Co-design for the development of legged robots

Gabriele Fadini

Université Fédérale
Toulouse Midi-Pyrénées

THÈSE

En vue de l'obtention du
DOCTORAT DE L'UNIVERSITÉ DE TOULOUSE

Délivré par l'Université Toulouse 3 - Paul Sabatier

Présentée et soutenue par

Gabriele FADINI

Le 26 octobre 2023

Un cadre générique de co-conception pour l'optimisation du design et de la commande des robots

---

Ecole doctorale : **SYSTEMES**

Spécialité : **Robotique**

Unité de recherche :
LAAS - Laboratoire d'Analyse et d'Architecture des Systèmes

Thèse dirigée par
Philippe SOUERES et Thomas FLAYOLS

Jury

M. Patrick WENSING, Rapporteur
M. Christian David REMY, Rapporteur
M. Philippe SOUERES, Directeur de thèse
M. Thomas FLAYOLS, Co-directeur de thèse
Mme Christine CHEVALLEREAU, Présidente

CO-DESIGN FOR THE DEVELOPMENT OF LEGGED ROBOTS

GABRIELE FADINI

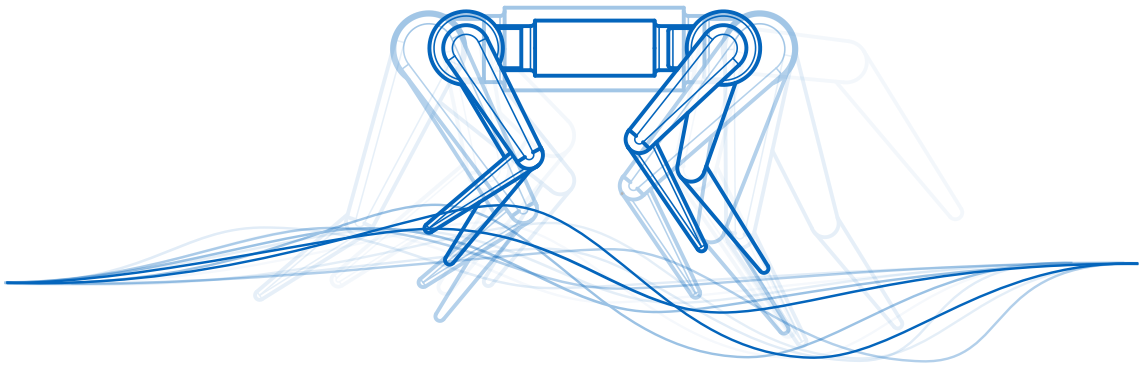

Développement de techniques de co-design
pour la conception et la commande de robots quadrupèdes

October 2023 – Final version

Gabriele Fadini,
Co-design for the development of legged robots,
Développement de techniques de co-design
pour la conception et la commande de robots quadrupèdes,
Doctoral degree in Robotics from the University of Toulouse,

JURY COMPOSITION

THESIS ADVISORS:		
	Philippe Souères,	LAAS-CNRS
	Thomas Flayols,	LAAS-CNRS
CHAIR:		
	Christine Chavallereau,	INRIA
RAPPORTEURS:		
	C. David Remy,	University of Stuttgart
	Patrick M. Wensing,	University of Notre Dame
INVITED MEMBERS:		
	Andrea Del Prete,	University of Trento
	Shivesh Kumar,	DFKI-RIC

Defended at LAAS-CNRS *on the 26th of October 2023.*

"Extrapolated, technology wants what life wants:
Increasing efficiency
Increasing opportunity
Increasing emergence
Increasing complexity
Increasing diversity
Increasing specialization
Increasing ubiquity
Increasing freedom
Increasing mutualism
Increasing beauty
Increasing sentience
Increasing structure
Increasing evolvability"
— *Kevin Kelly, What Technology Wants*

ABSTRACT

Keywords — concurrent design, co-design, optimization, quadruped, scaling, power efficiency

THIS dissertation focuses on concurrent design optimization for robotic systems, specifically in the context of co-designing legged robots. We explore the domain of legged robots and the innovative concept of co-design. By leveraging together hardware, software, and control algorithms, new possibilities for creating efficient, adaptable, and versatile robotic systems are possible. This alternative vision of robot design provides a new paradigm and holds potential for quadruped robots. The main investigated goals are performance in task execution and energy efficiency. A bi-level framework, combining both trajectory and hardware optimization, is proposed. This method proves to be versatile, scalable and generic, by combining genetic algorithms and trajectory optimization techniques. Such a tool is then applied with success to several optimization problems challenging complex tasks and systems, high dimensionality, mixed continuous-integer variables and multiple objectives. To properly account for hardware selection, *ad hoc* models were formulated, accounting for the power consumption and the scaling of the structure. To apply this approach to real systems, particularly to open-hardware quadrupeds, an extensive analysis was conducted based on their motor properties. Correlation models were developed to understand the relationship between motor mass and mechanical and electric parameters. Also, the scaling effect on the entire robotic system and individual actuation stages was analyzed. In this case, physical-based dimensional analysis was employed to ensure that dynamic and structural properties remain consistent. The method enhances the design of robotic systems by integrating power considerations and leads to the automatic discovery of some of the emerging design paradigms in the field of legged robotics.

RESUMÉ

Keywords — concurrent design, co-design, optimisation, quadruped, scaling,

CETTE thèse porte sur le développement de méthodes d'optimisation pour la conception simultanée de systèmes robotiques. Plus spécifiquement, nous nous intéressons au domaine innovant de la co-conception appliquée à des robots à pattes. En ajustant simultanément la mécanique, l'électronique ainsi que les algorithmes de contrôle d'un robot, de nouvelles possibilités d'améliorer les performances mais aussi l'adaptabilité et la polyvalence de ces systèmes émergent. Cette vision moderne de la conception robotique nous apparaît comme une piste prometteuse pour étendre les capacités des robots quadrupèdes. Le principal objectif de ce travail est d'améliorer les performances des robots dans l'exécution de tâches spécifiques tout en maximisant leur efficacité énergétique. Un cadre à deux niveaux, optimisant simultanément trajectoires de contrôle et spécificités matérielles, est proposé. Cette méthode s'avère polyvalente, évolutive et générique, en combinant des algorithmes génétiques et des techniques d'optimisation de trajectoire. Cet outil est ensuite appliqué avec succès à plusieurs problèmes d'optimisation caractérisés par des tâches et des systèmes complexes, une grande dimensionalité, des variables continues et mixtes entières ainsi que des objectifs multiples. Pour tenir compte de la sélection du matériel, des modèles *ad hoc* ont été formulés, en tenant compte de la consommation d'énergie et de la mise à l'échelle de la structure. Afin d'appliquer cette approche à des systèmes réels, des quadrupèdes open source dans notre cas, une analyse approfondie a été menée sur la base de leurs propriétés motrices. Des modèles de corrélation ont été développés pour comprendre la relation entre la masse du moteur et les paramètres mécaniques et électriques. En outre, l'effet d'échelle sur l'ensemble du système robotique et sur les étapes d'actionnement individuelles a été analysé. Dans ce cas, une analyse dimensionnelle basée sur la physique a été employée pour s'assurer que les propriétés dynamiques et structurelles restent cohérentes. Notre méthode facilite la conception des systèmes robotiques en intégrant des considérations de puissance et de découvrir certains paradigmes de conception émergents dans le domaine de la robotique à pattes.

RIASSUNTO

Keywords — progettazione concorrente, robotica, robot a gambe, *co-design*, co-progettazione, ottimizzazione, robot quadrupedi, effetto di scala, efficienza energetica

Questa tesi di dottorato si concentra sull'ottimizzazione di sistemi robotici attraverso la progettazione concorrente, in particolare sul *co-design* di robot a gambe (in inglese *legged robots*). Sfruttando intelligentement hardware, software e algoritmi di controllo, si aprono nuove possibilità per creare robot piú efficienti, adattabili e versatili. Tale visione alternativa alla progettazione tradizionale costituisce un paradigma innovativo e possiede un grande potenziale per l'ingegnerizzazione di sistemi complessi, e in particolare dei robot quadrupedi. I principali obiettivi indagati sono le prestazioni nell'esecuzione delle operazioni e l'efficienza energetica. Viene proposto un metodo di ottimizzazione a due livelli, che combina controllo ottimo per la generezione delle traittorie e un algoritmo genetico per la selezione dell'hardware. Questo metodo si rivela versatile, scalabile e generico. Tale strumento è stato applicato con successo a diversi problemi che comportano la sintesi di compiti e sistemi complessi, con un alto numero di variabili, anche discrete, ed eventualmente con obiettivi multipli. Per tenere adeguatamente conto della selezione dell'hardware, sono stati formulati modelli *ad hoc*, che tengono conto del consumo di energia e del fattore di scala della struttura. Per applicare questo approccio a sistemi reali, in particolare ai robot quadrupedi *open-hardware*, è stata condotta un'analisi approfondita in base alle proprietà del motore. Delle correlazioni fisicamente accurate sono state sviluppate al fine di descrivere la relazione tra la massa del motore e i realtivi parametri elettromecanici. Inoltre, è stato analizzato l'effetto di scala sull'intero sistema robotico e sui suoi attuatori. In questo caso, è stata impiegata un'analisi dimensionale per garantire la coerenza delle proprietà dinamiche e strutturali. Il metodo migliora il processo di selezione di sistemi robotici integrando considerazioni sulla loro efficienza e conduce inoltre alla scoperta automatica di alcuni dei paradigmi di progettazione emergenti in questo campo della robotica.

ACKNOWLEDGEMENTS

I would like to express my sincere gratitude to everyone who contributed to the development of this work, with a special acknowledgment to my thesis advisors Philippe Souères and Thomas Flayols. I am also extremely grateful to Andrea Del Prete. Thanks to him I got first involved in co-design and later on he kept closely following and advising my advancements in this domain. To these mentors goes my deep gratitude for the invaluable advice and suggestions through the years spent at Laboratoire d'analyse et d'architecture des systèmes (LAAS)-Centre national de la recherche scientifique (CNRS) in Toulouse. Their guidance supported not only this work but also my growth as a researcher and a person.

I also thank the members of the defense jury, in particular Christine Chevallereau, and the rapporteurs Patrick Wensing and David Remy, who agreed to review this thesis. It was also thanks to their contributions to this domain which fascinated me and greatly inspired me to pursue this scientific investigation.

I am also grateful to the many talented roboticists in the Gepetto team, who motivated me through discussions and provided constructive comments. In particular, a big thanks goes to Oliver, Nicolas, Nahuel, Carlos, Rohan and Justin for the exchanges about countless technical topics. Among the fellow students, which are way too many to mention on this short page, a special mention goes to Fanny, Sabrina, Pierre-Alexandre, Filip and Côme. Sharing ideas and struggles with them allowed me to keep curious about different topics in robotics. In addition, even if they just spent a short time in Toulouse, I express my gratitude to the so-called *italian gang*, Giulio, Filippo, Alessandro and Gianluigi, for their fresh and positive outlook at times when it was most needed.

Far from Toulouse, a sincere thank goes also to Shivesh Kumar, who invited me to collaborate on co-design in the Underactuated Robotics Lab at Deutsches Forschungszentrum für Künstliche Intelligenz (DFKI) in Bremen. Sharing the common objective of optimizing a quadruped platform helped me apply new ideas and insights into the problem. While, again in France, I will also remember fondly the many wonderful human beings I met along this journey and that made it lighter by sharing a laugh or a smile.

Lastly, but certainly not least, I extend my heartfelt thanks to my loving family and friends. Despite the physical distance, their unwavering support has always been by my side. Their belief in me and their continuous encouragement in my studies and personal life is something I will never adequately express my gratitude for.

Grazie a tutti,

Gabriele Fadini

CONTENTS

LIST OF SYMBOLS

Dynamical modeling

t	time $[s]$
$\mathbf{q}$	position vector
$\mathbf{q}_a$	actuated position state vector
$\mathbf{v}$	velocity vector
$\mathbf{v}_a$	actuated velocity vector
$\mathbf{u}$	control variable vector
$\mathbf{x}$	state vector
$\mathbf{a}$	acceleration vector
$\mathbf{x}^\star$	optimal state derivative vector
$\mathbf{u}^\star$	optimal control variable vector
$\mathbf{M}(\mathbf{q})$	inertia matrix at the joints
$\mathbf{\Omega}$	Generalized forces
$h(q, \dot{q})$	bias forces
C	Coriolis and centrifugal forces
g	Gravity forces
$\mathbf{\Phi}$	Integration function
$\mathrm{d}t$	integration infinitesimal
$\mathbf{f}$	contact forces
$\mathcal{L}$	optimal cost
$\mathcal{L}_{\tilde{\zeta}}$	robust optimal cost
$\mathbf{J_c}$	contact jacobian
$\boldsymbol{\tau}$	torques at the controlled joints
$\boldsymbol{S}$	selection matrix of the actuated joints
f	contact forces
$\mathbf{I}$	identity matrix
n_b	number of bodies
$\mathbf{n}, \mathbf{t}, \mathbf{b}$	normal, tangential, binormal unit vectors in the contact frame

Actuator and system parameters

ρ	density $[kg/m^3]$
K_v	speed constant
K_t	torque constant
K_e	electric constant
K_m	machine constant
V_t	voltage supplied $[V]$
V_m	voltage at the motor terminals $[V]$
i_0	stall current $[A]$
i	current flowing into the motor $[A]$
r_g	gap radius
R	winding resistance of the motor $[V/A]$
R_0	winding resistance at ambient temperature $[V/A]$
K_0	torque constant at ambient temperature $[Nm/A]$
ω_0	no load speed $[rad/s]$
τ_0	static motor torque $[Nm]$
τ_m	motor torque $[Nm]$
ω_m	motor angular speed $[rad/s]$
τ_l	load torque $[Nm]$
τ_f	friction torque $[Nm]$
τ_μ	Couloumb friction torque $[Nm]$
b	viscous friction coefficient $[Nms]$
ω_l	load angular speed $[rad/s]$
$\mathcal{I}_m$	rotor inertia $[kgm^2]$
$\mathcal{I}_l$	load inertia $[kgm^2]$
$n = \frac{\omega_m}{\omega_l}$	transmission ratio $[-]$

μ static friction coefficient

ε	torque conversion factor $[-]$
α	low-pass filter parameter
f_c	cut-off frequency

Power balance

P_m mechanical power withstood by the motor $[W]$
P_l mechanical power required by the load $[W]$
P_t thermal power out of the motor $[W]$
P_{el} electrical power $[W]$
P_f power consumed by the joint friction forces $[W]$
E_m mechanical energy $[J]$
E_t energy lost due to Joule effect $[J]$
E_{el} electrical energy $[J]$
L motor characteristic dimension $[m]$
A_s motor exposed surface $[m^2]$
η electromechanical power efficiency of the actuator $[-]$

Scaling

K beam flexural stiffness
E Young modulus $[Pa]$
l limb lengths $[m]$
Y inertia moment of area $[m^4]$
λ_l scaling factor for the limb linear length $[-]$
λ_s scaling factor for section linear dimension $[-]$
λ_a scaling factor for the accelerations $[-]$

Optimization

$\mathcal{D}$	design optimization variables
$\mathcal{C}$	control optimization variables
T	total time
T_c	time in contact
N	number of optimization nodes
N_{pop}	number of individuals candidates per generation
N_{gen}	number of generations to evaluate
N_{sim}	number of simulations to estimate the robust cost
$\mathcal{K}$	Riccati gains
γ	scaling factor of the Riccati gains
m_m	motor mass
$\mathbf{X}$	State optimization variables vector
$\mathbf{U}$	Control optimization variables vector
$\mathbf{A}$	Acceleration optimization variables vector
$\mathbf{\Gamma}$	Slack optimization variables vector
$\mathbf{F}$	Contact forces optimization variables vector
$\mathbf{Z}$	Optimization variables vector
$\mathbf{\Phi}$	Integration function

LIST OF SYMBOLS

Dynamical modeling

t	time $[s]$
$\mathbf{q}$	position vector
$\mathbf{q}_a$	actuated position state vector
$\mathbf{v}$	velocity vector
$\mathbf{v}_a$	actuated velocity vector
$\mathbf{u}$	control variable vector
$\mathbf{x}$	state vector
$\mathbf{a}$	acceleration vector
$\mathbf{x}^\star$	optimal state derivative vector
$\mathbf{u}^\star$	optimal control variable vector
$\mathbf{M}(\mathbf{q})$	inertia matrix at the joints
$\mathbf{\Omega}$	Generalized forces
$h(q, \dot{q})$	bias forces
C	Coriolis and centrifugal forces
g	Gravity forces
$\mathbf{\Phi}$	Integration function
$\mathrm{d}t$	integration infinitesimal
$\mathbf{f}$	contact forces
$\mathcal{L}$	optimal cost
$\mathcal{L}_\xi$	robust optimal cost
$\mathbf{J_c}$	contact jacobian
$\boldsymbol{\tau}$	torques at the controlled joints
S	selection matrix of the actuated joints
f	contact forces
$\mathbf{I}$	identity matrix
n_b	number of bodies
$\mathbf{n}, \mathbf{t}, \mathbf{b}$	normal, tangential, binormal unit vectors in the contact frame

Actuator and system parameters

ρ	density $[kg/m^3]$
K_v	speed constant
K_t	torque constant
K_e	electric constant
K_m	machine constant
V_t	voltage supplied $[V]$
V_m	voltage at the motor terminals $[V]$
i_0	stall current $[A]$
i	current flowing into the motor $[A]$
r_g	gap radius
R	winding resistance of the motor $[V/A]$
R_0	winding resistance at ambient temperature $[V/A]$
K_0	torque constant at ambient temperature $[Nm/A]$
ω_0	no load speed $[rad/s]$
τ_0	static motor torque $[Nm]$
τ_m	motor torque $[Nm]$
ω_m	motor angular speed $[rad/s]$
τ_l	load torque $[Nm]$
τ_f	friction torque $[Nm]$
τ_μ	Couloumb friction torque $[Nm]$
b	viscous friction coefficient $[Nms]$
ω_l	load angular speed $[rad/s]$
$\mathcal{I}_m$	rotor inertia $[kgm^2]$
$\mathcal{I}_l$	load inertia $[kgm^2]$
$n = \frac{\omega_m}{\omega_l}$	transmission ratio $[-]$

μ static friction coefficient

ε	torque conversion factor $[-]$
α	low-pass filter parameter
f_c	cut-off frequency

Power balance

P_m mechanical power withstood by the motor $[W]$
P_l mechanical power required by the load $[W]$
P_t thermal power out of the motor $[W]$
P_{el} electrical power $[W]$
P_f power consumed by the joint friction forces $[W]$
E_m mechanical energy $[J]$
E_t energy lost due to Joule effect $[J]$
E_{el} electrical energy $[J]$
L motor characteristic dimension $[m]$
A_s motor exposed surface $[m^2]$
η electromechanical power efficiency of the actuator $[-]$

Scaling

K beam flexural stiffness
E Young modulus $[Pa]$
l limb lengths $[m]$
Y inertia moment of area $[m^4]$
λ_l scaling factor for the limb linear length $[-]$
λ_s scaling factor for section linear dimension $[-]$
λ_a scaling factor for the accelerations $[-]$

Optimization

$\mathcal{D}$	design optimization variables
$\mathcal{C}$	control optimization variables
T	total time
T_c	time in contact
N	number of optimization nodes
N_{pop}	number of individuals candidates per generation
N_{gen}	number of generations to evaluate
N_{sim}	number of simulations to estimate the robust cost
$\mathcal{K}$	Riccati gains
γ	scaling factor of the Riccati gains
m_m	motor mass
$\mathbf{X}$	State optimization variables vector
$\mathbf{U}$	Control optimization variables vector
$\mathbf{A}$	Acceleration optimization variables vector
$\mathbf{\Gamma}$	Slack optimization variables vector
$\mathbf{F}$	Contact forces optimization variables vector
$\mathbf{Z}$	Optimization variables vector
$\mathbf{\Phi}$	Integration function

ACRONYMS

ABA	Articulated-Body Algorithm
ADMM	Alternating Direction Method of Multipliers
AI	Artificial Intelligence
AM	Additive Manufacturing
BLDC	Brushless Direct Current
CAD	Computer Assisted Design
CEA	Commissariat à l'énergie atomique et aux énergies alternatives (Alternative Energies and Atomic Energy Commission)
CoM	Centre of mass
CoG	Centre of gravity
CoT	Cost of Transportation
CMA-ES	Covariance Matrix Adaptation Evolution Strategy
CNRS	Centre national de la recherche scientifique (French National Centre for Scientific Research)
CRBA	Composite Rigid-Body Algorithm
CRP	Composite-Reinforced Polymer
CPG	Central Pattern Generator
DAE	Differential-Algebraic system of Equations
DARPA	Defence Advanced Projects Agency
DC	Direct Current
DD	Direct-Drive
DDP	Differential Dynamic Programming
DFC	Design-For-Control
DFKI	Deutsches Forschungszentrum für Künstliche Intelligenz (German Research Center for Artificial Intelligence)
DoF	Degree of freedom
EA	Evolutionary algorithm
ESA	European Space Agency
FDDP	Feasibility-driven Differential Dynamic Programming
FDM	Fused Deposition Modeling

FOC	Field-Oriented Control
GA	Genetic Algorithm
HPC	High-Performance Cluster
ICE	Internal Combustion Engine
IIT	Istituto Italiano di Tecnologia Italian Institute of Technology
iLQR	Iterative Linear Quadratic Regulator
IMU	Inertia Measurement Unit
IS	International system
LAAS	Laboratoire d'analyse et d'architecture des systèmes Laboratory for the Analysis and Architecture of Systems
LIP	Linear Inverted Pendulum
LQR	Linear Quadratic Regulator
OCP	Optimal Control Problem
NLP	Non-Linear Program
nMPC	Non-Linear Model Predictive Control
MIT	Massachusetts Institute of Technology
MPC	Model Predictive Control
MPI	Max Planck Institute
OCP	Optimal Control Problem
ODRI	Open Dynamic Robot Initiative
OSHWA	Open Source Hardware Association
PD	Proportional Derivative
PID	Proportional Integral Derivative
PLA	Polylactic Acid
PMSM	Permanent Magnet Synchronous Motors
PPO	Proximal policy optimization
QDD	Quasi Direct-Drive
RIC	Robotics Innovation Center
RL	Reinforcement Learning
ROS	Robot Operating System
RNEA	Recursive Newton-Euler Algorithm
SAC	Soft actor critic
SEA	Series Elastic Actuator
SLA	Stereolithography

SLIP	Spring-Loaded Inverted Pendulum
SLS	Selective Laser Sintering
SMA	Shape Memory Alloy
SP	Stochastic Programming
SQP	Sequential Quadratic Programming
TIT	Tokyo Institute of Technology
TRPO	Trust-region policy optimization

Part I

INTRODUCTION

In this part the goal of the thesis will be presented at a higher level. The questions connected to the Ph.D. research activity are presented, with some general simplifying examples. The subsequent steps associated with this study are then summarized, offering an overview of the progression of the work. The summary of the research contributions, is a concise synthesis of the evolution of the thesis. It sets the stage for the subsequent chapters and sections, establishing the framework within which the research has been conducted and the objectives have been achieved.

1

UNDERSTANDING THE CO-DESIGN APPROACH

In Short

In this chapter, the core of the thesis work is explained. The concept of co-design is introduced as a high-level statement and its motivations are explained with some examples. We remark some of its primary goals and provide explanations for its significance to the robotics community. The final section concludes the introduction to the topic by highlighting the contributions made during the course of the Ph.D. study.

Contents

1 EMBRACING CO-DESIGN PHILOSOPHY IN ENGINEERING

Over time, engineering products have become increasingly complex, often demanding a combination of multi-domain expertise and extensive design optimization/system integration phases. In addition to product development, modern engineers frequently face the task of designing an effective control policy for the system to achieve specific objectives. While this heightened complexity presents challenges, it also offers great opportunities to develop innovative solutions, necessitating the exploration of new design paradigms. Today, it is possible to tackle larger, multi-domain problems by leveraging modern modeling, simulation, and optimization techniques to significantly enhance the whole system. For instance, let us just consider the development of:

This is especially true whenever an autonomous logic or smart behaviours are implemented e. g. in portable devices, cars, appliances . . .

- Automotive industry
- Avionics
- Mechatronics
- Embedded systems design
- Robotics

In any of these domains, the engineering problem requires to face both the physical system implementation and a more functional phase related to making the product perform a specific task. In the case of complex systems, the trend is also to automatize the control inserting some kind of behavioral intelligence. This ranges from the assistive driving and piloting technologies developed for automotive and avionics to the synthesis of higher levels of autonomy, which is one of the main goals of robotics research. Constantly adding new features to the products makes them more useful but also more difficult to properly develop, design and test. Innovative design tools are employed to build such systems while test such their deployment and functionalities. This allows to reduce costs, it provides the engineers with useful intuition and allows for faster design cycles. Advancements in computational power and optimization enable nowadays the simulation of intricate interactions between the governing logic and the system. The development of microprocessors and information technology allowed us to progressively increase the intelligence and complexity of the product. This requires a synergistic approach among different fields, navigating through multiple domains and complex trade-offs among various designs. This is the case of mechatronics, a branch of canonical mechanical engineering, which includes also electronics and control engineering, that was first proposed as a trademark word in the 70s in Japan. In essence, mechatronics deals with engineering computer-controlled electro-mechanical systems. According to its paradigm, the mechanical system must be conceived as a whole system, together with the electrical/electronic and computer control. Similarly, also robotics is a multi-disciplinary field as well and the synthesis of intelligence is even more challenging because of the incredibly high complexity of the systems. In this work, the focus is on the design of optimized legged robots. To develop successful systems, an even tighter integration between different domains such as mechanical engineering, electronic engineering, control theory and computer science is needed. Based on some hardware current design, the goal is to optimize the robot to achieve a given task. In the past, several methods have been proposed for this same goal For instance, to design the platform, biological inspiration has been extensively used in the field of legged robotics. As animals have evolved over millions of years to navigate in complex environments, the mechanical design of robots should learn from that and reflect complexity of the biological systems. This however could lead to systems with unnecessarily high complexity. To reduce this problem, instead of biological inspiration, "technological inspiration" would be useful to keep the complexity of the system low and exploit the currently available technologies. While biological systems are still incredibly well adapted, they may be a chimera in robotics. For instance, no biological structure competes for speed with completely artificial designs, such as a racing car or a jet engine. And yet none of these systems show the high level of complexity of biological systems. One could even argue that, in the case of aviation, surely the flight of the birds has been a source of inspiration, but it was not necessary to copy all of the structural complexity to be successful in flying. The same approach should also be used in legged robotics, just as an inspiration driver, focusing on the essential functional aspects. The current technology limits what can be achieved, (e. g. materials, actuators or sensors are not yet comparable with their

Hence design both the plant and its control

In the sense that the technology should be considered when designing a system

biological equivalents). It is hence necessary to deal with this limitation and discover what kind of design adapts the best to the desired application. For instance, in the case of the robot ATRIAS [125], the force profile of the walk is functionally similar to that of humans. Yet it is an achievement based on technology: no biological system shows a similar leg topology. This thesis is based on a similar assumption. Inspired by recent popular robotics implementations, which will be described in detail, and current technology a specific design is selected and optimized both from the point of view of the mechanical design with the control. We start with a high-level nominal design of a robot (e. g. structure, actuator types and limits) and, within the current technological limits, try to improve on it.

2 WHY CO-DESIGN?

In the past, various techniques have been developed and employed to tackle the design and control problem in different fields. These approaches have typically been tailored to meet the specific requirements of each domain separately. The design phase involves numerous intricacies, with the potential for optimizing various aspects of the product. However, traditionally, this optimization has been carried out sequentially, treating mechanical design and control design as separate problems. Yet, the physical system and its associated control system are inherently interconnected, and employing conventional approaches may yield suboptimal results. For instance, in legged robotics, when producing contact forces, badly implemented leg designs may be affected by an uneven redistribution of torque across the joints. An optimized design, with more intelligent control, would distribute loads more evenly on the actuators hence avoiding excessive burden or damage to the joints. The interdependency between the designed physical system, the plant, and the governing intelligence, the control, is profound. In legged robots, the control strategy is influenced by the joint dynamics: e. g. mechanical characteristics of the actuators, such as bandwidth limitations or torque saturation, which impact the capabilities of the system. Furthermore, the characteristics of the plant itself also affect the performance, for instance when considering the influence of its inertia on the dynamics.

The actuation is contingent upon the physical parameters

WHAT A SYSTEM DESIGNER NEEDS Computerized tools can be used for two main different goals:

- Physical implementation validation
- Functional/behavioral synthesis and validation

These needs present some kind of duality: one is related to the plant's properties, while the other to its control. We may wonder if considering the two approaches together, let's say holistically, thanks to the use of novel computational tools, could empower engineering intuition even further. The answer is yes, and a lot of cutting-edge research has been recently carried out in this direction.

Co-design is one of the innovative design methodologies that adopt the vision of bringing the hardware design closer to its behavior synthesis. This new paradigm aims

at finding optimal solutions by simultaneously addressing the challenges of control and plant design. Leveraging the interplay of these two intelligent systems can be conceived while improving several metrics. Co-design has been successfully used in the past and seems to be a rapidly growing approach in robotics as a whole, see Fig. 1. In the same chart, it is possible to see that, even if legged robots have been associated with the earliest developments in co-design, only recently has the method gotten some traction. The

As several parts that have to be designed, assembled and controlled together, the word system design is often used

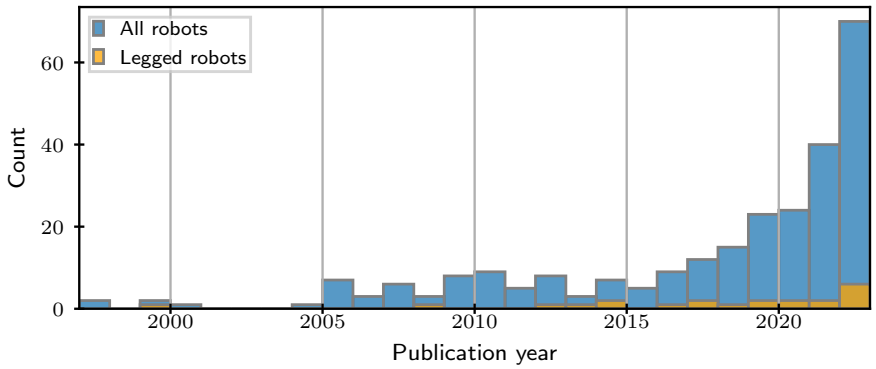

Figure 1: General and legged robotics co-design publications per year

Fig. 1 Source: IEEE Xplore Queries: 1) all: "co-design" AND "robot" IN metadata" 2) legged: "co-design" AND "(robot OR leg OR legged OR quadruped OR humanoid) " IN metadata"

conception of the system can follow different approaches to make it functional. It can even accomplish the task in a completely autonomous way (without external control, like in the case of passive walkers). In this case, the property that makes the system useful, the intelligence, can be directly embedded in the physical system itself. In the opposite case, we can envision steering the platform to perform a given task and in this case, control authority needs to be introduced. The intelligence here is added inside a control policy, which generally increases the robustness and versatility of the system. Fig. 2 visually explains this trade-off. The contribution of the control and the plant to

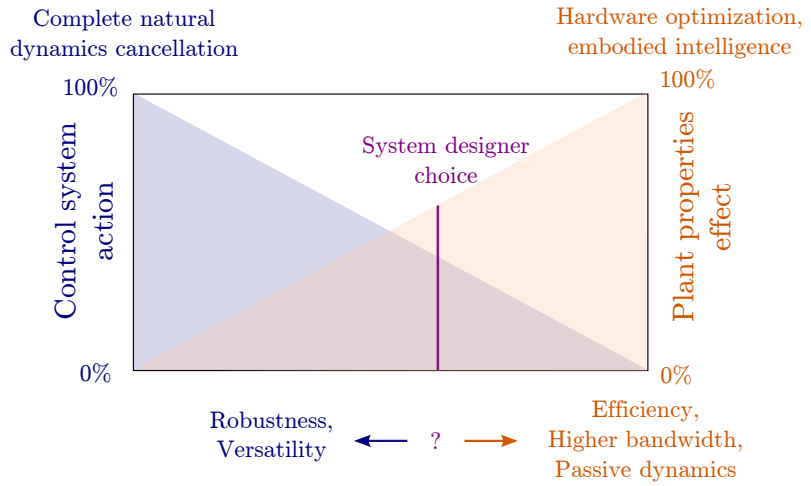

Figure 2: Design implementation trade-off between exploiting control strategy or plant characteristics.

task achievement are shown with different colors, respectively blue and orange. The poles are: (right) hardware that can execute the task without any control action (e. g. passive walkers, efficient but task-limited) and (left) a control architecture that completely cancels out the effect of dynamics (i. e. the hardware properties have no role in task fulfillment). However, in general, no system presents these polar properties, but shows a mixture of the two. The designer's choice is then to find a trade-off choice of design and control between these two extremes.

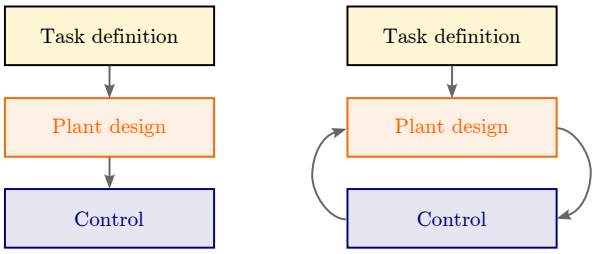

(a) Sequential approach (b) Integrated approach

Figure 3: *Sequential vs integrated* approach

Fig. 3 shows the classic approach of system integration Fig. 3a and a simultaneous definition of plant and control to follow a task Fig. 3b. According to Allison and Han [7], co-design is a design methodology that explicitly manages the interaction between the physical system and its control system, leading to system-optimal designs that outperform conventional sequential methods. In the literature, Allison and Nazari [10] referred to co-design as concurrent design, integrated design, or design-for-control, highlighting the minor or non-existent nuances between these terms. Some of the questions that co-design allows to answer are the following:

- Can the structure of the system be leveraged to complete the task?
- How can the best design of a robot be chosen for a given application?
- How can the computational approaches improve the design workflow?
- How can the material and manufacturing approaches help in customized robot creation?
- How to include the controller information in the design phase?

3 OBJECTIVE AND OUTLINE OF THE THESIS

The objective of this thesis is to propose and exploit a systematic framework to answer some of the previous questions. In particular, the objective is to find the best-suited legged robot hardware for a given high-level task. Different approaches for different challenges can be handled with the same unified problem-resolution strategy. The application of the method ultimately will allow a better understanding of the relationships between hardware and behavior, which is crucial for the new challenges in robotics. This

thesis is based on the interconnection between optimization, control, mechanical design, and robotics as parts of a larger, more challenging problem, which is how to automatize the robot design process for a specific purpose. We do not aim at completely solving it in its entirety and we rather focused on several open problems in the field. A considerable part of the investigation was dedicated to framing the co-design process, trying to understand its core elements and how to apply them to study cases in legged robotics. The co-optimization of robot design and motion is framed, in a general and realistic way. To achieve this, the robot design is considered a fundamental part. For this reason, this dissertation starts with a description of legged robots and their design and presents the technologies that are used in their implementation. In particular, the initial part provides a general introduction to the legged robot development, models and technological paradigms, covering the main ideas used later on in the text. It includes a presentation of the following points:

- Quadruped robot history and applications
- Some fundamentals on articulated robot dynamics modeling.
- The model of contact, necessary for manipulation and locomotion.

A the second part, the model of the actuators is detailed through the following focuses:

- Limitations and trade-offs in robotics actuator selection,
- A description of the friction model,
- A description of the power consumption model.

The third part of the thesis focuses on the co-design problem itself. First, a general approach is outlined, connecting it to the state of the art. The proposed method is explained as a complete co-design problem. The proposed framework, which is the actual core of the research is presented later on, highlighting the criticalities of the problem and motivating the solution strategy. Additionally, details on trajectory optimization strategies and the scaling model of the system are provided in the implementation section. Some results, building upon this framework and involving different systems are shown in the third part of the dissertation. The same foundation is then re-adapted, in the applications part of the thesis, in order to study, through co-design, some platforms and tasks. This thesis resulted in three contributions that showcase the application of the core idea and methodology to various systems and problems, each research representing a different level of complexity and stage of maturity.

- The first contribution addresses a specific system and problem, laying the foundation for the co-design framework. It explores a relatively simple monoped system, chosen as a minimal test case to explore the capabilities of the leg with respect to energy efficiency. This allowed an easily interpretable and focused examination of the research output. This initial stage involves a modeling phase of the actuators.
- Building upon the first contribution, a second extension focuses on the application of the core methodology to choose hardware robust to perturbation with co-design. In this stage, the scalability and adaptability of the research approach are tested. The results demonstrate the generality of the methodology with different systems and highlight the potential for solving more complex problems.

- The third contribution represents the culmination of the research journey, tackling a highly complex problem, quadruped optimization, for cyclic tasks. This stage incorporates more advanced techniques and tackles challenges that required numerous technical modifications but are still based on the same core intuition and methodology. By addressing such a complex system, the strength of the chosen approach is showcased, and validation on hardware further solidifies its effectiveness.

Taken together, these different contributions form a cohesive body of work that progressively adapts a shared vision and solution strategy. They demonstrate the ability to apply the approach to different levels of complexity, showcasing its adaptability, generality, and effectiveness. A final, conclusive part sums up the findings and speculates on the future extension of this work.

4 PUBLICATIONS

This thesis was directed at LAAS-CNRS under the supervision of Philippe Souères and Thomas Flayols. The presented work benefitted since the beginning of the continuous collaboration with Andrea Del Prete and the University of Trento, his knowledge, especially concerning numerical optimization and control of legged robots, was crucial in developing the framework. This thesis led to the writing of three articles. The first two were respectively presented at the conference IEEE ICRA 2021 and IEEE/RSJ IROS 2022 (the latter was also published in the journal IEEE RA-L). The most recent one has been submitted to the journal Robotica.

- G. Fadini, T. Flayols, A. Del Prete, N. Mansard, P. Souères, "Computational design of energy-efficient legged robots: Optimizing for size and actuators", *IEEE International Conference on Robotics and Automation (ICRA)*, May 2021,
- G. Fadini, T. Flayols, A. Del Prete, P. Souères, "Simulation aided co-design for robust robot optimization", *IEEE Robotics and Automation Letters*, Oct. 2022.
- G. Fadini, S. Kumar, R. Kumar, T. Flayols, A. Del Prete, J. Carpentier, P. Souères, "Co-designing versatile quadruped robots for dynamic and energy-efficient motions", *submitted to Robotica*, 2023.

Part II

FOUNDATIONS ON QUADRUPED ROBOTS

This part of the manuscript provides a general introduction to the field of legged robotics. In particular, it presents their history and development, focusing especially on quadrupeds, and describes the modeling of these systems and their dynamics.

2

STEPPING THROUGH TIME: PAST AND FUTURE OF LEGGED ROBOTS

In Short

In this chapter the state of the art is presented with a particular focus on:

- Legged systems historical development and technology
- Quadruped applications and limitations

Contents

1 LEGGED ROBOTS

1.1 *The promise of legged robotics*

Robotics, as a field, presents unique challenges due to the inherent complexity of the systems involved and the intricate control issues that arise. Within this broad domain, legged robots represent interesting platforms and demanding area of study. The generation of movement on these platforms presents lots of challenges, the main ones being:

Most of the fascination is probably tied to their similarity with biological systems.

- Under-actuation: the number of control inputs is fewer than the number of Degree of freedom (DoF) of the system. In other words, the system has fewer actuators than the number of DoF to define its position (e. g. the pose of the base of the robot cannot be controlled directly).
- Kinematic redundancy: Often there are more DoF or joints available than necessary to achieve a specific task or motion (e. g. redundant joints or closed-loop kinematics)
- Contact dynamics: Physical interactions occur when a robot comes into contact with the environment. Contact modeling is necessary to describe the forces, motions, and behaviors that arise during locomotion or manipulation in contact.

- IMPACT DYNAMICS: For quick motions, legged robots are subject to impulses, namely, changes in momentum caused by forces acting for a short time. It is necessary to assess the effect of these forces during motion.
- FOOTSTEP-PLANNING: Footstep planning refers to the process of determining the placement of a robot's feet to achieve desired locomotion or task execution. It involves generating a sequence of footstep locations that enable effective navigation.
- STABILITY, LOCOMOTION AND BALANCE: Achieving stable locomotion and balance is one of the main challenges in legged robotics. To ensure that the robot maintains balance there are constraints on its placement, its center of mass, support polygon, and allowable disturbances to avoid the risk of falling or losing stability.

Legged robots differ significantly from other counterparts (i. e. wheeled ones), so traditional methods often fall short when applied to these robots. The design, development, and control of legged robots requires tailored methodologies that can address these specific challenges. The mechanical compliance of robotic legs enables them to traverse diverse environments and adopt various walking patterns. Such versatility, coupled with kinematic redundancy resulting from multiple legs, allows legged robots to navigate obstacles such as rubble and stairs. The drive to develop novel legged platforms (and the associated control strategies) is crucial for several reasons. Firstly, legged robots have the potential to surpass wheeled systems in terms of mobility and versatility. Secondly, legged robots have a structure, which closely resembles biological systems, such as humans and animals. This is crucial in assistive applications and to traverse human environments. However, addressing the control and design challenges associated with these capabilities remains an open problem in research. Legged robotics is still a rather young field (even though investigations around legged locomotion date back even centuries ago). The promise is that by devising improved, tailored approaches, researchers will eventually unlock their full potential, paving the way for advancements in various fields, making strides towards even more capable, agile, and intelligent systems. Solving some of the open problems presented in the text already proves that the synthesis and control of highly dynamic behaviors is at reach (as exemplified for instance by the incredible achievements of the Atlas platform by Boston Dynamics [31]).

1.2 *Quadruped robots*

Quadruped robots are a fascinating subset of legged robots. These robots closely resemble and mimic animal movements and characteristics. They are capable of walking, running, climbing, and navigating over uneven surfaces while maintaining stability. These robots are getting a lot of interest and their widespread use is building up a community of domain experts and enthusiasts. In recent years, private companies showcased the capabilities of legged robots with several commercial products. Furthermore, there is a growing number of legged robot platforms used purely for research or in education. In the following section, the history of these platforms is outlined, and possible future evolutions are also discussed. The presented platforms show a high variability (for instance in sizes, and different technologies). The question on how to automatically

design a platform that is adaptable and can be deployed to achieving the designer's goals is one of the main drivers of this thesis.

1.2.1 *Historical implementations*

In-depth historical reconstructions of the development of mechanical quadrupeds can be found in multiple reviews, some publications covering this topic are the following: [25], [47], [149], [158]. The creation of a mechanical *automaton* with quadrupedal form is lost in time, as a statement of the human fascination with the recreation of animal movement. Firstly there are some examples during the Sui-Tang period in China and also in Europe. For instance, during the Italian Renaissance, there is a famous example of the mechanical lion developed by Leonardo da Vinci on a commission from Pope Leo X to amuse the French king François I. Later, this concept was developed further with some rudimentary legged systems like Hooke's chart Fig. 4a and Chebyshev's robots. During the Second Industrial Revolution, legged systems were conceived to reproduce animal-like motions, this is the case of several mechanical horses model Fig. 4b, 4c. Some examples of these mechanical curiosities can be found dating back to the 30s and 40s. For instance a human-controlled legged vehicle was conceived (Fig. 4d) and, in England, Hutchinson made a remotely controlled, cable-actuated, quadruped system (Fig. 4e). In the United States, a mechanical automaton was made by Messmore to reproduce the galloping motion of a horse Fig. 4f.

In the earliest systems, automatization heavily relied on the mechanical platform design and human control. It is just recently, in the second half of the 19^{th} century, that we start seeing systems more similar to what we may call today a "quadruped robot". A robot representing the earliest wave of these modern quadrupeds is the Walking Truck developed by General Electric [160] Fig. 5a. By a clever choice of mechanical linkage the Walking Truck could allow precise operation in the working environment and even provide some haptic feedback to the human operator [1]. Controlling these machines with computerized systems became viable just later in the 70s. McGhee's group at Ohio University was one of the first employers of this approach [169]. The Phony Pony [65] (Fig. 5b) was the first machine in which the control logic was not relying on a human operator (which was the case e. g. for the Walking Truck). It was a decade later that some form of intelligence could be embedded in the system itself. A quadruped robot featuring a microprocessor was designed from the University of Tokyo, KUMO-I [117] Fig. 5c, dating back to the 70s. Hirose and Kato's research allowed the PV-II Fig. 5d quadruped to climb obstacles [116], the leg design further simplified control. In the 80s some studies related to motion generation were performed by Raibert's group. Before this, the legged robots movement heavily relied on quasi-static movement to maintain balance with conservative motions, this class of robots is called "static crawlers". McGhee and Frank in the 60s first defined the criterion of static stability for legged systems. The locomotion can be performed stably if, at any time, the Centre of gravity (CoG) of the robot can be projected inside the support polygon created by the legs in contact with the ground. This static stability criterion was inspired by the observation of arthropods and their

1 Video description

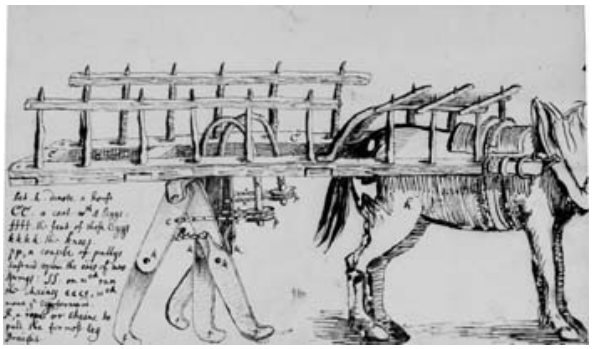

(a) Hooke's chart with Legs

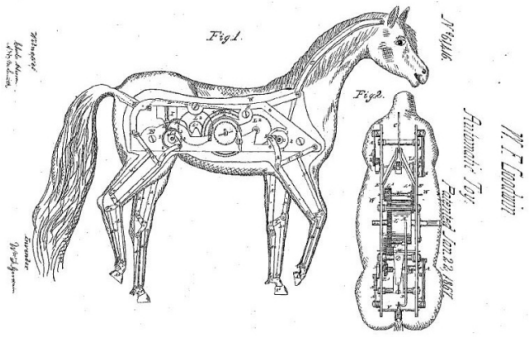

(b) Mechanical horse

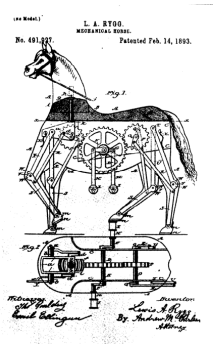

(c) Another mechanical horse

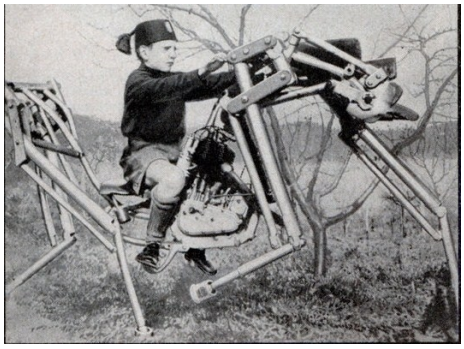

(d) Legged contraption by Alzetta 1932

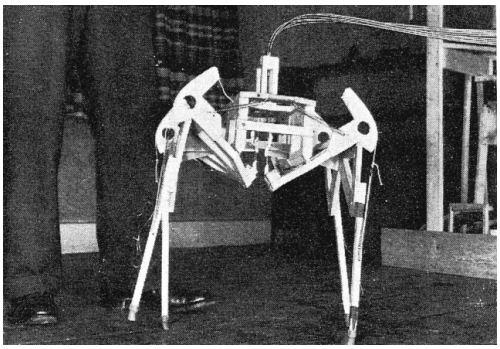

(e) Hutchinson 1940

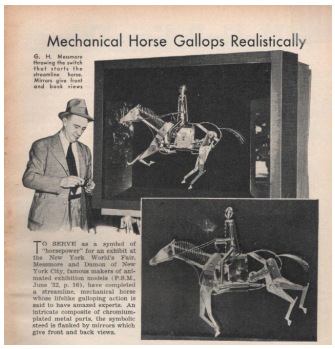

(f) Messmore's Horse

Figure 4: *Different legged contraptions*

motion. The first generation of machines adopted this criterion [156]. However heavy limbs were difficult to control [247], as the non-linear inertial effects were not negligible, so just slower motions could be achieved. Biological systems often move away from static stability to perform movement. To increase the motion speed it was necessary to consider the robot dynamics inside the control algorithm. This intuition first led Raibert to investigate more dynamic motions [197]. The complexity of the complete robot dynamics, though, pushed the realization of some preliminary simplified structures to this goal. His research, targeted to increasing mobility, was using 2D legged systems monopeds [198] or quadrupeds with prismatic legs Fig. 5e.

at the pace of Moore's law

The main limitations of this progress were the incremental improvements on the platforms which often were relying on a high engineering cost and on custom hardware and automatic control implementation. Later, with advancements in control and exponential computerization, it became possible to embed progressively more intelligence into robotic systems. Back in the 90s robots started greatly improving performance from the automatic control point of view. In Japan, the Titan series of robots was developed (Fig. 5f) at Tokyo University, and Sony started to produce in the late 90s the popular Aibo series of robots (Fig. 5g) [85]. The robots of this phase could perform rather simple tasks, such as quasi-static motions, kinetostatic planning or following simplified heuristics. For instance Scout-II [20], [191] is a robot that used passive prismatic joints to allow compliant locomotion on a variety of terrains with minimal actuation (a single actuated hip joint or leg). In its frame, this quadruped contained all that was needed for running and galloping even if, due to the lack of additional joints, the heading could not be controlled. It was necessary to wait for another decade to start seeing successful robots, capable of dynamic motions with more DoFs, whole-body control, and more interesting behaviors. Some major impulse in this sector was made by the development of BigDog [196], by Boston Dynamics. This hydraulic-driven machine, developed with Defence Advanced Projects Agency (DARPA) funding, had the goal of high payload-carrying capability and versatility on rough terrain. It was powered by a combustion engine and could traverse different terrains, including snow and debris. In 2012 Boston Dynamics revealed another quadruped, Cheetah [100]. Quadrupedal robots have gained significant traction and recognition, especially in research. Laboratories and research centers have nowadays access to dynamic platforms actuated by high-power density electric motors or hydraulic actuation. Several quadrupedal robots were developed as research platforms, including HyQ from Istituto Italiano di Tecnologia (IIT) [232] (Fig. 5j), with a hydraulic actuation capable of dynamic motion and high-payload carrying capabilities. In the domain of bipeds, some work explored the use of mechanical compliance in the structure. In 2007, a mechanically adjustable compliant robot BiMASC [129] was developed by the team of Johnatan Hurst at Carnegie Mellon. As a following development, another platform MABLE [99] was presented in 2009 by the University of Michigan. The platform featured non-linear springs capable of effectively isolating the motors from the impact forces and storing mechanical energy. This idea of decoupling the motors by the use of mechanical elements was reutilized also in the field of quadrupeds robots' design. Some years later, Roland Siegwart's group at ETH Zurich developed StarlETH, a

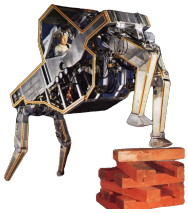

(a) 1965 Walking Truck

(b) 1968 Phony Pony

(c) 1976 Kumo I

(d) 1977 PV-II

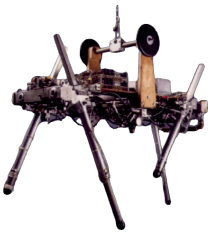

(e) 1986 Raibert

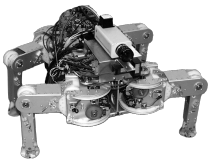

(f) 1996 Titan VIII

(g) 2001 Aibo ERS-110

(h) 2005 Scout II

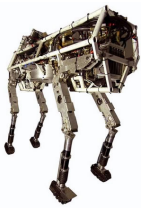

(i) 2008 Big Dog

(j) 2011 HyQ

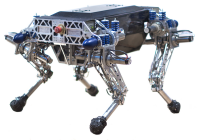

(k) 2012 StarlETH

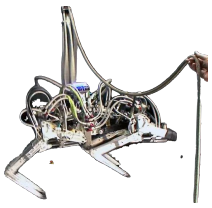

(l) 2012 Cheetah

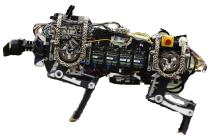

(m) 2013 MIT Cheetah

(n) 2013 CheetahCub

(o) 2013 WildCat

(p) 2015 MIT Mini Cheetah

(q) 2016 Minitaur

(r) 2016 Titan XIII

(s) 2017 Anymal

(t) 2019 Laikago

(u) 2019 Solo 12

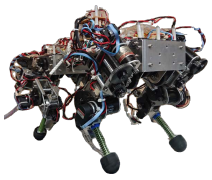

(v) 2020 Kurama

(w) 2020 Unitree A1

(x) 2020 Spot

(y) 2020 Alphred

(z) 2020 QGV series

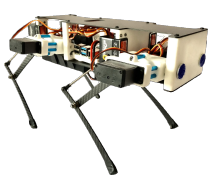

(aa) 2021 Pupper

(ab) 2022 Morti

(ac) 2022 Kirin

(ad) 2023 Sassa

Figure 5: History: Different quadruped robots concepts in time.

quadruped robot driven by Series Elastic Actuator (SEA) (Fig. 5k) [130]. In 2013 EPFL introduced the small-scale bio-inspired Cheetah-Cub robot featuring different compliant substructures (Fig. 5n) [251]. Passive elements (mechanical springs and dampers) are used in the structure and the joints are cable-driven. The design of this robot is made to be a relatively cheap and safe research testbed, with a remarkable weight of roughly 1.1 kg. Following a trend of highly transparent and back-drivable actuators, used for haptic devices, since the seminal work for the PHANTOM interface [213], the design of transparent actuators took off. Mini Cheetah (Fig. 5p) [32], [145], has been developed for research purposes following this approach, minimizing the reflected inertia of the leg, in a design paradigm that reduces the effect of impacts on the control [272]. Closed-loop kinematic and elastic elements were successfully used in the Jerboa robot, a small-sized planar biped with a controlled tail from the University of Pennsylvania [64] [2]. The robot was capable of different motions and base re-orientation exploiting the tail dynamics and recovering impact energy. MiniTaur (Fig. 5q) [27] was developed with a light-weight frame and used in reinforced learning simulation, successfully filling the sim-to-real gap [254]. The leg structure featured lightweight and robust closed-loop kinematics. Marco Hutter, one of the designers of StarlETH, more recently proposed an updated version, ANYmal, capable of improved performance [79], [131] (Fig. 5s). A new series of efficient robots, driven by high torque density actuators was developed at Massachusetts Institute of Technology (MIT). The design of these robots MIT Cheetah 1, 2 and 3 [28], [184], [272] (Fig. 5m) features a proprioceptive actuator and allowed to run up to 6 m/s. Boston Dynamics in 2015, following the acquisition by Google, revealed a smaller quadruped, with examples such as Boston Dynamics' Spot and Spot Mini [13] making an impact on the market [100]. In 2016, the Tokyo Institute of Technology (TIT) revealed a new sprawling-type robot, successor of the Titan series, Titan XIII [150] (Fig. 5r). The platform was made with efficiency and walking velocity in mind [3]. The structure was realized with Composite-Reinforced Polymer (CRP) and the actuation wire-driven (high specific strength Dyneema cables) to limit the weight distributed along the legs. Alphred is another sprawling-like quadruped developed by the RoMeLa laboratory [120] (Fig. 5y). It is made to allow interesting locomotion and manipulation capabilities, featuring a structure capable of to locking the foot position on the ground for a more stable contact [4]. Kirin is a quadruped robot using electric motors and prismatic legs with a structure allowing it to carry very heavy payloads [144] (Fig. 5ac). Also the robot Kurama [148], for running, presents a passive spring-loaded prismatic joint at lower legs' segments. Sharing a similar idea about proprioceptive actuation with MIT Mini Cheetah robot, several projects started to develop open-source platforms.
Developed under the Open Dynamic Robot Initiative (ODRI), the quadruped Solo was launched in 2016 by Max Planck Institute (MPI) Felix Grimminger and Ludovic Righetti, leader of the Dynamic Locomotion Research Group [98]. The whole robot just weights 2.2 kg and is made as a research platform to test new control algorithms. The actuators are extremely back-drivable and allow proprioceptive actuation, while aiming also at

2 Jerboa robot video
3 Titan XIII video
4 Alphred article, video, unofficial second version

keeping system complexity low. While Solo is a platform dedicated to cutting-edge control algorithm testing, simpler platforms are also developed for educational robotics. For instance, Stanford's Pupper robot is made to be an inexpensive and accessible resources [146] (Fig. 5aa). It can be easily produced, even if it is not made for additive manufacturing, and uses off-the-shelf servo motors. The goal of the platform is to target the field of educational robotics. Morti is the successor of Cheetah-Cub from Spröwitz's lab at MPI and was made with Artificial Intelligence (AI) applications in mind. It features elastic elements allowing compliance in the leg and it is driven by brush-less Direct Current (DC) motors. In [211] the parameters of Central Pattern Generator (CPG) were optimized to perform stable locomotion.
Several companies started the production of quadrupeds. For instance, Ghost Robotics, which introduced the parallel design small-scale robot Minitaur [27], is now proposing quadrupeds for security, military and inspection applications with the rugged Q-UGVs series [92] (Fig. 5z). These robots are capable of continuous operations for up to 3 hours with a payload of 10 kg in harsh environments. Targeting a different set of applications, the Chinese Unitree recently built an electric quadruped, Laikago Fig. 5t [5]. This quadruped, which now is discontinued, was developed for several different projects, like as the consumer-oriented Go series (Fig. 5w) [262]. The robots from this series, which are still on sale to this day are very popular in robotics research, thanks to their reasonable selling-point and perception hardware capabilities. Moreover, the Aliengo series packs features and certifications that make it amenable also to industrial applications. Some variations of these platforms feature hybrid locomotion modes (equipping wheels) or additional limbs to allow interaction with the external environment. Although quadruped robots were primarily used as research platforms, they start to see practical application use in several domains. They are now starting to be commercially available for automated task [271]. These platforms show great promise for security, patrolling, monitoring and inspection (e.g. in secluded sites such as off-shore platforms [14]).

1.3 *Applications*

Quadruped robots have a wide range of potential applications, their high versatility is due to:

- Sensing and Perception: these robots require advanced sensing capabilities to perceive and process the environment. They are equipped with cameras, depth sensors, and Inertia Measurement Unit (IMU) to gather visual, depth, and proprioceptive information. Algorithms are employed to interpret this sensory data stream and enable the robots to recognize objects, detect obstacles, and interact with their surroundings.
- Manipulation and Dexterity: Quadrupeds may also be designed to possess dexterous interaction capabilities. This involves usually additional robotic arms capable of grasping and manipulating objects with precision.

5 Laikago video

Quadrupeds have been successfully used in a lot of different domains, thanks to previously described capabilities. In the following list, we sum up some of the domains in which these robots have been used the most, and are driving some shifts.

- SUPPORT MILITARY OPERATIONS: As they require robust locomotion on a variety of terrains, which can be irregular. Examples of robots which are covering this application scenario are:
  - A prototype developed by Hutchinson, sponsored by the British War Department
  - The Iron Mule Train sponsored by the US Army
  - ASV funded by DARPA
  - Big Dog, funded by DARPA
  - Ghost robotics UGVs
- DE-MINING, robots are used for the detection of unexploded landmines:
  - The Titan VIII was one of the first robots used for this task
  - Comet-I is the first robot specifically designed for this purpose [225]
  - IAI-CSIC developed RIMHO-2 and DYLEMA as antipersonnel landmine detection and systems [65]
- REMOTE EXPLORATION (including space, submarine) Quadrupeds may be used for inspection application and remote data collection, possibly in far-away environments, where the human presence is not possible. In this field also completely unmanned operations may be included e. g. space rover explorations.
- SAFETY AND HAZARDOUS ENVIRONMENTS, INSPECTION of nuclear power facilities, these robots can help in handling radioactive materials, and safety in nuclear power plants, some legged robots that were built with this application in mind are [65], [260]:
  - ODEX by Odetics Inc.
  - RIMHO, a four-legged robot made in Spain to test the feasibility of the application (Jimenez et alia 1993)
  - Sherpa, by the French government Commissariat à l'énergie atomique et aux énergies alternatives (CEA) (Berns, 2005)
- AGRICULTURAL TASKS: These robots are designed to navigate in agricultural environments (without damaging the crops), assist with the management of the fields, soil monitoring, and perform tasks that would traditionally require manual labor. In particular, they may be interesting for precision agriculture (e. g. seeding, planting, applying herbicide)
- CONSTRUCTION: In particular for construction sites navigation, support of heavy loads, inspection, and other activities that require specialized equipment.
- ASSISTIVE ROBOTICS: They can also serve as companions or social robots, providing emotional support, entertainment, or educational assistance.
- RESEARCH: Lastly, thanks to a smaller scale and control complexity, increased robustness, stability and redundancy (if compared to their humanoid robots for instance), they are getting attention in the robotic researcher's community as great

(a) HyQ 2 Max [231] - pulling a Plane

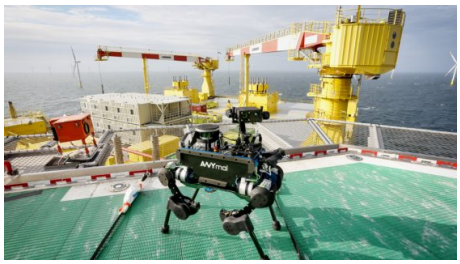

(b) Anymal on an off-shore platform

(c) Anymal on wheels

Figure 6: *Different quadruped applications and and trends*

research platforms for cutting-edge algorithm deployment and testing [15], [16], [210], [244], [245]. Another aspect that makes them even more appealing to the tinkerer researcher is the total freedom on the coming from some open-source open-hardware projects [98]. Some of the main sectors of research involve:

- Development of AI (sensors, control, intelligent behavior)
- Study of legged systems' motion
- Mimicking biological systems

1.4 *Limitations and current challenges to the application of legged robots*

Despite significant advancements, several challenges persist in the development of quadruped robots. Overcoming these issues requires interdisciplinary research that combines robotics, mechanical engineering, materials science and electronics. Possible limitations to the use of legged robots for an even broader set of applications are related, and not limited to:

- COMPLEXITY AND COST: Quadruped robots are rather complex systems. The locomotion control, sensor integration, and coordination required for quadrupedal movement involves many motors, sensors and precise algorithms and control systems. Designing and programming such complex systems is challenging, requiring expertise in robotics, control theory, and mechanical engineering. The cost involved in their development, production and maintenance is still rather high. Additionally, specialized components, such as high-torque density motors or custom-designed actuators, risk to further increase the overall cost of the robot. Recent custom designs inspired the industrialization of actuators or integrated solutions making components more accessible.

e.g. mini Cheetah-like actuators which are now readily available

- FRAGILITY AND FAULT TOLERANCE: Due to their complexity and numerous actuated joints which have to withstand repeated impacts, there is a challenge coming from the robust design of the platform. Ensuring fault tolerance in quadruped robots is also crucial for their reliable operation. When a fault or failure occurs in one of the robot's components, such as a motor or sensor, which can affect the robot's ability to walk or maintain stability. Developing fault detection and recovery mechanisms,

redundancy in critical components, and robust control strategies are essential to enhance the fault tolerance of quadruped robots.

- AUTONOMY: In the context of quadruped robots, achieving a higher level of autonomy can be challenging. The complex nature of quadrupedal locomotion, sensor integration, and environmental perception requires sophisticated algorithms and computational power. Developing robust perception systems, efficient motion planning algorithms, and decision-making capabilities are crucial for enhancing the autonomy of quadruped robots.
- OPERATIONAL CONSTRAINTS: Quadruped robots face operational limitations for instance in terms of speed. While they can achieve impressive walking and running gaits, their maximum speed is typically slower than that of wheeled robots. The mechanical constraints, such as the need for balance and stability, can limit the top speed of quadruped robots. Additionally, energy efficiency and power limitations may also influence their movements.
- ENERGY EFFICIENCY: Energy efficiency is a critical consideration for quadruped robots, as their mobility relies on limited resources (e. g. batteries). This can restrict their operational time and range. Efficient power management, lightweight design, and energy-saving control strategies are important factors to improve the energy efficiency of quadruped robots. Additionally, exploring alternative power saving methods, such as energy harvesting techniques or optimized energy storage solutions, can contribute to prolonged operation and increased autonomy.

Overcoming these limitations requires ongoing research and advancements in robotics technology, including improved component affordability, simplified control architectures, enhanced fault detection and recovery systems, and innovative mechanical designs. By addressing these limitations, quadruped robots can become more accessible, efficient, and versatile However, system designers have to face numerous challenges when creating new robotic platforms. Given the complexity of legged robots, it is not trivial to predict how to select the best platform to perform a given set of tasks. This is even exacerbated by the fact that design and control are usually considered separately, while in reality, they are deeply interconnected. Splitting them into different phases leads to inefficiencies and can potentially lead to sub-optimal results. To smartly conceive new platforms, the optimization of hardware for the task is necessary. Exploiting this concurrent-optimization approach motivates and guides this thesis.

2 CONCLUSION

In this chapter, the field of legged robotics has been introduced. We focused on the presentation of several legged robots through time and the possibilities that these systems allow. Moreover, some of the challenges of these platforms have been detailed. In the following chapters, we will tackle some of them, in particular, the problem of motion generation, system design and energy efficiency which are some of the limiting factors for legged robotics.

3

LEGGED SYSTEMS MODELING

In Short

In this chapter the modeling of legged robots is addressed by considering successively the following questions:

- Kinematic model, and possible kinematics
- Quadruped dynamic model
- Contact model
- Friction model

Contents

1 ROBOT ANATOMY AND KINEMATICS

Quadruped robots are built to have an animaloid form factor, with a head, torso, arms, and legs. They often incorporate joints and limbs that mimic biological anatomy to enable versatile and natural movements. The design aims to facilitate interactions and enhance the robot's ability to navigate and interact in human-centric environments. There are several possible configurations of the joints for the quadruped. They mainly depend upon the leg characteristics. The distinction may be of functional type, depending on the motion they enable, or kinematic, if the distinction is based on the link types, displacement and degrees of freedom. Concerning the allowed motions, we may find, as shown in Fig. 7, a distinction among two possible structures:

- Mammal-like structure (Fig. 7a), they feature joints which allow abduction, adduction, extension and flexion. This joint displacement closely resembles the one of the legs of animals or humans. The only difference is in the decoupling of motion in separate degrees of freedom (as it is difficult to actuate a completely spherical joint).

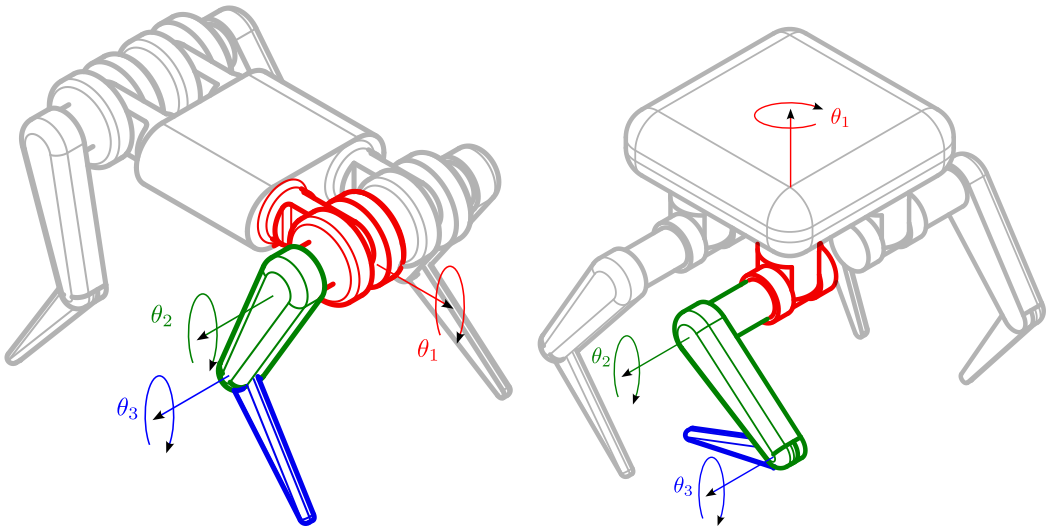

(a) Mammal-like (b) Sprawling-like

Figure 7: *Possible configurations of joints*

- Sprawling-like structure (Fig. 7b), the leg include successive revolute joints which allows its reorientation in the plane. The resulting motions that are closer to the motion of insects.
- Hybrid structure: mixing the two above with additional degrees of freedom

Concerning the leg structure itself, we may differentiate among different kinematic chain types (Fig. 8), both of them have found success in legged robotics applications:

- Serial structure (Fig. 8a): the kinematic graph spans a tree. Each joint can be reached in a single way from the root link.
- Parallel structure (Fig. 8b): the kinematic graphs presents some closed kinematic loops. This means that it is possible to reach some joints following multiple paths from the root-link. Some examples include the Cassie biped [276] [1] or ATRIAS [125].

An interesting discussion about the use of serial or parallel mechanisms to drive multiple joints in legged systems can be found in [2], The focus goes mostly on the concept of antagonism and power quality to perform the motion. These metrics can be optimized for different topologies. The main difference comes from the control and mechanical implementation point of view. Also in [1] several design considerations are provided in the case of passive legs.

Finally, a distinction can be made concerning the degrees of freedom in the leg. It is possible to have actuated joints or passive joints featuring compliant elements. Kinematically the use of revolute joints for the legs is the most common, it is nonetheless possible to encounter robots with prismatic joints. In Fig. 9 some of the most common

1 Cassie video

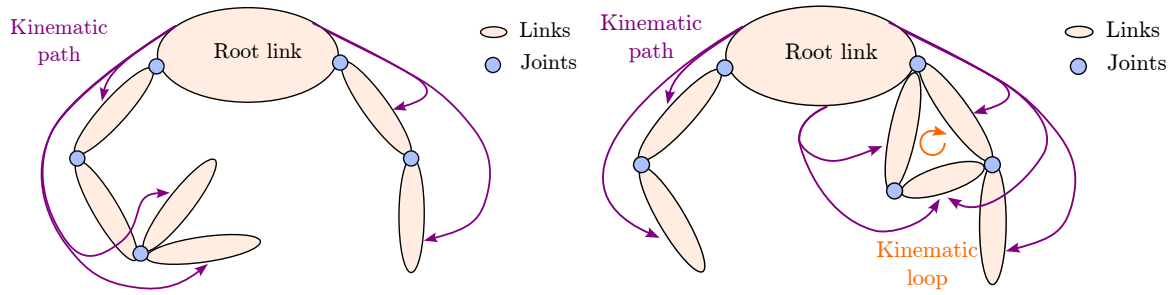

(a) Serial kinematic tree (b) Closed-loop kinematics

Figure 8: *Possible robot kinematic structure*

solutions to drive the joints are shown. Fig. 9a is a serial leg with revolute joints, by far one of the most common solutions. It allows easier control, especially if closed-loop is considered and proprioception. Fig. 9c presents a prismatic leg, which can be actuated or passive. This structure simplifies a lot of the control and was mainly used in the early prototypes of quadrupeds. From the mechanical point of view, it is challenging to manufacture linear actuated joints. Some of the solutions rely on hydraulic or pneumatic pistons. In some recent applications, prismatic joints are made by using ball screws. The latter solution allows at the same time pretty high stiffness, load-bearing capability and back-drivability of the motion. Some robots featuring this kind of mechanical solution are: Skippy [74] from IIT, using a ring-screw mechanism [83], [112] and PAL Robotics' Kangaroo [182]. Fig. 9d shows a leg design that was used in some small-scale quadrupeds. It presents an actuated joint that drives two linkages. This design allows force multiplication through the link leverages and generally leads to higher dynamic capabilities. The redundancy in the links makes the leg sturdier mechanically, but it also renders the control of the robot more complex. Fig. 9e shows another closed-loop kinematic structure. In this case, too the advantage is to have a sturdier redundant structure at the loss of easiness to control the leg. Atrias is a biped featuring this type of mechanism in the lower leg [125]. As you can see, generally the parallel designs allow to displace further away the driver of the joint, meaning that the motors can be put directly in the base without adding weight to the leg. This has several benefits and greatly reduces the leg's reflected inertia, thus enabling more dynamic motions. A downside of parallel planar mechanisms is the loss of manipulability in some spatial directions and a high degree of directionality in the applications of forces. A further development of these mechanisms, which aims at solving these problems, is the usage of parallel 3D mechanisms. This has several benefits such as the increase in manipulability and directionality allowing to precisely apply forces at any given direction, while resulting, at the same time, in a more robust structure. The downsides are however a significant reduction of the leg workspace and increased complexity in the control architecture. An example of this mechanism applied to quadrupeds is the GOAT leg prototype [140].

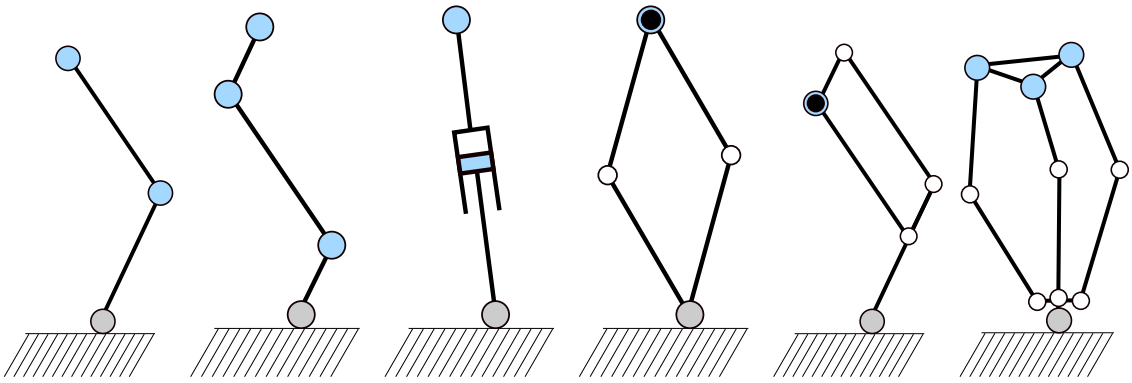

(a) Serial (b) Redundant Serial (c) Prismatic (d) Parallel 2D A (e) Parallel 2D B (f) Parallel 3D

Figure 9: *Possible leg topology and actuation*

2 ROBOTS IN MOTION: DYNAMIC MODEL

In the case of legged robots, the robot dynamic is rather challenging: the system is highly non-linear and underactuated, with many degrees of freedom (DoFs). [2] The system is generally controlled in torque at the joints, with the control vector $\mathbf{u} \in \mathbb{R}^{n_u}$. The adopted model generally includes the floating base pose (position and orientation of the root frame and the joint angles) in the configuration vector $\mathbf{q} \in \mathbb{R}^{n_q}$. As such, the robot configuration vector $\mathbf{q}$, as in (1), includes both the underacuated and the actuated DoF as shown in Fig. 10.

$$\mathbf{q} = [\underbrace{\underbrace{\underbrace{OO'}_{\text{Position}}, \underbrace{r}_{\text{Rotation}}}_{\text{Underactuated}}, \underbrace{\underbrace{q_1, q_2, ..., q_{n_u}}_{\text{joint angles}}}_{\text{Actuated}}}]^\top \in \mathbb{R}^{n_q} \tag{1}$$

One of the most commonly used model is exploiting quaternions to specify the base orientation without ambiguities due to singularities. In that case, the vector belongs to the special Euclidean group SE3, but this representation is redundant. A hidden constraint on the unitarity of the norm of the quaternion is eliminating one degree of freedom. This is intuitive as to specify the pose of the free-flyer, the minimal representation requires to determine the position and rotation angles. The velocity vector $\mathbf{v} \in \mathbb{R}^{n_v}$ specifies the rate of change of the position. However, in the case of redundant representation of the free-flyer, $n_v \neq n_q$ as the constraint is eliminating some DoF. If there are no constraints, then generally $n_v = n_q$. Through the position and velocity vectors, the complete state of the robot can be determined. We denote it with $\mathbf{x}$ and it is made by concatenating the position and velocity vectors (2).

$$\mathbf{x} = [\mathbf{q}, \mathbf{v}]^\top \in \mathbb{R}^{n_x = n_q + n_v} \tag{2}$$

2 Even if it is possible to consider some simplifications and symmetries.

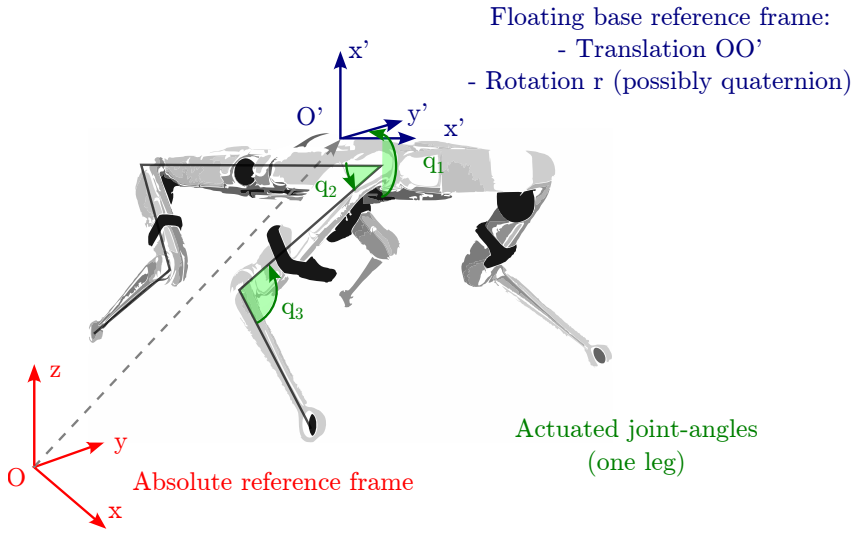

Figure 10: DOF of the robot and coordinate system of the floating base

UNCONSTRAINED DYNAMICS: For what concerns the robot's unconstrained dynamics, we can write down the equations of motion in the complete form or derive them from the Lagrangian formalism. The kinetic energy K is given by the summation of the kinetic energies of all the bodies n_b as follows:

$$\mathbf{K}(\mathbf{q}, \mathbf{v}) = \sum_{i=1}^{n_b} \frac{1}{2} \mathbf{v}^{\mathbf{T}} \mathbf{M} \mathbf{v} \tag{3}$$

where the joint inertia matrix can be obtained from the bodies mass matrix and Jacobians is given by (4):

$$\mathbf{M}(\mathbf{q}) = \sum_{i=1}^{n_b} \mathbf{J}_i^T(\mathbf{q}) \mathbf{M}_i \mathbf{J}_i(\mathbf{q}) \tag{4}$$

The total potential energy of the system can be written as the sum of the gravitational potential for all the bodies of the system.

$$\mathbf{U}(\mathbf{q}) = \sum_{i=1}^{n_b} g m_i \Delta z_i(\mathbf{q}) \tag{5}$$

According to the Lagrange equation, the dynamics of the system can be computed in matrix form:

$$\frac{d}{dt} \frac{\partial(\mathbf{K}(\mathbf{q}, \mathbf{v}) - \mathbf{U}(\mathbf{q}))}{\partial \mathbf{v}} - \frac{\partial(\mathbf{K}(\mathbf{q}, \mathbf{v}) - \mathbf{U}(\mathbf{q}))}{\partial \mathbf{q}} = \mathbf{\Omega} \tag{6}$$

where $\mathbf{\Omega}$ is the vector of the generalized forces acting on the system. For conservative autonomous systems $\mathbf{\Omega} = 0$, but, in the case of legged robots, among the generalized forces we include the joint torque control vector $\mathbf{u} \in \mathbb{R}^{n_u}$ and external forces.

$$\mathbf{M}(\mathbf{q})\dot{\mathbf{v}} + \underbrace{\left(\dot{\mathbf{M}}(\mathbf{q}) - \frac{1}{2}\mathbf{v}^\top \frac{\partial \mathbf{M}}{\partial \mathbf{q}}\right)\mathbf{v}}_{\mathbf{C}(\mathbf{q},\mathbf{v})} + \underbrace{\frac{\partial \mathbf{U}(\mathbf{q})}{\partial \mathbf{q}}}_{\mathbf{g}(\mathbf{q})} = \boldsymbol{\Omega} \tag{7}$$

Which can be written in compact form as follows:

$$\mathbf{M}(\mathbf{q})\dot{\mathbf{v}} + \mathbf{h}(\mathbf{q},\mathbf{v}) = \boldsymbol{\Omega} \tag{8}$$

Where $\mathbf{M}$ is the joint-space inertia matrix and $\mathbf{h}(\mathbf{q},\mathbf{v})$ depends on the nonlinear effects of gravity $\mathbf{g}(\mathbf{q})$ and centrifugal and Coriolis forces $\mathbf{C}(\mathbf{q},\mathbf{v})$, as expressed by (9).

$$\mathbf{h}(\mathbf{q},\mathbf{v}) = \mathbf{g}(\mathbf{q}) + \mathbf{C}(\mathbf{q},\mathbf{v}) \tag{9}$$

Based on the free dynamic (8), from the joint acceleration $\dot{\mathbf{v}}$ (also commonly denoted with $\mathbf{a}$), it is possible to determine the time evolution of the robot state $\mathbf{x}$, under the influence of $\boldsymbol{\Omega}$.

CONSTRAINED DYNAMICS:

In the constrained case, the generalized forces $\boldsymbol{\Omega}$ can be found by considering the control action $\mathbf{u}$ and the forces due to constraints.

$$\boldsymbol{\Omega} = \mathbf{u} + \mathbf{F} \tag{10}$$

The virtual work principle can be applied to find the value contact forces applied on the outside. The legged system has a dynamic which is constrained by the contact point positions $\mathbf{p_c}(\mathbf{q})$, which depend on the configuration of the robot. The externally applied contact reaction forces will affect the dynamics, through the matrix of the contact Jacobians $\mathbf{J_c} = \dfrac{\partial \mathbf{p_c}(\mathbf{q})}{\partial \mathbf{q}}$.

$$\mathbf{f}^\top \delta \mathbf{p_c}(\mathbf{q}) = \mathbf{f}^\top \mathbf{J_c} \delta \mathbf{q} = \mathbf{F}^\top \delta \mathbf{q} \tag{11}$$

Since the relationship must hold for any virtual displacement $\delta\mathbf{q}$

$$\mathbf{F} = \mathbf{J_c}^\top \mathbf{f} \tag{12}$$

The constraint at the contact point and the dynamics can be combined in a single compact formulation:

$$\begin{bmatrix} \mathbf{M}(\mathbf{q}) & \mathbf{J}_c^\top \\ \mathbf{J}_c & \mathbf{0} \end{bmatrix} \begin{bmatrix} \dot{\mathbf{v}} \\ -f \end{bmatrix} = \begin{bmatrix} \mathbf{u} - \mathbf{h}(\mathbf{q},\mathbf{v}) \\ -\mathbf{J}_c\mathbf{v} \end{bmatrix} \tag{13}$$

This leads to the following equation:

$$\mathbf{M}(\mathbf{q})\dot{\mathbf{v}} + \mathbf{h}(\mathbf{q},\mathbf{v}) = \mathbf{u} + \mathbf{J}_c^\top f \tag{14}$$

From (13), the robot state $\mathbf{x}$ evolves under the influence of the joint torques and contact forces as described by the constrained rigid body dynamics, a more detailed derivation can be found in [82]. The first row of equations of the system is the free robot dynamics, while the second set of equation represents the nonslip condition at the contact points, enforcing that the accelerations are null. Another interpretation can be also found: as the robot dynamic is constrained by the rigid contacts, there are constraints on their velocities and accelerations. This means that the contact points $\mathbf{p_c}$ do not move during the contact phase, and as a consequence their velocities are null:

$$\frac{\partial \mathbf{p_c}(\mathbf{q})}{\partial t} = 0 = \frac{\partial \mathbf{p_c}(\mathbf{q})}{\partial \mathbf{q}}\mathbf{v} = \mathbf{J_c}\mathbf{v} \tag{15}$$

The same also holds at the acceleration level:

$$\frac{\partial^2 \mathbf{p_c}(\mathbf{q})}{\partial t^2} = 0 = \dot{\mathbf{J}}_\mathbf{c}\mathbf{v} + \mathbf{J_c}\dot{\mathbf{v}} \tag{16}$$

A common way to take into account rigid contacts in the dynamics is by solving a set of Differential-Algebraic system of Equations (DAE) reduced to the first order. For mechanical systems, with constraints in position, this usually resolves to a set of ordinary differential equations (ODEs) including some stabilization terms to correct possible integration drifts (Baumgarte stabilization terms). Depending on the scope of the analysis, from the relationship in (13), different algorithms can be used for solving the dynamics of the system. The direct dynamics computation provides accelerations given $\mathbf{u}, \mathbf{q}, \mathbf{v}$. The inverse dynamics is the process that allows us to get the torques from the information related to the system and $\mathbf{q}, \mathbf{v}, \dot{\mathbf{v}}$. Legged systems are not fully actuated, so the inverse dynamics computation is not straightforward. The pseudo-inverse can be used, but the problem is in general under-determined. In the literature, some of the most used algorithms for solving the dynamics of these systems, include:

Thanks to their efficient implementation [82]

- Recursive Newton-Euler Algorithm (RNEA) for the inverse dynamics
- Articulated-Body Algorithm (ABA) for forward dynamics
- Composite Rigid-Body Algorithm (CRBA) solves the forward dynamics and recomputes the joint inertia matrix

3 FRICTION CONES

A legged robot will move on a surface thanks to the effect of the reaction forces applied to it. However, in the real world, some conditions arise on their value. To apply forces on the surface without the sliding of the contact point, these conditions on the forces need to be imposed. We consider the normal, tangent and bi-normal direction at the surface $\mathbf{n}, \mathbf{t}, \mathbf{b}$ respectively. Non-sliding of the contact is achieved under the static friction hypothesis: the contact point is not sliding if the resultant of all the forces applied at the contact point along the tangential direction to the surface is not greater than the

Coulomb friction in that tangential direction. This imposes a condition in the local frame of contact as shown in Fig. 11:

$$\begin{cases} F_n = \mathbf{f} \cdot \mathbf{n} > 0 & \text{Normal reaction with the ground} \\ |\mathbf{f} - F_n \mathbf{n}| \leq F_t & \text{No sliding } (F_t = \mu F_n \text{ maximum static friction}) \end{cases} \tag{17}$$

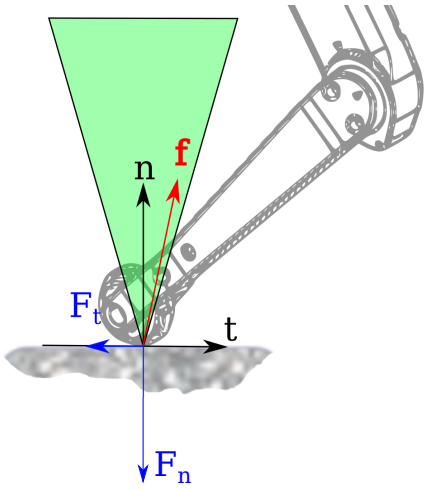

Figure 11: Friction cones in the local contact frame

where $\mathbf{f}$ is the contact force and μ is the friction coefficient. Visually this condition can be seen in Fig. 11: the contact is stable if the contact force belongs to the volume delimited by the cone.

LINEARIZED FRICTION CONES

To use the previous relationships in practical implementation (e. g. in CROCODDYL), which often cannot deal with the exact constraint, an approximation is usually made. Introducing an approximation, a linearized domain, where the contact forces can lie without sliding, can be considered instead. Geometrically this corresponds to a smaller region of space, usually a pyramid, as shown in Fig. 12.

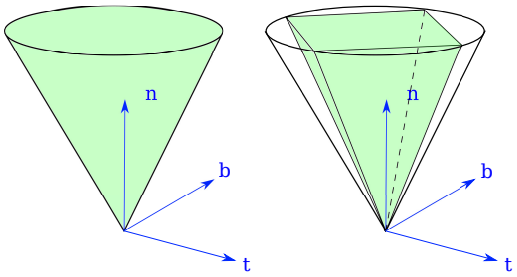

Figure 12: Linearized friction cone region

By decomposing the contact force vector along the axes of the local reference frame, the conditions become, for the 4-sided pyramid in Fig. 12:

$$\begin{cases} F_n = \mathbf{f} \cdot \mathbf{n} > 0 & \text{Normal reaction with the ground} \\ |\mathbf{f} \cdot \mathbf{t}| \leq F_t & \text{No sliding } (F_t = \mu F_n \text{ maximum static friction}) \\ |\mathbf{f} \cdot \mathbf{b}| \leq F_t & \text{"} \end{cases} \tag{18}$$

HIGHER ORDER APPROXIMATIONS This approach can be extended to a higher number of sides of the cone linearization, leading to a set of linear inequalities. For instance, on flat ground, letting $n \in \mathbb{N}$ to be the even number of sides and $f = [f_x, f_y, f_z]^\top$ the force decomposed in the local contact frame, (18) a reworking of (18) leads to the following set of $n+1$ equations:

$$\begin{bmatrix} 0 & 0 & 1 \\ \dots & & \\ -\cos(\alpha_k) & -\sin(\alpha_k) & \mu \\ \cos(\alpha_k) & \sin(\alpha_k) & \mu \\ \dots & & \end{bmatrix} \begin{bmatrix} f_x \\ f_y \\ f_z \end{bmatrix} \geq 0 \tag{19}$$

Where $\alpha_k = \frac{2k\pi}{n}$ and $k \in [0, ..., n-1]$ is the number of directions. Each of the inequalities corresponds to the projection of the tangential force in a given direction. By construction the set of inequalities are independent (as $\mu > 0$) and for $n \to \infty$ they recover exactly the friction cone constraints. According to the degree of conservatism, inner and outer approximations of the friction cone is possible. The friction coefficient can be modified to make the linearized friction cone an inward approximation. In this case (19) still holds, with a reduced friction coefficient $\tilde{\mu} = \cos(\frac{\pi}{n})\mu$.

SIMULATORS FOR ROBOTIC SYSTEMS

The constraints imposed in the system are both in the multi-body relationships among the frames and in the external contact points constraints, which expresses the relation of non-penetration among two different bodies. Such a relationship is expressed as an inequality constraint $\Phi_c(q) \geq 0$. To deal with these constraints there are two possible solutions. One is to solve a nonlinear complementarity problem (NCP), and the other one is to cast it to a linear complementarity problem (LCP) or to use an approximation, via quadratic programming. The advantages of the second formulation, which represents the application of Gauss' least constraint principle to the problem, is that the problem has a unique solution if it is defined, and has a lower computational expense. There are many open-source research robotic libraries to perform such computations, especially for the control of the robot, for instance `pinocchio`, developed at LAAS [42], Kinematics and Dynamics Library (KDL) [38] and Rigid Body Dynamics Library (RBDL) [84], DRAKE [256] are worth mentioning. In the field, apart from the libraries, that can be used more for the deployment of control algorithms, and for optimization, simulation software can be used to validate the performance and safety of the developed control algorithms *in silico*. Such simulators are based on physical engines and allow

forward dynamic simulation in potentially real-time environments. Some of the most used simulators there are: Bullet [58], Dynamic Animation and Robotic Toolkit (DART) [162], Open Dynamics Engine (ODE) [246], MuJoCo [258] and SimBody [236]. In recent years some additional flavors of robotics simulators got attention. For instance, simulators with GPU parallelization became commonly available allowing great speed-up gains. This kind of simulator is especially used for reinforcement learning [133], [163]. Another last class is made up of differentiable simulators, which allow to obtain derivatives through the implemented algorithms (often involving contact and impulses) [90], [123], [224]. The applicability of this latter class is quite large, ranging from optimal control to policy search [253] and identification [157].

4 CONCLUSION

In this chapter, some of the key details about the kinematic modeling and the dynamics of legged systems have been described. Such formalism is necessary to mathematically express the relationships which are used for the problems involving these systems, in particular numerical optimization. Finally, some of the tools, that we use in practice, both for dynamic modeling and for simulation, have been introduced.

Part III

SOME HARDWARE CONSIDERATIONS

CO-DESIGN is deeply connected to the hardware. In this part of the manuscript a discussion upon the robot technology, trends in actuator engineering and implementation is given. Successively, the question of modeling the actuators is considered and the implementation of the open-hardware actuators, on which part of the work is based on, is presented.

4

POWERING ROBOTICS: ACTUATOR MODELS

In Short

In this chapter, the question of the actuator model for robotics systems is addressed. The actuator model can vary depending on the type of actuator being considered, each actuator type having its specific characteristics and dynamics. A mathematical description of the actuator is required to analyze and design controls for real systems. By considering such models, engineers and researchers can simulate and analyze the system's behavior, stability, and performance. In this work, we mainly focus on electric actuators, so we present the non-linearities affecting these devices and their energy flows.

Contents

1 IDEAL MOTOR MODEL

The majority of actuated systems are composed of an active element that can be selected during the design phase and whose task is to provide mechanical power to a passive load or resist an external force, namely a motor. In robotics, the motor is needed to provide interaction power with the environment. For a legged robot, it is necessary to consider different models of the motors to properly choose the actuation system best

e.g. it's reasonable to think that a bigger robot will also need a more powerful actuation system and this usually means increased inertia and a slower response

suited for the application. The fundamental quantities to consider for motors are pro-

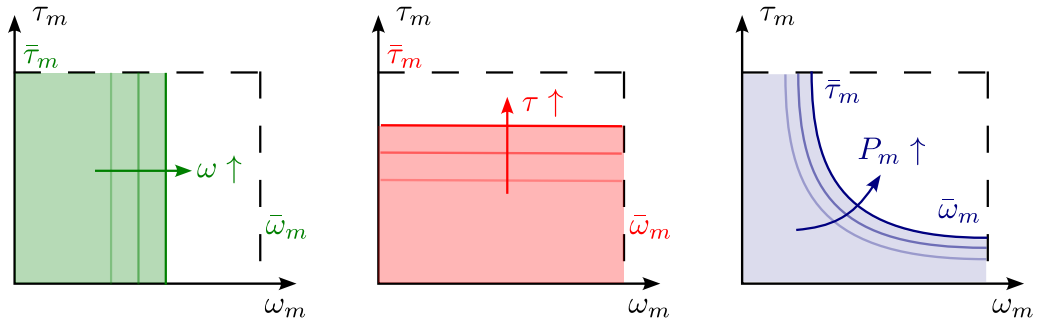

(a) Velocity source (b) Torque source (c) Power source

Figure 13: *Motor characteristic curves* in the idealized cases of ideal torque, speed and power source

duced torques and angular velocities. Every motor has its characteristic curve, namely a curve that correlates the output torque τ_m that can be provided by the motor to the load at a certain angular velocity ω_m. As shown in Fig. 13, there are some high-level idealizations on the motor selection. We can describe the motor outputs in terms of produced torque τ_m and the angular velocity ω_m. The regions of possible output combinations can be plotted in the same graph producing motors characteristic curves. In Fig 13 these operating areas are shown together with the maximum values, denoted with upper bars. According to their characteristic, motors can be simplified as ideals sources of the following quantities:

- Velocity (Fig. 13a): The characteristic curve is a vertical line, the motor is turning at a constant speed, no matter the load. Usually, this assumption is used for the DC motors with speed control. Moreover, it is a good approximation for hydraulic motors that allow very high torques and quick, impulsive dynamics.
- Torque (Fig. 13b): This characteristic curve is a horizontal line, the motor will provide the same torque at a very wide range of speeds. The assumption is correct for a DC motor that is controlled in current. The actuation is closer to the actual physical model of the system, the interaction between the motor and the transmission needs to be modelled.
- Power (Fig. 13b): The characteristic curve is an equilateral hyperbola, the product of the torque and speed is constant. The assumption is correct for DC excited in series.

2 MOTOR CLASSES

It is possible to use different sources to power a motor. The most commonly used technologies are of three types:

- ELECTRIC MOTORS: They produce motion thanks to the interaction force produced between a current and a magnetic field. They generally allow a rather compact system as the electric power is directly convertible into mechanical power (without the need for additional power generators or buffer elements, e. g. tanks for pneumatic and hydraulic actuators). This allows also easier control of the system, which can potentially reach a very high bandwidth. They are generally performing well for fast applications, but may suffer from overheating due to Joule losses when applying static interaction forces for extended periods of time. For this reason, cooling may be needed in the case of heavy-duty applications. Overall they are hence cheaper, less bulky and require less maintenance. Inside this class of motors, there are many other divisions, depending upon their technology. The DC motors are those motors that can be powered by a DC source. All motors need a variable magnet field to spin and such motors need to constantly change the coils in which the current flows. This commutation can either be mechanical (via brushes) or electronic (hence brush-less). For the applications in legged robotics, the majority of motors are Permanent Magnet Synchronous Motors (PMSM), which are also commonly called Brushless Direct Current (BLDC).
- PNEUMATIC POWER SOURCES: They convert the energy stored in a high pressure tank to mechanical energy. They need a compressor as a power source and utilize the aperture of distribution valves as the control signal. They can reach pretty high-speed values in the release phase and apply constant interaction forces. They are generally lightweight and allow compliant interactions. This makes them amenable in the case of gippers and some artificial muscles, but they show limitations in terms of peak values and back-drivability, efficiency, bandwidth and the capability of precise output. They are also utilized in the soft robotics domain, where simple actuators can also be 3D-printed via Additive Manufacturing (AM).
- HYDRAULIC POWER SOURCES: They produce interaction power by pressurizing an incompressible fluid (usually mineral oil). Due to this, they are also more complex, as to generate pressure pumps and additional motors need to be added to the platforms. This adds to the weight (large overhead infrastructure) and requires generally miniaturized components (such as custom-made pumps, Internal Combustion Engine (ICE) or electrical actuators), leading to higher costs. Efficiency moreover is reduced by the viscous losses and the distribution, which requires a manifold and several valves and tubes. The presence of several moving elements requires periodic maintenance, is rather noisy and can potentially catastrophically fail, producing oil leaks. Nonetheless, these actuators can produce remarkably high interaction forces with the environment, but are more complex to manufacture and more costly. Remarkably they can exert force in highly demanding conditions (e. g. static lifting or pulling), without big losses or the risk of overheating (which is a major cause of failure of electric motors in this scenario). Several high-performance and rather successful hydraulic robots have been developed in the past, in particular from Boston Dynamics Inc. (the high performance humanoid Atlas [31] and the quadruped Big Dog [196]) and from IIT (the quadruped series

HyQ [231], [232]). These robots shine in the area of high payload and impulsive force interaction generation, but they are less suited for applications in which compliant behavior is needed. Compliance can be mechanically introduced by modifying the distribution circuit (e. g. inserting tunable valves and bypasses) with a very high engineering cost. Moreover, to partially cope with the energy efficiency problem, some hybrid electro-hydraulic actuators are currently being developed to locally pressurize the fluid and avoid distribution losses. This is however adding to the complexity and distributed inertia of the structure. A passive mechanism of mechanical energy storage can be achieved by adding to the circuit reservoirs to pressurize fluid for later release.

Other actuation technologies exist, for instance, just to mention some, based on Shape Memory Alloy (SMA), contractile polymers, piezo-electric materials or magnetostriction [128]. However they have not seen so far major applications in legged robotics. Each of the major technologies has particular characteristics which make it useful for some specific applications. The main go-for choices nowadays for legged-robots are electrical and hydraulic-driven systems. The advantage of electric ones is precise control and generally lower weight and higher efficiency. The motors are acting as a power source. If a reduction is introduced, then additional friction, inertia are added to the system and they need to be compensated by the controller. Models covering hydraulic actuators can be found in [60], [229], while for a pneumatic actuator model, one can refer to [179].

3 TRANSMISSION SYSTEMS

The motion generated by the motor often cannot be exploited directly to actuate the joint for different reasons:

- The joint to actuate is far from the motor axis or the output axis of motion needs to be reoriented.
- The motor generally outputs high speed and low torque, so to make use of them we need to reduce the angular speed and increase torque for common applications.
- The motion needs to be converted (e. g. from linear to angular)

The mechanical elements make these different functions possible are the actuators' transmissions. There exist multiple different types. There are cable-driven systems (e. g. Bowden cables), systems with gears (compact planetary or epicycloid gears, often integrated with the motors), flexible splines (strain wave gears), or, in case the motion needs to be transmitted to another axis, chains or belt transmissions (timing belts for precise motion control), clutches. Finally, also direct coupling is possible when the actuator is direct-drive. Moreover, in the case of hydraulic pistons (a similar force multiplication effect can be obtained by exploiting the piston and rod geometry).

In Fig. 14 a generic transmission is shown. The motor (red) is connected to the load (blue) via a transmission element (green). The transmission enforces a constraint be-

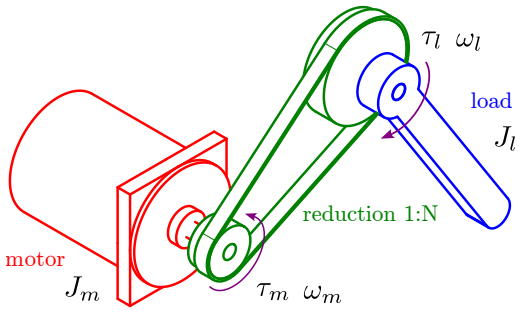

Figure 14: *Generic transmission*, in the figure belt-driven

tween the motor and the load. Where n indicates the ratio between the load and motor angular speed (respectively ω_l and ω_m):

$$n = \frac{\omega_m}{\omega_l} \tag{20}$$

Usually, as the motor speed needs to be reduced to be coupled with the load, $n \geq 1$. If we suppose a perfect transmission (without friction losses), then the mechanical power from the motor to the load is conserved. Hence we find, that the torque is increased by a factor n.

$$\begin{aligned} &\omega_m \tau_m - \omega_l \tau_l = 0 \\ &\omega_m \tau_m = \omega_l \tau_l \\ &\tau_l = n \tau_m \end{aligned} \tag{21}$$

If friction is present, from a dynamics point of view, the joint dynamics equation from the motor shaft is modified by adding a friction term τ_f

$$\tau - \frac{\tau_l}{n} = \mathcal{I}\dot{\omega}_m + \tau_f \tag{22}$$

Notation-wise, τ_m indicates the value of the interaction torque exchanged with the environment, while with τ indicates the value of the torque including friction $\tau = \tau_m + \tau_f$ at the motor side. $\mathcal{I}$ is the equivalent inertia at the motor shaft, which includes the load inertia $\mathcal{I}_l$:

$$\mathcal{I} = \mathcal{I}_m + \frac{\mathcal{I}_l}{n^2} \tag{23}$$

However other friction components exist in the transmission, e. g. dry-friction. The model of these components depends on the transmission type Fig. 15 and generally Coulomb friction becomes more and more important in the case of high-geared systems. The parameters of friction are also depending on lubrication, load and velocity as reported in [87]. Classical transmission introduces also further complexity in the model, especially for the control-related aspect. While they multiply the produced torque, they

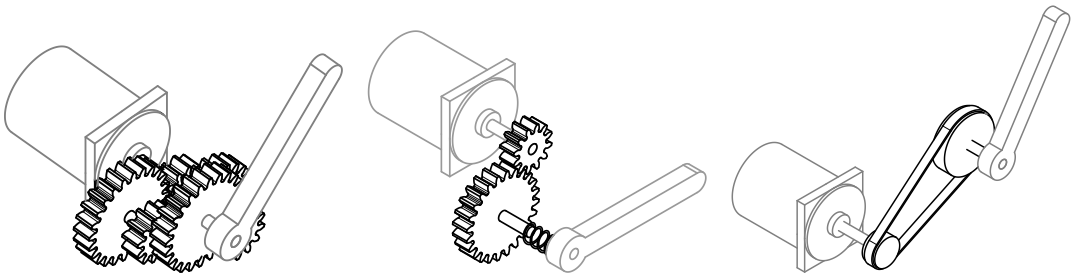

(a) Gear (b) Series elastic (c) Belt (or timing belt)

Figure 15: *Transmission types*

may also introduce backslash and friction among other non-linearities. These undesirable components contribute to increasing the mechanical impedance of the system.

4 JOINT FRICTION MODEL

The two dissipative mechanisms that are commonly introduced are in form of Coulomb and viscous damping at the transmission level. According to this simple model, requiring two parameters (Coulomb friction τ_μ and damping b), the friction torque at the motor axis is then:

The price of this friction model is to be blind to other non-linear effects, such as stick-slip conditions and Stribeck effect. For our application, this is generally acceptable.

$$\boldsymbol{\tau}_f = \begin{cases} \text{if } \omega_m = 0\text{: } \max\left(\tau_m, \tau_\mu\right) \\ \text{if } \omega_m \neq 0\text{: } \tau_\mu \text{sign}(\omega_m) + b\omega_m \approx \tau_\mu \tanh(\gamma\omega_m) + b\omega_m \end{cases} \tag{24}$$

where ω_m $\left[\frac{\text{rad}}{\text{s}}\right]$ is the motor angular speed, τ_μ [Nm] is the Coulomb friction parameter, b [Nms] is the viscous friction parameter. The first line in (24) corresponds to a "dry" friction condition, when there is no motion (stick condition) and this regime holds as long as $\tau_m < \tau_\mu$. When the motor torque wins the Coulomb friction value, the load motor can accelerate (slip condition). If a joint motion is produced, then the regime is called of "kinetic" friction and the second line of (24) is used. To approximate the non-differentiable sign function we use the hyperbolic tangent with $\gamma \gg 1$. Composing friction from different sources can be done and the overall equivalent damping factor at the load can be found as:

$$b = b_m + \frac{b_l}{n^2} \tag{25}$$

Where b_m is the damping at the motor side and b_l is the damping at the load side. Friction in robot actuation imposes additional load on the joints. The motor needs to compensate for this external perturbation. This will make the motors require more power with respect to a frictionless case.

To account for the effects of friction, it is possible either to use some online estimation of the parameters or to go for a model-based approach or online/offline identifications. The advantage of the online estimation is a better approximation of the real system

evolution, but it may be unfeasible or overcomplicated from the point of view of the instrumentation involved.

ANALYTIC JOINT FRICTION MODELS FOR SOME REVOLUTE JOINTS Friction in revolute joints, can be modelled with some knowledge on the moving parts. This requires generally a-priori information on the transmission and its geometry. For instance torque and a Herzian model of contact between two cylindrical axisymmetric surfaces (for journal bearings) or between a ball and the inner surface of a cylinder (bearings). In the ideal point-wise contact case between surfaces, without deformations the following equilibrium holds, referring to Fig. 16:

$$\begin{cases} -F_n \sin\theta + \mu F_n \cos\theta = 0 \\ F_n \cos\theta + \mu F_n \sin\theta = F \\ \mu F_n R = Fl \end{cases} \tag{26}$$

(26) can be resolved to obtain:

$$\begin{cases} \tan\theta = \mu \\ F_n = \dfrac{F}{1+\mu^2} \\ \dfrac{l}{R} = \dfrac{\mu}{\sqrt{1+\mu^2}} \end{cases} \tag{27}$$

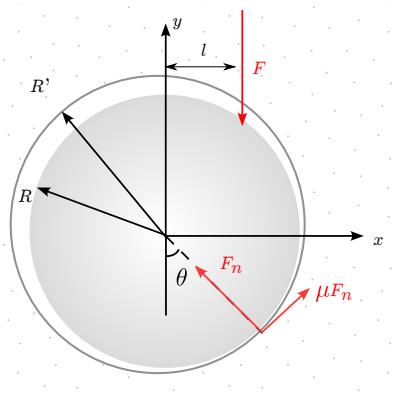

Figure 16: Friction in the bearing supposing the presence of clearance

$$\tau_\mu = \frac{F_n R \mu}{\sqrt{1+\mu^2}} \qquad \text{for } \mu \approx 0 \qquad \tau_\mu = F_n R \mu \tag{28}$$

In the case of Hertzian contact among surfaces the friction force will depend on a pressure distribution on a localized surface area. In particular, according to Faraz and Pay [80], the friction model can be corrected with a geometric and dimensional parameter C_α that includes the effects of Hertzian contact and body deformations. C_α depends on the Young modulus of the materials E, the Poisson ratio ν and the geometry R, R'. Then, the friction torque will be depending on the external load, geometry, and

the contact angle θ of the support. This angle is a function of the material and the geometry of the revolute joint, so it varies case by case. There are several known cases:

- SOCKET BALL: $C_\alpha = \frac{3}{4}\left(\frac{\cos(\alpha)}{\sin^2(\alpha)} - \alpha\frac{\cos(2\alpha)}{\sin^3(\alpha)}\right)$
- JOURNAL BEARING: $C_\alpha = f(\alpha)$ becomes a polynomial approximation of an elliptic integral
- ROLLING-ELEMENT BEARINGS: Given their complexity, an analytical relation is difficult to find, but empirical correlations are found in some manufacturers' catalogs. According to these conservative correlations, friction torque is depending on: $\tau_f = \frac{1}{2}\mu P d_m$ where $P = F_r + YF_a$ with:
  - Y, a coefficient depending on the bearing type
  - F_r, F_a the total radial and axial loads respectively, and P is the equivalent dynamic bearing load,
  - d_m the mean diameter of the bearing.

for instance SKF catalogs and guidelines

TAKE HOME MESSAGE: Overall, friction scales with the type of joint, the external load and geometry (e. g. the diameter of the bearing), but also, with the characteristics of the load. So, from an engineering point of view, it is possible to calculate the friction in an actuation system by analyzing its working regime and loads. However, this is not a practical approach, even if it is possible in some cases, often is not easy to predict a variable load on the transmission elements. For some types of actuators, it is difficult to come out with analytical laws, so identification is needed. A method to identify the friction parameters for a specific class of actuators is explained in chapter 6. Then in co-design this information is used. Based on these identified values an extrapolation is proposed, for a specific type of transmission, to describe how the friction is modified by changes in the actuator choice (notably the motor selection and the gear ratio). This allows us to describe how the properties scale with the system.

5 PERMANENT MAGNETS SYNCHRONOUS MOTORS

Here we consider an important subclass of electric motors, the PMSM-BLDC motors, due to their large presence on the market, the easiness to use and their importance in legged robotics. The case studies that will be presented will use these motors. Here a motor model is produced to address:

- PERFORMANCE (limits of the motor)
- EFFICIENCY

Such model holds for DC motors (with mechanical commutation) or for PMSM-BLDC controlled via Field-Oriented Control (FOC).

Preliminary, some variables related to the motor peak performance are defined:

- STALL TORQUE τ_0: the torque the motor can withstand in static conditions (when the angular velocity is zero $\omega_m \approx 0$)

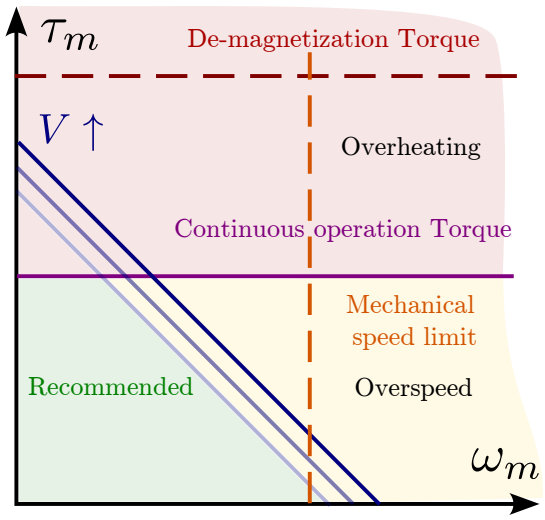

Figure 17: BLDC *motor operating regime*

- MAXIMUM ALLOWED ANGULAR SPEED ω_0: Value of the angular speed that can be achieved when no load is attached, (when $\tau_m \approx 0$). This value, due to friction, is less than $\frac{V_t}{K_e}$
- MAXIMUM POWER: According to some datasheets, the maximum mechanical power P_m can be found when $\tau_m = \frac{\tau_0}{2}$ and $\omega_m = \frac{\omega_0}{2}$

5.1 *Motor constants*

An electric motor is powered by a voltage V_t and a current i. In the case of BLDC motors, it is common practice to use linear relations between the electrical and mechanical variables, using the following constants:

- K_v the SPEED CONSTANT, it is defined as the ratio between the angular speed of the rotor and the voltage at the terminals of the motor $K_v = \frac{\omega_0}{V_m} \left[\frac{rad}{sV}\right]$. Can be measured by making the motor spin without load and measuring the back EMF at the terminals.
- K_t the TORQUE CONSTANT, it is defined as the ratio between the torque output by the motor and the current flowing into its coils $K_t = \frac{\tau_m}{i} \left[\frac{Nm}{A}\right]$
- K_e the ELECTRICAL CONSTANT, it represents the ratio between the voltage drop at the motor terminals during the motion, and the angular speed of the motor $K_e = \frac{V_m}{\omega_m} \left[\frac{Vs}{rad}\right]$

The values found in the catalogs usually differ significantly, depending on the convention used for the units (usually in rpm). Moreover, K_e is simply the International system (IS) unit inverse of the speed constant. Regulating the source voltage high enough

with respect to the nominal voltage, the torque is no more dependent on the angular velocity Fig. 17. These constants are sufficient to specify all the characteristic of the motors; however, another useful design constant is commonly used: the motor constant, K_m. It is defined as the ratio of the torque output and the power losses of the motor

$$K_m = \frac{\tau_m}{\sqrt{P_t}} = \frac{K_t i}{\sqrt{i^2 R}} = \frac{K_t}{\sqrt{R}} \left[\frac{Nm}{\sqrt{W}}\right] \tag{29}$$

K_m can be used for selecting the size of a motor for a specific application, while K_v can be chosen to determine the motor design materials, in particular for the windings. Since the torque of the DC motor is related to the current ($\tau_m = K_t i$) and the losses are connected to the Joule effect dissipations $P_t = i^2 R$, this quantity represents ideally how much torque output the motor can deliver over the unit of power lost. Additionally the slope that can be seen from the blue curves of Fig. 17, which establishes a relationship between the angular speed and the torque, is commonly called *speed-torque gradient*.

5.2 *Electromechanical equivalence*

We can consider the back electromotive force generated by the motor at its terminals and show the connection with the mechanical torque that has to be provided by the motor.

$$V_m = K_e \omega_m, \tag{30}$$

where we recall that the electrical power can be seen as a drop of voltage at the motor terminals. The torque that the motor produces is proportional to the current:

$$\tau_m = K_t i \tag{31}$$

In an idealized case, the electrical power provided to the motor will exactly equal the mechanical work performed by the motor.

$$\underbrace{V_m i}_{P_{el}\text{, Electrical power}} = K_e \omega_m i = K_t \omega_m i = \underbrace{\tau_m \omega_m}_{P_m\text{, Mechanical power}} \tag{32}$$

This means that, in IS units, the torque constant and the electrical constant have the same value, even though they represent different phenomena.

$$K_e = K_t = \frac{60}{2\pi K_v} \tag{33}$$

6 MOTOR GEOMETRY AND RELATIONSHIP WITH PERFORMANCE

A detailed discussion on how the geometrical parameters of the motor are impacting its property can be found in [235]. Using custom actuators can provide more torque density. The motor torque is proportional to the square of the radius gap [126]. In [235] it has

been proven from experiments that torque density is proportional to the gap radius r_g of the electromagnetic (EM) motor. This value is the radius between the motor axis to the center of the gap between the permanent magnets and the stator as shown in Fig. 18. Rotor inertia also goes as $m_m r_g^2 \sim r_g^3$ so there is a trade-off between the two. From a practical point of view also increasing the rotor length is possible, but this has a lower impact on torque density and is negatively impacting cooling.

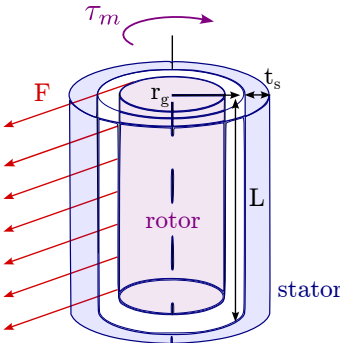

Figure 18: *Motor geometric sketch*

The total torque output of the motor is

$$\tau_m = FAr_g \approx 2\pi(Bi_a)r_g^2 L \tag{34}$$

Where F is the shearing force density produced by the integration of the product of the magnetic flux and current on the surface (of area $A = 2\pi r_g L$) of the rotor, B is the average magnetic flux and i_a the average axial current. By dimensional analysis and experimental fitting, it was found in [235] that the following relationships could be established, considering the gap diameter as the main geometric parameter and by keeping the electromagnetic characteristics of the section constant:

- Motor mass: $m_m \sim r_g$
- Motor torque: $\tau_m \sim r_g^2$ (volume of the rotor $\sim r_g^2$). r_g has two main effects, which can be superimposed: it increases the moment arm and it increases the tangential component of the magnetic force.
- Motor inertia: $\mathcal{I}_m \sim r_g^3$
- Torque Density: $\frac{\tau_m}{m_m} \sim r_g$
- Acceleration: $\frac{\tau_m}{\mathcal{I}_m} \sim \frac{1}{r_g}$
- Motor constant: $K_m^2 = \frac{K_t^2}{R} \sim r_g^3$

These relationships are based on some assumptions about the shape of the motor. It can be observed however that another favorable way to increase the torque, without increasing the rotor inertia $\sim r_g^3$, is to change the motor aspect ratio, i. e. to make it longer along its revolution axis. This second design option can be beneficial to reduce the effect of the rotor inertia on the dynamics.

DIFFERENT MOTOR STRUCTURES' PERFORMANCE: IN-RUNNER AND OUT-RUNNER

For motors, it is possible to have two main designs. One in which the permanent magnets are attached to the rotor and the coils are on the stator, and another in which the coils are on the rotor. These two designs are commonly called in-runner and out-runner and show different compromises as reported in Tab. 1. Generally, outer-runner designs allow higher torque production and less moving inertia at the price of envelope and heat dissipation.

The table is mostly qualitative and shows these trade-offs when comparing motors of similar weight in the case of motors for compact applications [114]

	OUTRUNNER	INRUNNER
Diameter	↑	↓
Length	↓	↑
Torque density	↑	↓
Heat Dissipation	↓	↑

Table 1: Advantages of in-runner vs out-runner motor designs

7 ENERGETIC ANALYSIS OF ELECTRIC ACTUATORS

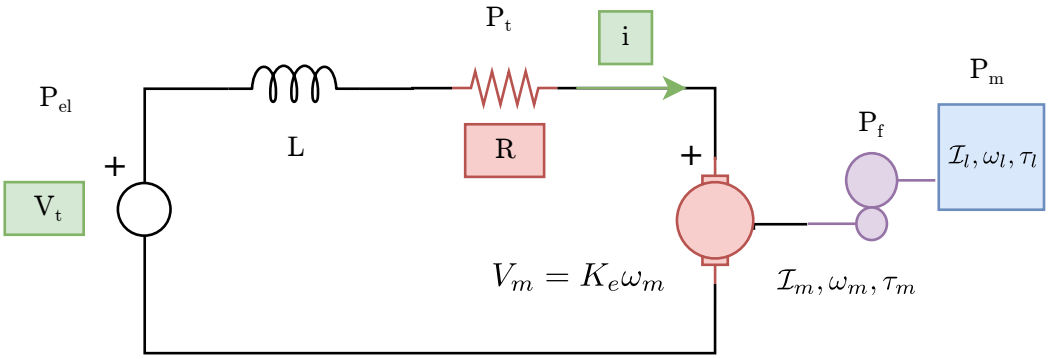

Figure 19: Electromechanical model of a single actuator

$$\underbrace{iV_t}_{P_{el}} = \underbrace{\tau_m \omega_m}_{P_m} + \underbrace{\tau_f \omega_m}_{P_f} + \underbrace{i^2 R}_{P_t} + \overbrace{iL\frac{di}{dt}}^{\approx 0} \tag{35}$$

In (35) the power equation of the electromechanical model of one motor, described in Fig. 19, is expressed. The total power given by the power supply P_{el} is the sum of the mechanical power P_m, the Joule losses in the motor windings P_t, the motor induction loading and friction losses in the joint P_f. Whereas the other losses can be taken into account, generally the dynamics of the inductance has a much faster timescale and can be neglected in the analysis. This energy flow is equivalent to the one proposed in other

formulations for the evaluation of power consumption in industrial scenarios Boscariol, Scalera, and Gasparetto [30] or for robotic systems Yesilevskiy, Gan, and Remy [279]. The difference concerning is allowing energy regeneration on the power supply side when $P_m \leq 0$. From the total torque at the motor side, with friction compensation it yields, according to (24):

$$\tau = \frac{1}{n}\tau_l + \mathcal{I}_m\dot{\omega}_m + \tau_\mu sign(\omega_m) + b\omega_m^2 \tag{36}$$

CAVEAT In the following, with a slight abuse of notation, the variables collecting several joint information are represented with bold symbols. Those are to be interpreted as the vectorial version of torque and speed collecting the values on all the joints. The reasoning of the energy balance is still valid and it extends naturally to the whole system.

7.1 *Mechanical power*

Mechanical motor power is defined as the scalar product of the motor speed ω_m and the interaction torque τ_m

$$P_m = \tau_m\omega_m \tag{37}$$

the total mechanical power exerted on/by all the joints can be compactly written as:

$$P_m = \sum_{i=1}^{N_{\text{motors}}} \tau_{m,i}\omega_{m,i} = \boldsymbol{\tau}_m^\top\boldsymbol{\omega}_m \tag{38}$$

where $\boldsymbol{\tau}_m$ and $\boldsymbol{\omega}_m$ are the vectors containing all the joint information. The power can be both positive or negative, taking only the positive part into account neglects the fact that the mechanical power, when the motor is acting as a generator, could be restored. In this analysis, this is a desirable effect to exploit.

With this in mind the mechanical energy consumed during the motion is the integral over time interval $[0, T]$.

$$E_m = \int_0^T P_m(t)dt \tag{39}$$

7.2 *Dissipations, thermal losses*

There are two main sources of dissipations, one is related to the heating of motor coils (Joule effect), the other to the energy lost as friction in the joint.

JOULE EFFECT : The winding resistance and the torque constant are considered in a model of the thermal losses due to the coil resistance. So for a single joint the following equation can be written:

$$P_t = i^2R = \frac{\tau^2}{K_t^2}R = \frac{\tau^2}{K_m^2} \tag{40}$$

In compact form, considering all of the joints, it writes:

$$P_t = \boldsymbol{\tau}^\top \mathbf{K} \boldsymbol{\tau} \qquad [\mathrm{W}], \tag{41}$$

where $\boldsymbol{K}$ is a diagonal matrix mapping the motor torques to the power dissipated by the Joule effect (its diagonal contains the squared reciprocal of the motor constants K_m).

As a side note, from the same values, a common performance indicator of the motors is defined. The *thermal torque value*, which is the root mean square of the motor torque that gives us an indication of the overall loading and energy lost during a given task or cycle.

$$\tau_{m,\mathrm{RMS}} = \sqrt{\frac{\int_0^T \tau_m^2 dt}{T}} \tag{42}$$

JOINT FRICTION LOSSES : The value of $\boldsymbol{\tau}_f$ (24) is used to compute the energy dissipated in the joints as the scalar product of the friction torque and speed computed at the motor side:

$$P_f = \tau_f \omega_m \qquad [\mathrm{W}] \tag{43}$$

Similarly as before the reasoning holds for several joints:

$$P_f = \boldsymbol{\tau}_f^\top \boldsymbol{\omega}_m \tag{44}$$

Even if this power can end up heating the system, it is a different phenomenon than the Joule effect and so it is treated separately.

7.3 *Electrical power and power flows*

The quantities introduced in Eq. (44) and Eq. (41) are non-negative and the formulation is also able to encompass the non-perfect regeneration of the electrical energy Joule when the system is in a regenerative phase. In that case, even if the current is back-flowing, there is still some dissipation in the coils of the motor and at the joint level. The total electrical power is given by the interaction power plus the dissipations terms:

$$P_{el} = \boldsymbol{\tau}_m^\top \boldsymbol{\omega}_m + \boldsymbol{\tau}_f^\top \boldsymbol{\omega}_m + \boldsymbol{\tau}^\top \mathbf{K} \boldsymbol{\tau} = \boldsymbol{\tau}^\top \boldsymbol{\omega}_m + \boldsymbol{\tau}^\top \mathbf{K} \boldsymbol{\tau} \tag{45}$$

Here the total motor torque, including friction is called $\boldsymbol{\tau} = \boldsymbol{\tau}_m + \boldsymbol{\tau}_f$. The total electrical energy can be computed as the integral in time of the electrical power:

$$E_e = \int_0^{\mathcal{T}} P_{el} dt \tag{46}$$

In the studied case, for generality, if P_m is negative, it can overcompensate for the friction losses and regenerate some power on the motor side. If this is not possible, it is more reasonable to use the total positive electrical power:

$$P_{el}^{+} = \max\left(\boldsymbol{\tau}^{\top}\boldsymbol{\omega}_m + \boldsymbol{\tau}^{\top}\mathbf{K}\boldsymbol{\tau}, 0\right) \tag{47}$$

Clearly $P_{el} > P_m$. We assume moreover that the robot cannot store the negative mechanical work, this mechanism may be interesting and used to partially compensate for the overheating effect on the robot. Note also that P_{el} is an important parameter also for the total energy consumption and could be related to the dimensioning of the batteries of the robot.

From the power balance:

$$P_{el} - P_m - P_f - P_t = 0 \tag{48}$$

Some additional power components (e. g. power consumed by on-board electronics) can be included in this balance. The convention for the signs is:

- $P_{el} > 0$ when the source is providing power otherwise if $P_{el} < 0$ the source is regenerating power.
- $P_m > 0$ when the load is getting power from the source, otherwise if $P_m < 0$ the load is regenerating power.
- $P_f, P_t > 0$ when friction, thermal losses by Joule effect cannot inject power to the system so their sign is positive

The mechanical power by the motor will be considering also possible power going to charge the batteries.

$$P_{el} = \boldsymbol{V}_t\boldsymbol{i} = \boldsymbol{\tau}^{\top}\boldsymbol{\omega}_m + \boldsymbol{\tau}^{\top}\mathbf{K}\boldsymbol{\tau} \tag{49}$$

In this case, from the joint friction identification and friction model, $\boldsymbol{\tau}$ comprises also the dissipation losses.

8 POWER MODEL WITH REGENERATION

In case of regeneration, there are 4 cases, which can be assessed on a single motor energy balance:

- FORWARD MOTOR: $\omega_m > 0$ and $\tau_m > 0$
  $V_m > 0$ and $i > 0$, in this case the current flowing is $i = \dfrac{V_t - K_t\omega_m}{R}$
- GENERATOR: $\omega_m > 0$ and $\tau_m < 0$
  $V_m > 0$ and $i < 0$, in this case the current flowing is $i = \dfrac{V_t - K_t\omega_m}{R}$
- GENERATOR: $\omega_m < 0$ and $\tau_m > 0$
  $V_m < 0$ and $i > 0$, in this case the current flowing is $i = \dfrac{V_t - K_t\omega_m}{R}$
- BACKWARD MOTOR: $\omega_m < 0$ and $\tau_m < 0$
  $V_m < 0$ and $i < 0$, in this case the current flowing is $i = \dfrac{V_t - K_t\omega_m}{R}$

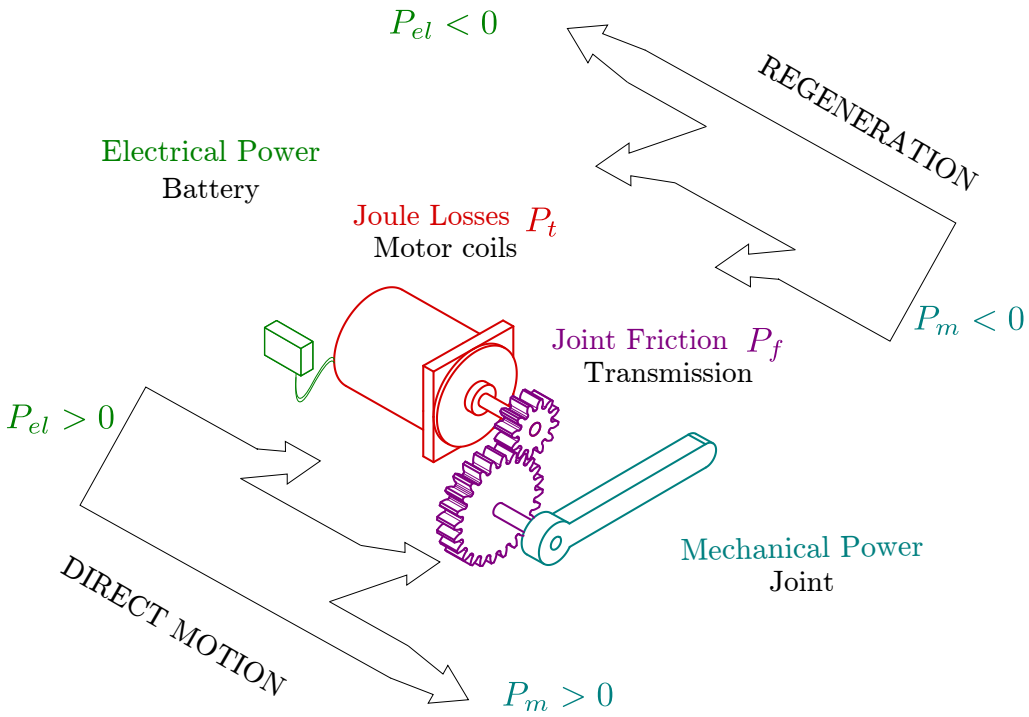

Figure 20: Direct and backward motion of the motor

9 CONCLUSION

This chapter focused on the actuator model for robotics systems. Different types of actuators have distinct characteristics and dynamics, necessitating specific mathematical descriptions. Accurate actuator models enable analysis, control design, and simulation of the system's behavior, stability, and performance. The main emphasis was on electric actuators, and the chapter addressed the non-linearities and energy flows that affect these devices.

5

ENGINEERING LEGGED ROBOTS: PARADIGMS FOR ACTUATOR SELECTION

In Short

In this chapter, some of the difficulties tied to the selection of the right actuators are presented. General conditions to the selection of the actuators indeed exist, but multiple possible choices depend on the envisioned application. The positive and negative aspects of each mainstream actuator technology are summed up. Then we focus on electric actuators, which are the main focus of this thesis. Some of the most used implementations in legged robotics together with their trade-offs are presented. Among these, the proprioceptive paradigm, which our work investigates, is detailed.

Contents

Motor selection is a very important aspect to consider in the design phase, because a wrong choice can lead to inefficiencies.:

- Wrongly dimensioning the motor may be problematic in highly dynamic conditions and transient loads,
- Over-sized motors may be needlessly more costly,
- Choosing a bigger motor may increase the maximum power available, but also, add useless weight to the robot.

For the selection phase, it is crucial to determine the right parameters of the motors. A first choice is to find if, for a given task, the motor can provide appropriate torques and speed to the joint by looking at its characteristic curve. In this phase, the transmission

must also be determined: a high transmission ratio will reduce the load on the motor and have an impact on the dynamic behavior, but will result also in increased friction, which is undesirable. In this sense, it is necessary to consider the impact of motor selection and transmission together and, based on that, assess the impact of the power losses due to dissipative effects.

1 NECESSARY CONDITIONS FOR ACTUATOR SELECTION

The choice of one specific actuator over another depends on the task to be performed. Motors will be appropriately chosen for the dynamic loading if, for all the duration of the task, they satisfy the following conditions:

- the instantaneous torque provided by the motor is greater than that of the load, reduced to the motor axis $\tau_m(t) \geq \left|\left(n\mathcal{I}_m + \frac{1}{n}\mathcal{I}_l\right)\dot{\omega}_l + \frac{1}{n}\tau_l\right|$,
- the root mean square value of the motor torque is higher than the one of the load reduced to the motor axis $\tau_m^{rms} \geq \frac{\tau_l^{rms}}{n}$,
- the nominal maximum angular speed of the motor is higher than the one of the load, reduced to the motor axis $\omega_0 \geq n\omega_{l,max}$,
- the motor peak or continuous power (depending on the load characteristics) is higher than the one required by the load $P_m \geq (\tau_l + \mathcal{I}_l\dot{\omega}_l)\omega_l$

2 DESIRABLE PROPERTIES FOR ROBOTICS-ORIENTED ACTUATORS

In legged robotics applications, when selecting actuators the designer is generally interested in maximizing some performance indicators. For instance, it seems reasonable to optimize the motor via criteria that, at the same time:

MAXIMIZE:

- Torque/torque density
- Bandwidth
- Operating speed
- Available power
- Force transparency
- Proprioception
- Control bandwidth
- Sensing bandwidth
- Energy-efficiency
- Back-drivability (safety)
- Mechanical robustness

MINIMIZE:

- Inertia
- Friction
- System complexity
- Envelope

There are a lot of factors that interplay in this choice. No design is meeting all the possible requirements, and no perfect actuator exists. What usually must be defined is the actuator that is the most suited to the envisioned application. Among the technologies that are commonly used, some of the different motor properties are summed up

in Table 2. Actuators for low-complexity systems and fast applications in which torque control is achievable are Direct-Drive (DD) and Quasi Direct-Drive (QDD), but as can be seen, the major disadvantage is the lower torque density compared with the other alternatives. The major direction of this work is to understand how they can be properly selected in systems in which efficiency is important.

This table is mainly qualitative, so it has to be taken with a pinch of salt, a quantitative review of different robotic actuator technologies can be found in [128], here some common downsides of the different actuator types are reported. Another review paper, specifically tailored to multi-legged systems (including some sensor and control elements) can be found here [110]

Actuator Type	DD	QDD	SEA	HGR	HYD
Torque density	Lowest	Lower	Base	Higher	Highest
Transparency	Highest	Higher	Base	Lower	Lowest
Bandwidth	Highest	Higher	Lowest	Base	Base
Efficiency	Base	Base	Highest	Higher	Lowest
Impact robustness	Higher	Base	Base	Lower	Higher
Back-drivability	Highest	Higher	Base	Lower	Lower
System simplicity	Highest	Higher	Base	Higher	Lowest

DD - Direct drive QDD - Quasi-direct drive ($n < 10$)

SEA - Series elastic actuators HGR - High gear ratio ($n > 10$) HYD - Hydraulics

Table 2: Qualitative comparison between different actuator properties.

3 ELECTRIC MOTORS DESIGN PARADIGMS FOR LEGGED ROBOTICS

3.1 *Link with interaction control*

Hardware selection cannot be explained without an application. To discuss the trends of actuators for legged robotics, also considering their control strategy is needed. In the past, the oldest legged-robot's design were following rigid control policies, in which the system was tracking joint positions and joint velocities. It was not long to find out that this approach, albeit very effective in fields where precision and accuracy are needed (e. g. such as industrial manipulators), was insufficient in terms of the variety of interactions that a robot can have with the environment. The seminal work about impedance control [118], [119] showed how the classical trajectory-following tracking was limiting the spectrum of interactions with the environment. In particular, in the case of contacts, robots are not able to compliantly follow tasks that require the application of forces (e. g. to apply constant pressure on a surface while moving) if also the joint positions are fixed. It was clear that in some tasks, there is a link between forces and motions. This interaction is of paramount importance for legged systems as the control of forces exerted with the ground impacts motion and stabilization of the system.

Robots allowing this interaction with the environment involved more advanced control and hardware implementations. In recent legged robots' development, to cope with the problem of controlling precisely force interactions, several designs have been proposed. Feedback impedance control is possible but requires a precise model of the sys-

tem and hence is very much affected by sim-to-real imperfections, in particular, those relating to:

- model mismatches (i. e. geometry and inertias, un-modelled flexibilities),
- sensor dynamics,
- actuator dynamics,
- processing delays (i. e. computation or communication).

To mitigate the impact of these issues, some approaches have been used in the past. For electric motors, these solutions need to resolve the problem of the power density of the motors, possibly adding sensors or compliance in the system, a small chart with the problems and solutions to problems is shown in Fig. 21. Three main design paradigms can be found, and a small discussion is proposed together with an explanation of the goals of each solution.

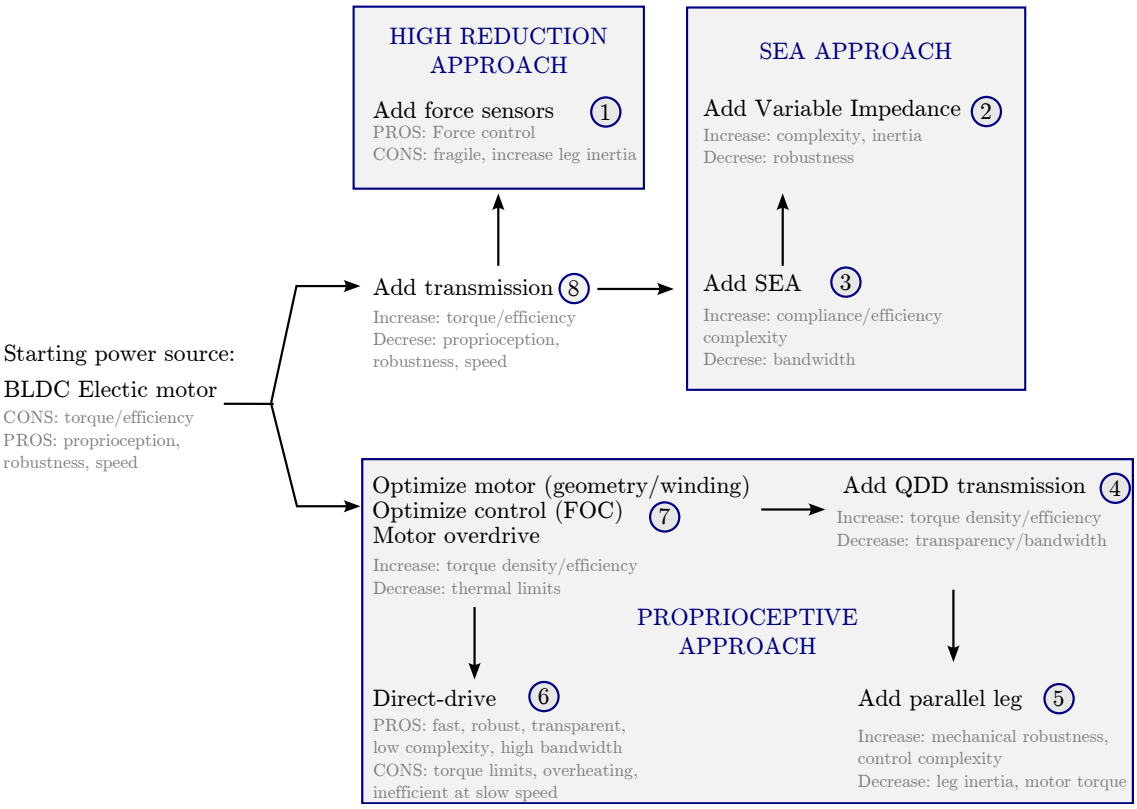

Figure 21: Possible design workflows

3.2 *Torque controlled with high-gear ratio and additional sensors*

Following a traditional mechanical design approach, an easy way to improve the torque density of the actuator is by using a higher reduction ratio. For instance, strain wave gears like harmonic drives are used extensively in high-end robotics applications with

the advantage of achieving higher torques within a very compact envelope (co-axially). In these actuators, the motor is moving an elliptical element, called wave generator

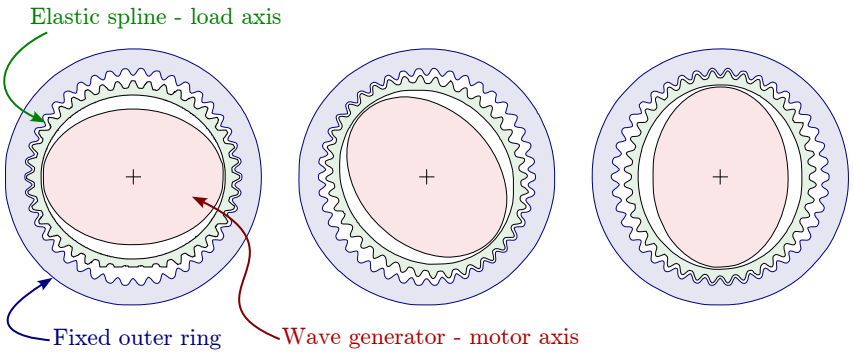

Figure 22: Strain wave gearing system

which is deforming an elastic spline (fixed on the output shaft) forcing contact with a fixed outer ring as shown in Fig. 22. Other advantages are that they allow rather precise control, and very high torque output as they present almost zero backlash. These actuators are however rather costly and fragile. They sacrifice a lot in terms of robustness to shocks and back-drivability. Moreover, the mechanism that they exploit is rather prone to add losses in the transmission (i. e. friction, hysteresis of the elastic element). As a result of this, and of and huge reflected inertia, transparency is lost. Since the actuator by itself is not compliant, the solution is to compensate for that in software, by the use of advanced control techniques which allow to perform force interaction control. To allow this, additional force sensors are needed and installed on the actuation stages. This adds the downsides of increased system complexity and added weight. Such an approach has been rather popular in legged robots in particular for a series of successful humanoid systems such as the ASIMO [212], HRP series [141]–[143], HUBO [136], [185], JAXON [153] and Talos [252] (the first commercial torque-controlled humanoid robot launched by PAL Robotics). On this side, the technology of transmission is evolving, however, there is no free lunch. Other than harmonic drive, also epicycloidal gear trains (Fig. 23) and hypocycloid drives alteratives exist. The first present a considerable backslash, but can be miniaturized and are co-axial while the second are affected by problems in shaft alignment that may require very low tolerances to avoid bending and jamming.

3.3 *Series Elastic Actuators*

Trying to cope with the problem of reducing the negative effects of impulses that impact the mechanical structure and still add some force-control/sensing capability, a proposal was advanced in [192] with SEA. The compliant interaction is embedded in the actuator's physical design. The core idea is to decouple the load from transmission by inserting of a compliant mechanical element in series. By knowing the properties of these elements (usually acting as linear torsional springs) such as the material's elastic modulus and ge-

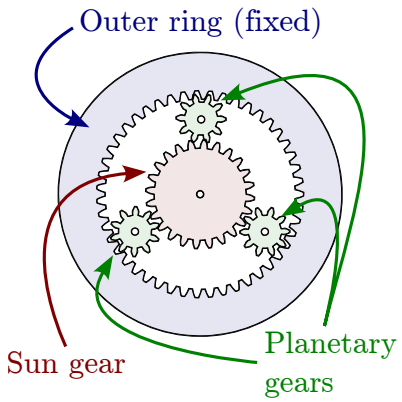

Figure 23: Epicycloidal gearing system

ometry, it is possible to relate the displacement field to the force stress field. This allows angular displacement sensors to be used to perform force control and sensing. Robots using this solution are showing also naturally dynamic and energy-efficient motions, as SEA draw parallels with bio-inspired structures. However SEA come at the price of added compliance, and often they require a more complex model, because of complex joint dynamics [132]. There are also several trade-offs from the spring characteristics themselves: a stiff spring is not adequate to absorb impacts and presents poor sensing resolution while a softer spring introduces a more complex dynamical coupling between motor and load and reduces the overall bandwidth of the actuator [207].

Among the robots featuring elastic elements in the actuation there are some important cases of humanoids: such as ATRIAS [124], [125], MABEL [99], THOR [121] and ESCHER [151]. From IIT we can cite also the WALK-MAN robot [259] and iCub [171]. Among the quadruped robots instead, StarlETH is utilizing SEA actuators [130]. Furthermore, bio-inspired studies [251] were conducted on CheetahCUB, a small-sized robot featuring high-gear ratio servo-motors and spring elements on parallel legs. Recently, still using elastic components, Morti [211] a lightweight quadruped driven by brushless motors via cables has been introduced

From a practical point of view, it may be interesting to regulate the value of the stiffness itself and this leads to another series of actuators and research Variable Impedance Actuators, as presented in this review on the topic [264].

3.4 *Proprioceptive actuator design*

An ingenious way to perform sensing, which does not require additional expensive sensors is through proprioceptive design [149], [272]. This design paradigm was inspired by solutions from the domain of haptics (in particular from the PHANTOM interface), rather back drivable and transparent, i. e. opposing low resistance to motion. The idea of proprioception is to directly achieve force control via current control which is al-

lowed by BLDC motors. In order not to introduce too many non-linearities, an extremely minimal, transparent actuation (QDD to accomplish higher efficiency) is needed. QDD transmissions oppose low resistance to the transmission of actuator force from motion and vice-versa, in other terms they have a low mechanical impedance. However, to obtain the same torque output, QDD actuators require motors with higher torque density compared to other solutions. Factors that must be limited to keep the impedance low include: inertia, damping and friction. Another way to increase back-drivability is by optimizing the leg itself (inertia). This was done efficiently using bio-inspired tensegrity [11] or topological optimization. The proprioceptive approach was first detailed for legged robots from MIT bio-inspired robotics lab: MIT Cheetah and MIT mini Cheetah [28], [184]. Surprisingly, these robots, while being highly performance-oriented were still quite energy-efficient. As they present fewer losses in the regenerative regime, they allow to restore negative power into batteries [233]. The efficiency of power electronics in absorbing negative mechanical into batteries is still an open challenge. With further advancements, it will allow some active compliance to be embodied inside the actuator itself. A lot of new robots are pushing this new approach to the extreme. For instance Solo [98] is featuring minimal actuator stages with a weight of ≈150 g or other robots such as Minitaur [27], Jerboa and Delta Hopper [147] is even eliminating the transmission itself and exploiting the robustness of closed kinematic chains (fast and rigid). However the selection of the right actuator, allowing both a good performance without increasing the energy consumption is not straightforward and investigating this trade-off is still an open problem. Moreover, to make the decision even harder the choice of the structure also plays a role and should be taken into account from the initial case

The decisions associated with this engineering problem are perfectly aligned with the philosophy of co-design

4 CONCLUSION

In this chapter, the challenges related to selecting appropriate actuators were discussed. While there are general selection guidelines, specific choices depend on the application. The pros and cons of mainstream actuator technologies were outlined, with a focus on electric actuators, which are the main subject of the thesis. The chapter also presented commonly used implementations in legged robotics, including the proprioceptive paradigm, which is the primary focus of the research. Due to the importance of this class of actuators, chapter 6 is dedicated to showing in detail the implementation that drives this thesis and its identification.

6

QUASI-DIRECT DRIVE ACTUATORS: AN OPEN-HARDWARE CASE

In Short

In this chapter, the QDD actuators used on the Solo robot are quickly presented in terms of technological implementation and design and control choices. For our co-design investigation, it constitutes the "building block" for new robotic platforms. The properties of this actuator can be easily identified and the open-hardware nature of the project allows easier customization. The credits for the design implementation go to Felix Grimminger [98] and to the other contributors to ODRI [a]. A part dedicated to the identification of the friction parameters is also included.

a Project page, Github page

Contents

1 ACTUATOR MODULE CHARACTERISTICS

The actuator module used for the ODRI platforms can be re-adapted in a series of different robot topologies as can be seen from recent projects as shown in Fig. 24.

Figure 24: Different robots sharing the same modular actuator from the ODRI project [98]

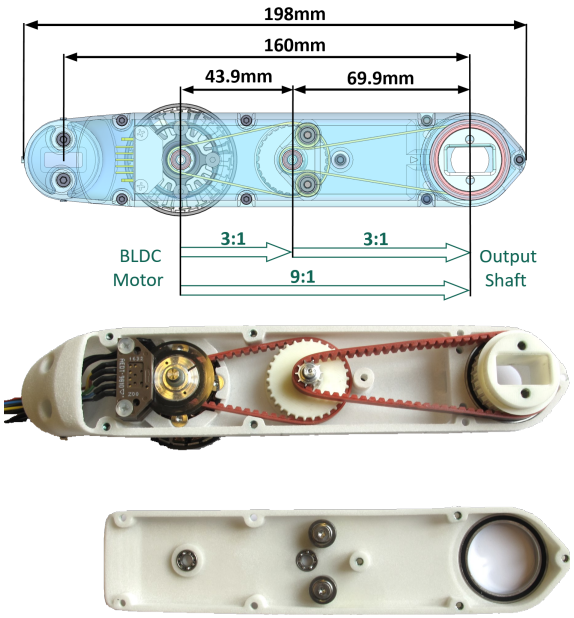

Figure 25: Actuation stage of the ODRI project [98]

The module is a compact QDD system that can be repurposed for a variety of projects with common control logic and interface to the low-level hardware. With this approach, it is possible to obtain at a reduced engineering cost, platforms capable of torque-control and proprioception. Each actuator module, shown in Fig. 25, has a segment length of 160 mm inter-axis, weighs 150 g and outputs 2.5 Nm at 12 A.

MOTOR: The motors used are from the Antigravity series of the T-motors, they are out-runner BLDC designed for drone applications. The advantages are low weight for rather high torque density and compactness. Moreover, they present adequate efficiency and low cogging torque. The link structure allows to place the motor always be at the distal location with respect to the actuated joint, this reduces the moving masses and the rotational inertia.

TRANSMISSION: Each actuator reduction is made by a compact transmission system. The overall gear ratio is realized by two almost identical stages featuring synchronous belts and custom-made pulleys. The shafts had to be custom-made and are challenging because the smaller pulleys have just a few teeth in contact with the belt. The pulleys and belts require two stages to reach the adequate gear ratio in such a reduced space. From the design point of view, n depends on the ratio of the number of teeth or, for the timing belt, between the diameters of the motor and the driven wheel. For $n = 9$, it would mean obtaining a very large cross-section, which is unfeasible. The shafts are inserted on rotary bearings which are fitted on some slots in the frames. Other elements, such as belt pre-tensioners are also similarly inserted.

SENSORS: On the actuator, for sensing position, industrial-grade high-resolution optical incremental encoder modules are used allowing robust, high-precision motion control. From these sensors, fine control laws can be implemented.

FRAME SHELLS: The structure of each actuator module is made to be built by AM. The chosen technology for larger structural is Fused Deposition Modeling (FDM) or Selective Laser Sintering (SLS) parts (the first is generally cheaper and allowed quicker prototyping, but is a bit more constraining and results in less sturdy parts). For all the precision parts Stereolithography (SLA) is used to meet the thigh tolerances (e. g. for the custom pulleys which need to be mounted on the machined micro shafts). The actuator link is made of two outer shells that cover the moving transmission part and hold the structure together using screws inserted in the plastic by reinforcing the tapping with helicoils. This structure is rather lightweight and it has an adequate level of stiffness. The design of this structure is hollow to easily fit the belt transmission, cables and sensors (rotary encoder).

CONTROL BOARD AND POWER SOURCE: The low-level controller was made from scratch including the hardware part allowing deep access to the hardware capabilities. To get the most out of the motors FOC, presented in [269], is used to finely control the power generation and get the most out of the torque. This technique, albeit rather old, has just recently been possible to correctly be implemented on compact-sized hardware. The actuator can be powered with different energy sources, thanks to the use of batteries it allows more versatile usage on legged systems. Regeneration is not generally used, because of the additional complexity. However it is an important element to consider in the case of larger robots where the deceleration of larger inertias may regenerate a considerable amount of power which would otherwise be lost overheating the motors.

2 ACTUATOR SYSTEM IDENTIFICATION

Some tests were made to identify some physical parameters of the system. MPI already identified the actuator with some measurements utilizing a torque sensor. The same goal has to be replicated without these sensors with an identification procedure that we developed and that we present in this section. Proprioception, reference profiles and known inertias can be used instead to estimate the torque values and, by linking the currents to torques, the friction values can be recovered. This way performing system identification becomes easier and more accessible. At LAAS a simple system was built in order to characterize the friction parameters Fig. 26. The objective is to control a single actuation stage in positions and velocities, by sending reference trajectories and making it move a rather high load inertia. This resulted in the testbed in Fig. 26, featuring a flywheel for which the geometry and material are known.

Additionally, the Polylactic Acid (PLA) structure is made heavier by the addition of bolts, with standardized mass at predefined radial positions. A fixed base allows fitting an actuator module and connecting the flywheel to the output shaft. The angular posi-

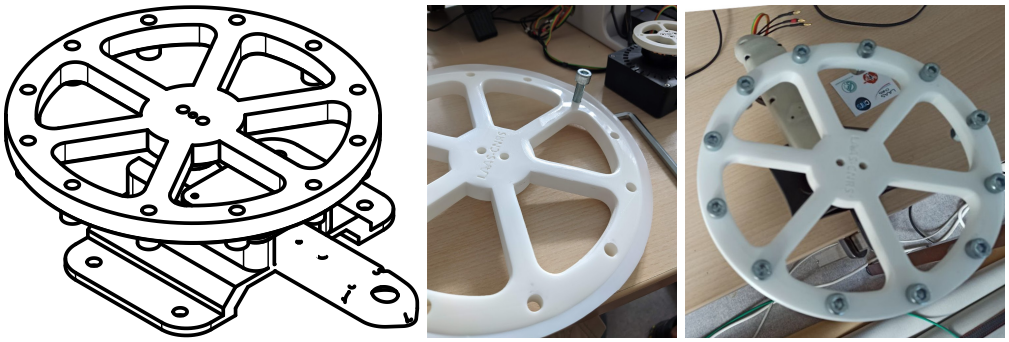

(a) Measurement testbed

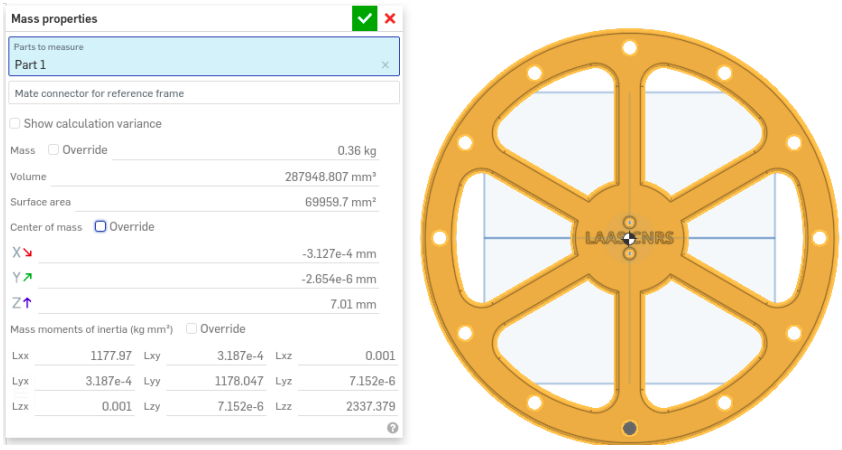

(b) Inertia values obtained from model, Onshape Computer Assisted Design (CAD)

Figure 26: Flywheel to perform system identification

tion of the motor (and hence the load, as the transmission is considered rigid) can be tracked with a Proportional Derivative (PD) controller on predefined trajectories thanks to the low-level interface to the hardware. With the knowledge of the load and by choosing the references to follow, the interaction torque can be deduced (either by using the ideal acceleration or by processing the data with a Savitzky-Golay filter, recovering higher-order derivatives), and the motor torque is tied to the current (as explained in chapter. 5). The effects of Coulomb friction and viscous damping are included in the model (50) (with a smoothed version of the sign function, substituting it with tanh). The torque acting at the motor is given by:

$$\tau_m \approx \mathcal{I}_m^\star \dot{\omega}_m + b\omega_m + \tau_\mu \tanh(\gamma\omega_m) \tag{50}$$

Where $\mathcal{I}_m^\star$ is the reflected inertia on the motor axis. The value of such inertia is obtained from the rotor and flywheel inertia.
For what concerns the chosen trajectories for the tests two cases are used:

- SINUSOIDAL TRAJECTORY: The advantage is that by controlling reference position and velocity (Fig. 27a), the acceleration is automatically tracked, as shown by the tracking in Fig. 27b. This is useful for performing transient tests and the identification of several parameters. In this case different values of frequencies and amplitudes were tested.
- CONSTANT VELOCITY TRAJECTORY: This profile makes the robot follow some ramp-up profiles in velocity, which later is kept to constant values for a given amount of time as shown in Fig. 28a.

For slow motions, Coulomb friction can be identified, while for fast movements the mechanism will be the viscous one. The data from the measurements is used to fit the model (50) with non-linear least squares. We obtained the values reported in Table 3. Moreover, it was possible to also verify that, from the collected data (which is shown in

PARAMETER	VALUE
$K_{t,u}$	0.230 Nm/A
$K_{t,l}$	0.235 Nm/A
τ_μ	5.054 10^{-3} Nm
b	1.02 10^{-5} Nms
γ	4.65 10^{8}

Table 3: Identified values with non-linear least squares

Fig. 27c), the ground truth for the torque constant K_t = 0.023 Nm/A is rather close to the estimated one. The identification of the viscous friction with the sinusoidal profile was quite noisy, this motivated the use of the ramp profiles, in which the velocity is constant and the dynamic effect due to acceleration is not present.

In this case, b =3.29 10^{-5}Nms provides a better identification, on a wider domain but with more data dispersion. More work on the identification side can be done with

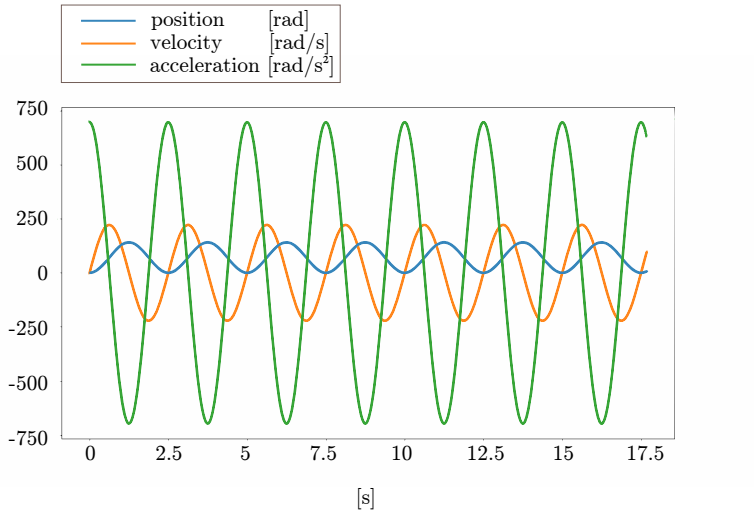

(a) Example of reference sinusoidal trajectories

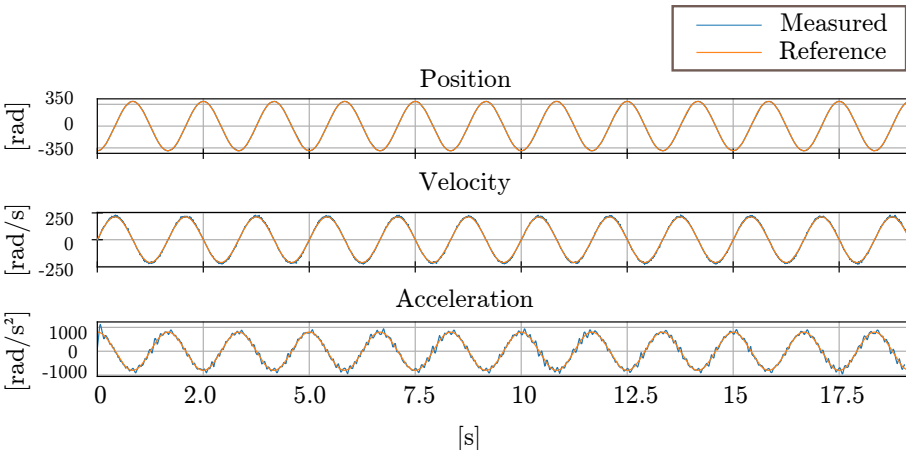

(b) Tracking of the references

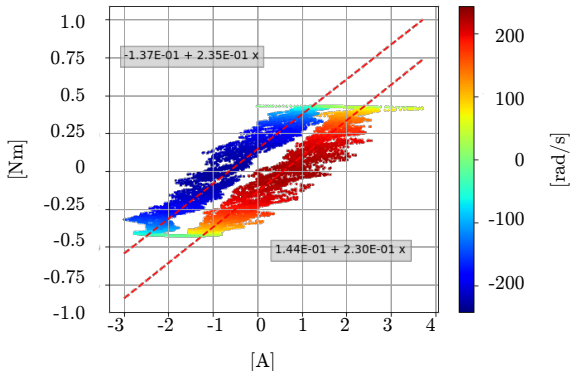

(c) Estimation of the torque constant

Figure 27: Sinusoidal reference trajectories used for system identification

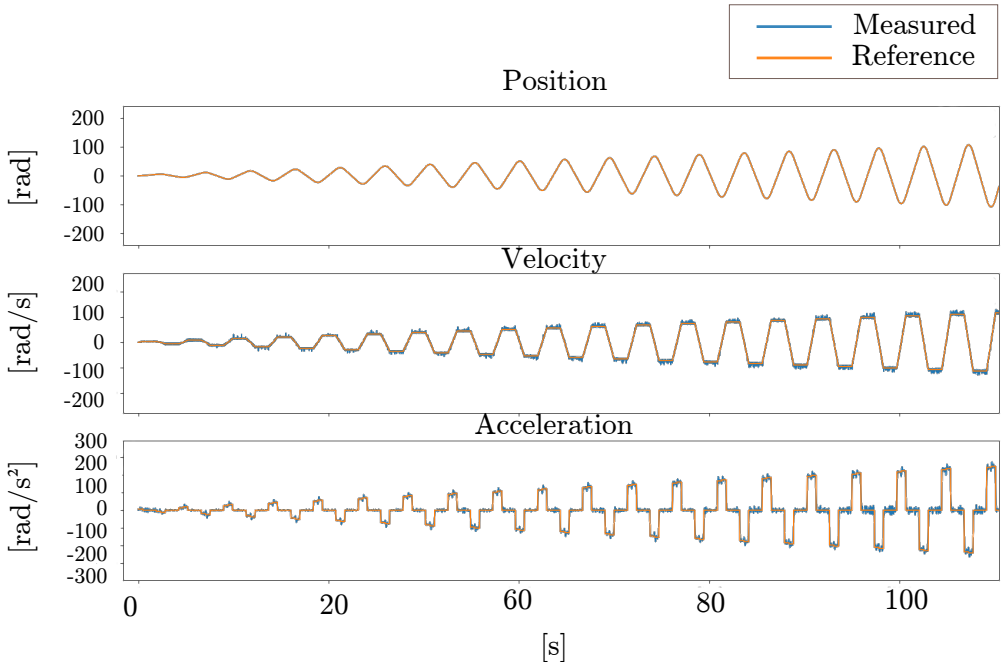

(a) Tracking of the references

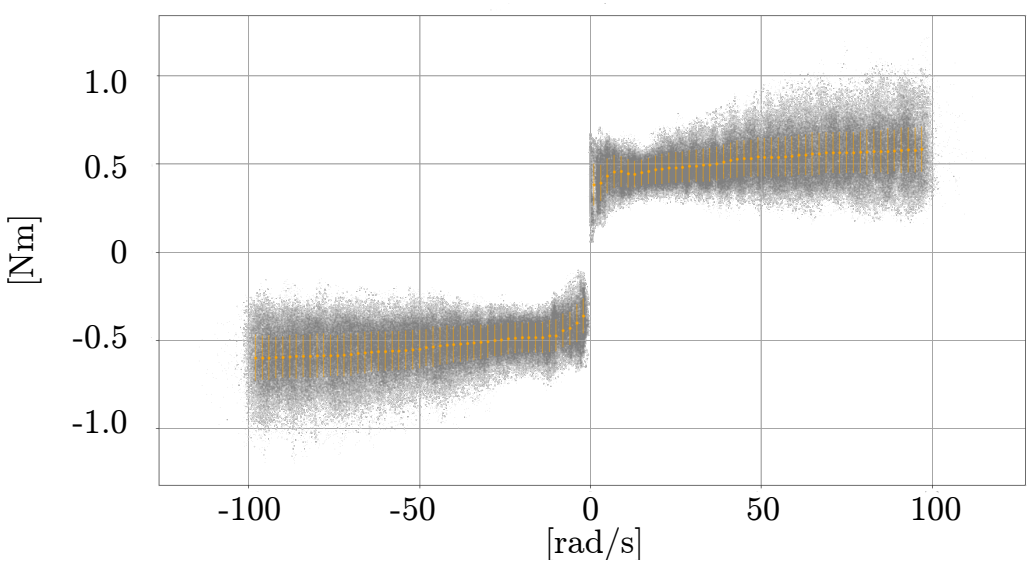

(b) Impact of viscous friction for different velocty levels

Figure 28: Ramp trajectory test viscous friction identification

the use of the power board, which was not available at the time of testing. The same platform, paired with a double encoder, one on the output shaft could also, be used for identifying the backlash or elasticity of the actuator and provide precise information about its bandwidth.

3 CONCLUSION

In this chapter, the QDD actuators employed in the Solo robot and other projects were presented. We focused on technological implementation, design, and control choices. The open-hardware nature of the project allows for easy customization, as they can be re-purposed to build new modular robotic platforms. Thanks to this property, these actuators have been selected for our co-design investigation (in particular the first two papers). As accurate identification of their nominal characteristics is needed, the chapter included a whole section dedicated to the friction parameters identification.

Part IV

CO-DESIGN: CHALLENGES AND SOLUTIONS

In this part, our research on co-design is presented. Initially, we provide a detailed explanation of the co-design problem and explore existing solutions in the literature. We then introduce our solving framework, which is tailored to the specific characteristics of the problem and incorporates features to enhance its robustness and versatility. This framework is applied to various problems. Firstly, we use the framework to optimize a monoped hopper structure and its actuators, which feature the proprioceptive approach described in the previous chapters. Next, we address the challenge of increasing the co-designed output's robustness to noise. To achieve this, we develop a method that utilizes the information from Differential Dynamic Programming (DDP) to evaluate the controller's performance in the presence of noise. Finally, we extend the method to a quadruped robot and optimize such a platform for multiple complex cyclic tasks. This allows us to demonstrate the flexibility and effectiveness of our co-design approach across different applications and scenarios.

7

OPTIMIZATION METHODS AND FRAMEWORKS FOR LEGGED ROBOTS DESIGN

In Short

In this chapter the problem of co-design and its goals are discussed envisioning applications in the field of legged robotics. Different successful implementations of co-design solutions to tackle relevant problems in robotics are presented.

Contents

1 PROBLEM STATEMENT

As stated in the introduction, legged robotic systems, and more specifically quadrupeds, have some advantages over wheeled robots. The redundancy of the legs can be useful for the stabilization of the body and may allow to overcome uneven surfaces with ease. The state of the art in their construction and control also makes it possible to compensate for high perturbations from the outside, while maintaining a reasonable level of compliance. The advantages of kinematic redundancy in the quadrupedal structure may also allow more energy-efficient actuation patterns (e. g. motions or gaits) to recover energy with antagonistic actuation and regeneration. Energy management is particularly crucial in the case of electric actuators. Moreover, a requirement for these quadrupeds is to have the right size to perform a given task. This latter property is needed to guarantee their usefulness, and to navigate in a given environment, but is not an easy target to optimize, because of a high interconnection among plant properties and control. For instance, bigger robots may need bulkier motors unless smarter control strategies are used. On the other hand, even if smaller robots may be more agile and better performing, if their

dimensions are not suited for the task, their applicability becomes highly reduced. This motivates the need for a tool that can explore all of the design and control possibilities. In addition to the scaling problem, the necessity for the robots to have an adequate mobility range for the robots needs them to be able to use energy efficiently. This goal needs a model of the energy dissipations of the systems and, especially for QDD actuator, the possibility of energy recovery from the motor in case of motion inversion. With such a model, the robot design step will also take into account possible regeneration and thus optimize the control of the body exploiting this capability. To achieve enhanced robot efficiency, control, and design, it is necessary to develop an optimization framework that addresses all of these key aspects.

2 OPTIMIZE THE DESIGN OF LEGGED ROBOTS

Numerous approaches for model-based design have been suggested in prior research, in particular hardware design for legged systems, these works have roots in engineering intuition or trial and error. Various design criteria have been suggested based on good heuristics or intuitions. For instance in [251] the addition of multi-segment, compliant legs was proposed to ease the task of controlling quadrupeds. Passive compliant elements are added in the leg mechanics to achieve at the same time higher speed and efficiency. These observations are motivated by bio-inspired considerations. At a higher level, purely motivated by technological choices, some selection criteria for energy-efficient motor-transmission combinations were proposed for some pre-defined tasks [206]. The approach was used to determine some of the hardware employed on the ATRIAS robot. One of the main limitations of this method comes from the choice of the task, which is fixed and may be sub-optimal. As already mentioned in [272] the idea of proprioceptive actuators has later been formalized, with implications on both hardware and control. This implementation became particularly popular in the area of legged robots, but it poses still some challenges from the hardware selection point of view. A major issue comes from the energy efficiency of the actuator, which needs to be properly handled. The proprioceptive design approach was empirical, and mainly targeted to increase performance and proprioception. Surprisingly for MIT Cheetah robot efficiency turned out to be rather high as well. In more recent publications i. e. [205] an entire constructive framework approach is dedicated to robot leg design, specifically optimizing power consumption. In this framework, the hardware optimization is progressive and starts with energy-efficient template models, which capture the essence of the locomotion dynamics and, in subsequent phases, optimize for the energy losses of the complete system and the actuator choice. This sequential pipeline follows an approach that, from a general abstract sketch of the system, embodies the real robot design by making it progressively more detailed. However, as the variables are added sequentially to the problem, the optimization cannot exploit possible relationships between them. The method can also be impacted by some bias in the selection of the high-level templates which are artificial and do not express the whole complexity of the robot. In [230] a multiple-objective optimization framework (featuring a Genetic Algorithm (GA)

and the possibility of optimizing discrete variables) was proposed paired with metrics encompassing energy efficiency, joint impedance and time response of the system. In this case, however, the joint trajectories were fixed *a priori* and not taken as possible optimization variables. This, in high-level problems (when just a high-level task is fixed), may be not versatile enough as it overfits a specific choice. It is clear to see that also this approach is missing a complete view of the interconnections between the plant and the control that need to be expressed. The way to exploit this dependency is with a more general co-design approach. In the following section, a review of the co-design literature is presented to then discuss some results applied to legged robots.

3 UNDERSTANDING THE CO-DESIGN APPROACH

The co-design approach allows to optimize hardware and control for a task. It allows a better, more general and systematic vision with respect to the standard methods presented in Section 2. By nature, the purpose of this design technique is to exploit the relationships between physical parameters and governing intelligence. The technique was first used in computer graphics, seminal work in this field was performed by Karl Sims in [239], [240]. In his results the morphology and behavior of simulated creatures were optimized in a competitive environment thanks to an Evolutionary algorithm (EA). This first achievement proved the feasibility of the technique for complex sensorimotor problems. Co-design then quickly developed for robotics applications, exploiting the high interdisciplinarity of this field. The concept of co-design, involving the optimization of both motion and controller, was initially explored in [186] and Reyer and Khatib [204], where the optimal trajectory and associated gains were discovered solving a Non-Linear Program (NLP). In [159] the idea of Design-For-Control (DFC) was formalized. In this paper approach to synthesize robot design taking into consideration their control was applied for different scenarios and the optimization of a four-bar linkage system. A systematic definition of the problem of generating platform for dynamic behaviors and the techniques to solve it can be found in [8]. Additionally, some structured approaches, defining the problem of co-design from a mathematical point of view, can be found in the following works [43]–[45], [282]. While several works exploited NLP for many different applications (e. g. in [40] co-design was used for drones and multi-robot design selection), the use of EA approaches kept being quite popular, a review on EA optimization applied to robotics can be found in [194]. One of the advantages is that evolutionary co-design can be adapted to a variety of systems, in [24] EA have been used to deal with the synthesis of winged drones, considering also the trade-offs among different objectives. Related to actuator optimization, very promising results quickly followed. Limited to some manipulator examples [237] tested several optimization algorithms such as Simple Genetic Algorithms, Genetic Algorithms with elitism, and Differential Evolution finding optimal designs of SCARA and articulated manipulators. From the point of view of optimal hardware selection, some results were achieved in Ouyang, Li, Zhang, *et al.* [181], where co-design was employed to reduce peak torque and power in servomotors while tracking a predefined trajectory. The actuator model was rather

The work of Park and Asada is almost contemporary to that of Sims, and still the focus of the analysis is remarkably different.

complex, combining a constant velocity motor and a servomotor in a hybrid mechanical system. Recent literature has also explored the use of co-design to optimize mechanical systems by harnessing their passivity. By minimizing control torques and input energy, the dynamics of the plant is utilized to follow an energy-optimal trajectory as closely as possible, thereby reducing the applied control torques required for task execution. Further formalization of the approach can be found in [10] (a more recent review on different optimization techniques can be found in [6]). These methods have been used in several domains, from the selection of suspension systems [7] to air filters [214]. The use of sequential formulations of the co-design approach was discussed in [67], [187], trying to split the problem complexity into subsequent phases. In [9] the approach demonstrated a decrease in energy requirements by optimally selecting the link dimensions of a pick-and-place mechanism, while making limited modifications to the plant. The feasibility of passive walking devices that relied solely on gravity to maintain stable walking patterns was demonstrated in [168]. This concept can be extended to a broader range of robotic systems and proves particularly advantageous for repetitive tasks and predefined motions. Studies have shown that increasing the mass of the system's links can be beneficial for minimizing energy consumption since it enables better utilization of the system's passivity. Promising approaches for the design of passive walkers have been proposed in [39] and [217] and used similar methods. These approaches hold the potential for enhancing the efficiency of legged systems. Related to optimal plant selection for minimal energy consumption the effect of the inertia of the system has also been studied for passive bipedal motion [109] where the motion was produced by redistributing the system mass. In recent work, the optimization of rather involved physics has been proposed by ground-breaking work showing the maturity of the approach. As an example, related to the designing of soft/compliant mechanisms, in [50], [57], [170], [242] computational tools were used to best select the structure of soft mechanical figures in several locomotion scenarios or swimming. Similarly, in the case of closed-loop kinematic chains, the selection of the hardware of mechanical avatars was automatized. In [56] the kinematic design parameters were selected to generate smooth motion for mechanical avatars. The approach was extended in successive work [257]. Further studies have investigated the impact of different energy cost functions on the electromechanical actuation of monoped hopping systems [279] and the tradeoff between energy policies in series and parallel actuation systems [278] using co-design techniques. Previous studies in biomechanical systems aimed to achieve natural simulations of animal-like models. For example, [55] utilized a flexible spine and a GA to determine the optimal control sequence for a quadruped avatar, resulting in a more natural motion. In [89] a GA was applied to optimize the timing and plant modifications of a bipedal model with muscular actuators, aiming for optimal motion performance. The use of passive dynamics to reduce power consumption under fixed trajectories has proven effective in the study and optimization of robotic systems [53], [168]. Additionally, considering the characteristics of the actuator, such as exploring the potential for energy recovery, can lead to better system representation. However, developing a custom plant model

(that incorporates energy recovery phenomena and accounts for dissipation losses) is necessary to facilitate such considerations.

4 CO-DESIGN APPLIED TO LEGGED ROBOTS

MOTION GENERATION Concerning the generation of motions for legged systems, several works have covered the topics, showing the maturity of model-based methods to synthetize interesting behaviors. They are generally based on the formulation of an Optimal Control Problem (OCP) and have a quite high degree of versatility. For instance in [199], the animation of dynamic legged locomotion was proposed for different robot topologies. Transitions between different behaviors were additionally obtained with limited user intervention. In the same spirit, in [263] a method to synthesize parametrized motions was proposed for different behaviors and for high-level parameters, such as speed, leap size and turning rate. More recently, in [154] several dynamic maneuvers were chosen for a galloping 3D quadruped robot by using a multiple-objective evolutionary algorithm. In [111] a real-time technique to re-target motion on different creatures' morphologies was proposed and used in the videogame Spore. In [155] the locomotion of a character was linked to the natural modes of the system, based on its length, mass and stiffness. In [268] an approach was proposed to synthesize optimal gaits for several legged systems topologies. In [54] a generalized real-time walking controller was proposed with generality for gait, motion and morphology. In [3] the generation of the motion was optimized together with some physical parameters of the model itself.

CO-DESIGN OF LEGGED-ROBOTS Several studies have tackled the problem of legged robot co-design, each focusing on different aspects and objectives. In Mombaur et al. [174], optimization was performed on the motion and kinematic parameters of a biped to achieve stable running by combining local trajectory optimization with genetic optimization for hardware parameters. Saurel et al. [218] and Buondonno et al. [39] optimized the actuators of passive walkers for cyclic motions. Quadruped motion was also obtained on StarlETH, a robot with a rather complex joint dynamics, in [88]. Digumarti, Gehring, Coros, *et al.* in [71] optimized the leg design of the StarlETH robot to maximize peak speed. In [250] several simple legged-robots were designed solving a single NLP, optimizing both the hardware and motion and allowing the inclusion of task fulfillment constraints. Other works focused on the optimality of motion and design. Yesilevskiy, Gan, and David Remy [278] and Yesilevskiy, Gan, and Remy [279] designed monopeds to minimize various cost functions, aiming for energy efficiency under the optimization of different metrics. Ha, Coros, Alspach, *et al.* in [104] co-design was applied to study the relationship between motion and design selection for legged systems including different motion tasks with semplified models. The same authors in [105] proposed the use of the implicit function theorem, and sensitivity analysis, to clearly establish a relationship between optimal control (task-execution) and robot design (to be later used in optimization). The key intuition is that motion and task constraints implicitly define a manifold of valid designs recovering it allows to perform optimization on a reduced

space. The results featured optimized designs of a quadruped and a manipulator, with a final hardware validation. Finally, in [106] robot designs were optimized by changing the link scaling of the legs to follow user-defined trajectories. The framework could greatly reduce the effort of the system while performing the motion. A methodology to optimize legged robot design for tracking trajectories planned under the assumption of single rigid body dynamics was introduced in [46]. Recently in [221] a Deep Reinforcement Learning approach is used to optimize concurrently the physical design of a robot and its policy. In [91] the simultaneous synthesis of hardware and control was used to obtain skating robots. In Dallas, Machairas, Koutsoukis, *et al.* [62] a method to select optimally the design of legged systems has been introduced showcasing two sequential stages (centroidal model and quadruped robot dynamics). A computational design tool, based on co-design was presented in [69], [70]. It allowed user inputs to guide robot design in several scenarios to avoid self-collisions and perform locomotion tasks. Some following work in this domain tried also to optimize quadrupeds taking into account the control, by inverse-dynamics differentiation, [66]. In some recent work, [52], biped leg design was optimized for mono-articular or bi-articular linear actuation. The problem is split into an analytic phase for the design, with some heuristics, and a subsequent optimization using Sequential Quadratic Programming (SQP) algorithm for the task. The performance of the design is evaluated based on the optimized trajectories. Optimization targeting leg design of a high-performance platform (Skippy) was proposed in [74], [95], [96] under several different criteria. The goal of these works was to also test the simulation of the optimized hardware to possibly close some sim-to-real gaps from the design phase itself. Additionally, the Pareto set was obtained to provide additional insights into the design phase. In [73] a co-optimization algorithm was presented for the quadruped Solo, it utilized the differentiation of the motion planner for faster convergence and the imposition of arbitrary design constraints. Palacios et al. [37] used the Alternating Direction Method of Multipliers (ADMM) to optimize robot design with a focus on increasing control robustness in different scenarios, featuring the optimization of a planar quadruped bounding gait for the mini Cheetah robot [32]. In recent work, co-design has been also applied to cooperative humanoid robotics, in [215] co-design is used in a NLP to best select the hardware parameters of a humanoid robot to perform collaborative payload lifting with a human operator. In [189] the controller and the design (including closed-loop structures) of a simple manipulator arm were selected, moreover, the use of a custom hardware specification allowed a high versatility and the automatic code generation for the controller was achieved. A cascaded robust optimization approach, applied to manipulators was also proposed in [216], exploiting a staged structure ensuring optimality and robustness to hardware parameter variations. In [277] the design of a manipulator was optimized for a contact-aware manipulation task. The method features a differentiable parametrization of the hardware and meshes. In [228] the automatic generation of robots from a set of primitives was achieved by taking into account the user input and the final fabrication step. The algorithm optimized the specifications of hardware components from a database of discrete choices (made-up of structures that could be obtained with folding). The generation of designs was

proven in real and the framework could optimize structure and gaits for several goals. Co-design of robots was also applied to demonstration learning, in [94] a framework for modular robots were proposed and could choose their structure and behavior based on human demonstrations.

DATA-DRIVEN METHODS Related to evolutionary approaches and neural network control, they stated getting some recent traction in order to solve the problem of robot control. On this side, seminal work was performed in co-design by Auerbach and Bongard in [17]–[19], proposing a framework to automatically select a robot design and his mind by encoding it with neural network parameters and optimizing with an EA called CPPN-NEAT. In [103] the co-design of a system and its control policy was explored with Reinforcement Learning (RL). The agent was allowed to jointly modify environment parameters along with its policy. Also in [161] performed optimization of hardware and task in a very data-efficient way with a tailored Soft actor critic (SAC) approach [107]. One key finding is that joint learning of body design makes policy learning more efficient and leads to a higher reward. In [48], the Trust-region policy optimization (TRPO) [226] algorithm was used, similarly also in this case, the hardware was treated as a policy parameter and was used successfully on a toy 1D problem and an underactuated hand design. In [101] the generative design of legged robot topologies was combined sequentially with RL to select locomotion policies and to evolve a population of robots. Also in [23] a meta-RL algorithm was used to learn a policy for different designs. Such policy was utilized to evaluate each design for optimization, achieving close-to-optimal performance. The approach used Proximal policy optimization (PPO) [227] combined with Covariance Matrix Adaptation Evolution Strategy (CMA-ES). In the same year Schaff and Walter [220] used RL to optimize different behaviors for multi-legged systems (sprinting, obstacle crossing and wall climbing), this work used PPO to select a design-conditioned policy. In a subsequent work [219] a similar approach was also applied to soft robots exploiting the SAC algorithm to design a policy and optimize actuator placement. Another take on the problem is given in [115]: in which the design of a robot is learned to generalize over different tasks. The method involves optimizing an information-theoretic quantity to enable an agent to explore and control the environment. The method uses a Graph Neural Network (GNN) to predict the action primitive which a morphology should execute to reach a specific state. This predictive capability is used to mutate agents with high fitness, ultimately leading to the discovery of morphologies that are functional across a significant portion of the environment without requiring predefined task specifications. A focus on designing agents that facilitate learning has been posed in [248]. In this work, the information from training is efficiently used in a morphology-agnostic controller. Related to real quadruped design, recent result exploiting RL is [26], in this work, using the platform Anymal. In an initial step, a design-conditioned policy was trained with a model-free RL to control the robot in a given range of design parameters. Then, bayesian optimization was employed to find the best design given the selected policy. A data-driven approach was also exploited in [183] to select several designs for several objects to grasp via a bayesian optimization technique that leverages

The difference here is to achieve a robust "good enough" control, thus often leading to a solution far from the optimal one.

the latent space of design and control parameters for achieving higher efficiency. Related to sensorimotor skills, advancements in the problem of sensor placement for soft robots have been achieved in [249], by the use of learning approaches.

5 GOALS OF THE PROPOSED APPROACH

The ultimate goal of a good co-design framework is to accurately represent the robot, the actuators and optimize a meaningful performance metric.

Observing the several contributions in co-design literature, few papers deal with the problem of actuator selection in a physically accurate manner. One initial issue is related just to the representation of the system. To retrieve information about the control, an optimization at the torque level is needed, but this increases the number of variables and makes the problem more complex. In many co-design works, the motion trajectory is optimized (potentially on simplified models) and the torques follow the pre-planned trajectory only in the second stage, but this could lead to sub-optimal (or even infeasible) trajectories. Hence, one motivation that drove our investigation is to make use of state-of-the-art optimization techniques that are tailored to whole-body torque-control optimization (this is what is referred to as whole-body in Tab. 4). This led to a hybrid approach that uses the strengths of gradient-based methods and evolutive strategies. As a second issue, often the model of the actuator relies on some assumptions. For accuracy, a proper model of the actuator has been developed accounting for the limits and also the bandwidth (in the most recent version of the framework). Finally, the minimized metrics are generally a surrogate of the real physical quantities. For instance, to represent the cost associated with a movement, usually, the squared norm of the torque vector is used. While being a simple and reasonable proxy, it generally falls short of being physically accurate (e. g. there is a cost when the robot regenerates energy). In the work, we aim to exploit a metric that matches without approximations the energy requirements associated with the movement Additionally in co-design, the problem of robustness has often been neglected, while it may be crucial for the final implementation, also this problem will be targeted.

In Table. 4 several methods are compared, in orange, we highlight our contributions' key features compared to some selected publications in legged robotics co-design.

6 CONCLUSION

In this chapter, the problem of co-design was discussed. Preliminary, several works about design optimization of robots were presented. Then, several remarkable contributions dealing with the problem of motion generation for legged systems were shown. Finally, our analysis moved to the approaches encompassing both problems with co-design. In this latter case, a particular focus was given to co-design approaches tailored to legged robots, which were discussed and compared.

Contribution	[46]	[106]	[250]	[174]	[71]	[37]	[73]	[76]	[78]	[77]
Whole-body*				✓	✓	✓	(✓)	✓	✓	✓
Bandwidth										✓
Hard constraints				✓	✓	✓				✓
Cyclicity				✓		✓				✓
Scaling	✓	✓	✓	✓	✓	✓	✓	✓	✓	✓
Energy optimization	✓					✓	✓	✓	✓	✓
Global exploration				✓				✓	✓	✓
Mixed-integer										✓
Robustness						✓			✓	
Controller						✓	✓		✓	
Hardware validation			✓		✓					✓

Table 4: Comparison between selected state-of-the art co-design approaches for legged robots.
* Exact dynamics instead of kinematic/reduced models.

8

SOLUTION STRATEGY AND NOMINAL BI-LEVEL FRAMEWORK

In Short

In this chapter details of the co-design problem are outlined, highlighting its structure and similarity with optimal control problems. Based on this observation a solution strategy is proposed trying to meet all the high-level implementation requirements.

Contents

1 CO-DESIGN PROBLEM STATEMENT AND FRAMEWORK GOALS

The focus of the thesis is designing robots capable to perform highly dynamic maneuvers while exploring the potential of changing the robot size and selecting an optimal actuation system that minimizes energy consumption for a specific task. The design of robotic hardware is a complex decision problem involving both integer and continuous variables, multiple objectives and constraints. The interaction among design parameters, control and system dynamics makes the optimization highly coupled. Standard design methods, based on an iterative or sequential workflow, are limited and not general enough. The outcome of this research is the development of an approach that can be adapted, with minor modifications, to various legged systems. This method will not only facilitate their design but also address critical actuation limitation issues and energy-saving challenges.

Such a framework aims to optimize the overall performance and capabilities of robots, with a particular focus on:

- Robot Efficiency: Optimizing efficiency involves minimizing losses, and reducing unnecessary actions. It can be achieved through several strategies, including optimal control to optimize motor torque and power usage.

- CONTROL: Precise and feasible robot movements need to be generated including a complete model of the constraints that the actuator selection poses on the system. This is a key feature in the case of electric motors that includes the transmission and motor choice.
- ROBOT DIMENSIONS: This refers to the capability of the framework to select the robot size.

And additionally, as additional, desirable, features, it should allow:

- MULTIPLE OBJECTIVES: Considering multiple performance criteria simultaneously should be possible. For example, the framework can optimize for both energy efficiency and task completion time, or for accuracy and robustness in uncertain environments. Multi-objective optimization techniques, such as Pareto optimization or weighted sum methods, can be employed to find optimal trade-offs between orthogonal objectives.
- DATA-DRIVEN ACCELERATION: To enhance efficiency and scalability, the optimization framework should be able to reuse data. This involves utilizing data processing and machine learning techniques.

This aspect can be combined with the warmstart capabilities of the solver to decrease computation times or effort coherence

By integrating these aspects, robot efficiency, control, and scaling can systematically be improved. The framework allows for the systematic exploration of design choices, algorithm parameters, and system configurations to maximize the overall performance and capabilities of robots in given scenarios.

As can been seen in Fig. 29, complete problem depends not only on the states and controls, which need to be determined for each task, but also upon some additional design and control parameters of the system to be designed. In the same picture, the way the variables intervene in the problem is visually highlighted. The optimization variables related to the trajectories are directly influenced by the choice of the ones related to the design (i. e. as different hardware implementation results in different problem constraints, which impact the choice of state and control pairs), while it is not straightforward to find an opposite relationship. This intuition is exploited in the next section to reduce the complexity of the problem.

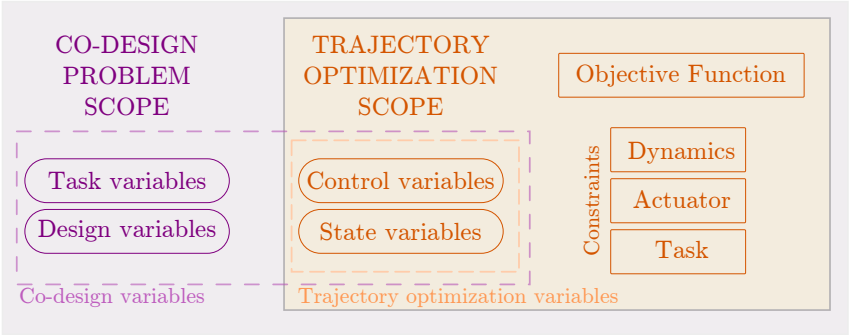

Figure 29: Co-design approach and its relationship with OCP

2 CHALLENGES OF THE PROBLEM

In addition to the computational complexity, the non-linearity and non-differentiability in the design parameters also constitute a challenge. Even when the gradient is defined, the problem may be ill-conditioned or require a good initial guess.

Moreover, as the optimization domain may be discrete, the functions are then dependent on integer parameters that are defined on discrete domains. In that case, the optimization problem becomes a mixed-integer program and requires special techniques and solvers to use gradient information (i. e. `gurobi`), since some parameters are tied to integer variables.

Another challenge comes from the non-linearity of the cost function, even if the function is continuous: the problem may have multiple local minima in the definition space. Such minima may be either absolute or local, and this can be shown with some benchmark mathematical functions, as shown in Fig. 30a and Fig. 30b. This effect with respect to the function is also called ruggedness, and requires non-local optimization strategies, in order not to fall in local minima, giving wrong results. The ideal solver will have to find all the minima and not just the local ones. Since gradient-based methods are impacted by these issues, letting the set of parameters related to the control and hardware be explored with some level of randomization allows more robustness. However, the optimization becomes slower since many more samples are needed.

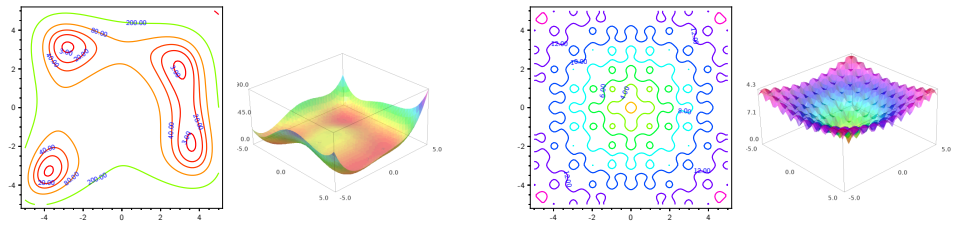

(a) Himmelblau function (b) Ackley function

Figure 30: Local minima issues for some non-convex functions

3 PROBLEM STRUCTURE: LINK WITH OPTIMAL CONTROL

For a robot to perform a specific task, a cost metric to minimize over a given time interval $[t_0, t_F]$ can be envisioned. In the most general form, this metric can depend upon a series of variables of interest. Let us define $\mathcal{D}$ the set of variables related to the platform hardware and $\mathcal{C}$ the set of controller-related parameters of the task. Using this notation and denoting by x and u the state and controls respectively, the co-design problem can be expressed as a constrained optimization problem as follows (51):

$$\begin{aligned} &\underset{x(t),u(t),\mathcal{D},\mathcal{C}}{\text{MINIMIZE}} && \Phi(x(t_0),u(t_0),x(t_F),u(t_F),\mathcal{D},\mathcal{C}) + \int_{t_0}^{t_F} \mathcal{L}((x(t),u(t),\mathcal{D},\mathcal{C}))dt \\ &\text{SUBJECT TO:} && \dot{x}(t) = f(t,x(t),u(t),\mathcal{D},\mathcal{C}) && \text{DYNAMIC CONSTRAINTS} \\ & && h(t,x(t),u(t),\mathcal{D},\mathcal{C}) \leq 0 && \text{PATH CONSTRAINTS} \\ & && g(t_0,t_F,x(t_0),x(t_F),\mathcal{D},\mathcal{C}) \leq 0 && \text{BOUNDARY CONSTRAINTS} \end{aligned} \tag{51}$$

where t_0 and t_F are the initial and final time values. The problem is to minimize the cost function $\mathcal{L}$ in (51) by finding the *best* trajectories of the control $\boldsymbol{u}$ and state $\boldsymbol{x}$, and the *best* parameters of the design $\mathcal{D}$ and control $\mathcal{C}$. This constitutes a standard OCP augmented with the pair $(\mathcal{D}, \mathcal{C})$. The task is fixed *a priori* (i. e. a target position to reach, within a fixed time) and a terminal cost Φ or a terminal constraint can be utilized to enforce it. In an optimal control problem, the solution will be affected by the so-called *curse of dimensionality* as described by Bellman [22], which states that the size of the problem increases exponentially as a function of the number of variables. A problem that already includes a high number of variables and constraints, such is the case for robots' optimal control, may become unsolvable when adding the design and control parameters.

The resolution of the problem can be highly aided by exploiting its structure. The selection of the parameters will not change with the dynamics of the system, they will be constant quantities in the optimization problem. A possible strategy is to select the parameter pair in $(\mathcal{D},\mathcal{C})$, solve the optimization problem for this pair and then assess the performance of the solution against the cost function. This strategy can be used in a bi-level optimization problem and it implies to divide the problem into two subproblems, in which the same cost function is considered by two subsequent phases, minimizing it according to different variables, one depending on the set of parameters $(\mathcal{D},\mathcal{C})$, the other one depending on trajectory optimization.

4 PROPOSED GENERAL OPTIMIZATION FRAMEWORK EMBODIMENT

In this co-optimization problem multiple hardware combinations are explored for a given task to study the design space, giving insights to the system designer since its conception phase. In the outer-loop a GA optimizes the design parameters considering their minimized optimal cost value $\mathcal{L}$ obtained in the inner loop (a trajectory optimization). The outer loop generates a population of random designs and for each design an Optimal Control Problem (OCP) is solved. After all the individuals in the population are evaluated, the outer loop proceeds with the evolution of the population, generating a new random population and propagating the information of the designs that provided the lower cost, so a higher performance. This process will then run iteratively until an exit condition is met. The use of this optimizer is quite robust and more global in the exploration. This is not generally true in the case of gradient-based co-design approaches which depend on an initial guess and may be impacted by local minima, a point discussed in [106].

The two optimizing loops work together in the sense that the outer optimization loop will select and feed the best parameters to the inner loop which in turn will select the optimal control policy for the plant and selected task. The outer loop optimizer is potentially capable of handling parameters from discrete sets, while the inner loop will be able to give the solution after setting an OCP with the dynamics of the plant.

Moreover this technique is quite general and allows also some additional modifications before the outer loop evaluates the next population.

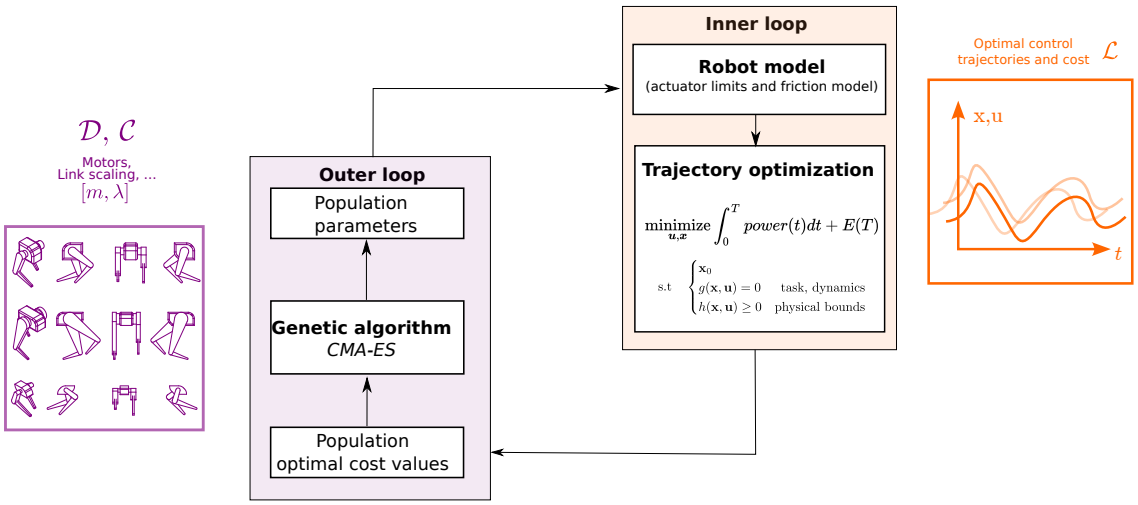

Figure 31: Co-design approach and the bi-level formulation

The proposed approach is suited to enable design optimization for a large variety of robots. The robot's design choice is parametrized by a set of hardware-related quantities $\mathcal{D}$ which fully determine its features. For a robotic system, multiple physical design parameters $\mathcal{D}$ impact the performance. These parameters are related to the geometry, material and masses of the structural part; and characteristics of the actuation system, both in terms of masses, inertia and peak capabilities.

For instance $\mathcal{D}$ includes:

- Joint position
- Link dimensions and shape
- Link material, impacting, Young modulus E and density ρ
- Structural length, masses and inertias and CENTRE OF MASS (CoM) of the links.
- Actuator choice, peak capabilities, torque and velocity limits.
- Transmission properties, for instance, gear ratio, friction, bandwidth.
- Motor mass, rotor inertia, electromechanical properties.

Some of the design variables may be discrete and this may be complicated to explore.

The control parameters $\mathcal{C}$ have the uttermost relevance, they are related to other high-level control and/or task hyper-parameters (e. g. contact timings). It may be of interest, for instance, to select a control policy, so the type of controller and task-related decisions are a nice plus to include. For instance, in the results part, some examples of variables to be optimized are in the form of phase timings for the task (e. g. contact time). Additionally, some gain scaling variables have been included for robustness to perturbation. In literature, controller parameters, such as Proportional Integral Derivative (PID) gains, have already been optimized with this approach [159], [283].

This intertwined problem needs to be broken down. The solution is performing optimization by a two-stage algorithm on a discretized version of problem (51) as shown in Fig. 31. Splitting the problem makes it tractable and was first proposed to study gait timing in [268]. Moreover, such an approach is fairly general and can be readily re-adapted, possibly to deal with high dimensional, mixed continuous-integer and multi-objective optimizations. The work-flow is structured as follows:

- An outer-loop black-box optimizer, i. e. GA, randomly samples the physical design and control parameters $(\mathcal{D}, \mathcal{C})$ for a given problem, the set of combinations is called population.
- For each combination of parameters of the population (individual), a lower-level, trajectory optimization problem is instantiated for the given task and cost function. At this stage, the co-design outer-loop variables $\mathcal{D}, \mathcal{C}$ are fixed and the problem takes the form of a standard OCP. Inside this problem, we enforce as constraints:
  - Control limits
  - Joint limitations
  - Collisions
  - Contacts
  - Task following
- The final values of the cost function are sent back to the GA, which will use this information to generate the next population to evaluate scoring *how fit* the individual is to solve the problem. After the trajectory optimization, the value of the cost function will be the lowest admissible for the specific choice of the control and state trajectory (within the limits of the solver and chosen tolerances). Such value will be returned to the outer optimizer that will use it to select new individuals in the population. This last step is connected to the first one and this loop is reiterated until convergence or an ending condition is met.

In this implementation, the two algorithms are minimizing the same cost function (which needs to reflect the hardware performance), each one specialized in a different set of optimization variables. Thanks to this nested structure, in the outer loop also the formulation of the optimal control problem can be modified to obtain even higher versatility. For instance, different locomotion modes, and different numbers of nodes can be initialized.

The selection of the most suited designs at each iteration enables a more efficient exploration of the different combinations of all parameters. The choice for a GA is motivated by the fact that co-design problems may be difficult to initialize and be impacted by local minima. The structure allows us to divide the complexity and extend some additional features to it. As it will be explained later on, with the right choice of the outer loop, it is possible to parallelize the computation of the inner loop. The guiding logic will be the outer loop which, cost function aside, will be able to collect other information from the inner loop to store or process it to improve the search (eg learning a better initial guess for the inner problem).

For what regards the optimization objective, $\mathcal{L}$, different metrics will be considered in the different problem applications.

5 CONCLUSION

The bi-level framework that was presented will be the workhorse used for solving different problems. Its characteristics, choice and high-level goals have been detailed in general. Different metrics, criteria, tools and additional components will be explained in the following to deal with three applications that try to build upon this approach playing with its capabilities and addressing specific problems.

9

DESIGN OF AN ENERGY-EFFICIENT MONOPED

In Short

A case study involving the test bed of the Solo [98] quadruped leg is used to illustrate the consistency of the method (see Fig. 35). The actuator presented in chapter 6 is used. The energy-driven cost function is formulated on the basis of the electro-mechanical actuator model. Moreover, understanding how size impacts power consumption is necessary to obtain efficient design. The modification of the robot size is performed to avoid structural weakening, an aspect that has been often overlooked in the literature. A method encompassing this problem is introduced. Thanks to these contributions, hardware can be reliably optimized.

Contents

1 ENERGY-AWARE ROBOTICS

Improved energy-aware control and planning algorithms enable autonomous locomotion and navigation capabilities at a reduced energetic cost. Moreover, on the hardware side, the development of lightweight materials, low-power electronics and more energy-efficient actuators can help limit power consumption and extend the operational time.

The two aspects can also be possibly used together in smart energy-harvesting and energy-regeneration techniques. For instance, in the case of the MIT Cheetah robot, it is possible to recover negative mechanical work by regenerating the batteries [234].

1.1 *Passivity and optimal motion*

Hardware that is optimized for energy efficiency can produce motion, potentially with no control power requirement. This concept can be seen in nature, where biological structures are made to exploit external energy sources. For example, birds of prey can exploit the streams of air to avoid moving their wings when hovering. Similarly, in [21] from experiments on dead fish bodies, it was found that also fish bodies are capable of harvesting the energy in water vortices moving upstream with no apparent energy consumption [1].

(a) 2011 Gubernare Strandbeest, credits Theo Jansen [135]

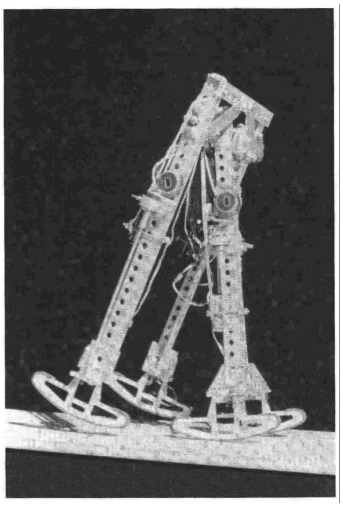

(b) Planar passive walker by Tad McGeers

This idea also transferred in legged robotics, where some moving sculptures were made to use wind energy as an external power source by Theo Jansen (Fig. 32a). Or with the passive walkers conceived by Tad McGeers (Fig. 32b) capable of moving on inclined surfaces. Also in the case of simple legged systems, optimal motions were synthetised, by taking into account an energy metric. In [202] a framework to optimize the energy efficiency of locomotion was proposed, producing several gaits. In recent work, energy optimal motion for a monoped featuring passive elements has been selected [195]. In [243] the gait energetics of a bipedal robot platform has been investigated. Additionally in [274] optimal gaits were found through contacts and impact for bipeds and monopeds running at different speeds. In [280] a passive element spine was inserted in a quadruped producing several different optimal gaits. Different speeds, under an energetic optimization criterion, led to the discovery of different gait cycles [275]. Overall,

1 Russ Tedrake's interview in Lex Fridman's podcast

improving autonomy and energy efficiency in legged robots will enhance their practicality, versatility, and endurance, allowing them to operate autonomously for extended periods while conserving energy resources. This approach is translated also in this work, where, with some tailored cost functions, the most energy-efficient trajectories and the most efficient robots are selected.

1.2 *Cost of transportation*

A commonly used criterion to assess the overall energy performance of a robot is the Cost of Transportation (CoT) (52) which according to [149], [261]. Such metric is commonly used to express the energetic economy of locomotion: and initially, it was applied in biomechanics publications to describe animal motions [223] [4], [5]. The CoT is a non-dimensional number obtained with the ratio of power used during a motion and a power expressed as the product of the robot's weight and the forward speed, it takes the following expression:

$$\mathrm{CoT} = \frac{P_{el}}{mgv} \tag{52}$$

where P_{el} is the electrical power input to the system, m is the total mass of the robot, g is the gravitational acceleration, and v is the robot's forward speed. A similar index historically was introduced by Gabrielli and Von Karman in the 50s to compare the efficiency of different vehicles [86]. In practical applications, it is common to redefine it by using averaged values over a finite time horizon which writes:

$$\mathrm{CoT} = \frac{\bar{P}_{el}}{mg\bar{v}} \triangleq \frac{\int_{t=0}^{T} P_{el}dt/T}{mg\int_{t=0}^{T} vdt/T} = \frac{E_{el}}{mg\Delta x} \tag{53}$$

Note also that (53) can be re-worked to use just quantities between the beginning and the end of the movement, as the required energy and the displacement produced, this yield to the last expression, based on macroscopic quantities [175]. By plotting the CoM versus the mass of the system m, some clustering classes and correlations appear for robots as shown in [150], [251]. So several expressions roughly represent the same idea, with slight variations, a review of the nuances can be found in [238]. Albeit being a quite popular metric in literature, it is not a quantity easy to use in custom OCP solvers. Considering (52) as running cost to minimize along the trajectory means that the velocity term at the denominator could pose issues when the robot starts from a standstill. Issues also arise for (53) when the motion has zero mean velocity (and hence when it produces no net displacement). The presence of two integral terms, one at the numerator and one at the denominator, needs to be treated carefully and cannot be used directly in the OCP formulation (an additional state may be needed so that the CoT can be expressed as a terminal constraint). Moreover, its definition is not quite general enough for our purposes (as it is mostly thought for forward locomotion modes, it does not cover other tasks, or systems, such as manipulators' motions for instance). Then the minimization of electrical power, without normalization, was considered instead.

i. e. in the sense that it depends on initial and final values, not instantaneous ones

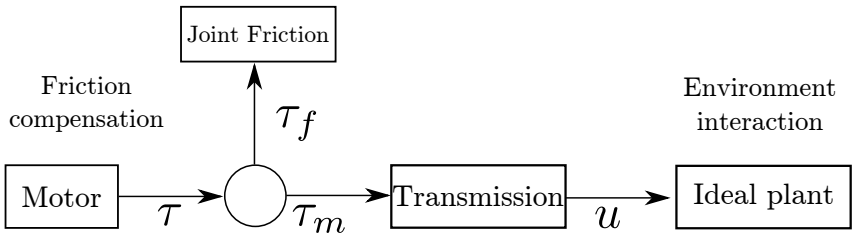

Figure 32: Scheme of the compensation of friction in the cost function

1.3 *Energy minimization*

The electro-mechanical parameters of the actuation are used to estimate the power losses in a physically-driven manner. The goal of the optimizer is to find the motion that achieves the task while minimizing the required electrical energy. A possible option to account for friction would be to include it in the system dynamics (in our case within `pinocchio`). But, as we assume to perfectly know the actuator model, this is unnecessary and we just minimize it in the OCP. From the values of the joint interaction torque u, the torque at the motor side can be obtained (also compensating for friction in the actuator as shown in Fig. 32):

$$\boldsymbol{\tau}_t = \boldsymbol{\tau}_m + \boldsymbol{\tau}_f = \frac{\boldsymbol{u}}{n} + \boldsymbol{\tau}_f \tag{54}$$

with n the gear ratio (see Fig. 32). A friction-less dynamics is used (as often done in robotic trajectory optimization) and friction just appears in the cost function. In the real system too, friction torques are usually compensated by a controller, and, from the outside, motions with friction compensation are indistinguishable from the ones obtained with friction-less dynamics. The role of the OCP is then to choose the ideal references state and control of x and u to minimize energy expenses.

POWER COMPONENTS The values of the electro-mechanical characteristics are utilized to compute the power components used as costs with the power expressed in chapter 7. The power components are summed to get the total electrical power, considering a perfect regeneration and efficiency of the electronic inverter. In the OCP, from friction-less dynamics the value of the friction compensation is reconstructed and then the overall associated power is minimized.

MECHANICAL ENERGY INVARIANCE FOR CYCLIC TRAJECTORIES The energy consumption model described in chapter 7 accounts for the non-ideal behavior of the actuators. We use the smoothed powers as running costs for the OCP. The minimum total mechanical energy needed will be a quantity that depends on the task. In some specific cases, it is not needed to directly optimize for it in the cost function. For instance, if the task consists in moving from a fixed initial state to a fixed fully specified state, the integral of the mechanical power P_m supplied is equal to the difference of the total mechanical energy between the final and the initial state and hence is a constant known value. Then the mechanical energy is fixed (i.e. independent of the chosen trajectory). This

holds also for any conservative energy component (e. g. elastic energy [178]), therefore P_m is not a quantity that needs to be added to the cost function. The periodic motions which minimize the overall dissipated power are obtained. For any periodic trajectory Ω, the electrical energy equals the integral of the losses ($P_{el} = P_f + P_t$). Therefore, it is not necessary to minimize explicitly the mechanical power because its circuitation is a conserved quantity and equals the difference in mechanical energy between the final and initial state (which is state-dependent and hence zero by definition of periodicity):

$$\oint_{\Omega} \mathbf{u}^{\top}(\gamma)\mathbf{v}_a(\gamma)d\gamma = (\mathrm{E}_{mec} = \mathrm{E}_{kin} + \mathrm{E}_{pot})|_{\mathbf{x}_0}^{\mathbf{x}_T} \triangleq 0 \text{ as } \mathbf{x}_0 = \mathbf{x}_T \tag{55}$$

This result can also be extended for semi-periodic trajectories. In particular, we consider the case in which joint velocities are the same and only the x position of the robot base changes. Any translation of the base along x is tolerated as it results in no net change in potential energy because:

- the base lands at the same z position it started from,
- the actuated joint position trajectories are cyclic.

This is a sufficient condition: the final height of each link CoM is equal to the initial one, so no difference in potential energy is induced, and kinetic energy is conserved as there is no difference in state velocity (and the joint space inertia is invariant to base translations).

2 SYSTEM MODEL

2.1 *Motor parameters*

this is an acceptable approximation for the type of sytem we consider, especially considering that for fabrication a choice needs to be done on the real set of motors e. g. choosing the one closest in terms of mass and characteristics.

Following the methodology proposed in [278], [279], the characteristics of the PMSM are parametrized as a function of the motor mass m_m [kg], this is done with data from similar motors from different manufacturers (*Antigravity*, *Turnigy*, *MultiStar* and *PropDrive*). This provides a model to describe the performance of the drone motors used for the actuators in ODRI [98]. The final design can either be chosen from the catalogs (e. g. according to off-shelf availability) or custom-built (as for the motors of MIT Cheetah [28]). With the exponential regression (56), the peak torque of the real actuator was found with about 15% surplus:

$$\begin{cases} \text{Stall torque} & \tau_{max} = 5.48\ m_m^{0.97} & [\text{Nm}] \\ \text{Motor constant} & K_m = 0.15\ m_m^{1.39} & [\text{Nms}] \\ \text{Rotor inertia} & \mathcal{I}_m = 7.19 \cdot 10^{-4}\ m_m^{1.67} & [\text{Kg m}^2] \end{cases} \tag{56}$$

The motor bodies are considered as localized mass m_m and the effect of their inertia $\mathcal{I}_m$ is included in the dynamics as suggested in [81], through a modification of the joint mass matrix $\mathbf{M}(q)$. This step is neglecting some components of the inertia tensor of the

motor, as they could not all be easily recovered with a parametrization. This is good approximation for drone or pancake motors, which may not hold in the case the motors possess a non negligible inertia around the other axes e. g. very long motors.

$$\mathbf{M}_{\text{corrected}}(q) = \mathbf{M}(q) + \underbrace{\begin{bmatrix} n_0^2\mathcal{I}_{m,0} & 0 & \dots & 0 \\ 0 & n_1^2\mathcal{I}_{m_1} & \dots & 0 \\ 0 & 0 & \dots & 0 \\ 0 & 0 & \dots & n_{nu}^2\mathcal{I}_{m_{nu}} \end{bmatrix}}_{\text{correction term}} \tag{57}$$

2.2 *Friction*

Modifying the transmission (i. e. its gear ratio n) impacts the actuator friction. The approach is to modify the identified parameters for a single reduction stage with a gear ratio of $\eta = 3$ (which corresponds to a half-stage of the Solo actuator Fig 25). For this nominal value, viscous friction b_0 and Coulomb friction $\tau_{\mu,0}$ are known on the input side. Then, a new gear ratio can be obtained, by thinking of stacking together multiple identical transmission stages. With a series of k identical stages with the same gear ratio η, the total gear ratio n from input to output is obtained as

$$n = \eta^k \tag{58}$$

In this passage, we extend the reasoning to the continuum, in general, this is to capture the main effect of the modification in the QDD range.

The friction of each stage is considered proportional to the input torque. Intuitively, a higher input torque can be obtained by increasing the number of actuators working in parallel with a similar belt type and reduction η. With this approximation, the friction will be scaled proportionally to the torque. Also in practice, higher torques need wider belts and pulleys thus increasing the friction. A similar consideration was used also in [279] for gearboxes. Coulomb friction of a stage is then proportional to the maximum input torque. By reporting the Coulomb friction for each stage i to the motor axis, considering the reduction stack, the overall Coulomb friction on the motor side is:

$$\tau_\mu = \sum_{i=0}^{k} \frac{\tau_{\mu,0}\eta^i}{\eta^i} = k\tau_{\mu,0}, \quad \text{with } k \in \mathbb{N} \qquad \tau_\mu \propto \tau_{max} \tag{59}$$

Hence τ_μ is at the same time linearly proportional to the number of stages and to the motor torque. Extending this reasoning to a continuous space yields:

$$\begin{aligned} k &= \frac{\log(n)}{\log(\eta)} \in \mathbb{R} \\ \tau_\mu &= k\tau_{\mu,0} \end{aligned} \tag{60}$$

Any reduction ratio corresponding to a non-integer number of stages in the design phase be approached with slight variations in the number of teeth of the pulleys, which

can be adapted before system implementation. Here just the main effect of the actuator modification is captured. For the viscous friction constant, across the stages, each subsequent axis i has a lower angular velocity and the torque reported to the motor axis is also reduced by the same factor. So the overall torque on the motor axis resulting from all the viscous friction in the transmission is given by:

$$\tau_b = \sum_{i=0}^{k} \frac{b_0 \omega_m}{\eta^{2i}} = \underbrace{\left(1 + \frac{1 - \eta^{-2k}}{\eta^2 - 1}\right) b_0}_{b} \omega_m \tag{61}$$

The damping coefficient b, from the analytical form, is almost equal to b_0 since for $\eta^2 \gg 1$ each stage is adding a negligible contribution. This is also supported by the low value of the identified damping friction b and the small values of the gear ratio n for the envisioned QDD application.

2.3 *Parametric actuation model*

The actuator technology is detailed in chapter 6. For this hardware, a parametric model is used to find the actuator friction (damping $\mathbf{b}$ and Coulomb component $\boldsymbol{\tau}_\mu$) and motor properties (rotor inertia, winding resistance and motor constant). With the values obtained, the dynamics of the system will be modified by:

- modifying joint inertia adding the rotor inertia
- adding the motor mass to the link
- changing the cost function power-related parameters

3 ROBOT SIZE AND SCALING CHOICES

Several quadrupedal designs, including commercial and research platforms, have been developed, as seen in chapter 2. The ground-breaking work of some research groups showed the possibility of achieving back flips and athletic behaviors, with smaller-sized quadrupedal platforms. Smaller quadrupeds are capable of more dynamic behaviors (e. g. stepping faster and performing backflips). On the other hand, bigger quadrupeds can climb over obstacles and may be more useful in practical applications in human environments. A natural question arises: how can quadruped robots be designed so that they can perform a range of dynamic tasks? To make quadruped robots more useful for real uses, two potential avenues exist. One approach is to enhance the robustness and affordability of existing expensive, bigger solutions. Alternatively, also optimizing the scale of smaller robots should be possible. To do so, our approach is to change the link structure as exemplified in Fig. 33. Two mechanisms are considered: a linear scaling of the link along its main dimension (62) and a homogeneous scaling of the cross-section in the two directions (63). In the analysis, we use a cylinder as an approximation of the link geometry, but similar equations can be found also in the case of more complex shapes. Two scaling factors are introduced:

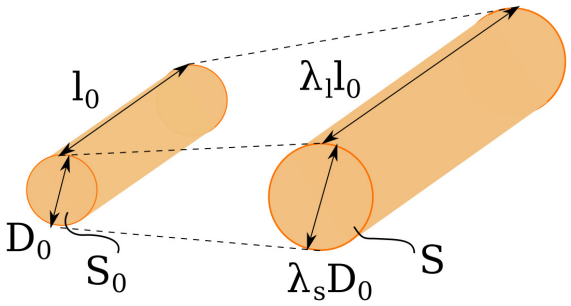

Figure 33: Scaling transformation for one limb

- λ_l with respect to its length,
- λ_s in both directions of its cross-section.

If the nominal model has a limb main dimension l_0 and a cross-section area S_0, the scaled version has limb dimension can be found as:

$$l = \lambda_l l_0 \tag{62}$$

In the case of the section area, the relationship expresses as follows:

$$S = \lambda_s^2 S_0 \tag{63}$$

It follows that the scaling factors become:

$$\lambda_s = \sqrt{\frac{S}{S_0}} \tag{64}$$

$$\lambda_l = \frac{l}{l_0} \tag{65}$$

There are some caveats when dealing with structural shaping: the robot link shape cannot be modified freely because this might yield a weak and unusable design. Thus, we exploit the current knowledge of the system under the following simplifying assumptions:

- The same material is used, and no material property will change (e.g., density ρ, Young modulus E).
- The shape of the system is fixed, only the aspect ratio can change: for each body, we consider a homothetic scaling along the principal length with a ratio λ_l and uniform cross-section dimension scaling ratio λ_s with respect to the nominal sizes.
- For structural integrity the deflection δ, normalized with respect to the principal link length l, must be kept constant across the scaling.

$$\frac{\delta}{l} \propto \frac{Fl^2}{YE} \propto F\frac{\lambda_l^2}{\lambda_s^4} \propto ma\frac{\lambda_l^2}{\lambda_s^4} \propto a\frac{\lambda_l^3}{\lambda_s^2} \tag{66}$$

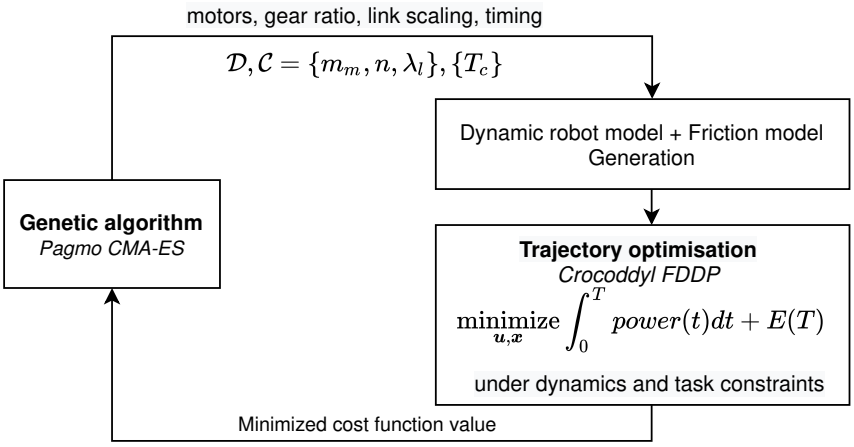

Figure 34: Simplified scheme of the bi-level implementation with CROCODDYL.

Such a quantity depends on section inertia moment of area $Y[\mathrm{m}^4]$and the inertial load F, which scales linearly with the mass ($m \propto \lambda_l \lambda_s^2$), and the acceleration of the link a.

The last requirement, under Froude dynamical similitude [5] (a constant across scaling), results in the relationship

$$\lambda_s = \lambda_l^{3/2} \tag{67}$$

If such scaling law is used as a constraint, the design variables are reduced (the section scaling would depend on the length scaling) moreover, structural integrity is enforced. This choice penalizes larger structures even more than geometric scaling ($\lambda_s = \lambda_l$). Other, more favorable, scaling choices, would not make the moving inertia increase this much, and may be adopted losing some safety margin. Another possibility is to make the structure lighter with topology optimization in the second stage. In our scope, this is not considered and the focus is on relatively small modifications from the nominal design. Under these assumptions, the mass and the inertia tensor of the bodies that build the model are modified consistently to the transformation, as well as all the lengths that are involved in the problem.

4 IMPLEMENTATION

Our first framework implementation, which can be seen in Fig. 34, a local gradient method DDP is used for the inner loop and CMA-ES for the outer loop, these two choices are briefly explained here. For trajectory optimization, this work uses CROCODDYL, an open-source library developed for the optimal control of legged robots [165]. In particular, we use the Feasibility-driven Differential Dynamic Programming (FDDP) algorithm, which is more robust to the initial guess than the classic DDP. For the robot dynamics modeling and computations the `pinocchio` library is used [41], [42]. The gradients and Hessians of the highly nonlinear power cost are analytically derived and used through custom cost classes. Additional constraints are introduced as penalties in the cost func-

CROCODDYL *actually implements an algorithm closer to iLQR as the second order derivatives of the dynamics are not used. In the energy cost we use the exact Hessians, as generally they are obtained with Gauss approximation*

tion. This is actually necessary just because Crocoddyl cannot handle hard equality or inequality constraints. The latter are approximated with penalty functions that are null, as long as the values are within the limits, and grow quadratically when the limits are violated. This is done for the friction cones cost, control bounds and position limits, while the terminal constraint is enforced with a high penalty. Dealing with cost constraints is moreover possible in DDP with squashing functions [255]. For genetic optimization the `Pagmo` library from European Space Agency (ESA) [134] is exploited for its versatility and the variety of interchangeable algorithms. Among them, the black-box CMA-ES [108] is selected to optimize the co-design parameters. The reasons for this choice are its good convergence properties and its capacity to avoid local minima. The same algorithm was previously chosen for the design of robotic feet [164] and other integrated design problems [89].

Another interesting feature of this library is in some additional evolutionary mechanism. For instance, in order to avoid initialization issues, it is the possible to evolute different populations on different "islands" and use "migration" across the island.

5 RESULTS: MONOPED JUMP

5.1 *Case Study Model*

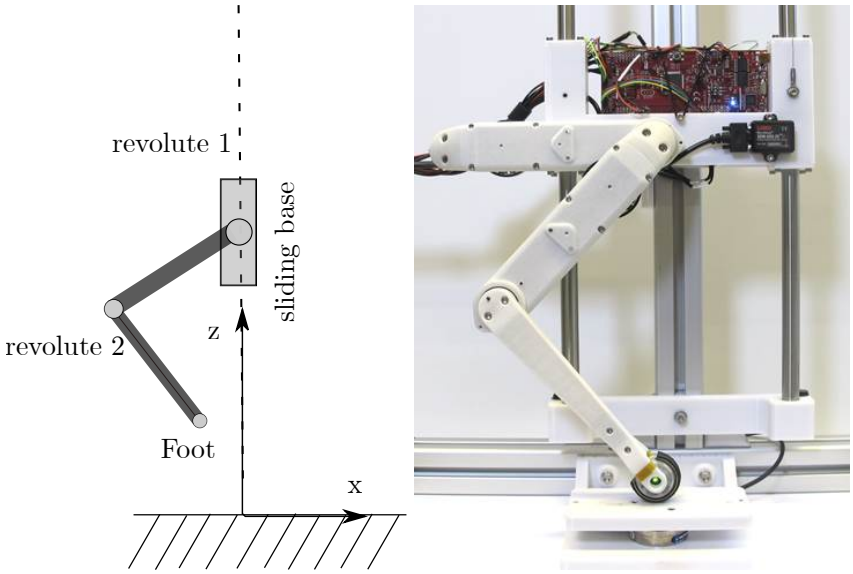

Figure 35: Structure of the monoped and the real platform used in [29]

The presented approach is applied to the case of a jumping monoped, whose body is constrained to move along a vertical prismatic joint (see Fig. 35). This model reproduces the testbed of the Solo robot leg [29]. Its underactuated dynamics, the contact constraints and timing issue, make it a minimal, yet complete, benchmark case of a legged robot. The leg includes two actuated revolute joints and a body with mass m_b =0.37 kg.

TASK FORMULATION The chosen task is a jump, with a fixed completion time of $T = 1$s. Initially, the robot is standing in contact with the ground and with a straight leg

for a total duration of time T_c. After this phase, the robot must jump, in order to reach the target position $\boldsymbol{p} = [0, 0, 0.64]^\top$m with the foot. The reaching task is expressed as a terminal cost on the complete state: the foot must reach $\boldsymbol{p}$ with a fully stretched vertical leg configuration and null velocities (the base position is found according to this final configuration). In particular, penalties on the control bounds and on the penetration of the ground were introduced as running costs. Joint position and velocity limits are also added in a similar way. The energy term is computed as a running cost, consisting of the integral of the power losses. The weights of each term of the cost function are shown in Table 5. For integrating the system dynamics we have used an explicit Euler integration scheme with time-steps of $\Delta t = 10^{-3}$s. This choice is motivated by the fact that Euler integration may introduce a high error in the reconstruction of the total energy needed, so a finer discretization is necessary.

Table 5: Jump problem weights

TYPE	COST COMPONENT	VALUE
Terminal cost	Task completion	5e3
Running cost	Power	2e0
	Torque bounds	1e1
	Penalty Ground violation contact phase	1e6
	Penalty Ground violation flying phase	1e3

DESIGN VARIABLES: In the design parameters are included:

- motor mass $\boldsymbol{m_m} \in [0.05, 1]$kg,
- gear ratios $\boldsymbol{n} \in [3, 20]$,
- scaling of the links $\pm 20\%$ with respect to the nominal leg design $\boldsymbol{\lambda_l} \in [0.8, 1.2]$.

To reduce the number of design variables, the same motor and gear ratio are used for all joints. In the task-related control variables, the contact time $T_c \in [0.2, 0.8]$s is included.

5.2 *Numerical Results*

With respect to the optimal solution found fixing $T_c = 0.7s$ and using the current design version of the actuator that will be referred to as the Nominal Case (A), the following two optimizations are considered:

- Actuator-Only Case (B): The scale and the timing are fixed ($\lambda_l = 1$ and $T_c = 0.7$s), whereas the actuator parameters m_m and n are optimized.
- Complete Case (C): The size, the timing and the actuator parameters are optimized.

The results obtained for these cases are described and compared in the following.

ACTUATOR-ONLY CASE To better understand the impact of the actuator choice, a preliminary study was made by fixing $T_c = 0.7$s and $\lambda_l = 1$. In this case, given the small dimension of the search space, the optimization was performed directly by sampling the space $m_m \times n$ with a 19×18 uniformly spaced grid as shown in Fig. 36. In this case the routine took 1 hour and 19 min, with an average time for trajectory optimization of 14.72s. This figure depicts the trade-off between n and m_m. It appears that small motors with very low reduction lead to high costs because they produce $\boldsymbol{\tau}_m$ at the expense of an increased P_t. At the same time high values of m_m and n seem to be sub-optimal since they induce an increase of P_f and of the mass to be moved. Therefore, for fixed scaling and timing, the best combination was obtained in between those extreme cases, with $m_m = 0.1\text{kg}, n = 12$. Additionally, for any choice of m_m there seems to exist an optimal value of n, ideally providing the best trade-off between higher friction torque $\boldsymbol{\tau}_f$ and increased output $\boldsymbol{\tau}_m$. The optimal trajectories of the robot links (Fig. 37b) and of $\boldsymbol{x}, \boldsymbol{u}$ (Fig. 37c) highlight how the system in the contact phase converts the potential energy of the floating base into kinetic energy by letting it slide downward. At the same time bending the knee provides a way to apply a reaction force to push the system upward during the jumping phase.

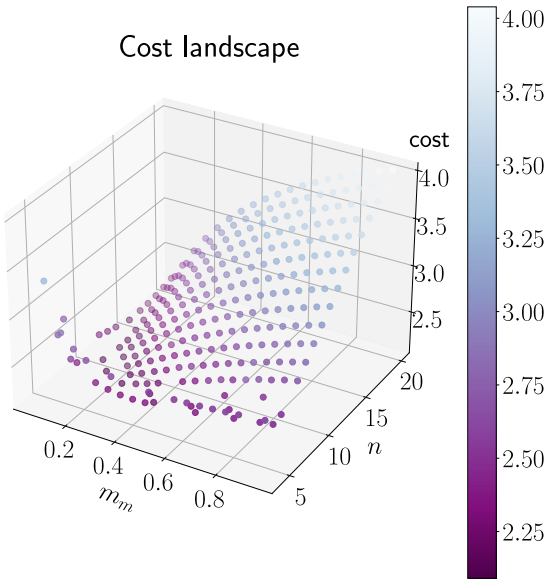

Figure 36: Cost landscape versus m_m and n, Actuator-Only Case

COMPLETE CASE Here the idea is that, by exploiting additional degrees of freedom, we can find optimal design and control for the system. In this case, after evolving a population of 10^2 individuals for 10 times, for solving the co-design optimization, for

Table 6: Benchmark of the energy minimization

TYPE	NOMINAL CASE	ACTUATOR-ONLY CASE	COMPLETE CASE
Mechanical Energy	0.96 J	1.32 J	1.47 J
Joint friction	0.87 J	1.60 J	0.38 J
Joule dissipation	4.37 J	1.87 J	0.53 J
Total	6.19 J	4.79 J	2.38 J

10^3 trajectory optimization problems, the overall time was about 9 hours, taking on average 33.72s for each CROCODDYL solver call. The optimum is found for:

$$\begin{cases} m_m & = 9.85 \cdot 10^{-2} [\text{kg}] \\ n & = 4.5 \\ \boldsymbol{\lambda}_l & = [0.83, 0.99] \\ T_c & = 0.729\text{s} \end{cases} \tag{68}$$

The actuators have a higher mass and a lower gear ratio. While the second link is close to the nominal length, the first one almost hits the lower bound of its search space. The optimal trajectories of the frames (Fig. 37b) and of $\boldsymbol{x}, \boldsymbol{u}$ (Fig. 37d) are quite different from the ones found as the optimal solutions of the Actuator-Only Case. In the Complete Case, having a lower n allows higher joint velocities without incurring an excessive P_f. This, together with the structural change, allows the joint torque to be reduced compared to the result of the Actuator-Only Case, Fig. 37c.

DISCUSSION

The total energy for the Complete Case is reduced with respect to both the Nominal Case and the Actuator-Only Case as shown in Table 6. As expected, the Complete Case is showing the best improvement, around 61.5%, from the Nominal Case. The mechanical energy for the Complete Case is higher than the reference because motors are twice as large, while the limb size is only slightly changed (17%). This is counter-intuitive and reflects the fact that Joule effects may be extremely detrimental for small motors, as can be seen in the Nominal Case. The Complete Case has much lower friction losses, which can be explained by a lower reduction and lower $\boldsymbol{u}$ concerning the Actuator-Only Case, which minimizes the losses from the Joule effect. The effect of timing (Fig. 38b) is less trivial to observe and discuss, but there seems to exist a minimum of around 0.729s. Higher values may not give enough time to the flight phase to reach the goal, while smaller values would not allow applying efficiently a force on the ground. In Fig. 38a we can appreciate the convergence of the optimization for the Complete Case, as the

number of iterations increases there seems to be a diminishing return in the improvement of the cost.

6 CONCLUSION

In this chapter, we have presented the computational structure we proposed and implemented for co-designing legged robots, which constitutes our first contribution. The results show that it is possible to exploit the trade-offs between the robot structure, the actuators and the control to achieve a given task with minimal energy consumption. Design parameters aside, it was also possible to optimize the contact timing of the task of the task together with the rest of the variables. This approach can be applied to a variety of legged systems, considering even more complex design choices and metrics. However, since the optimization is computationally expensive and the complexity would increase even further, strategies to make the computation faster were needed. This steered part of the work to the parallel evaluation of the GA. Additionally, more complex multi-objective strategies may be necessary to find the best design as in [7], [266]. It was also found out that the OCP resolution using CROCODDYL could be rather brittle to tuning parameters and this motivated the search for more robust methods. In this work, the information on actuator bandwidth was missing. A reformulation of the problem to include also such limits was achieved, as presented in the next two chapters.

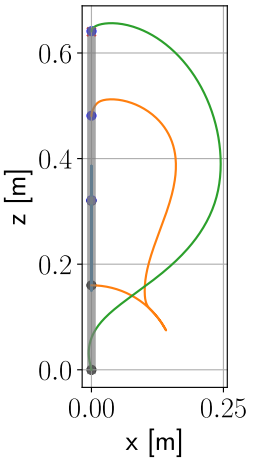

(a) Actuator-Only Case

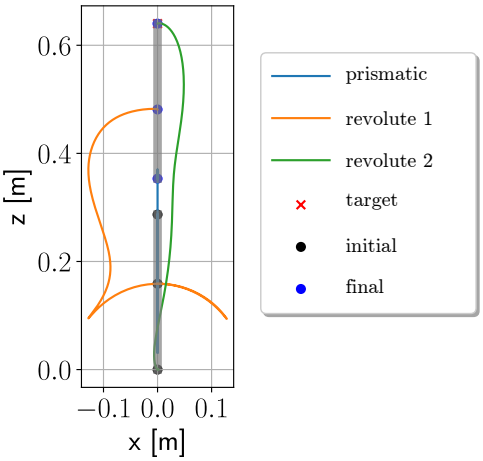

(b) Complete Case Motion

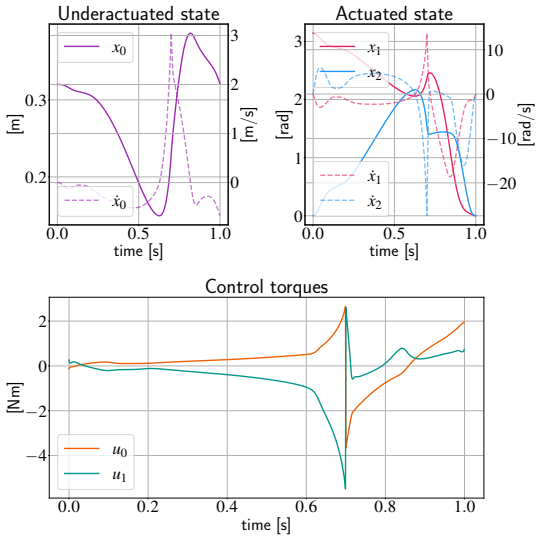

(c) Actuator-Only Case

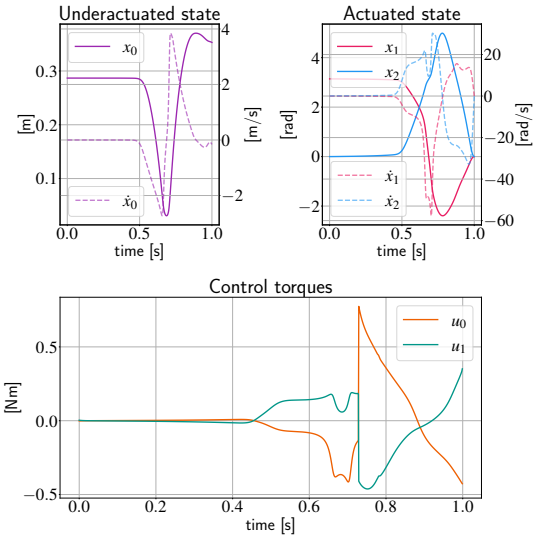

(d) Complete Case

Figure 37: Optimal solution in terms of state and control

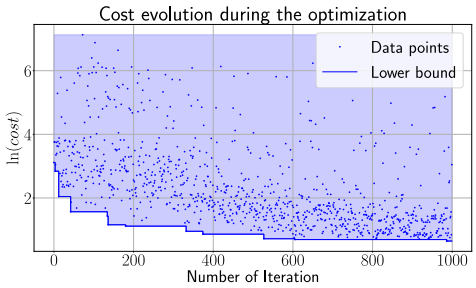

(a) Cost evolution versus the iterations

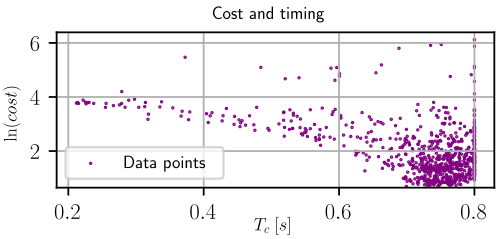

(b) Effect of timing on the cost

Figure 38: Complete Case: CMA-ES optimization

10 ROBUSTNESS ANALYSIS

In Short

Starting from the results presented in the previous chapter, the following questions arise: How robust is the found optimal trajectory? Can we use it on the system zero-shot? Can the solution be used for practical applications in real where noise is present? To find an answer to these issues, we proposed to modify the framework to take into account perturbation and a feedback controller in the co-design framework. Our strategy is detailed in this chapter. After a brief comparison of similar works in literature, the method is presented. We use the information from the inner loop in a series of perturbed simulations introducing a new robust metric. This is made possible by the structure of our framework that we modified on purpose. The implementation is explained in detail, encompassing the technical choices. In a conclusive part, some results are shown for the robust co-design of a monoped hopper and a serial manipulator.

Contents

1 ROBUSTNESS OF MOTION IN ROBOTICS

Robustness can be defined as the ability of a system to mitigate the impact of uncertainty while performing a plan. A common approach to deal with the stability of perturbed complex robotic hardware is to optimize a metric that represents the sensitivity of the trajectory to perturbation. This can be done in open-loop [173] or with closed-loop sensitivity analysis [34], [93]. Both options rely on custom-made and differentiable cost

formulations that increase the complexity and nonlinearity of the problem itself. In the same way, another work was dedicated to the selection of robust limit cycles for the motion of passive quadrupedal systems [203]. The importance of the natural dynamics of the systems and their impact on robustness was also studied in [113]. In this paper, instead of focusing on self-stability and the basin of attraction of stable trajectories, the focus was put on the the viability of the robust solution. This provides another interpretation of the link between a given design and its stability properties, which remains a problem still open. Another possibility to account for robustness is via Stochastic Programming (SP), in which the optimal trajectory is found for a set of perturbed scenarios [35], [36], [176]. These approaches produce motions that can be replayed more easily on the system, even in the case of unmodelled dynamics. However, such methods do not scale favorably as the dimension of the problem increases significantly for each additional scenario. Another possibility is to include the controller in the optimization problem, with additional decision variables. However, optimizing the controller is a hard problem and cannot be done on high-dimensional systems. Especially in the case of co-design, this becomes prohibitive in terms of computational complexity, because of the already large state dimension and time horizon [33], [67]. A technique that was proposed in [37] is the optimization of several perturbed scenarios with the ADMM, also taking into account the optimal controller selection. Thanks to this approach the complexity of the overall problem can be greatly reduced, and a larger number of perturbed scenarios can be explored. Controller optimization is often performed with some assumptions such as the use of reduced models [214], sequential optimization [187] or constant gains along the trajectory. In the domain of co-design, some heuristic approaches to generate controllers, such as PD gains tuning, have also been used after the optimal trajectories were found [72]. In addition, swarm exploration [200] and multi-objective co-design with gain tuning have been proposed in the past, but without specifically addressing robustness [127]. On the control side, in [265] the impact of both control and hardware selection has also been studied to minimize its impact on the task execution. Recently in [167] a preliminary result was achieved by considering trajectory stabilization in the design phase for simple underactuated systems around a set point of the state space. Our approach shares some similarities to the technique of *domain randomization* used in RL [254], which aims to learn a control policy that performs well with a variety of (possibly perturbed) robot models. Instead, our approach tries to discover the hardware that leads to the locally optimal linear controller that can perform at best under different perturbations. However, robustness remains challenging in co-design, while being crucial to ensure the practical applicability of the found solutions. This becomes even more challenging for inherently unstable systems, such as legged robots. Our previous results were mainly targeting the adequacy of the hardware for optimizing the motion. However, the optimal trajectories may be unfeasible in a real system, e. g. , as the system cannot stabilize external perturbations due to unmodeled dynamics, noise, delays, saturation or actuator dynamics. So, even if optimality is still a very important aspect, robustness needs to be considered as well before the real system integration.

2 ROBUST BI-LEVEL CO-DESIGN OPTIMIZATION SCHEME

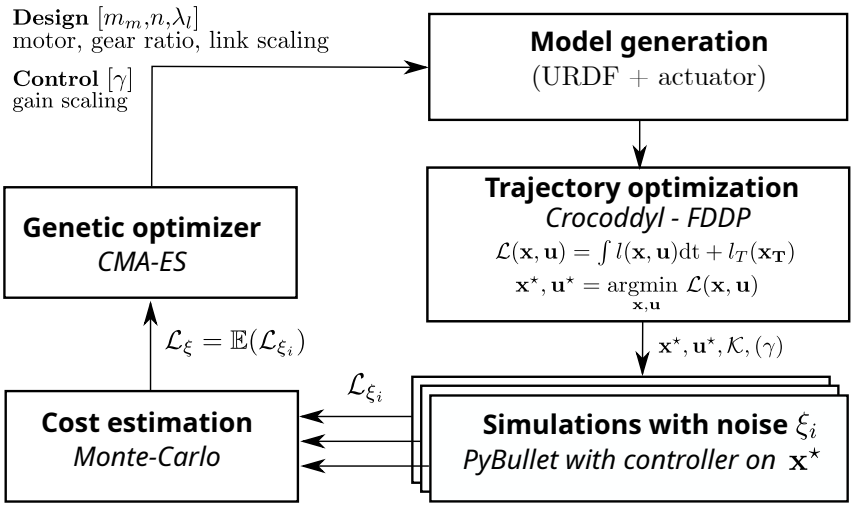

Figure 39: Robust bi-level scheme with additional simulations

Some modifications to our co-design algorithm are added to ensure robust performance and faster implementation. The bi-level optimization scheme is parallelized (parallel evaluation for CMA-ES [273]). Moreover to account for robustness, instead of the minimized cost, in the outer loop, a metric that averages the performance of the controller over multiple simulations [59] (each one including noise and the actuator model) is used. In these simulations, the system is stabilized around an optimal trajectory with the Riccati gains [63], automatically computed by the DDP algorithm, to avoid the extra computational complexity of explicitly optimizing for a control policy. Much better scaling of the algorithm is achieved (introducing perturbed scenarios in simulation is cheaper than in OCP) if compared to the other approaches optimizing for the controller's robustness directly. This comes at the price of the blindness of the inner loop (DDP) to perturbations, which can be limiting as the nominal references are selected in a way that does not consider them explicitly. Nonetheless, our tests show promising results for the design of an energy-efficient robot manipulator and a jumping monoped, which are performing better under perturbations. Finally, in the outer loop it is still possible to further optimize the controller: the explicit optimization of the proposed state-feedback controller scaling leads to a robustness improvement.

The robustness metric is obtained by adding a simulation step with perturbations and a controller as shown in Fig. 39 and in Algorithm 1 line 9.

IMPLEMENTATION: As usual, in an outer loop, the co-design parameters (hardware and optional gain scaling γ) are optimized with CMA-ES. Initially, a population pop of N_{pop} possible robot hardware configurations are randomly initialized. Then, for each set of parameters, $params \in pop$, a model of the robot is generated and the corresponding OCP is solved, optimizing the reference trajectories. Each optimal trajectory $\mathbf{x}^\star, \mathbf{u}^\star$ is

Algorithm 1: Bi-level optimization

Input : N_{gen}, N_{pop}, N_{sim}, tol, $setup$
Output: $file$
`Initialization:`
$N_p \leftarrow 0$
$population \leftarrow$ random N_{pop} combination of co-design parameters
`Outer loop:`
while $N_p < N_{gen}$ OR *stop condition* $\leq tol$ **do**
  `Inner loop:`
  $\mathcal{L}_\xi \leftarrow [\,]$
  for $params \in population$ **do**
    $model \leftarrow$ `initRobotModel`$(params)$
    OCP $\leftarrow$ `initOCP`$(model)$
    $\mathbf{x}^\star, \mathbf{u}^\star, \mathcal{K} \leftarrow$ `solveDDP`$(params)$
    $\mathcal{L}_\xi$`.append(`$\texttt{simulate}(params, \mathbf{x}^\star, \mathbf{u}^\star, \mathcal{K}, \gamma, N_{sim})$`)`
    $file \leftarrow params, \mathbf{x}^\star, \mathbf{u}^\star, \mathcal{L}, \mathcal{L}_\xi$
  $population \leftarrow$ `evolveCMEAS`$(population, \mathcal{L}_\xi)$
  $N_p \leftarrow N_p + 1$

then tracked in N_{sim} simulations with a controller using the Riccati gains $\mathcal{K}$ computed by DDP and optionally scaled by a linear coefficient γ. Each simulation includes a perturbation source ξ acting at the joint torques. To solve the OCP and obtain the Riccati gains, `crocoddyl` [165] is used. A custom `URDF` [208] is shared between the OCP and the simulator `PyBullet` [59]. It is generated parametrically using the Robot Operating System (ROS) module `xacro` [193], [209]. Moreover, the robot model corresponding to *params* is tested in simulations that include a model of friction and actuator dynamics. The problem cost function $\mathcal{L}$ is then averaged on the ensemble of N_{sim} simulation trajectories $\mathbf{x}_\xi, \mathbf{u}_\xi$ with a Monte-Carlo approach to obtain the robust metric under perturbations $\mathcal{L}_\xi$ as in (70). Then, the outer loop gets the values of the robust cost after the simulation step. With this information, a new population is generated and the outer loop keeps iterating until a termination condition is attained. In the implementation, for each generation, the collection of the costs $\mathcal{L}_\xi$ is parallelized asynchronously leading to a computation speed-up. Unlike in stochastic optimization, the number of perturbed scenarios can be rather high (up to 10^3), at a reduced computational cost of multiple simulation runs (linear in the number of time-steps and simulations $O(N_{sim})$).

2.1 *Selection of the local state feedback controller*

Many approaches can be applied to perform feedback control of unstable and underactuated systems. A promising one, used on real systems, is to re-plan online the ideal trajectory using Model Predictive Control (MPC) [177], [201]. Another way is to learn offline a robust control policy using RL. This method is quite interesting as it automatically produces robustness in the synthesized policy and has seen some interesting

application in the domain of co-design (even if not targeting actuator selection). These two methods are computationally expensive and often require problem-specific tuning that limits their use for co-design. Furthermore, if the goal is to treat local deviations from the reference trajectory, the methods may be unnecessarily too complex. Close to optimality, the dynamics can be linearized and the MPC controller is then equivalent to a local linear controller. This makes it possible to follow a pre-planned trajectory while counteracting small disturbances [63]. This consideration is used in our approach to make the problem tractable inside our framework. Riccati gains prove to be a natural way to synthesize a local controller around the optimal trajectory. For the unconstrained Linear Quadratic Regulator (LQR) problem, such gains are optimal, as detailed in [241], and an extension may be possible also with equality or inequality constraints. To follow the reference $\mathbf{x}^\star$ from $\mathbf{x} \approx \mathbf{x}^\star$, the control $\mathbf{u}$ includes a feedback term linear with respect to the state error:

$$\mathbf{u} = \mathbf{u}^\star + \gamma \mathcal{K}(\mathbf{x} - \mathbf{x}^\star) \tag{69}$$

Actually, Riccati gains could be also recovered through sensitivity analysis. However from first investigationst the resolution of DDP problem seems to recover them also with a lower computational cost.

The gain matrix $\mathcal{K}$ maps state deviations to corrections of the control input. Such matrix can optionally be multiplied by a gain scaling factor $\gamma \in \mathbb{R}$, ($\gamma = 1$ by default). This controller requires almost no tuning once the OCP is solved with DDP, contrary to other techniques such as PD control with gain scheduling. Furthermore the scaling parameter is to avoid stiff or weak gains and can be tuned automatically. A drawback is that this feedback is guaranteed to work only in the vicinity of the optimal trajectory. If the perturbations on $\mathbf{x}$ are too large, or if the dynamic is too nonlinear, or chaotic, these considerations may not hold anymore and other strategies must be used instead. This controller was preliminary validated for robustness in simulation with a serial manipulator robot model and a monoped, where the perturbations are coming from heavy objects thrown at high speed to the robots video. Additionally several sources of noise have been tested, both in the joint positions and torques. The take is that that the local policy performs better than the simple controllers that can be selected otherwise.

The reason behind γ is to introduce a policy parameter, as the policy is not directly an optimization target anymore, but obtained through DDP.

3 ENSEMBLED FINAL COST

In the outer loop, the robust cost metric $\mathcal{L}_\xi$ considers an ensemble of joint torque perturbation sources for each simulation $\boldsymbol{\xi} \in \mathbb{R}^{N_{sim} \times n_u \times N}$, where n_u is the number of actuated joints and N the number of time steps. A joint torque noise realization $\boldsymbol{\xi}_i$ with $i \in \{0, ..., N_{sim} - 1\}$ acts on the ideal joint torque $\mathbf{u}^\star$, proportionally to its value: $\boldsymbol{\xi}_i \sim \mathcal{N}(0, \sigma^2)\ \mathbf{u}^\star$. This noise model was chosen as it was found that the source of noise does not significantly change the robust solution in [68]. Given $\boldsymbol{\xi}_i$, the state trajectories $\mathbf{x}_{\xi_i}, \mathbf{u}_{\xi_i}$ in simulation with controlled torque are used to re-evaluate the cost function $\mathcal{L}(\mathbf{x}_{\xi_i}, \mathbf{u}_{\xi_i})$, (encompassing both task fulfillment and energy minimization). This metric shares similar information with the optimal cost from the OCP ($\mathcal{L}(\mathbf{x}^\star, \mathbf{u}^\star)$), but it is enriched also with tracking in simulation. Since $\mathcal{L}_{\xi_i}$ is a random variable, depending on the realizations of the noise ξ_i, its expected value $\mathcal{L}_\xi$ is obtained using a Monte-Carlo

approach, increasing the number of simulations high enough leads to a stabilization of the estimated $\mathcal{L}_{\tilde{\xi}}$ value as can be seen in Fig. 40.

$$\mathcal{L}_{\tilde{\xi}} = \mathbb{E}(\mathcal{L}_{\tilde{\xi}_i}) \approx \frac{1}{N_{sim}} \sum_{i=0}^{N_{sim}-1} \mathcal{L}(\mathbf{x}_{\tilde{\xi}_i}, \mathbf{u}_{\tilde{\xi}_i}) \tag{70}$$

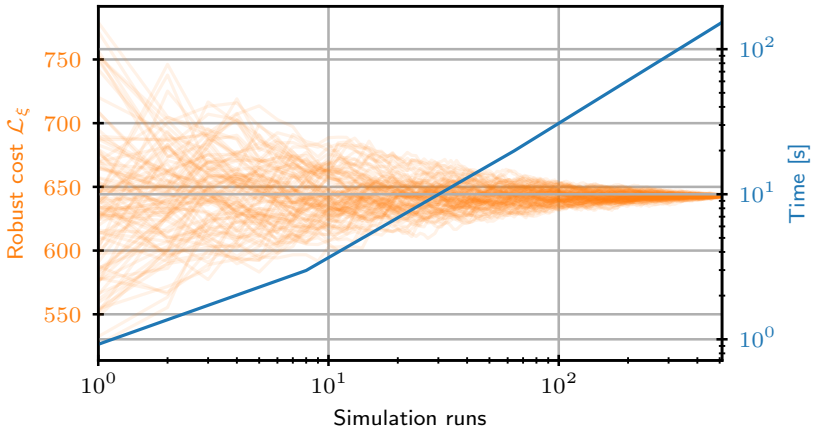

Figure 40: Monte Carlo evaluation of the robust cost $\mathcal{L}_{\tilde{\xi}}$ progressively increasing the number of simulations N_{sim}. For several simulation runs, each orange curve represents the value of $\mathcal{L}_{\tilde{\xi}}$ obtained with a different random seed. The associated computation time is plotted in blue.

From the results of the co-design optimization, it was also verified that there is some trade-off between the optimization of the robust cost and the optimization of the ideal one from the OCP: a lower robust cost leads to a decrease in energy efficiency in the ideal case Fig. 41.

4 SIMULATION OF THE JOINTS' DYNAMICS

This is indeed a simple first order filter whose goals is to capture the smoothing effect of the mechanics of the actuator. More involded strategies may be introduced linking different the varaibles of the problem. Communication delays can also be introduced in simulation.

In the simulations, the full actuator model is considered (including friction and bandwidth). From the ideal torque $\mathbf{u}^\star$ in the OCP the control $\boldsymbol{\tau}$ is computed to compensate for friction. In addition to friction compensation, the actuator dynamics is modeled as a first-order low-pass filter in Eq. (71):

$$\mathbf{u}_k = \alpha \boldsymbol{\tau}_k + (1-\alpha)\boldsymbol{\tau}_{k-1}, \text{ for } k \in 1,..N-1 \tag{71}$$

where the initial torque is imposed, $\mathbf{u}_0 = \mathbf{u}_0^\star$, and α is a parameter depending on the cut-off frequency that was fixed to 20 Hz based on testing. This filtering is introduced to simulate joint torques that can reasonably be applied within the limitations of each actuator, which in previous work were not taken into account. In parallel also a methodology to take into account these limits in the OCP directly was developed for DDP. But we did not include such development in this work because it required augmenting the

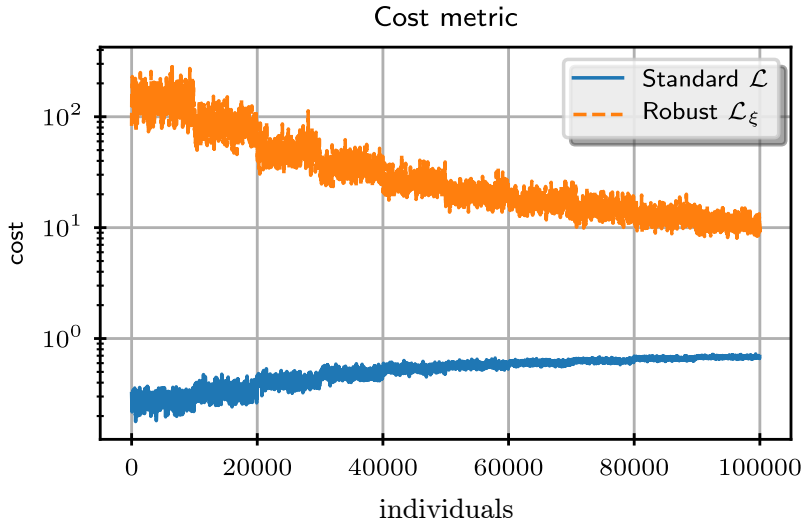

Figure 41: Robust cost metric $\mathcal{L}_\xi$ evolution trend during CMA-ES (orange curve). $\mathcal{L}_\xi$ diminishes increasing the number of runs of Alg. 1 (the number of the overall evaluated individuals), while the standard cost $\mathcal{L}$ increases (blue curve).

state with the control dynamics (and such a strategy was rather expensive). Finally, saturation is introduced to enforce the torque limits before sending the control to the simulated joint: $\underline{\mathbf{u}} < \mathbf{u}_k < \overline{\mathbf{u}}$.

5 RESULTS

Some results, including robustness in our framework, are presented. In the initial phase, we optimize just hardware parameters (fixing the gain scaling $\gamma = 1$). Two types of robots, shown in Fig. 42, are optimized for robust task tracking. Each one is made up of variants of the actuator module developed in ODRI [98]:

These two example represent interesting study cases which embody different characteristics: one is fully-actuated and redundant while the other is underactuated and to move has to explot the contact dynamics.

- SERIAL MANIPULATOR (Fig. 42a): With a fixed base (red), it includes 4 links actuated by 4 motors ($R_Z - 3 \times R_X$). Only the sizes of the last 3 links are optimized, while the shape of the base and the Z-axis link (orange) are fixed. Since each actuator can differ from the others in terms of motor and transmission selection, the hardware optimization variables are 11.
- MONOPED (Fig. 42b): With a non-actuated base (blue) that can move freely along a vertical prismatic link (2 bars), it includes two optimized links and two actuated revolute joints [29], [76], [98].

CO-DESIGN VARIABLES The hardware optimization involves:

- Motor mass $m_m \in [0.05, 1]$ kg
- Gear ratio $n \in [3, 20]$

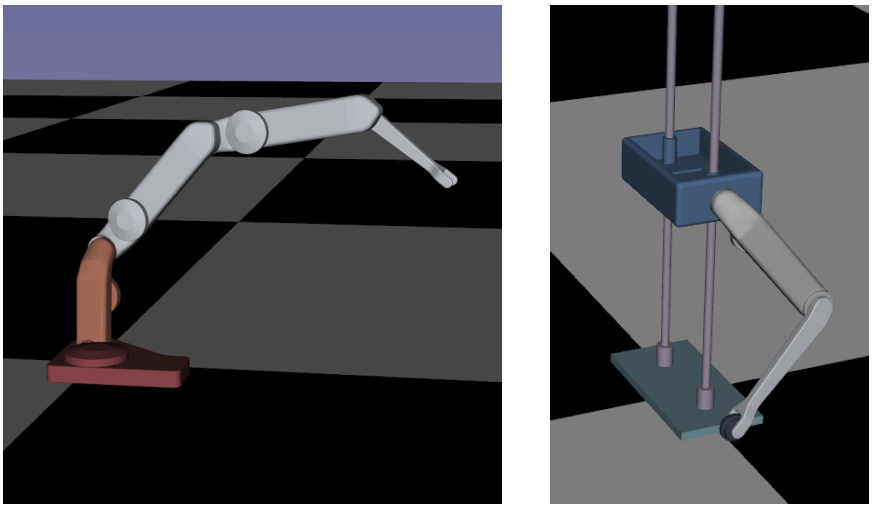

(a) Manipulator (b) Monoped

Figure 42: Robot models used in our tests.

- Link scaling $\lambda_l \in [0.8, 1.2]$ ($\lambda = 1$ is the nominal case)

The joint friction parameters and the electro-mechanical properties of the actuator can be estimated from the first two variables. The link scaling λ_l represents the ratio between the link length and the current module design length. A single scaling parameter is used to keep the relative deflection of the link constant, the section needs to change too according to the scaling previously outlined. The change modifies also the inertia of the links. In the latest results, hardware and controller parameters are optimized together in the case of the manipulator. This way it is possible to increase robustness by adding the gain scaling parameter γ (introduced in (69)) to the co-design variables.

6 MANIPULATOR BACK AND FORTH TASK

TASK The task is to displace a fixed mass payload of 0.1 kg from an initial position $\boldsymbol{p}_0$ (with an initial pose which depend on $\boldsymbol{q}_0 = 0$) up to a given point with a fixed displacement $\boldsymbol{p} = \boldsymbol{p}_0 + [-0.1, -0.1, 0.1]^\top$ m and then to bring it back to $\mathbf{p}_0$. At the intermediate and final positions the joint velocities must be zero.

HYPER-PARAMETERS The parameters related to CMA-ES are the number of generations $N_{gen} = 10$, and the number of problems per generation $N_{pop} = 10000$. Parallelization is used to speed up computation. On a standard desktop computer, ≈102 hours were necessary for solving 10^5 problems, with a mean time per problem of 3.7 s, including the simulation phase. The OCP has 1000 nodes and $dt = 1$ ms; the cost weights are reported in Tab. 7. For the realization $\boldsymbol{\xi}$ the value of $\sigma_{\xi} = 0.2$ was selected and $N_{sim} = 100$. Aside from the power losses due to Coulomb friction and Joule effects, here mechanical energy was introduced. Indeed, as the final state (in particular the

WEIGHT	TYPE	VALUE
Mechanical power	Running	1e−2
Power losses	"	1e−2
Final frame position	Terminal	1e4
Final frame velocity	"	1e6
Penalty on the max torque	Penalty	1e4
Intermediate frame position	"	1e6
Intermediate frame velocity	"	1e6

Table 7: Manipulator cost function weights

pose) is not specified, it is necessary to minimize the total electrical power. This ensures that the system does not reach the goal with an excess of mechanical energy (potential and kinetic). The running cost includes all the power components, summed with the same weight, and the input power is minimized considering perfect regeneration.

DISCUSSION The values obtained with the standard method (without robustness optimization) and its robust counterpart are compared. Fig. 44b shows that the standard method applies very high torques when the joint velocities are null (initial, intermediate and final configurations) to minimize the mechanical power. However, this solution is hardly applicable to the real system due to bandwidth limitations. Position and velocity tracking is better for the robust case, as illustrated qualitatively in Fig. 44a and quantitatively by the lower rooted mean squared error along the state trajectories $\text{RMSE} = \sqrt{\Sigma_{i=0}^{N_{sim}} ||\mathbf{x}_{,i} - \mathbf{x}^{\star}||_2^2 / N_{sim}}$ in Tab. 8. The hardware parameters in Tab. 8 show that to provide high impulsive torque, the standard method selects bulkier motors, dissipating less energy by Joule effect and more energy by Coulomb friction as reported in Tab. 8. On the other hand, the robust method induces higher Joule losses, and selects smaller motors, but overall require less torque and adds less mass to the system Tab. 8. Reasonably, both methods select the link size to reduce the moving masses and system inertia. In Fig. 41 the cost metric profiles in the case of the standard and the robust approach are shown versus the evolution of CMA-ES (all the evaluated individuals of each generation). The improvement of the robust metric $\mathcal{L}_{\xi}$ is accompanied by a degradation of the standard metric $\mathcal{L}$. The robust version penalizes a lot of the designs and controls that are not able to fulfill closely the task (given the high weight of the final position, this results in a cost order of magnitude greater than the standard one). Despite this (expected) trade-off, the optimization of $\mathcal{L}_{\xi}$ produces designs that can follow more closely the task under perturbations. In Fig. 40 the convergence of $\mathcal{L}_{\xi}$ to the empirical expected value is shown, for different histories of ξ and different random seeds. From the trend, it is noticeable that after around 100 simulations the deviation is two standard deviations from the empirical expected value, while for 1000 simulations we can consider $\mathcal{L}_{\xi}$ completely converged. Fig. 40 also shows that the computational time is roughly linear with the number of simulations (blue curve).

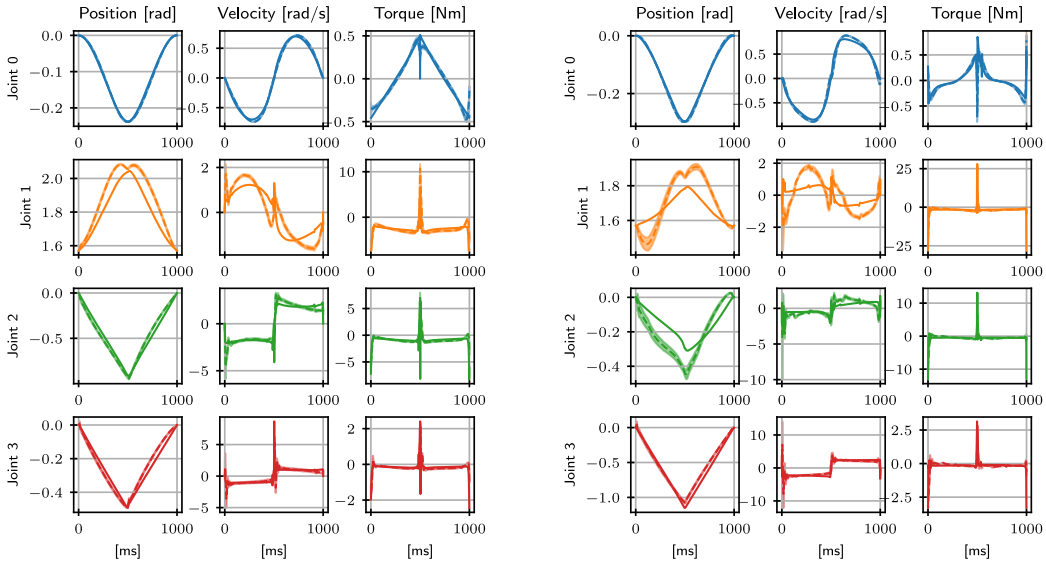

(a) Robust method. (b) Standard method.

Figure 43: Manipulator back-and-forth tracking. Solid lines represent reference trajectories, dashed lines represent the mean of simulated trajectories; shaded regions show the deviation $\pm 3\sigma$ around the mean.

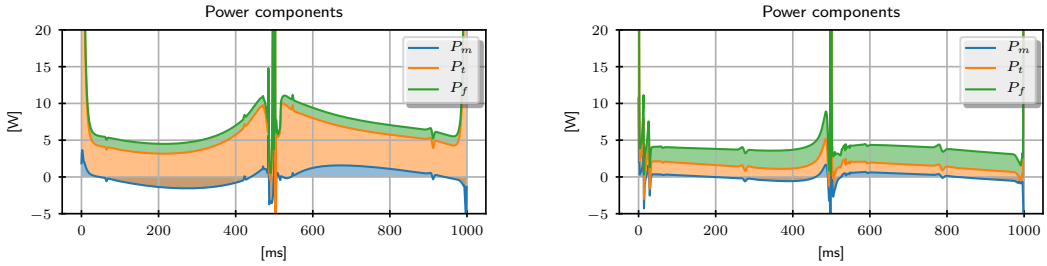

(a) Robust method. (b) Standard method.

Figure 44: Power components required by the back and forth task. Colored areas are proportional to the energetic expense. The upper bound of the curve is the sum of all the power components.

QUANTITY	ROBUST	STANDARD
Cost $\mathcal{L}$	9.58e-3	3.5e-3
Cost $\mathcal{L}_\xi$	33.42	2e3
λ_l	[0.83, 1.02, 0.86]	[0.80, 0.80, 1.08]
m_m	[0.05, 0.05, 0.05, 0.06]	[0.2, 0.76, 0.49, 0.4]
n	[16.7, 11.6, 11.8, 15.2]	[17.1, 11.8, 11.4, 15.3]
RMSE	0.287	1.836
$\sum_i P_{m,i}$dt [J]	-0.9	-1.7
$\sum_i P_{t,i}$dt [J]	6.5	1.8
$\sum_i P_{f,i}$dt [J]	1.3	3.2

Table 8: Results for the manipulator back and forth task.

	ROBUST		STANDARD	
QUANTITY	$\mu(\sum r)$	$\sigma(\sum r)$	$\mu(\sum r)$	$\sigma(\sum r)$
Actuation penalty	0.00	0.00	0.00	0.00
Mechanical power	-0.44	1.54	64.54	10.2
Joule losses	8445.60	32.3	2408.0	143.6
Joint friction	1983.59	49.6	8343.0	223.5
Placing position	4.7e-5	2.19e-6	1e-6	2.8e-10
Placing zero velocity	0.531	0.173	6.44	4.74
Final position	0.193	0.136	21.41	13.2

Table 9: Non-weighted cost residuals after perturbation for the manipulator case.

The optimal solution in this case is also more aggressive in terms of magnitude of the control input, meaning that it is rejecting noise requiring more energy. This is shown in Tab. 10, where the standard method selects hardware parameters that requires less dissipation at the level of the transmission. This results in fewer Joule losses from bulkier motors and a higher torque constant. On the contrary, the robust method selects smaller motors, which lead to more Joule losses, but at the same time also decreases the total mass of the system. Since the motion is rather fast, lower inertia is beneficial. With smaller motors, the system requires fewer control corrections to track the trajectories and the discrepancy between the reference torques and the simulated ones is reduced.

7 MONOPED JUMP

TASK The robot has to perform a jump with the base in a given time and stabilize the base after touch-down. In the OCP such task is enforced weakly as a penalty on the prismatic joint z position.

$$l_{jump}(z) = \begin{cases} 0 & \text{if } z \geq z_{ref} \\ ||z - z_{ref}||_2^2 & \text{if } z < z_{ref} \end{cases} \tag{72}$$

This task encourages motions that are jumping above the reference height threshold ($z_{ref} = 0.4$ m), but still allows smaller structures that underperformed the task. At the same time, letting the maximum height unspecified is beneficial to find solutions that satisfy the task timing sequence, which is chosen *a priori*. In the OCP there are four predefined phases for the jumping motion:

- *Contact phase*: the foot contact with the ground is enforced in the dynamics for a fixed number of nodes
- *Flying phase*: the contact with the ground is broken and the monoped is jumping. At the intermediate node the cost (72) is applied.
- *Impact phase*: the foot velocity at the new contact point is set to zero and a small regularization is added to penalize landing of the foot far from the origin.
- *(Post-impact) contact phase*: the leg, while in contact with the ground, can decelerate the base motion and stop the system.

HYPER-PARAMETERS For CMA-ES the following parameters were chosen: $N_{gen} = 5$, $N_{pop} = 1000$. The OCP has 1000 nodes and $dt = 1$ ms; the cost weights are reported in Tab. 10. For the realization $\boldsymbol{\xi}$ the value of $\sigma_{\xi} = 0.2$ was selected and $N_{sim} = 100$.

COST COMPARISON Fig. 45 shows the reference joint velocities for robust and standard methods. Qualitatively the simulated trajectories are similar to the ideal trajectories. A jump of the base is performed even if perturbations and actuator bandwidth limitations make the monoped perform worse, anticipating the contact phase with the ground. This means that the optimized motion needs high accelerations that are not feasible with the more accurate hardware modeling introduced in the simulation. The

Quantity	Robust	Standard	Weights
Hardware			
Scaling	[1.2 , 0.973]	[0.87, 0.8]	
Motor mass	[0.125, 0.282]	[0.812, 0.05]	
Gear ratio	[5.43, 7.83]	[5.19, 7.00]	
Metrics			
Cost $\mathcal{L}$	50.91	13.67	
Cost $\mathcal{L}_{\xi}$	631.08	1.09e4	
RMSE on $x^{\star}$	1.893	4.675	
Mechanical power	-16.67	-111.24	10
Joule power	49.02	76.03	10
Joint friction	16.00	48.21	10
Penalty			
Base penalty	0	0	10^3
Foot penalty	0	0	10^4
Knee penalty	0	0	10^4
Actuation penalty	0.0035	0.012	10^4
Regularization			
Friction cone	1.52	1.054	10^{-1}
Jump threshold	2.53	0.00	10^5
Contact at zero	0.046	0.021	10^3
Terminal state	1.27	0.028	10^3

Table 10: Results for the monoped co-design

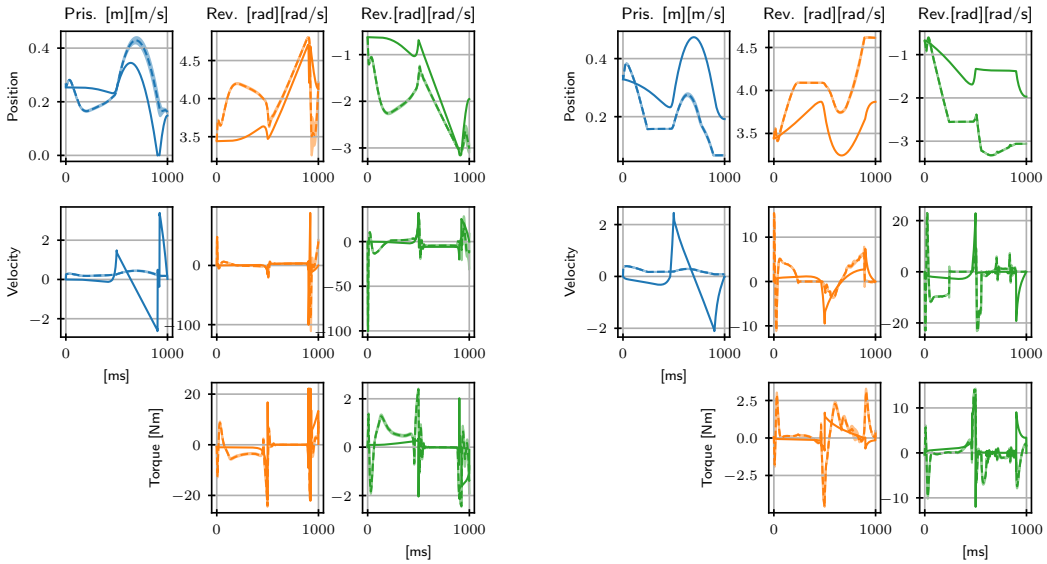

(a) Robust method. (b) Standard method.

Figure 45: Monoped jump: solid lines represent reference trajectories, dashed lines the mean of the simulated trajectories, while shaded regions show the deviation $\pm 3\sigma$ around the mean. Note that the prismatic joint is underactuated.

reference trajectories of the standard case are minimizing the cost, but such optimality does not translate into robustness, as these trajectories are also more brittle and not easy to follow in perturbed scenarios.

A property of the robustly optimized trajectory can be seen in Fig. 46, which shows the ratio between lateral and vertical contact forces. The forces obtained with the robust method are further away from the friction cone bounds, whereas the standard method stays closer to them, and even slightly violates the limits (friction cones are modeled as penalties in DDP). Having a higher margin proves to be beneficial in simulation. In this case, the controller, counteracting the perturbations, may produce additional lateral contact forces, which then cause sliding of the contact point. Such sliding is unmodelled in the OCP dynamics, so it is a major source of tracking failure. The proposed method can account for this unwanted behavior without explicitly adding custom terms in the cost function.

COST LANDSCAPE

In the case of the monoped, an additional investigation is proposed. It explores the value of the standard and robust cost against different combinations of actuator parameters. The costs have been evaluated on a grid, reconstructing the landscape of the standard cost $\mathcal{L}$ and the robust one $\mathcal{L}_{\xi}$. The task and problem formulation do not change but, in this exploration, the actuator is chosen to be the same for both joints (link lengths are fixed to the nominal values) so two parameters are explored, as seen in Fig. 47. The robust cost adds insights that the standard cost does not capture, and this results in

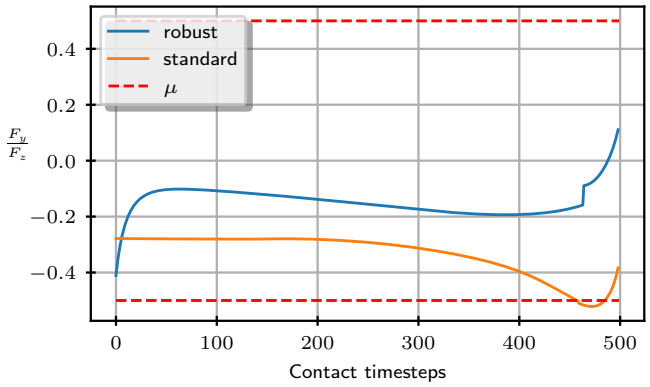

Figure 46: Monoped jump: ratio between vertical and lateral contact forces, and friction cone bounds $\pm\mu$.

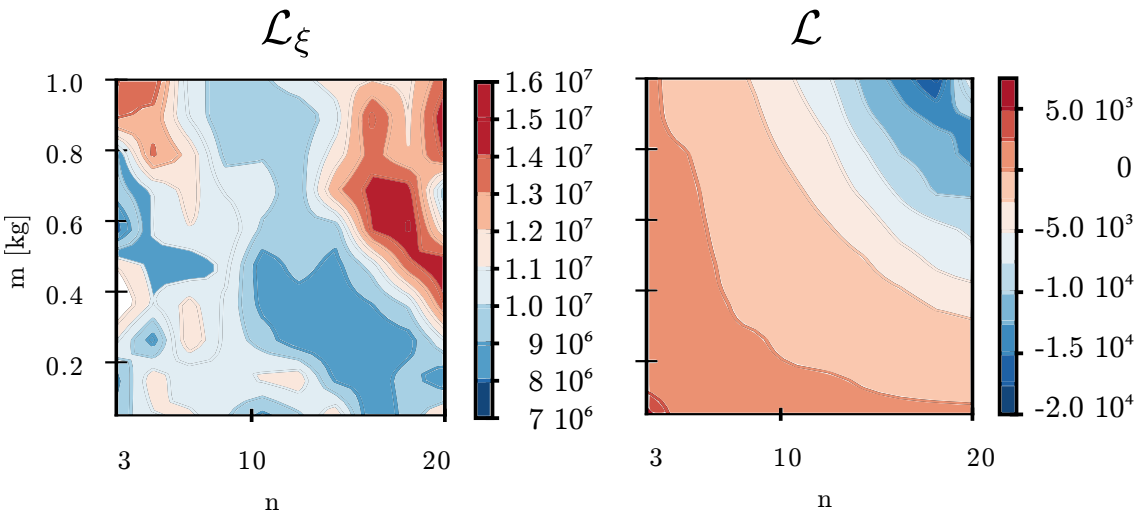

Figure 47: Monoped jump: contour plot of the robust and standard cost as functions of the motor mass m_m and gear ratio n. Two very different optimal regions are present.

different cost landscapes. Minimizing just $\mathcal{L}$, as already seen, the best hardware combination involves large motors and large reductions. Conversely, such choice is highly penalized in the robust case, when joint friction and actuator bandwidth are accounted for. One explanation is that the increased motor size increases the inertia and nonlinear dynamic effects, so the controller has to apply higher feedback torques to compensate for perturbations. Moreover, larger motors are accompanied by increased rotor inertias, and thus greater reflected inertias. In the robust case instead, smaller motors are selected with reductions that do not reach the maximum values. This seems to hint that, when robustness comes into play, more transparent actuators perform better. As detailed in [272], transparent actuators can be obtained by minimizing friction and reflected inertias at the joint level, so with quasi-direct-drive actuation and low rotor inertia. This way the actuator bandwidth and back-drivability are both increased. These properties are necessary for proprioception and rapid control corrections.

8 CONTROLLER PARAMETERS OPTIMIZATION

To further improve the controller robustness, the optimization of the gain scaling factor γ (as in (69)) was introduced in the outer loop. In this case, for the same back-and-forth task as in Section 6, a single actuator choice was optimized to be used in all joints and with $\gamma \in [0.1, 10]$. The optimization was done with a population of 1000 individuals evolved for 5 generations. The optimum was found for hardware values in a similar range of the previous manipulator results, at $m_m = 0.05$, $n = 15.7$, $\lambda = 1.13$ and for $\gamma = 6.57$. The value of the robust cost though is significantly lower than what is observed in the case of unscaled gains, with the value $\mathcal{L}_{\tilde{\zeta}} = 10.17$. Plotting the values of $\mathcal{L}_{\tilde{\zeta}}$ against γ results in Fig. 50. Here a value of γ greater than the unit is overall leading to a decrease of $\mathcal{L}_{\tilde{\zeta}}$. The explanation is that the Riccati gains obtained by DDP are optimal but only locally. This is not the case with the addition of perturbations: amplification of the correction improves tracking. It can be observed however that this trend stops at higher values of γ, where a sharp increase in the robust cost is induced instead. This last example shows that, with this framework, optimizing even simple controller parameters is possible at a reduced computational cost.

GAIN OPTIMIZATION ON THE NOMINAL HARDWARE Further tests on the qualitative behavior of the system with respect to the scaling was performed. For these tests, we just took the nominal hardware and evaluated the impact of the scaling on the energy costs and on the joint torque trajectories. In Fig.49 the control trajectories from several perturbed simulations are superimposed. Each with a higher transparency for lower values of γ. If the scaling factor is higher than the optimal ($\gamma > \gamma^\star$), the control action becomes more aggressive, and it sharply increases the cost $\mathcal{L}_{\tilde{\zeta}}$. Empirically it can be observed that the control trajectories are more impacted by both saturation and oscillations around the nominal torque reference, (which is plotted in black). Similarly, if the correction with the Riccati gains is reduced ($\gamma < \gamma^\star$), the performance is not adequate to counteract perturbation. Upscaling the gains ($\gamma > 1$) results in solutions that

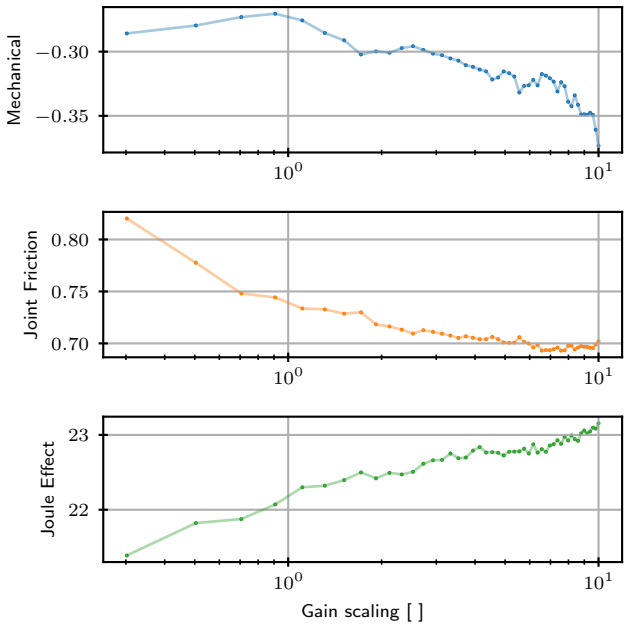

Figure 48: Effect of the gain scaling parameter on the cost components

σ	0	0.32	0.64	0.95	1.26
MECHANICAL	-0.27	-0.28	-0.32	-0.39	-0.41
JOULE	22.15	22.48	22.56	23.59	23.77
COULOMB	0.74	0.75	0.82	1.00	1.09
$\mathcal{L}_\xi$	193.4	223.9	354.2	581.5	681.4

Table 11: Evolution of the cost and the energy components for various values of the standard deviation of the perturbation

are closer to the nominal torque reference and at a lower robust cost. Qualitatively the energy components (corresponding to the mechanical energy, joint friction dissipation, and Joule effect in the motor) are shown in Fig. 48. There it can be noticed that the major impact is on the Joule effect, which increases drastically. Curiously the joint friction is reduced instead. Finally, the mechanical energy values are slightly decreasing, but overall this effect is small and mostly explained by the oscillations due to higher gains.

Impact of noise on the framework

Another study we made was on the entity of the noise distribution $\sim \mathcal{N}(0, \sigma)$. We evaluated the impact of σ on the cost components. In this case, we fixed the nominal design of the actuator. The values of σ are varied within $[0, 3]$ where zero corresponds to a simulation alone run. In Tab. 11 we observe that σ is leading to an increase of the cost components and that the combination simulation with noise is not impacted by vari-

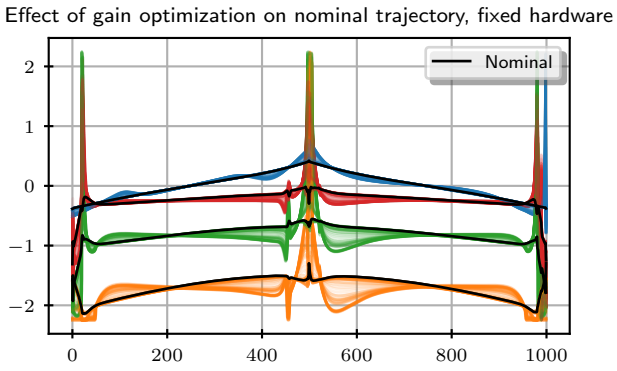

Figure 49: Control trajectories with perturbation, noise and controller for different values of the scaling compared with the robust nominal in black

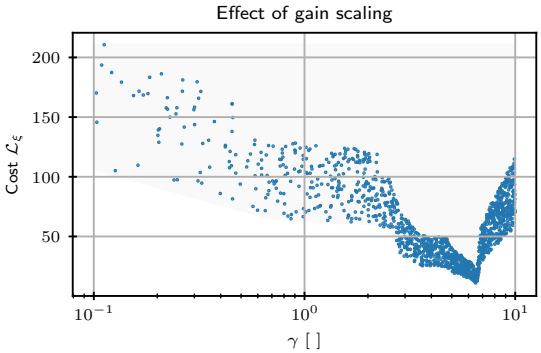

Figure 50: Effect of the scaling γ with respect to the robust cost $\mathcal{L}_\xi$. Each dot represents an individual of the optimization. The presence of a minimum can be seen.

ability in the region of lower values of noise when $\sigma \in [0, 1.26]$, with ensembled means of the energy costs rather close to each other. An increase in the noise is accompanied by a higher correction to compensate for it, so this resolves in a general increase of the dissipation components and $\mathcal{L}_{\xi}$.

9 LIMITATIONS

The proposed method scales favorably, and is simple to consider in our framework, but it has several draw-backs:

- We assume to have a perfect controller with no communication delay or noise on the measurements of the state. The additional bandwidth limitation dynamics allow us to partially account for it, but other mismatches with reality may be present.
- If the state moves from the nominal trajectory we cannot re-plan a new reference to follow as happens in the case of Non-Linear Model Predictive Control (nMPC) approaches, moreover in the controller we cannot properly handle saturation limits, they are included in the penalization by the trajectory optimization, and hardly enforced in the simulation,
- In legged locomotion it may be problematic to correctly execute time phases and dynamics changes (such as creating and breaking a contact): the trajectory must follow a strict time evolution,
- In some cases, the Riccati gains can be very aggressive when a critical task objective needs to be fulfilled (such a high terminal cost, hard constraint), then, their applicability to the system, which has some physical limits, may not be possible and lead to instability.

10 CONCLUSION

The main contribution in this chapter is the modification of the co-design framework to include the information of a feedback controller performance. This addition to the approach presented in the previous chapter constitutes an important step in the direction of evaluating hardware properties before starting the system integration in real prototypes. The method shows improvements to robust tracking and requires little tuning: hardware and trajectories less impacted by noise are selected without explicitly introducing robustness in the OCP itself. This technique has been used for two different robotic platforms. Interestingly in both cases, the selected hardware is more transparent, suggesting a trade-off between optimality and the capability to counteract perturbations. The impact of the gain scaling choice and the noise is studied in a separate part, supporting this intuition. The major drawback lies in the local nature of the controller, which is not general enough and requires reference trajectories. The controller has been chosen *a priori* (local feedback controller). This can be done rather efficiently by reusing information from DDP, but it is limiting the generalization. The substitution of the controller with even more general approaches, such as MPC or RL, which allow an online replan-

ning of the trajectory, seems a promising choice but at a very high computational price. To overcome this limitation, an extension was proposed to also include the controller parameters in the optimization loop. It consists in optimizing the gain scaling factor together with the design parameters, in the outer loop.

11

QUADRUPED ROBOT OPTIMIZATION FOR MULTIPLE CYCLIC TRAJECTORIES

IN SHORT

This chapter presents the third step of our co-design development which aims to extend the framework for complex movements while ensuring the satisfaction of hard constraints. Our method to design robots using computational techniques is then applied to co-design a quadruped robot for achieving dynamic cyclic behaviors. The prototype developed at DFKI, Bremen, serves as a platform for successfully applying such a vision. The optimization considers various cyclic tasks and selects the robot size and QDD actuators from off-shelf catalogs to ensure efficient bounding and backflips. The platform and theoretical aspects of the framework are outlined in the first part of the chapter. To deal with such complex tasks a new trajectory optimization formulation is used. so, the problem formulation is detailed, The actuator model features a new bandwidth limitation inequality constraint. The power model presented in chapter 4 is then proven to provide adequate estimates of the first prototype iteration through experimental validation. A co-design study is performed on the platform, starting with preliminary optimization for each individual task. A refinement that considers the Pareto set from the two tasks is used to select an improved design for future implementation.

Contents

THE DFKI QUADRUPED PROTOTYPE

The work in this chapter was developed as the result of a collaboration between LAAS-CNRS and the DFKI. To cooperate on the subject of quadruped co-optimization I was invited by Dr. Shivesh Kumar as visiting researcher in the Underactuated lab at Robotics Innovation Center (RIC) in Bremen. In this project, also Justin Carpentier was involved and he kindly provided his expertise with frequent exchanges on the optimization and he extended some new features' in `pinocchio` to integrate it with Casadi. DFKI RIC recently developed a new robot quadruped (see Fig. 51). The validation and co-design results are based on the preliminary prototype. The robot consists of a central body with four identical legs. Each of them with 3 degrees of freedom (DoF), which are actuated by off-the-shelf QDD actuators with an integrated reduction stage. The leg topology is mammal-like and the physical dimensions for the initial design are inspired by the open-source project Mjbots-quad [188]. To keep the leg's inertia low, the knee joint's motor was shifted to the pitch axis of the hip joint and coupled to the knee joint via a belt with a gear ratio of $1/2$. All structural elements of the robot can be manufactured by waterjet cutting, even the gearbox pulleys for coupling the knee joint. This allows quick replacement of parts and adaptation of the kinematics. For example, the leg segments' length or the belt drive's transmission ratio can be adapted, resulting in a cost-effective and adaptable design. This will prove useful in later prototyping, as a final design can be quickly produced. The components of the body consist of Carbon Fiber-Reinforced Plastic (CFRP) plates with a thickness of 1 mm. This allows easier manufacturability and assembly, without sacrificing rigidity and lightness. The analysis starts from the nominal design, and focuses on the selection of the motors and the scaling of the links with respect to the first version.

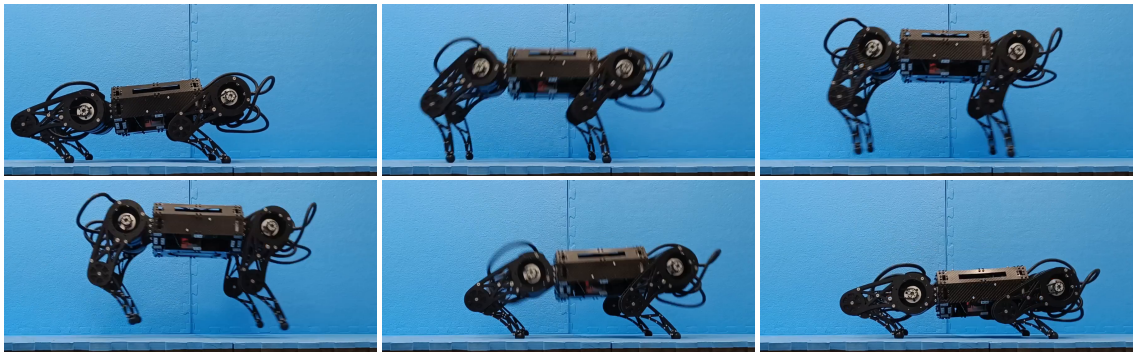

Figure 51: QUADRUPED PROTOTYPE bounding tests at DFKI RIC [1]

1 MODIFICATIONS TO THE FRAMEWORK

For this problem, a parallelized bi-level scheme is still used (Fig. 52). The main differences with our previous developments are in the implementation of the inner-optimization

1 Companion video at https://peertube.laas.fr/w/iUscYk7iigi4v3sgk97XxV

which require a more robust and versatile implementation. In the practical application we target, the optimized motions are cyclic and highly dynamic and these characteristics forced us to explore new trajectory optimization approaches. In our previous works hard constraints could not be exactly enforced, but only approximated via penalties in the cost function. This was rather limiting because it required hand-tuning the weights and parameters associated with penalties. This was a main source of brittleness, which we have overcome in this work by relying on *Casadi* [12] and *Pinocchio* [41], [42]. Now more versatile, yet complex, optimal control problem formulations can be solved with robust general-purpose optimizers. One of them is *IpOPT* [267], which comes with a robust optimization routine that allows better globalization compared to other state-of-the-art gradient-based solutions. However, this comes at the expense of:

- Increased computation time compared to iLQR or DDP [166], as the specific sparsity pattern of the OCP is not exploited. Such sparsity in the Hessian matrix is just partially recovered by the linear solver `MA57` [75], which we selected because of its efficiency and robustness. Depending on the complexity, each OCP problem's computation time varies between $\approx 10\,\text{s}$ and 10 min. Moreover, the addition of hard constraints drastically increases the complexity.
- Warmstart capability, because of the barrier initialization, interior point methods are more difficult to warm start. This usually limits the re-using of previously computed solutions to solve a new problem instance [270], [281].

For the outer loop we still rely on GA. The use of CMA-ES[108] enables us to explore globally the combination of hardware parameters, while in general gradient-based methods are more impacted by initialization issues. These features provide an edge over state-of-the-art methods for complex design problems. The main modification we introduced in the loop has to do with CMA-ES, as it works on continuous domains while the motors are off-shelf, from a discrete set. A continuous parametrization of such an integer design set allows optimizing for discrete variables (e. g. off-shelf motors). The discrete motor choice is optimized at the same level as the other design variables by CMA-ES, which by default works on a continuous space. Internally, all the design-related quantities are continuous, a remapping strategy is employed to pass from the continuous variables associated with the motor selection to the discrete equivalent before solving the problem. CMA-ES then optimizes over a set of continuous variables exploring all the motor combinations, and internally, before computing the associated OCP, a projection to the integer set is performed. Thanks to this remapping, the motor characteristics are found in tables without the need for an explicit parametrization as used in previous work [76], [78], [278], [279]. This mechanism becomes necessary also when the motor technologies are rather different from each other and a parametrization is not viable. Finally, the genetic approach in the outer loop is *massively parallelizable*. The overall computation time is reduced, as the whole optimization was adapted for parallelization on a High-Performance Cluster (HPC), using *SLURM*[222] as shown in Fig. 52 to solve a large number of OCP problems.

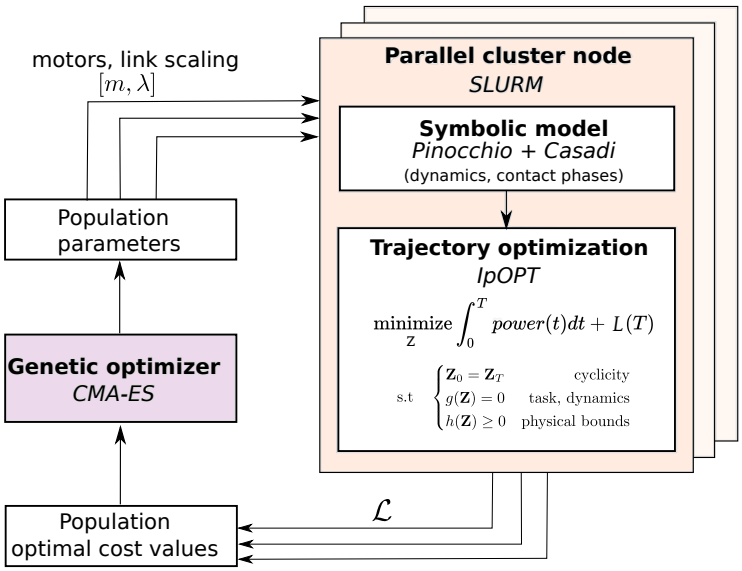

Figure 52: Overview of the approach. Stack of the parallelized bi-level optimization scheme with arbitrary hard constraints on the primal optimization variables

2 TRAJECTORY OPTIMIZATION PROBLEM

2.1 *Trajectory optimization formulation*

VARIABLES For the OCP on a discretized horizon with nodes $[0..N]$, we use direct collocation with an augmented set of variables: $\mathbf{Z} = [\mathbf{X}, \mathbf{U}, \mathbf{A}, \mathbf{F}, \mathbf{\Gamma}]$ where:

- $\mathbf{X}$ is the decision vector collecting the evaluations of states of the robot $\mathbf{x}$, each state includes the configuration and velocity of all its degrees of freedom. where $\mathbf{q}_\text{b}$ is the underactuated base position and $\mathbf{q}_\text{a}$ is the vector of actuated joint positions.

$$\mathbf{x} = [\underbrace{x, z, \theta, q_{1..n_u}}_{\mathbf{q}=[\mathbf{q}_\text{b},\mathbf{q}_\text{a}]\in\mathbb{R}^{n_q}} \underbrace{\dot{x}, \dot{z}, \dot{\theta}, \dot{q}_{1..n_u}}_{\mathbf{v}=[\dot{\mathbf{q}}_\text{b},\mathbf{v}_\text{a}]\in\mathbb{R}^{n_v}}] \in \mathbb{R}^{(n_x=n_q+n_v)} \tag{73}$$

- $\mathbf{U}$ contains the actuated joint torques $\mathbf{u} \in \mathbb{R}^{n_u}$.
- $\mathbf{A}$ is the vector of the joint accelerations $\mathbf{a} = \dot{\mathbf{v}} \in \mathbb{R}^{n_v}$.

Just for the contact phase nodes $C = [N_{c,0}..N_{c,T}] \subseteq [0..N]$, the foot position $\mathbf{p}_{c,f}$ for the feet f in contact is fixed. For any foot f in contact, we define additionally:

- $\mathbf{F}$: the contact force vector, which stacks the contact forces $\mathbf{f} = \bigcup_C \bigcup_p (\mathbf{f}_{c,p} \in \mathbb{R}^{n_c})$, where n_c is the contact point dimension, which depends on the contact model. For instance, in planar models $n_c = 2$, while for three dimensional and contact wrench models it equals $n_c = 3$ and $n_c = 6$, respectively.
- $\mathbf{\Gamma}$: a slack variable vector, which collects the contact slack variables $\gamma = \bigcup_C \bigcup_p \{\gamma_p \in \mathbb{R}^{n_c}\}$, following the formulation in [190], to impose constraints on the feet position

and velocity. These variables are introduced only in the contact phases to avoid contact drift.

MODEL CHOICE The considered augmented set of variables, at torque and acceleration level, is motivated by the intention of imposing physically driven constraints on the trajectory considering the physical limitations of the actuator. This is not directly possible in the case of simplified models such as Linear Inverted Pendulum (LIP) [137], [139], Spring-Loaded Inverted Pendulum (SLIP) [138] or centroidal model [61], [180], which do not include the joint torques. Finally, highly-dynamic behaviours are difficult to discover as they are often far from the simplified model assumptions.

CONTACT PHASES This study is limited to the case of trajectories with pre-specified phases and timing (the sequence of contacts is fixed a-priori). We follow a holistic approach inspired by [172] (and later [152], [174]) where the motion of a biped is synthesized by imposing periodic constraints on the trajectory. As in [51], the joint trajectories of a planar biped are optimized to obtain cyclic behaviors imposing contact constraints and joint limits. The main advantage of our method is the automatic discovery of the footholds, as the contact location is left free. It is nonetheless possible to further refine the phase timing with black-box techniques as in [76] or with methods that optimize the length of each contact phase in the optimal control problem directly [174].

2.2 *Optimal Control Problem Constraints*

With the formulation outlined in Section 2.1, constraints can be imposed directly on the primal variables both in the form of equality and inequality constraints. This is an aspect of the utmost importance for co-design, as the feasibility of the motion needs to be guaranteed from the optimization stage.

ROBOT DYNAMICS Recalling (13), the accelerations can be solved using the Forward Dynamics (FD) [82], leading to a constraint on $\mathbf{a}$. Joint accelerations must then be integrated numerically to obtain joint velocities and positions. To this aim, we introduce an integration function $\mathbf{\Phi}$, which we used to formulate the following constraints (in the implementation, it is an explicit Euler scheme, with length Δt), with direct collocation:

$$\mathbf{x}^{+} = \mathbf{\Phi}(\mathbf{x}, \mathbf{a}, \mathbf{u}, \gamma, \Delta t), \tag{74}$$

To improve numerical conditioning, the contact point velocity is corrected with a slack variable γ as proposed in [190]. This allows to impose redundant constraints on the contact location and its velocity, avoiding drift. This modification is propagated in the integrator law (74), as shown in Eq. (13) of [190]. In the cost function, these slack variables are penalized for converging to physically accurate solution. Our integrator hence depends also on γ because, instead of the state velocity $\mathbf{v}$, the value $\tilde{\mathbf{v}}$ is used in the

integration step, where $\tilde{\mathbf{v}}$ can be interpreted as the velocity projected in the kernel space of the contact velocity $\mathbf{J}_c\mathbf{v}$:

$$\tilde{\mathbf{v}} = \mathbf{v} + \mathbf{J}_c^\top \gamma \tag{75}$$

Contact constraints

The rigid contact model leads to several constraints described in the following.

FORCES The non-sliding and unilaterality conditions impose the following constraints on any contact force (for flat ground) $\mathbf{f}_c = [f_{c,x}, f_{c,y}, f_{c,z}]^\top$, given the friction coefficient μ:

$$\begin{cases} \mu^2 f_{c,z}^2 \geq f_{c,x}^2 + f_{c,y}^2 \\ f_{c,z} \geq 0 \end{cases} \tag{76}$$

NON-SLIDING CONTACT POINTS During any contact phase of horizon $C = [N_{c,0}..N_{c,T}] \subseteq [0..N]$, the position $\mathbf{p}_{c,f}$ of any foot f in contact is constant for the whole phase. In particular, we set it equal to the value at the beginning of the phase:

$$\mathbf{p}_{c,f}(\mathbf{q}_i) = \mathbf{p}_{c,f}(\mathbf{q}_{N_{c,0}}), \quad \forall\, i \in C, i \neq N_{c,0} \tag{77}$$

NON-PENETRATION The z coordinate of the contact point must be at ground level (flat ground assumption):

$$\mathbf{p}_{c,f}(\mathbf{q}_{N_{c,0}})|_z = 0 \tag{78}$$

Because of (77), this condition can be imposed just on the initial contact node $N_{c,0}$.

CONTACT VELOCITY The velocity of the feet in contact must be zero:

$$\mathbf{v}_{c,f}(\mathbf{q}_i) = 0, \quad \forall\, i \in C \tag{79}$$

Key-frames collision avoidance with the ground

To produce a feasible motion, constraints on the vertical position of some key-frames (e.g. shoulder and knee joints, indicated with the subscript kf) need to be imposed in order to not penetrate the ground. This is enforced along the whole optimization horizon through inequalities of the type:

$$\mathbf{p}_{kf}(\mathbf{q}_i)|_z \geq 0, \quad \forall\, i \in [0..N] \tag{80}$$

Cyclicity

Cyclic motion patterns are the target of the optimization. This choice allows us to keep the optimization horizon per cycle short enough without sacrificing numerical precision. Once the motion primitive is obtained, a locomotion pattern that is representative of the robot's main operation can be achieved by replicating the cycle multiple times. The periodicity of the solution is introduced in the OCP with non-Markovian constraints between the optimization variables at the initial and final nodes of the problem. Depending on the problem requirements, these constraints can involve the full set of decision variables $\mathbf{z}$ or just a subset of it.

$$\mathbf{g}(\mathbf{z}_0, \mathbf{z}_N) = 0 \tag{81}$$

For instance, some offsets or inequalities can be introduced just on specific parts of the state to enforce a given behavior (e.g., in a forward jump, we want that the base position translates at least of a given amount, but all the other variables match the values at the beginning of the trajectory).

$$\mathbf{h}(\mathbf{z}_0, \mathbf{z}_N) \leq 0 \tag{82}$$

As these constraints enforce a dependency between the initial and final nodes. A major drawback is that the requirements to define a Markov chain are not respected anymore. This renders using faster iterative algorithms as DDP [166] not viable.

Actuator model and limits

All the main actuator limits are taken into account:

- *Position*: joint position bounds are considered (e.g., the knee joint angle is delimited by the presence of stoppers).
- *Velocity*: each actuator speed limit is considered by imposing bounds on the joint angular velocity. For highly dynamic trajectories, this aspect is essential as these thresholds may easily be reached.
- *Torque*: Generally, torque limits are modeled as fixed bounds on $\mathbf{u}$. This is a necessary but not sufficient condition because the actuator cannot instantly provide any torque value: the intrinsic limitation due to the bandwidth of the actuation needs to be addressed. Approaches to treating it were proposed in [97], [102] working in the frequency domain respectively on the cost function and to obtain feedback gains that can be applied to the real system. Our approach is to impose physically-driven bounds on the torque values themselves. The rationale is that, considering the joint transmission, the elastic elements (particularly the transmission belt) can store energy through small deformations. This acts as a low-pass filter from the motor to the connected joint, which can be approximated by a first-order filter whose cut-off frequency depends on the actuator technology (for DC motors, it can be estimated $f_c \approx 20Hz$). In the time domain, the filter presents a straightforward

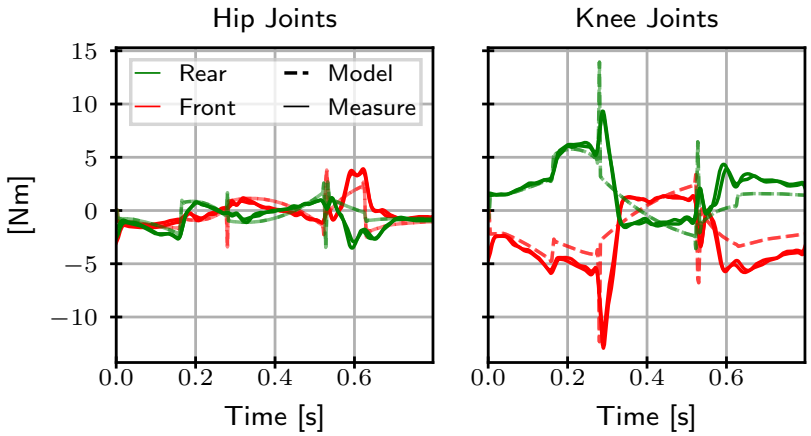

Figure 53: The actuator model allows a close match between the ideal trajectories with friction compensation and the ideal torque applied to the system from measurement data.

implementation. For each node $k \in [1..N]$ it results in the following inequality constraints:

$$\begin{cases} \mathbf{u}_k \leq (1-\alpha)\mathbf{u}_{k-1} + \alpha\overline{\mathbf{u}} \\ \mathbf{u}_k \geq (1-\alpha)\mathbf{u}_{k-1} + \alpha\underline{\mathbf{u}} \\ \underline{\mathbf{u}} \leq \mathbf{u}_0 \leq \overline{\mathbf{u}} \end{cases}, \tag{83}$$

where $\alpha \in [0,1]$ depends on f_c and the discretization step Δt as follows:

$$\alpha = \frac{2\pi\Delta t f_c}{2\pi\Delta t f_c + 1}. \tag{84}$$

$\underline{\mathbf{u}}, \overline{\mathbf{u}}$ are respectively the minimum and maximum torque that can be achieved by the actuator. By construction, (83) respects peak limits, as $\underline{\mathbf{u}} \leq \mathbf{u}_k \leq \overline{\mathbf{u}}\ \forall k \in [1..N]$.

3 VALIDATION OF THE ENERGY MODEL WITH REAL HARDWARE RESULTS

For what concerns the cost function that is minimized, in the Lagrange term, the total electrical energy consumption is expressed as the time integral $\int_0^T P_{el}(t)dt$ of electrical power P_{el}, as in [76], [78]. P_{el} is computed with the non-ideal dissipations of the actuators. In this section, the actuator model and the power consumption models introduced in Section 7 are validated on the prototype in production at DFKI.

ACTUATOR MODEL AND POWER CONSUMPTION VALIDATION The trajectory optimization formulation introduced in Section 2 is used to produce an energy-optimal bounding motion (for more details on the task, see Section 4.4). By tracking the optimal reference trajectory with the prototype, the gap between model and reality is assessed, and the models are validated. Fig. 53 shows that the actuator model with the identi-

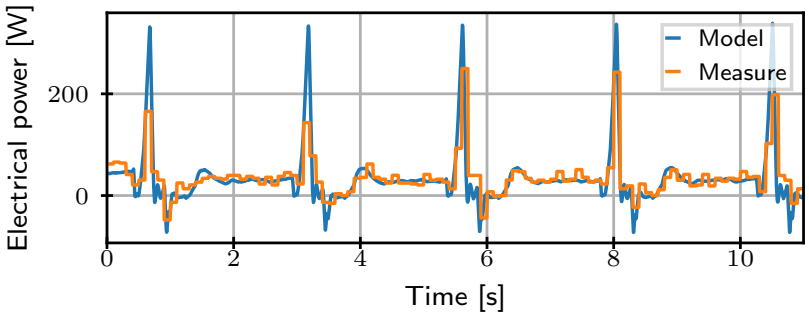

Figure 54: The electrical power estimation closely follows the values measured on the system

Table 12: Energy consumption values for the jump

Case	Measured	Reference
Energy optimal	39.69J	39.64J
Heuristic	56.75J	68.47J

fied parameters, closely predicts the total joint torque τ (including joint friction τ_f) as in (24). A jumping trajectory cycle lasts 0.8 s, so it is repeated multiple times, with a phase in which the system resets to the initial position. To stabilize the trajectory, a PD joint-position controller is used, with additional feed-forward torques from the OCP. The value of the joint torques predicted by the model closely follows the measures, with the main difference in the flying phase [0.3s,0.5s], which can be attributed to the unmodelled controller dynamics. In Fig. 54, the power prediction from joint data measurements (torque and velocity) are shown together with the measured data. The estimation of the total electrical power is given by $P_{el} = P_{mech} + P_t + P_f$, with the notation introduced in Section 7. To compute the values, τ_f is inferred by our joint friction model. Fig. 54 shows that the prediction, which solely uses joint measurements (velocities and commanded torques), follows the measurements of the electrical power provided by the power source, which is measured as the time average product of voltage V and current i, $P_{el} = iV$ (at a lower sampling rate). Nonetheless, the integrated values of the total electrical consumption are accurate, despite the controller dynamics and the sim-to-real gap. These findings are reported for the energy optimal trajectory in Table 12. In addition, a hand-tuned heuristic was used to produce similar jumps with the prototype (with a similar time horizon and jump displacement). On this heuristic, the same method was applied to assess the electrical power consumption. It was found that the consumption of the heuristic was higher than the energy optimal trajectories (which are 30% more efficient with respect to the measured values). The optimal energy expenditure is rather accurately estimated by the method, while for the heuristic, the prediction on the reference trajectory overestimates the power consumption.

4 CO-DESIGN OPTIMIZATION RESULTS

4.1 *Problem requirements and assumptions*

The high-level requirements for the platform are: i) to produce stable locomotion in the forward direction x, ii) to be capable of dynamic motions along the z axis as shown in Fig. 55. To consider representative-legged robot movements, we focus on the generation of iii) stable and periodic motion patterns. Such movements need to be performed while being iv) energy efficient. Taking this into account, periodic bounding and backflip were selected as benchmark tasks to achieve.

ROBOT MODEL Fig. 55 shows a sketch of the joint placements on a complete robot. The general design choice is to place the motors as close as possible to the base to limit the reflected inertia of the leg links. Another preliminary design choice is to drive both the abduction joint and the hip joint directly, while using a belt transmission with a reduction factor of 2 for the knee joint. Since the motion of leg abduction in the lateral plane (y, z) is not strictly needed for bounding or jumping, a planar model was used instead of the complete one, to avoid unnecessary complexity. The masses of the motors are lumped on a single axis and the abduction of the leg (rotation around x of the first leg joint) is blocked. The motor of the blocked DoF is located in the base, while the hip and knee motors are on the same axis and are shown in grey. Nonetheless, the mass of the motors responsible for the leg abduction is considered in the base. This choice simplifies the problem by reducing and coupling some DoFs. The robot model for this task exploits the symmetry of the motion about the (x, z) plane. The optimization then removes the burden of discovering symmetrical behaviors by encoding them directly in the dynamics. Under these constraints, the dynamical equivalence between the complete model and the planar one is ensured by lumping each link inertia and control effort on a unique joint for each symmetrical hip and knee. The command torque on the joints

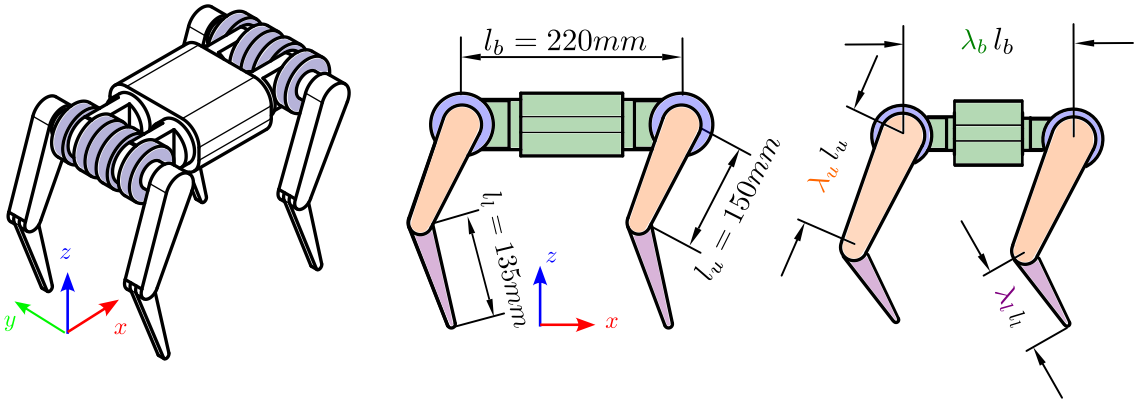

Figure 55: Complete robot model (left), its planar simplification (center) and scaling of the base, upper leg and lower leg links.

(and limits) is then doubled, and they need to be equally divided into two legs to pass on the real system.

4.2 *Structural scaling of the model*

The legs and torso structure are then modeled as fixed payloads, corresponding mainly to the mass of the motors. Additionally, there is a smaller contribution to the mass from embedded electronics and fixating frames for the panels. Taking this into account, and knowing that the rigidity of the system for bending is higher than with additive manufacturing, we can envision scaling up the link along its main nominal dimension with a factor λ (see Fig. 55). For the planar quadruped model of Fig. 55, three scaling factors are considered: λ_u, λ_l and λ_b, respectively for the upper leg, lower leg, and base of the robot. This scaling is just acting on the links. The mass and dimension of the fixed payload (e.g., motors) do not scale with the rest of the rigid bodies. The material density is assumed constant, and the section of the links is not modified. This scaling affects the link inertial parameters as follows:

- The link mass scales linearly $\propto \lambda$.
- The center of mass position scales linearly $\propto \lambda$.
- Inertia: for the inertial parameters, each link geometry is simplified with box primitives, and each component of the inertia tensor is modified independently after the scaling. However, it is possible to intuitively envision the major contribution to the tensor. For this scaling, the effect on the inertia tensor is twofold: there is a purely geometric scaling with respect to the main link dimension ($\propto \lambda^2$), and a second one just related to the mass scaling ($\propto \lambda$).

4.3 *Design variables*

For both co-design tasks, the same set of variables is used, they are presented in the following paragraphs.

CONTINUOUS DESIGN VARIABLES: Starting from the nominal design the following continuous design parameters are:

- lower leg link scaling $\lambda_l \in [0.5, 1.5]$
- upper leg link scaling $\lambda_u \in [0.5, 1.5]$
- base scaling $\lambda_b \in [0.5, 1.5]$

DISCRETE DESIGN VARIABLES:
For the specific co-design application the motors are chosen from the off-shelf Antigravity AK series as reported in Table 13. In particular, among AK80-6 and AK80-9, these two motors differ mainly in the reduction of the integrated rotary gear, which is reported as the last number. Negligible differences are found for the other parameters, especially concerning the motor constant and the winding resistance. In the co-

Table 13: Properties of the motor selection integer variables

Motor type	AK80-9	AK80-6
Mass [kg]	0.48	0.48
Rotor inertia [kg m^2]	6.1E-05	6.1E-05
K [Nm/$\sqrt{W}$]	0.22	0.22
Gear reduction [-]	9	6
Nominal torque Nm	9.83	6.55
Peak speed [rad/s]	25.66	38.22

optimization problem the same leg design, and consequently actuator choice, is used for all four legs. The possible motor combinations for the hip and knee motors (respectively m_{hip}, m_{knee}) are then four.

Actuator choice

The actuator properties are taken into account by modifying the robot dynamics, the constraints of the OCP, and the cost function. The main effects of the actuator are as follows:

INERTIA The added rotor inertia is considered in the model via the technique explained in chapter 9.6 of [82]: the rotor inertia is multiplied by the value of the squared reduction and added to the corresponding diagonal element of the joint space mass matrix. Moreover, each motor mass contribution is added to the parent link mass and inertia as a concentrated mass.

TRANSMISSION FRICTION Given a motor and its transmission, the overall viscous and Coulomb friction are considered in the cost function that minimizes the overall energy, following the same approach as in [76].

MOTOR PLACEMENT The contribution given by the motor masses is also taken into account by the structural base scaling. Each motor is modeled as a localized mass and the rotational inertia is modified accordingly.

4.4 *Co-design for bounding*

The first optimized task is a bounding motion, where the robot must perform a jump of at least 0.30 m. The cyclic constraints enforce the robot state to be equal at the beginning and the end of the trajectory, except for the base x position. Finally, a constraint is added to obtain zero joint velocities at the start and end of the trajectory. In this way, the system consumes just the energy required to perform the jump and decelerate to a full stop in the final part of the trajectory. The phases of such movement are as follows (Fig. 57c):

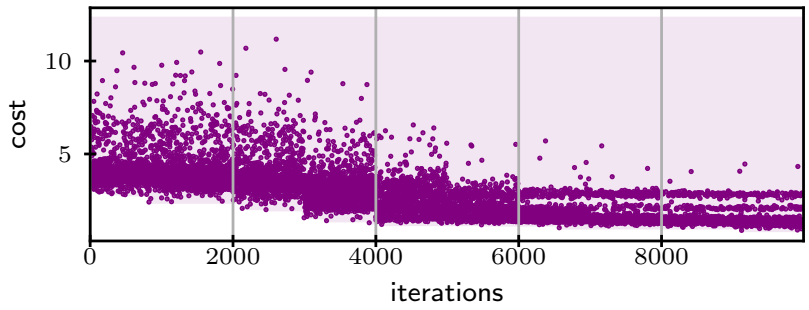

Figure 56: Convergence of the algorithm along the evolution of the populations

	NOMINAL	OPTIMIZED
Cost $\mathcal{L}$	1.78	0.41
λ_u	1.0	0.752
λ_l	1.0	0.514
λ_b	1.0	0.512
m_{hip}	AK80-6	AK80-9
m_{knee}	AK80-6	AK80-9

Table 14: Results of the optimization for the bounding task

- *Dual support*, with all feet in contact with the ground.
- *Flying phase*, with no contact with the ground.
- *Dual support*, with all feet again in contact with the ground.

This task is symmetrical, meaning that the time left for each contact phase is the same. For the overall problem, the time window for each cycle of the jump is 0.7 s, and the total number of nodes for the optimization horizon is 100.

OUTER LOOP HYPER-PARAMETERS For this optimization, the CMA-ES algorithm is initialized to evolve for 10 times a population of 1000 different individuals (different combinations of the design parameters). Fig. 56 shows that this is sufficient to reach stationary values in the cost. It is clear from the trends that there is a diminishing return in exploring further combinations of parameters. In particular, in the same figure different bands can be seen, which correspond to the various optimal design for the 4 combinations of the motors.

COST COMPARISON For this task, the optimal design is obtained for the values reported in Table 14. We see that, compared to the nominal design, the best solution is found for a smaller robot.

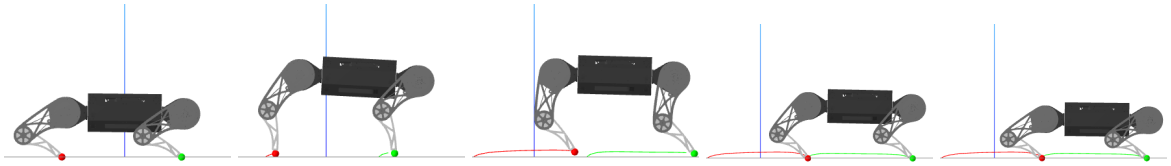

(a) Bounding motion

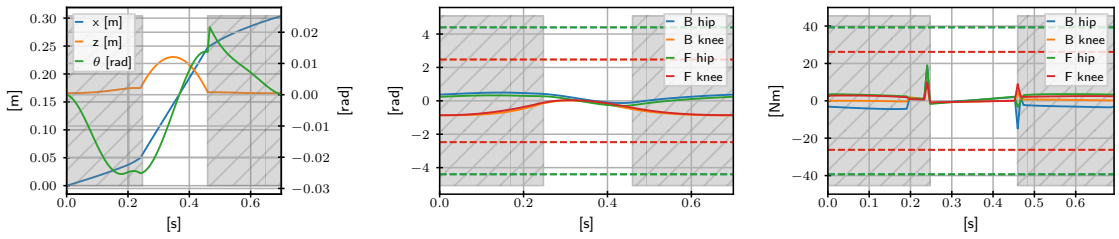

(b) Optimal design minimal energy trajectories

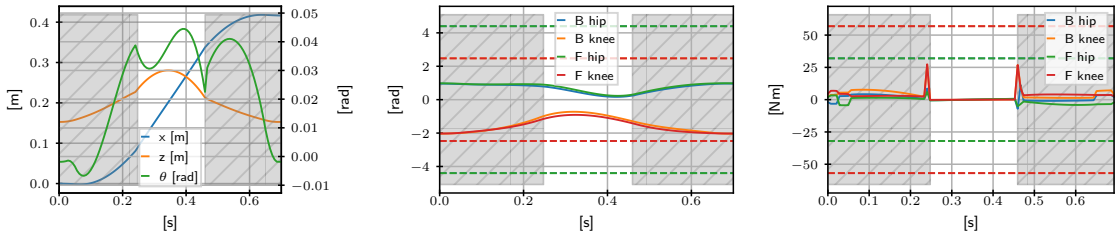

(c) Nominal design minimal energy trajectories

Figure 57: *Bounding task*: Fig. 57a shows the different motion phases. Trajectories for the optimal and the nominal designs are respectively shown in Fig. 57b and Fig. 57c. In both, from left to right, the plots show: base, joint positions and joint torques trajectories. Contact phases are highlighted with grey background.

DISCUSSION The method consistently provides results with $|\gamma| < 10^{-6}$. According to Table 14, the optimization selects a smaller robot, with a different scaling between thigh λ_u and shank λ_l, $\lambda_u/\lambda_l = 1.46$. For bounding it seems that robots with longer thighs are performing better. The optimal solution is chosen to be very close to the lower bound of the variables λ_b, λ_l. The effect of the base length can be observed in Fig. 57b: when its scaling is reduced (Table 14), the trajectories of knee and hip joints are showing a higher similarity. In the nominal case, the joint position is hitting the position limits, which does not happen for the optimized hardware. The optimal quadruped for bounding seems to be shaped as a planar biped: as energetically there is no advantage in carrying a longer and heavier base for this task, then the base length is chosen as short as possible. From the joint positions of the nominal design (Fig. 57c), the knee stopper can partially limit the robot's motion. Finding a re-design that does not impose a limitation would be advisable. For both designs the optimal joint trajectories are smooth and not hitting the velocity bounds. Concerning the actuator selection for this task, a motor capable of rapid motions is not necessary. Conversely, the choice of a higher gear ratio allows larger torque bounds and greatly decreases the Joule losses. Furthermore, a higher reduction is also impacting the system inertia and reducing transparency. However, for bounding with the optimal robot (which is smaller) there is no need to use more dynamic and less energy-efficient motors, hence a higher gear ratio is selected.

To produce the same torque, as the motors have the same motor constant, the ratio of the Joule dissipation is equal to the quotient between the squared values of their gear ratios, with +125% for the smaller one.

4.5 *Co-design for backflip*

As a second task we present the result of a backflip optimization, as shown in Fig. 58. This motion was selected as a complex and dynamic task example, exploiting the whole-body dynamics of the system. The robot starts with zero velocity and has to perform a full rotation of the base before landing. In the landing phase, the excess velocity needs to be damped to reach a full stop at the end of the trajectory. Moreover, also for this task, all joint positions except the base x component need to be equal at the beginning and the end of the trajectory. For this motion the total time to perform the task is 1 s. As represented in Fig. 58a, the different phases are as follows.

- *Dual support*, with all the feet in contact with the ground. In this phase the motors need to accelerate the base to produce enough vertical velocity to break the contact with the ground. Moreover the applied forces need to generate enough momentum for the upcoming rotation of the base.
- *Single support*, with the front legs taking off. This phase is added to allow the robot to start the rotation of the base and still push the ground with the back legs.
- *Flying phase*, in which there is no foot in contact with the ground and the base is following a ballistic movement. The motion of the legs is not contributing to the jump, but is useful to get the feet in the right position before landing (preparing for the impact phase).
- *Single support*, with the front legs touching the ground first.

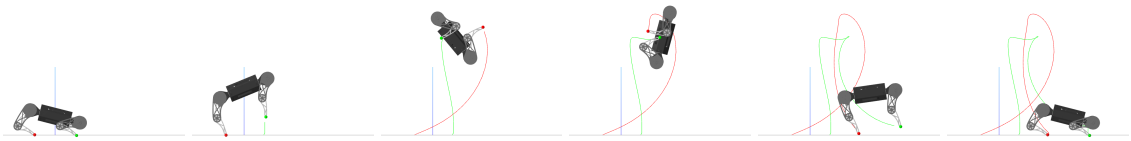

(a) Backflip movement: a full base rotation is required, the state trajectory is cyclic except for the x-translation. The robot must additionally also have zero joint velocity at the extremes of the trajectory.

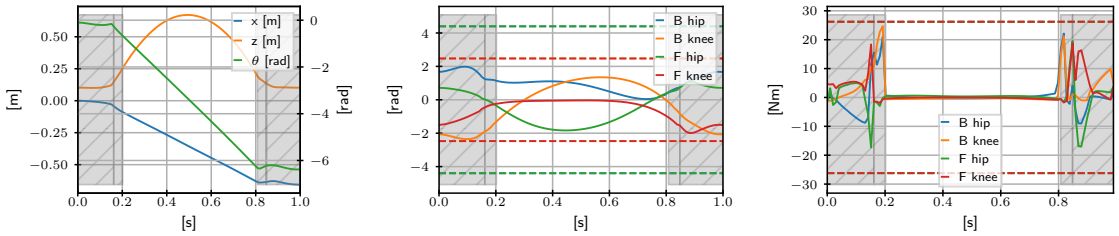

(b) Optimal design minimal energy trajectories

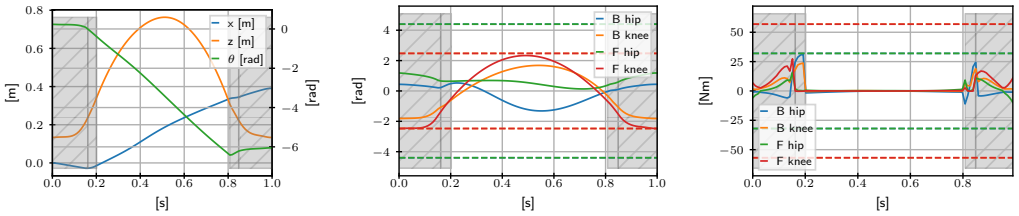

(c) Nominal design minimal energy trajectories

Figure 58: *Backflip task*: Fig. 58a shows the different motion phases. Trajectories for the optimal and the nominal designs are respectively shown in Fig. 58b and Fig. 58b. In both, from left to right, the plots show: base, joint positions and joint torques trajectories. Contact phases are highlighted with grey background.

	NOMINAL	OPTIMIZED
Cost $\mathcal{L}$	5.21	0.67
λ_u	1.0	0.50
λ_l	1.0	0.689
λ_b	1.0	1.07
m_{hip}	AK80-6	AK80-6
m_{knee}	AK80-6	AK80-6

Table 15: Results of the optimization for the backflip

- *Dual support*, with the rear legs reestablishing contact with the ground. The contact needs to be stable, so the forces are inside the friction cone and the motors bring the robot to a full stop at the end of the trajectory.

OUTER-LOOP HYPER-PARAMETERS: CMA-ES is initialized so that each generation is made up by 10^3 individuals and the number of overall evolutions of the population is fixed to 10. In this problem, as the task is more challenging, some design could not physically satisfy the constraints and perform the motion within the problem constraints. *IpOpt* provides debug information on the infeasibility of the problem. If an individual is unfeasible an arbitrary high cost value, higher than the other feasible designs, is assigned to it. The outer-loop algorithm is elitist, meaning that when generating a new population it will automatically discard the outlier designs.

COST COMPARISON: The results for this optimization are reported in Table 15. Running the optimization routine we notice that the leg size is reduced while the base dimensions are slightly increased.

DISCUSSION

The optimization selects a smaller robot, but interestingly a different optimal scaling of thigh λ_u and shank λ_u is found (with ratio $\lambda_u/\lambda_l = 0.73$) with respect to the bounding task. For backflips it seems then that robots with longer shanks are performing better. The optimal solution is very close to the lower bound of the variable λ_u. Fig. 58b and Fig. 58c report the optimal and nominal design trajectories. The optimal base scaling is obtained with a bigger base without reaching the upper bound. This can be explained as there is a trade-off between the base inertia and the capability to apply momentum to perform a full base rotation around θ of -2π rad. For the same applied contact forces, the longer the base, the easier the backflip can be performed. However, there is still a trade-off as a bigger base increases also the inertia of the rigid body. For the backflip, it seems that the most critical constraint is the maximum joint velocity. The nominal design, featuring a higher reduction, can exert more torque but reaches the joint velocity limit. For this task, the knee joint is reaching the position limits of the actuator, in both trajectories, so this constitutes another hint that this limit needs to be

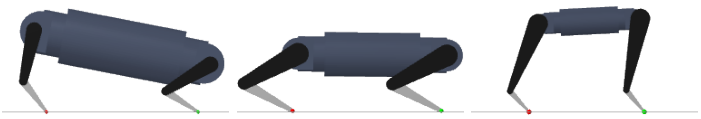

Figure 59: Left to right robot design for: optimized backflip, nominal, optimized bounding

taken into consideration for the final robot design. Compared to the torque required for bounding, in this case saturation is reached. In Fig. 58b and 58c, the low-pass filter effect can be noticed from the smooth torque trajectories that do not exceed the upper and lower torque bounds of the actuator, (shown with dotted lines). For the backflip, a motor that can produce faster motion is needed for task completion. So, for this task, the motor selection goes in the opposite direction to what was obtained for the bounding task, leading to a smaller reduction to achieve a higher joint velocity. In this case, as the motion is quicker, the effect of the rotor inertia is higher and a smaller reduction helps in accelerating the joint.

4.6 *Landscape analysis for multiple objectives*

As expected, rather different designs were produced for the two tasks by the co-design optimization (Table 14 and 15, Fig. 59). Therefore, an additional grid-search was performed to better understand the impact of the design selection. In this case the base was kept to the nominal length $\lambda_b = 1$, and we studied the leg design for the two tasks presented before. The scaling of the upper and lower leg link is then studied together with the motor selection. For the scaling a uniform grid of 50×50 was studied within the range $[0.5, 1.5]$. The results are depicted in Fig. 60a and 60b for the bounding and the backflip tasks, respectively. The plots show the value of the cost against the scaling of the upper link λ_u and lower link λ_l once a specific motor combination is chosen. From the trends of the optimal value $\mathcal{L}$ some orthogonality emerges between the two tasks in the design space. In Fig. 60b the white regions are associated with unfeasible problems, which occur consistently in the case of robots with short shanks and long thighs.

With the values obtained from the grid search the Pareto frontier was reconstructed (Fig. 61) for the two different tasks costs. The resulting Pareto front is reported in Table 16, it constitutes a reduced set of candidates that can perform both bounding and backflip reasonably well. As a second order criterion, the designs that involve less modifications to the nominal prototype are preferred. This is driven by practical considerations: modifying the shank link is easier than the thigh, as the modification of the latter involves a re-design of the transmission, which is more challenging. Moreover an optimized robot for bounding is preferred if this implies a sacrifice of performance for backflips (locomotion on the x direction is the main movement mode). So the closest options are the 2^{nd} and 3^{rd} rows of Table 16, which use the same motors and a lower

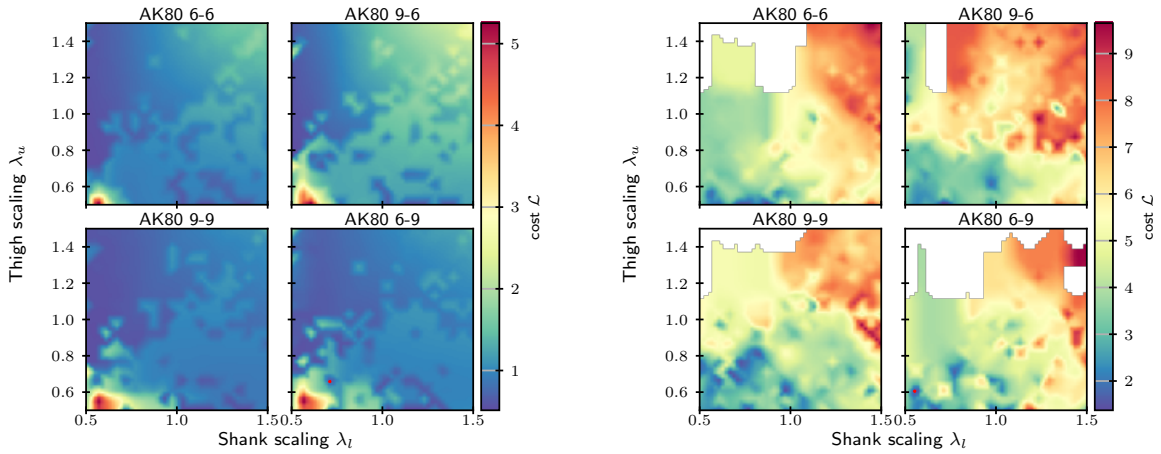

(a) Jumping task landscape

(b) Backflip task landscape

Figure 60: Landscapes for different combinations of motors and link scaling, for two different tasks

link very close to the nominal one. Among the two, the one with the scaling parameter of the thigh at $\lambda_u = 0.66$ was selected. The chosen design, decreases the cost for the motion as shown in Fig. 61. The relative improvement of this design with respect to the nominal one is 52% for backflip and 67% for bounding. Some performance was sacrificed for the sake of versatility, because this is less than what was found for the design that optimize a single task, with relative improvements of 87% and 77% respectively.

5 CONCLUSION

In this chapter, our co-design framework was improved to gain more completeness and versatility, and we applied it to the optimization of a quadruped robot developed at DFKI RIC. Two cyclic tasks were selected to represent different key motion capabilities. In the initial phase, optimal hardware solutions were found for each of the two tasks separately, showing an improvement of up to 87% for energy consumption. Related to these results, the scaling for bounding are similar (in the ratio between shank and thighs) to one found in a previous publication [62], even if based on other model assumptions (template models). Since the two optimizations led to rather different designs, we used a Pareto set approach to select a versatile and efficient trade-off, providing a computational basis to enhance the robot hardware design for the next prototype. This insight will be used for the development of the next quadruped version. The core elements of this work are: first, the development of a more robust and parallelizable bi-level scheme capable of handling mixed-integer variables and, second, a more versatile OCP formulation with equality and inequality constraints, which allows coping with actuation band-

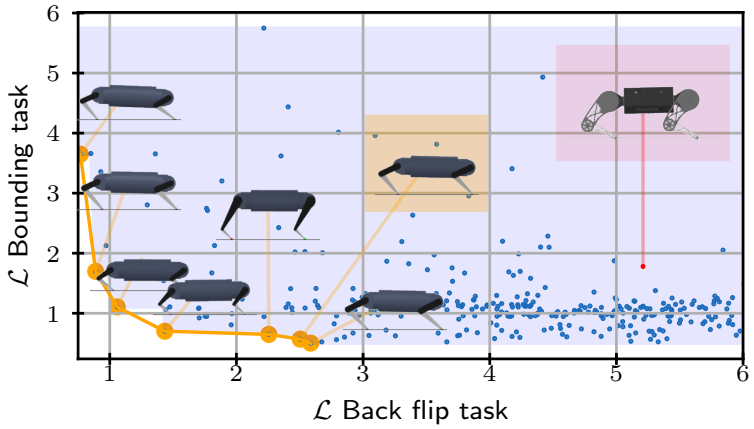

Figure 61: Pareto front approximation for the two tasks' cost. The designs are superimposed. The one highlighted in orange is the design which requires the least modifications to the nominal prototype, shown in red.

λ_u	λ_l	m_{hip}	m_{knee}	$\mathcal{L}$ BACKFLIP	$\mathcal{L}$ BOUNDING
0.50	0.87	AK80-6	AK80-6	1.06	1.11
0.50	1.03	AK80-6	AK80-6	2.59	0.50
0.66	1.03	AK80-6	AK80-6	2.50	0.57
0.71	0.55	AK80-6	AK80-6	0.77	3.65
0.50	0.71	AK80-9	AK80-9	0.89	1.70
0.61	0.97	AK80-9	AK80-9	1.43	0.70
1.08	0.50	AK80-9	AK80-9	2.26	0.65

Table 16: Pareto optimal designs for the two tasks, lower values of $\mathcal{L}$ indicate better performance.

width and motion cyclicity. The energy consumption and friction models of the actuator used in trajectory optimization were validated on the real robot prototype. Future work, and extension to this contribution will be detailed in the next chapter.

Part V

CONCLUSION

In this conclusive part, the thesis work is summarized, and the main findings and contributions are highlighted. The strengths and weaknesses of the research are evaluated, providing an assessment of the work's significance and limitations. Additionally, potential research directions for future development are suggested, outlining promising areas that could benefit from further investigation.

12

SUMMARY OF THE RESULTS AND OPEN QUESTIONS

In Short

In this final chapter the work presented in this thesis is wrapped-up. Some final remarks about the strengths and weaknesses of the contributions are highlighted and some promising research directions are suggested for future development.

Contents

1 MAIN FINDINGS

In this dissertation, optimal hardware for energy efficiency was optimized using co-design. The problem was tackled from the beginning with a general approach that allowed different extensions. The bi-level framework that was selected is quite general and can be adapted in different ways allowing several analyses of the systems and the tasks. The results follow these different stages of the work. In particular, the earliest work involved developing a reliable physical model of the actuators and the structural scaling. With this technique, the hardware for a jumping monoped was optimized leading to remarkable energy efficiency improvements in the optimization. The same framework was later used for addressing the robustness of hardware to perturbation. In this sense, a novel technique to evaluate the performance of hardware in perturbed simulations was proposed. This method exploits at best the use of DDP in optimization, allowing to efficiently re-use the optimal local feedback controller information to track the optimal trajectory in perturbed simulations. This work was also parallelized to make the computation times reasonable. In the time of several hours, hundreds of thousands of robot designs are computationally evaluated for a specific task, with little prior information. This provides some rather useful information to the user when a new platform has to be selected. This has also been the core goal of the collaboration with DFKI for the optimization of a quadruped prototype. Our framework was adapted in this case to deal with the design of a quadruped with different actuators and for more complex,

cyclic, locomotion tasks. This result required new tools to perform trajectory optimization, because it was needed to enforce hard constraints. In this case, the validation of the model for energy efficient cyclic tasks was achieved. The results of these presented contributions seem to point us in the right direction, and we can work to progressively increase the scope of our work even further as will be explained in the next chapter.

2 PROSPECTS AND UNSOLVED PROBLEMS

The work we performed in the study of legged robots with co-design progressively opened some new paths and made new questions arise. Solutions to some of them, such as the robustness problems have been suggested. Many others, however, due to the complexity of co-design, are still open. In particular, in the next paragraphs, some of the most promising directions for future research are summed up.

HARDWARE REFINEMENT AND TESTING Albeit we strive to be general, many final design choices (i. e. topological optimization) are left for the last implementation stage, possibly implying way too many modifications from the prototype design. If this is the case, the optimization output and the implementation of the robot would hopelessly diverge, impacting the quality of the optimized robot. Since in future work, it is planned to build and test the virtual systems, such eventuality has to be considered. To include it in the framework, more general robot models need to be developed. Moreovoer, experimental testing of hardware solutions is needed. Our co-design approach is not made to automatize completely the robot design, as it still needs user input and further model refinement. Since sim-to-real gaps are difficult to eliminate, some iterations, looping-back on the framework with data-driven information is crucial for the development and validation of various co-designed systems. Co-design should involve testing the hardware under controlled conditions to assess its functionality, performance, and reliability. With system identification and the validation of the power consumption on the quadruped robot, just a small part of this work has been achieved. For future applications, the ties with hardware should be explored even more in-depth. Possibly, the current representation of the robot characteristics, to use a genetic analogy, "the robot DNA", may not be sufficient. A systematic view on the automatic generation of robots can be found in [122], where the perspective of generating complete assemblies with rich kinematic and sensorimotor description is outlined.

ROBUSTNESS In the proposed robust controller selection, gain tuning is performed at a later stage, from the outer-loop, while it may be important for robustness to consider the controller in the inner loop. In-depth comparison with works that follow this approach, such as [36] may lead us to interesting results. In future work, we plan to address this, possibly including optimal gain selection in the OCP. However, the main limitation of the method remains the computational cost of the OCP, and we are aware that its resolution may become a bottleneck for more complex systems or tasks, even if we proposed a method that scales more favorably. A final very important step is

also to certify that the robustness translates into the real system. Especially when the optimized hardware implementation is finally built. In our latest work, the nominal trajectories could be easily tracked on the DFKI quadruped prototype, but in general, the entity of the *sim-to-real* gap has to be evaluated and some techniques to mitigate its effect may be necessary.

IMPROVING THE SYNTHESIS OF BEHAVIORS One of the strengths of our approach, which can be seen especially in the latest contribution, lies within its versatility: the problem can be specified in a rather high-level way. This is quite powerful: the task can be achieved with very little user specification, just imposing a cost and physical constraints based on the actuator type and the motion. Such freedom comes however at a price, working at the actuator level, which is necessary for the envisioned application is leading to a very complex OCP. In this work parallelization, symmetries and task cyclicity were exploited. However, for more complex motions and a higher number of DoFs, the computation time of the OCP may become a bottleneck. The resolution of such a problem is the most critical part of our method. Faster solvers or custom-made adaptations may be more efficient, but they are not the answer. They may be more constraining and more brittle requiring more tuning from the user. On this side, there is no clear winner, as there is a trade-off between the freedom from more general solvers and the speed from specialized ones. Along the thesis work, different implementations have been tried out, but they require way too much domain-specific knowledge to be used by non-experts. So two problems are still open: computation times and versatility of the approach. In our work, the mechanism of parallelization has been shown as a way to considerably speed up the computation. Another possibility is the use of warmstart of the OCP. Storing previously computed information, it is possible to associate a problem with an already computed "near" solution. With DDP especially, the gains from the computational point of view are remarkable and the framework allows a simple extension of a data-driven warmstart by creating a library of previously computed motions. Related to the versatility of the problem instead, some emerging data-driven approaches, such as RL, are capable of discovering very complex behaviors, with minimal user intervention. Their use in co-design may lead to some new applications, potentially difficult to formalize with OCP, in the field. Another advanced technical implementation would require the use of differentiable simulators in the OCP, which are getting popular for policy learning and optimization and co-design [90]. Thanks to their formulation, they would allow a more general description of the system (i. e. the capability of differentiating through the contact phases and the robot model). Some early work has already been moved in this direction, showing very promising results.

Near in the design space

MATURITY AND USABILITY Even if useful insights can be recovered with this tool, expert knowledge is still needed to select many details about the task (i. e. the OCP) or the design (i. e. the final design on the Pareto set or from the continuous approximation of motor selection). Of course, our method cannot completely automatize the whole workflow. We wonder, however, if using a different problem formulation, capable

of handling multiple objectives differently (e. g. with weights or hierarchically), may reduce this effect. Also, related to the choice of the representative tasks, which in our work was done following intuition, we wonder if it can be guided by an algorithm instead.

GENERATIVE DESIGN A possible evolution of the co-design framework in connection with generative design can be seen. Some frameworks can already generate design solutions for the synthesis of simple products under some user requirement specification [49]. It is possible that in the future, even a complete model of a robot (from the `urdf` to the bill of material) will be co-designed as the output of some generic description such as "build a bipedal robot that can run at 5 m/s". To achieve this goal, a lot of work has to be done on the formal description of the robots (which is still not general enough), and to convert the engineering workflow into a systematic computational algorithm.

CO-DESIGN FOR A COOPERATIVE ROBOTICS COMMUNITY

"Humans are the reproductive organs of technology.
We multiply manufactured artifacts and spread ideas and memes."

— Kevin Kelly, What Technology Wants

Sharing similar hardware makes it easier for researchers to replicate results, which is one of the compelling goals of open science.

Transparency and accountability can also be achieved more easily. With open platforms, it is possible to start discussions on potential safety risks, which would turn into a more aware use.

Co-design needs to start with hardware and good implementation ideas. The tools that have been presented are still rather experimental and not general enough to be used by a domain of non-expert users and most of all to replace engineers and roboticists: the decisions about the final implementation are still up to the system designers. Co-design will become an important component of designing future robots. However, there are some possible issues tied to its applicability, especially on the hardware side. To reduce the barrier to the synthesis of optimized robots, the approach should be accompanied by an open design philosophy. An open-hardware approach has already been used in many projects, for instance, ODRI, as seen in chapter 6. Freely sharing robotic technical knowledge is fostered by associations like the Open Source Hardware Association (OSHWA) [1], which encourages research that is accessible, collaborative and respects user freedom. The robotic community greatly benefits from these trends which enable collaboration, innovation, and accessibility. Co-design too would gain momentum through knowledge sharing within the robotic community, especially for what concerns hardware implementation and customization. By openly sharing designs, schematics, and specifications, developers and researchers can benefit from each other's expertise, and build upon existing work thanks to rapid prototyping and experimentation. Lowering the barrier to entry for creating new robotic systems would make the field of robotics advance, and address real-world challenges more effectively.

As individuals collaborate and improve upon the design process, they learn from each other, share insights, and collectively improve their understanding of robotics. I hope that this knowledge-sharing vision, without which this work would not have been possible, will be used in many other projects for the benefit of the future.

1 https://www.oshwa.org/

BIBLIOGRAPHY

[1] A. Abate, R. L. Hatton, and J. Hurst, "Passive-dynamic leg design for agile robots", in *2015 IEEE International Conference on Robotics and Automation (ICRA)*, Seattle, WA, USA: IEEE, May 2015, pp. 4519–4524. DOI: 10.1109/ICRA.2015.7139825. [Online]. Available: http://ieeexplore.ieee.org/document/7139825/ (cit. on p. 26).

[2] A. Abate, J. W. Hurst, and R. L. Hatton, "Mechanical antagonism in legged robots", in *Robotics: Science and Systems XII*, Robotics: Science and Systems Foundation, 2016. DOI: 10.15607/RSS.2016.XII.008. [Online]. Available: http://www.roboticsproceedings.org/rss12/p08.pdf (cit. on p. 26).

[3] S. Agrawal, Shuo Shen, and M. Van De Panne, "Diverse motions and character shapes for simulated skills", *IEEE Transactions on Visualization and Computer Graphics*, vol. 20, no. 10, pp. 1345–1355, Oct. 1, 2014. DOI: 10.1109/TVCG.2014.2314658. [Online]. Available: http://ieeexplore.ieee.org/document/6781622/ (cit. on p. 75).

[4] R. M. Alexander, *Principles of animal locomotion*. Princeton university press, 2003 (cit. on p. 91).

[5] R. M. Alexander, "The gaits of bipedal and quadrupedal animals", *The International Journal of Robotics Research*, vol. 3, no. 2, pp. 49–59, 1984. DOI: 10.1177/027836498400300205 (cit. on pp. 91, 97).

[6] J. Allison, "Complex system optimization: A review of analytical target cascading, collaborative optimization, and other formulations", Feb. 2020 (cit. on p. 74).

[7] J. Allison and Z. Han, "Co-design of an active suspension using simultaneous dynamic optimization", vol. 136, Jan. 2011. DOI: 10.1115/DETC2011-48521 (cit. on pp. 7, 74, 102).

[8] J. Allison and D. R. Herber, "Multidisciplinary design optimization of dynamic engineering systems", in *54th AIAA/ASME/ASCE/AHS/ASC Structures, Structural Dynamics, and Materials Conference*, Boston, Massachusetts: American Institute of Aeronautics and Astronautics, Apr. 8, 2013. DOI: 10.2514/6.2013-1462. [Online]. Available: https://arc.aiaa.org/doi/10.2514/6.2013-1462 (cit. on p. 73).

[9] J. T. Allison, "Engineering system co-design with limited plant redesign", *Engineering Optimization*, vol. 46, no. 2, pp. 200–217, 2014 (cit. on p. 74).

[10] J. T. Allison and S. Nazari, "Combined plant and controller design using decomposition based design optimization and the minimum principle", ser. International Design Engineering Technical Conferences and Computers and Information in Engineering Conference, vol. Volume 1: 36th Design Automation Conference, Parts A and B, Aug. 2010, pp. 765–774. DOI: 10.1115/DETC2010-28887.

eprint: https://asmedigitalcollection.asme.org/IDETC-CIE/proceedings-pdf/IDETC-CIE2010/44090/765/2696716/765_1.pdf (cit. on pp. 7, 74).

[11] A. Ananthanarayanan, M. Azadi, and S. Kim, "Towards a bio-inspired leg design for high-speed running", *Bioinspiration & Biomimetics*, vol. 7, no. 4, p. 046 005, Dec. 1, 2012. DOI: 10.1088/1748-3182/7/4/046005. [Online]. Available: https://iopscience.iop.org/article/10.1088/1748-3182/7/4/046005 (cit. on p. 59).

[12] J. A. E. Andersson, J. Gillis, G. Horn, *et al.*, "CasADi A software framework for nonlinear optimization and optimal control", *Mathematical Programming Computation*, vol. 11-(1), 2019 (cit. on p. 127).

[13] A. S. Anthony and A. P. Pallewatta, "Four legged walking robot with smart gravitational stabilization", 2017 (cit. on p. 19).

[14] Anybotics, *Anymal X*, https://www.anybotics.com/anymal-x-the-worlds-first-ex-proof-legged-robot/ (cit. on p. 20).

[15] M. Aractingi, P.-A. Leziart, T. Flayols, *et al.*, "Learning to Adapt the Trotting Gait of the Solo Quadruped", working paper or preprint, Oct. 2021, [Online]. Available: https://hal.laas.fr/hal-03409682 (cit. on p. 22).

[16] M. Aractingi, P.-A. Léziart, T. Flayols, *et al.*, "Controlling the Solo12 Quadruped Robot with Deep Reinforcement Learning", working paper or preprint, Aug. 2022, [Online]. Available: https://hal.laas.fr/hal-03761331 (cit. on p. 22).

[17] J. Auerbach, D. Aydin, A. Maesani, *et al.*, "RoboGen: Robot generation through artificial evolution", presented at the ALIFE 14: The Fourteenth International Conference on the Synthesis and Simulation of Living Systems, Jul. 1, 2014, pp. 136–137. DOI: 10.1162/978-0-262-32621-6-ch022. [Online]. Available: https://doi.org/10.1162/978-0-262-32621-6-ch022 (cit. on p. 77).

[18] J. E. Auerbach and J. C. Bongard, "Evolving complete robots with CPPN-NEAT: The utility of recurrent connections", in *Proceedings of the 13th annual conference on Genetic and evolutionary computation*, Dublin Ireland: ACM, Jul. 12, 2011, pp. 1475–1482. DOI: 10.1145/2001576.2001775. [Online]. Available: https://dl.acm.org/doi/10.1145/2001576.2001775 (cit. on p. 77).

[19] J. E. Auerbach and J. C. Bongard, "Dynamic resolution in the co-evolution of morphology and control", in *IEEE Symposium on Artificial Life*, 2010. [Online]. Available: https://api.semanticscholar.org/CorpusID:1020890 (cit. on p. 77).

[20] R. F. Battaglia, "Design of the scout ii quadruped with preliminary stair-climbing", 1999 (cit. on p. 17).

[21] D. N. Beal, F. S. Hover, M. S. Triantafyllou, *et al.*, "Passive propulsion in vortex wakes", *Journal of Fluid Mechanics*, vol. 549, no. -1, p. 385, Feb. 8, 2006. DOI: 10.1017/S0022112005007925. [Online]. Available: http://www.journals.cambridge.org/abstract_S0022112005007925 (cit. on p. 90).

[22] R. Bellman, *Dynamic Programming*, ser. Dover Books on Computer Science Series. Dover Publications, 2003. [Online]. Available: https://books.google.fr/books?id=fyVtp3EMxasC (cit. on p. 84).

[23] Á. Belmonte-Baeza, J. Lee, G. Valsecchi, *et al.*, "Meta reinforcement learning for optimal design of legged robots", *IEEE Robotics and Automation Letters*, vol. 7, no. 4, pp. 12 134–12 141, Oct. 2022. DOI: 10.1109/LRA.2022.3211785. arXiv: 2210.02750[cs,eess]. [Online]. Available: http://arxiv.org/abs/2210.02750 (cit. on p. 77).

[24] F. Bergonti, G. Nava, V. Wüest, *et al.*, "Co-design optimisation of morphing topology and control of winged drones", 2023, Publisher: arXiv Version Number: 1. DOI: 10.48550/ARXIV.2309.13948. [Online]. Available: https://arxiv.org/abs/2309.13948 (cit. on p. 73).

[25] P. Biswal and P. K. Mohanty, "Development of quadruped walking robots: A review", *Ain Shams Engineering Journal*, vol. 12, no. 2, pp. 2017–2031, Jun. 2021. DOI: 10.1016/j.asej.2020.11.005. [Online]. Available: https://linkinghub.elsevier.com/retrieve/pii/S2090447920302501 (cit. on p. 15).

[26] F. Bjelonic, J. Lee, P. Arm, *et al.*, "Learning-based design and control for quadrupedal robots with parallel-elastic actuators", *IEEE Robotics and Automation Letters*, vol. 8, no. 3, pp. 1611–1618, Mar. 2023. DOI: 10.1109/LRA.2023.3234809. [Online]. Available: https://ieeexplore.ieee.org/document/10008034/ (cit. on p. 77).

[27] D. J. Blackman, J. V. Nicholson, C. Ordonez, *et al.*, "Gait development on Minitaur, a direct drive quadrupedal robot", in *Unmanned Systems Technology XVIII*, R. E. Karlsen, D. W. Gage, C. M. Shoemaker, *et al.*, Eds., International Society for Optics and Photonics, vol. 9837, SPIE, 2016, pp. 141–155. DOI: 10.1117/12.2231105. [Online]. Available: https://doi.org/10.1117/12.2231105 (cit. on pp. 19, 20, 59).

[28] G. Bledt, M. J. Powell, B. Katz, *et al.*, "Mit cheetah 3: Design and control of a robust, dynamic quadruped robot", in *2018 IEEE/RSJ International Conference on Intelligent Robots and Systems (IROS)*, 2018, pp. 2245–2252. DOI: 10.1109/IROS.2018.8593885 (cit. on pp. 19, 59, 93).

[29] M. Bogdanovic, M. Khadiv, and L. Righetti, "Learning variable impedance control for contact sensitive tasks", *IEEE RAL*, vol. 5, pp. 6129–6136, 2020 (cit. on pp. 98, 111).

[30] P. Boscariol, L. Scalera, and A. Gasparetto, "Task-dependent energetic analysis of a 3 d.o.f. industrial manipulator", in. Jan. 2020, pp. 162–169. DOI: 10.1007/978-3-030-19648-6_19 (cit. on p. 49).

[31] Boston Dynamics Inc., *Atlas: Antropomorphic robot* (cit. on pp. 14, 39).

[32] W. Bosworth, S. Kim, and N. Hogan, "The MIT super mini cheetah: A small, low-cost quadrupedal robot for dynamic locomotion", in *IEEE SSRR*, 2015 (cit. on pp. 19, 76).

[33] S. Boyd, C. Baratt, and S. Norman, "Linear controller design: Limits of performance via convex optimization", *Proceedings of the IEEE*, vol. 78, no. 3, 1990 (cit. on p. 106).

[34] P. Brault, Q. Delamare, and P. Robuffo Giordano, "Robust trajectory planning with parametric uncertainties", in *IEEE Int. Conf. on Robotics & Automation*, 2021 (cit. on p. 105).

[35] G. Bravo-Palacios, A. Del Prete, and P. M. Wensing, "One robot for many tasks: Versatile co-design through stochastic programming", *IEEE RAL*, vol. 5, no. 2, pp. 1680–87, 2020 (cit. on p. 106).

[36] G. Bravo-Palacios, G. Grandesso, A. Del Prete, *et al.*, "Robust co-design: Coupling morphology and feedback design through stochastic programming", *Journal of Dynamic Systems, Measurement, and Control*, Feb. 1, 2022 (cit. on pp. 106, 150).

[37] G. Bravo-Palacios and P. M. Wensing, "Large-scale ADMM-based co-design of legged robots", in *IEEE/RSJ Int. Conf. on Intelligent Robots and Systems*, 2022 (cit. on pp. 76, 79, 106).

[38] H. Bruyninckx, P. Soetens, and B. Koninckx, "The real-time motion control core of the orocos project", in *2003 IEEE International Conference on Robotics and Automation (Cat. No.03CH37422)*, vol. 2, Sep. 2003, 2766–2771 vol.2. DOI: 10.1109/ROBOT.2003.1242011 (cit. on p. 33).

[39] G. Buondonno, J. Carpentier, G. Saurel, *et al.*, "Actuator design of compliant walkers via optimal control", in *IEEE/RSJ Int. Conf. on Intelligent Robots & Systems*, 2017 (cit. on pp. 74, 75).

[40] L. Carlone and C. Pinciroli, "Robot co-design: Beyond the monotone case", in *2019 International Conference on Robotics and Automation (ICRA)*, Montreal, QC, Canada: IEEE, May 2019, pp. 3024–3030. DOI: 10.1109/ICRA.2019.8793926. [Online]. Available: https://ieeexplore.ieee.org/document/8793926/ (cit. on p. 73).

[41] J. Carpentier and N. Mansard, "Analytical Derivatives of Rigid Body Dynamics Algorithms", in *Robotics: Science and Systems*, 2018 (cit. on pp. 97, 127).

[42] J. Carpentier, G. Saurel, G. Buondonno, *et al.*, "The Pinocchio C++ library – A fast and flexible implementation of rigid body dynamics algorithms and their analytical derivatives", in *IEEE/SICE Int. Symposium on System Integration*, 2019. DOI: 10.1109/SII.2019.8700380 (cit. on pp. 33, 97, 127).

[43] A. Censi, *A mathematical theory of co-design*, Oct. 12, 2016. arXiv: 1512.08055[cs, math]. [Online]. Available: http://arxiv.org/abs/1512.08055 (cit. on p. 73).

[44] ——, "Monotone co-design problems; or, everything is the same", in *2016 American Control Conference (ACC)*, Boston, MA, USA: IEEE, Jul. 2016, pp. 1227–1234. DOI: 10.1109/ACC.2016.7525085. [Online]. Available: http://ieeexplore.ieee.org/document/7525085/ (cit. on p. 73).

[45] ——, "Uncertainty in monotone codesign problems", *IEEE Robotics and Automation Letters*, vol. 2, no. 3, pp. 1556–1563, Jul. 2017. DOI: 10.1109/LRA.2017.2674970. [Online]. Available: http://ieeexplore.ieee.org/document/7864337/ (cit. on p. 73).

[46] M. Chadwick, H. Kolvenbach, F. Dubois, *et al.*, "Vitruvio: An open-source leg design optimization toolbox for walking robots", *IEEE Robotics and Automation Letters*, 2020 (cit. on pp. 76, 79).

[47] H. Chai, Y. Li, R. Song, *et al.*, "A survey of the development of quadruped robots: Joint configuration, dynamic locomotion control method and mobile manipulation approach", *Biomimetic Intelligence and Robotics*, vol. 2, no. 1, p. 100 029, Mar. 2022. DOI: 10.1016/j.birob.2021.100029. [Online]. Available: https://linkinghub.elsevier.com/retrieve/pii/S2667379721000292 (cit. on p. 15).

[48] T. Chen, Z. He, and M. T. Ciocarlie, "Hardware as policy: Mechanical and computational co-optimization using deep reinforcement learning", in *Conference on Robot Learning*, 2020. [Online]. Available: https://api.semanticscholar.org/CorpusID:221095482 (cit. on p. 77).

[49] X. '. Chen, Y. Tao, G. Wang, *et al.*, "Forte: User-driven generative design", in *Proceedings of the 2018 CHI Conference on Human Factors in Computing Systems*, Montreal QC Canada: ACM, Apr. 21, 2018, pp. 1–12. DOI: 10.1145/3173574.3174070. [Online]. Available: https://dl.acm.org/doi/10.1145/3173574.3174070 (cit. on p. 152).

[50] N. Cheney, R. MacCurdy, J. Clune, *et al.*, "Unshackling evolution: Evolving soft robots with multiple materials and a powerful generative encoding", *ACM SIGEVOlution*, vol. 7, no. 1, pp. 11–23, Aug. 2014. DOI: 10.1145/2661735.2661737. [Online]. Available: https://dl.acm.org/doi/10.1145/2661735.2661737 (cit. on p. 74).

[51] C. Chevallereau and Y. Aoustin, "Optimal reference trajectories for walking and running of a biped robot", *Robotica*, no. 5, 2001 (cit. on p. 129).

[52] C. Chevallereau, P. Wenger, Y. Aoustin, *et al.*, "Leg design for biped locomotion with mono-articular and bi-articular linear actuation", *Mechanism and Machine Theory*, vol. 156, p. 104 138, Feb. 2021. DOI: 10.1016/j.mechmachtheory.2020.104138. [Online]. Available: https://linkinghub.elsevier.com/retrieve/pii/S0094114X20303554 (cit. on p. 76).

[53] S. H. Collins, M. Wisse, and A. Ruina, "A three-dimensional passive-dynamic walking robot with two legs and knees", *The International Journal of Robotics Research*, vol. 20, no. 7, pp. 607–615, Jul. 2001. DOI: 10.1177/02783640122067561 (cit. on p. 74).

[54] S. Coros, P. Beaudoin, and M. Van De Panne, "Generalized biped walking control", *ACM Transactions on Graphics*, vol. 29, no. 4, pp. 1–9, Jul. 26, 2010. DOI: 10.1145/1778765.1781156. [Online]. Available: https://dl.acm.org/doi/10.1145/1778765.1781156 (cit. on p. 75).

[55] S. Coros, A. Karpathy, B. Jones, *et al.*, "Locomotion skills for simulated quadrupeds", *ACM Trans. Graph.*, vol. 30, p. 59, Jul. 2011. DOI: 10.1145/2010324.1964954 (cit. on p. 74).

[56] S. Coros, B. Thomaszewski, G. Noris, *et al.*, "Computational design of mechanical characters", *ACM Trans. on Graphics*, vol. 32-(4), 2013 (cit. on p. 74).

[57] F. Corucci, N. Cheney, F. Giorgio-Serchi, *et al.*, "Evolving soft locomotion in aquatic and terrestrial environments: Effects of material properties and environmental transitions", *Soft Robotics*, vol. 5, no. 4, pp. 475–495, Aug. 28, 2018. DOI: 10.1089/soro.2017.0055. [Online]. Available: https://www.liebertpub.com/doi/10.1089/soro.2017.0055 (cit. on p. 74).

[58] E. Coumans *et al.*, "Bullet physics library", *Open source: bulletphysics. org*, vol. 15, no. 49, p. 5, 2013 (cit. on p. 34).

[59] ——, "Bullet physics library", *Open source: bulletphysics. org*, vol. 15, no. 49, p. 5, (cit. on pp. 107, 108).

[60] J. J. Craig, "Introduction to robotics: Mechanics and control (3-rd edition)", *PEARSON Prentice Hall*, pp. 41–46, 2005 (cit. on p. 40).

[61] H. Dai, A. Valenzuela, and R. Tedrake, "Whole-body motion planning with centroidal dynamics and full kinematics", in *IEEE-RAS International Conference on Humanoid Robots*, 2014 (cit. on p. 129).

[62] S. Dallas, K. Machairas, K. Koutsoukis, *et al.*, "A leg design method for high speed quadrupedal locomotion", in *2017 IEEE/RSJ International Conference on Intelligent Robots and Systems (IROS)*, Vancouver, BC: IEEE, Sep. 2017, pp. 4877–4882. DOI: 10.1109/IROS.2017.8206365. [Online]. Available: http://ieeexplore.ieee.org/document/8206365/ (cit. on pp. 76, 143).

[63] E. L. Dantec, M. Taix, and N. Mansard, "First Order Approximation of Model Predictive Control Solutions for High Frequency Feedback", in *IEEE ICRA*, Philadelphia, US, 2022 (cit. on pp. 107, 109).

[64] A. De and D. E. Koditschek, "The Penn Jerboa: A platform for exploring parallel composition of templates", 2015, Publisher: arXiv Version Number: 2. DOI: 10.48550/ARXIV.1502.05347. [Online]. Available: https://arxiv.org/abs/1502.05347 (cit. on p. 19).

[65] P. G. De Santos, E. Garcia, and J. Estremera, *Quadrupedal locomotion: an introduction to the control of four-legged robots*. Springer, 2006, vol. 1 (cit. on pp. 15, 21).

[66] K. D. De Vincenti Flavio and S. Coros, "Control-aware design optimization for bio-inspired quadruped robots", *Control-Aware Design Optimization for Bio-Inspired Quadruped Robots*, 2021. [Online]. Available: http://crl.ethz.ch/papers/controlAwareDesign.pdf (cit. on p. 76).

[67] J. Deese and C. Vermillion, "Nested Plant/Controller Codesign Using G-Optimal Design and Continuous Time Adaptation Laws: Theoretical Framework and Application to an Airborne Wind Energy System", *Journal of Dynamic Systems, Measurement, and Control*, vol. 140, no. 12, Aug. 2018, 121013 (cit. on pp. 74, 106).

[68] A. Del Prete and N. Mansard, "Robustness to joint-torque-tracking errors in task-space inverse dynamics", *IEEE T-RO*, vol. 32, no. 5, pp. 1091–1105, 2016 (cit. on p. 109).

[69] R. Desai, B. Li, Y. Yuan, *et al.*, "Interactive co-design of form and function for legged robots using the adjoint method", *arXiv:1801.00385 [cs]*, Apr. 15, 2018. arXiv: 1801.00385. [Online]. Available: http://arxiv.org/abs/1801.00385 (cit. on p. 76).

[70] R. Desai, Y. Yuan, and S. Coros, "Computational abstractions for interactive design of robotic devices", in *2017 IEEE International Conference on Robotics and Automation (ICRA)*, Singapore, Singapore: IEEE, May 2017, pp. 1196–1203. DOI: 10.1109/ICRA.2017.7989143. [Online]. Available: http://ieeexplore.ieee.org/document/7989143/ (cit. on p. 76).

[71] K. M. Digumarti, C. Gehring, S. Coros, *et al.*, "Concurrent optimization of mechanical design and locomotion control of a legged robot", *Mobile Service Robotics*, pp. 315–323, 2014 (cit. on pp. 75, 79).

[72] T. Dinev, C. Mastalli, V. Ivan, *et al.*, "Co-designing robots by differentiating motion solvers", *ArXiv: 2103.04660*, 2021 (cit. on p. 106).

[73] ——, "A versatile co-design approach for dynamic legged robots", in *IEEE/RSJ Int. Conf. on Intelligent Robots and Systems*, 2022 (cit. on pp. 76, 79).

[74] J. Driessen, "Design of high-performance legged robots: A case study on a hopping and balancing robot", Jul. 11, 2019, Publisher: Universitá degli studi di Genova. DOI: 10.15167/DRIESSEN-JOSEPHUS_PHD2019-07-11. [Online]. Available: https://iris.unige.it//handle/11567/950662 (cit. on pp. 27, 76).

[75] I. S. Duff, "MA57 a code for the solution of sparse symmetric definite and indefinite systems", 2, vol. 30, New York, NY, USA: Association for Computing Machinery, 2004, pp. 118–144 (cit. on p. 127).

[76] G. Fadini, T. Flayols, A. Del Prete, *et al.*, "Computational design of energy-efficient legged robots: Optimizing for size and actuators", in *2021 IEEE International Conference on Robotics and Automation (ICRA)*, Xi'an, China: IEEE, May 30, 2021, pp. 9898–9904. DOI: 10.1109/ICRA48506.2021.9560988 (cit. on pp. 79, 111, 127, 129, 132, 136).

[77] G. Fadini, S. Kumar, R. Kumar, *et al.*, "Co-designing versatile quadruped robots for dynamic and energy-efficient motions", 2023 (cit. on p. 79).

[78] G. Fadini, T. Flayols, A. Del Prete, *et al.*, "Simulation aided co-design for robust robot optimization", *IEEE Robotics and Automation Letters*, vol. 7, no. 4, Oct. 2022 (cit. on pp. 79, 127, 132).

[79] P. Fankhauser and M. Hutter, "Anymal: A unique quadruped robot conquering harsh environments", *Research Features*, vol. 126, pp. 54–57, May 2018. DOI: 10.3929/ethz-b-000262484 (cit. on p. 19).

[80] A. Faraz and S. Pay, "Towards approximate models of coulomb frictional moments", vol. 40, Apr. 2003 (cit. on p. 43).

[81] R. Featherstone, "Gears", in *Robot Dynamics Algorithms*. Boston, MA: Springer US, 2008. [Online]. Available: https://doi.org/10.1007/978-0-387-74315-8 (cit. on p. 93).

[82] ——, *Rigid body dynamics algorithms*. Springer, 2014 (cit. on pp. 31, 129, 136).

[83] ——, "A ring screw mechanical transmission mechanism", 2023 (cit. on p. 27).

[84] M. L. Felis, "Rbdl: An efficient rigid-body dynamics library using recursive algorithms", *Autonomous Robots*, vol. 41, no. 2, pp. 495–511, 2017 (cit. on p. 33).

[85] M. Fujita, "AIBO: Toward the era of digital creatures", *The International Journal of Robotics Research*, vol. 20, no. 10, pp. 781–794, Oct. 2001. DOI: 10.1177/02783640122068092 (cit. on p. 17).

[86] G. Gabrielli, "What price speed? specific power required for propulsion of vehicles", *Mech. Eng.*, pp. 775–781, 1950 (cit. on p. 91).

[87] E. Garcia, P. Gonzalez De Santos, and C. Canudas De Wit, "Velocity dependence in the cyclic friction arising with gears", *The International Journal of Robotics Research*, vol. 21, no. 9, pp. 761–771, Sep. 2002. DOI: 10.1177/027836490202100987 7 (cit. on p. 41).

[88] C. Gehring, S. Coros, M. Hutter, *et al.*, "Control of dynamic gaits for a quadrupedal robot", in *2013 IEEE International Conference on Robotics and Automation*, Karlsruhe, Germany: IEEE, May 2013, pp. 3287–3292. DOI: 10.1109/ICRA.2013.6631035. [Online]. Available: http://ieeexplore.ieee.org/document/6631035/ (cit. on p. 75).

[89] T. Geijtenbeek, M. van de Panne, and A. F. van der Stappen, "Flexible muscle-based locomotion for bipedal creatures", *ACM Trans. Graph.*, vol. 32, no. 6, Nov. 2013. DOI: 10.1145/2508363.2508399. [Online]. Available: https://doi.org/10.1145/2508363.2508399 (cit. on pp. 74, 98).

[90] M. Geilinger, D. Hahn, J. Zehnder, *et al.*, "Add: Analytically differentiable dynamics for multi-body systems with frictional contact", *ACM Transactions on Graphics (TOG)*, vol. 39, no. 6, pp. 1–15, 2020 (cit. on pp. 34, 151).

[91] M. Geilinger, R. Poranne, R. Desai, *et al.*, "Skaterbots: Optimization-based design and motion synthesis for robotic creatures with legs and wheels", *ACM Transactions on Graphics*, vol. 37, no. 4, pp. 1–12, Aug. 10, 2018. DOI: 10.1145/3197517.3201368. [Online]. Available: https://dl.acm.org/doi/10.1145/3197517.3201368 (cit. on p. 76).

[92] Ghost robotics, *Q-UGVs*, https://www.ghostrobotics.io/vision-60 (cit. on p. 20).

[93] P. R. Giordano, Q. Delamare, and A. Franchi, "Trajectory generation for minimum closed-loop state sensitivity", in *IEEE Int. Conf. on Robotics & Automation*, Brisbane, Australia, 2018 (cit. on p. 105).

[94] A. Giusti, M. J. Zeestraten, E. Icer, *et al.*, "Flexible automation driven by demonstration: Leveraging strategies that simplify robotics", *IEEE Robotics & Automation Magazine*, vol. 25, no. 2, pp. 18–27, Jun. 2018. DOI: 10.1109/MRA.2018.2810543. [Online]. Available: https://ieeexplore.ieee.org/document/8356588/ (cit. on p. 77).

[95] A. E. Gkikakis and R. Featherstone, "Realistic mechanism and behaviour co-design of a one legged hopping robot", in *2021 International Conference on Computer, Control and Robotics (ICCCR)*, Shanghai, China: IEEE, Jan. 8, 2021, pp. 42–49. DOI: 10.1109/ICCCR49711.2021.9349280. [Online]. Available: https://ieeexplore.ieee.org/document/9349280/ (cit. on p. 76).

[96] ——, "Robust analysis for mechanism and behavior co-optimization of high-performance legged robots", in *2022 IEEE-RAS 21st International Conference on Humanoid Robots (Humanoids)*, Ginowan, Japan: IEEE, Nov. 28, 2022, pp. 752–758. DOI: 10.1109/Humanoids53995.2022.9999745. [Online]. Available: https://ieeexplore.ieee.org/document/9999745/ (cit. on p. 76).

[97] R. Grandia, F. Farshidian, R. Ranftl, *et al.*, "Feedback MPC for torque-controlled legged robots", in *IEEE/RSJ Int. Conf. on Intelligent Robots and Systems*, 2019 (cit. on p. 131).

[98] F. Grimminger, A. Meduri, M. Khadiv, *et al.*, "An open torque-controlled modular robot architecture for legged locomotion research", *IEEE RAL*, vol. 5, pp. 3650–3657, 2020 (cit. on pp. 19, 22, 59, 61, 62, 89, 93, 111).

[99] J. Grizzle, J. Hurst, B. Morris, *et al.*, "MABEL, a new robotic bipedal walker and runner", in *2009 American Control Conference*, St. Louis, MO, USA: IEEE, 2009, pp. 2030–2036. DOI: 10.1109/ACC.2009.5160550. [Online]. Available: http://ieeexplore.ieee.org/document/5160550/ (cit. on pp. 17, 58).

[100] E. Guizzo, "By leaps and bounds: An exclusive look at how Boston dynamics is redefining robot agility", *IEEE Spectrum*, vol. 56, no. 12, pp. 34–39, Dec. 2019. DOI: 10.1109/MSPEC.2019.8913831 (cit. on pp. 17, 19).

[101] A. Gupta, S. Savarese, S. Ganguli, *et al.*, "Embodied intelligence via learning and evolution", *Nature Communications*, vol. 12, no. 1, p. 5721, Oct. 6, 2021. DOI: 10.1038/s41467-021-25874-z. [Online]. Available: https://www.nature.com/articles/s41467-021-25874-z (cit. on p. 77).

[102] N. K. Gupta, "Frequency-shaped cost functionals - extension of linear-quadratic-gaussian design methods", *Jrnl. of Guidance Control and Dynamics*, vol. 3, 1980 (cit. on p. 131).

[103] D. Ha, "Reinforcement learning for improving agent design", *Artificial Life*, vol. 25, no. 4, pp. 352–365, Nov. 2019. DOI: 10.1162/artl_a_00301. [Online]. Available: https://direct.mit.edu/artl/article/25/4/352-365/93262 (cit. on p. 77).

[104] S. Ha, S. Coros, A. Alspach, *et al.*, "Task-based limb optimization for legged robots", in *2016 IEEE/RSJ International Conference on Intelligent Robots and Systems (IROS)*, Daejeon, South Korea: IEEE, Oct. 2016, pp. 2062–2068. DOI: 10.1109/IROS.2016.7759324. [Online]. Available: http://ieeexplore.ieee.org/document/7759324/ (cit. on p. 75).

[105] ——, "Joint optimization of robot design and motion parameters using the implicit function theorem", in *Robotics: Science and Systems XIII*, Robotics: Science and Systems Foundation, Jul. 12, 2017. DOI: 10.15607/RSS.2017.XIII.003. [Online]. Available: http://www.roboticsproceedings.org/rss13/p03.pdf (cit. on p. 75).

[106] ——, "Computational co-optimization of design parameters and motion trajectories for robotic systems", *Int. Journal of Robotics Research*, vol. 37, 2018 (cit. on pp. 76, 79, 84).

[107] T. Haarnoja, A. Zhou, P. Abbeel, *et al.*, "Soft actor-critic: Off-policy maximum entropy deep reinforcement learning with a stochastic actor", in *Proceedings of the 35th International Conference on Machine Learning*, J. Dy and A. Krause, Eds., ser. Proceedings of Machine Learning Research, vol. 80, PMLR, Jul. 10, 2018, pp. 1861–1870. [Online]. Available: https://proceedings.mlr.press/v80/haarnoja18b.html (cit. on p. 77).

[108] N. Hansen, "The CMA evolution strategy: A tutorial", *arXiv:1604.00772*, 2016 (cit. on pp. 98, 127).

[109] J. Hass, J. M. Herrmann, and T. Geisel, "Optimal mass distribution for passivity-based bipedal robots", *The International Journal of Robotics Research*, vol. 25, no. 11, pp. 1087–1098, Nov. 2006. DOI: 10.1177/0278364906072449 (cit. on p. 74).

[110] J. He and F. Gao, "Mechanism, actuation, perception, and control of highly dynamic multilegged robots: A review", *Chinese Journal of Mechanical Engineering*, vol. 33, no. 1, p. 79, Dec. 2020. DOI: 10.1186/s10033-020-00485-9. [Online]. Available: https://cjme.springeropen.com/articles/10.1186/s10033-020-00485-9 (cit. on p. 55).

[111] C. Hecker, B. Raabe, R. W. Enslow, *et al.*, "Real-time motion retargeting to highly varied user-created morphologies", *ACM Transactions on Graphics*, vol. 27, no. 3, pp. 1–11, Aug. 2008. DOI: 10.1145/1360612.1360626. [Online]. Available: https://dl.acm.org/doi/10.1145/1360612.1360626 (cit. on p. 75).

[112] E. Heijmink, "The ring screw: Modelling, development and evaluation of a novel screw transmission", 2018 (cit. on p. 27).

[113] S. Heim and A. Sprowitz, "Beyond basins of attraction: Quantifying robustness of natural dynamics", *IEEE Transactions on Robotics*, vol. 35, no. 4, pp. 939–952, Aug. 2019. DOI: 10.1109/TRO.2019.2910739. [Online]. Available: https://ieeexplore.ieee.org/document/8710301/ (cit. on p. 106).

[114] G. Heinzelmann, G. Liebhard, and H. Rosskamp, "Energy efficient drive train for a high-performance battery chain saw", in *2011 1st International Electric Drives Production Conference*, Nuremberg, Germany: IEEE, Sep. 2011, pp. 101–106. DOI: 10.1109/EDPC.2011.6085558. [Online]. Available: http://ieeexplore.ieee.org/document/6085558/ (cit. on p. 48).

[115] D. J. Hejna, P. Abbeel, and L. Pinto, "Task-agnostic morphology evolution", *ArXiv*, vol. abs/2102.13100, 2021. [Online]. Available: https://api.semanticscholar.org/CorpusID:232046055 (cit. on p. 77).

[116] S. Hirose, "A study of design and control of a quadruped walking vehicle", *The International Journal of Robotics Research*, vol. 3, no. 2, pp. 113–133, Jun. 1984. DOI: 10.1177/027836498400300210 (cit. on p. 15).

[117] S. Hirose and K. Kato, "Study on quadruped walking robot in tokyo institute of technology-past, present and future", in *Proceedings 2000 ICRA. Millennium Conference. IEEE International Conference on Robotics and Automation. Symposia Proceedings (Cat. No. 00CH37065)*, IEEE, vol. 1, 2000, pp. 414–419 (cit. on p. 15).

[118] N. Hogan, "Stable execution of contact tasks using impedance control", in *Proceedings. 1987 IEEE International Conference on Robotics and Automation*, vol. 4, Raleigh, NC, USA: Institute of Electrical and Electronics Engineers, 1987, pp. 1047–1054. DOI: 10.1109/ROBOT.1987.1087854. [Online]. Available: http://ieeexplore.ieee.org/document/1087854/ (cit. on p. 55).

[119] N. Hogan, "Impedance control: An approach to manipulation: Part i—theory", *Journal of Dynamic Systems, Measurement, and Control*, vol. 107, no. 1, pp. 1–7, Mar. 1, 1985. DOI: 10.1115/1.3140702. [Online]. Available: https://asmedigitalcollection.asme.org/dynamicsystems/article/107/1/1/400604/Impedance-Control-An-Approach-to-Manipulation-Part (cit. on p. 55).

[120] J. Hooks, M. S. Ahn, J. Yu, *et al.*, "Alphred: A multi-modal operations quadruped robot for package delivery applications", *IEEE Robotics and Automation Letters*, vol. 5, no. 4, pp. 5409–5416, 2020. DOI: 10.1109/LRA.2020.3007482 (cit. on p. 19).

[121] M. A. Hopkins, S. A. Ressler, D. F. Lahr, *et al.*, "Embedded joint-space control of a series elastic humanoid", in *2015 IEEE/RSJ International Conference on Intelligent Robots and Systems (IROS)*, Hamburg, Germany: IEEE, Sep. 2015, pp. 3358–3365. DOI: 10.1109/IROS.2015.7353845. [Online]. Available: http://ieeexplore.ieee.org/document/7353845/ (cit. on p. 58).

[122] D. Howard, A. E. Eiben, D. F. Kennedy, *et al.*, "Evolving embodied intelligence from materials to machines", *Nature Machine Intelligence*, vol. 1, no. 1, pp. 12–19, Jan. 7, 2019. DOI: 10.1038/s42256-018-0009-9. [Online]. Available: https://www.nature.com/articles/s42256-018-0009-9 (cit. on p. 150).

[123] T. A. Howell, S. L. Cleac'h, J. Brüdigam, *et al.*, *Dojo: A differentiable physics engine for robotics*, Mar. 30, 2023. arXiv: 2203.00806[cs]. [Online]. Available: http://arxiv.org/abs/2203.00806 (cit. on p. 34).

[124] C. Hubicki, A. Abate, P. Clary, *et al.*, "Walking and running with passive compliance: Lessons from engineering: A live demonstration of the ATRIAS biped", *IEEE Robotics & Automation Magazine*, vol. 25, no. 3, pp. 23–39, Sep. 2018. DOI: 10.1109/MRA.2017.2783922. [Online]. Available: https://ieeexplore.ieee.org/document/8360164/ (cit. on p. 58).

[125] C. Hubicki, J. Grimes, M. Jones, *et al.*, "ATRIAS: Design and validation of a tether-free 3d-capable spring-mass bipedal robot", *The International Journal of Robotics Research*, vol. 35, no. 12, pp. 1497–1521, Oct. 2016. DOI: 10.1177/0278364916648388 (cit. on pp. 5, 26, 27, 58).

[126] A. Hughes and B. Drury, *Electric motors and drives: fundamentals, types and applications*. Newnes, 2019 (cit. on p. 46).

[127] H. V. Hultmann Ayala and L. dos Santos Coelho, "Tuning of PID controller based on a multiobjective genetic algorithm applied to a robotic manipulator", *Expert Systems with Applications*, vol. 39, no. 10, pp. 8968–8974, 2012 (cit. on p. 106).

[128] I. W. Hunter, J. M. Hollerbach, and J. Ballantyne, "A comparative analysis of actuator technologies for robotics", *Robotics Review*, vol. 2, pp. 299–342, 1991 (cit. on pp. 40, 55).

[129] J. W. Hurst, J. E. Chestnutt, and A. A. Rizzi, "Design and philosophy of the BiMASC, a highly dynamic biped", in *Proceedings 2007 IEEE International Conference on Robotics and Automation*, Rome, Italy: IEEE, Apr. 2007, pp. 1863–1868. DOI: 10.1109/ROBOT.2007.363593. [Online]. Available: http://ieeexplore.ieee.org/document/4209357/ (cit. on p. 17).

[130] M. Hutter, C. Gehring, M. Bloesch, *et al.*, "StarlETH: A compliant quadrupedal robot for fast, efficient, and versatile locomotion", in *Adaptive Mobile Robotics*, World Scientific, 2012, pp. 483–490 (cit. on pp. 19, 58).

[131] M. Hutter, C. Gehring, D. Jud, *et al.*, "ANYmal - a highly mobile and dynamic quadrupedal robot", in *IEEE/RSJ Int. Conf. on Intelligent Robots and Systems*, 2016 (cit. on p. 19).

[132] M. Hutter, C. D. Remy, and R. Siegwart, "Adaptive control strategies for open-loop dynamic hopping", in *2009 IEEE/RSJ International Conference on Intelligent Robots and Systems*, St. Louis, MO, USA: IEEE, Oct. 2009, pp. 154–159. DOI: 10.1109/IROS.2009.5354474. [Online]. Available: http://ieeexplore.ieee.org/document/5354474/ (cit. on p. 58).

[133] J. Hwangbo, J. Lee, and M. Hutter, "Per-contact iteration method for solving contact dynamics", *IEEE Robotics and Automation Letters*, vol. 3, no. 2, pp. 895–902, 2018. [Online]. Available: www.raisim.com (cit. on p. 34).

[134] D. Izzo, "Pygmo and pykep: Open source tools for massively parallel optimization in astrodynamics (the case of interplanetary trajectory optimization)", Jan. 2012 (cit. on p. 98).

[135] T. Jansen, "Strandbeests", *Architectural Design*, vol. 78, no. 4, pp. 22–27, Jul. 2008. DOI: 10.1002/ad.701. [Online]. Available: https://onlinelibrary.wiley.com/doi/10.1002/ad.701 (cit. on p. 90).

[136] T. Jung, J. Lim, H. Bae, *et al.*, "Development of the humanoid disaster response platform DRC-HUBO+", *IEEE Transactions on Robotics*, vol. 34, no. 1, pp. 1–17, Feb. 2018. DOI: 10.1109/TRO.2017.2776287. [Online]. Available: http://ieeexplore.ieee.org/document/8281682/ (cit. on p. 57).

[137] S. Kajita, F. Kanehiro, K. Kaneko, *et al.*, "Biped walking pattern generation by using preview control of zero-moment point", in *IEEE Int. Conf. on Robotics & Automation*, vol. 2, 2003 (cit. on p. 129).

[138] S. Kajita, M. Morisawa, K. Miura, *et al.*, "Biped walking stabilization based on linear inverted pendulum tracking", in *IEEE/RSJ Int. Conf. on Intelligent Robots and Systems*, 2010 (cit. on p. 129).

[139] S. Kajita, T. Nagasaki, K. Kaneko, *et al.*, "ZMP-based biped running control", *IEEE Robotics & Automation Magazine*, vol. 14, no. 2, 2007 (cit. on p. 129).

[140] S. Kalouche, "GOAT: A legged robot with 3d agility and virtual compliance", in *2017 IEEE/RSJ International Conference on Intelligent Robots and Systems (IROS)*, Vancouver, BC: IEEE, Sep. 2017, pp. 4110–4117. DOI: 10.1109/IROS.2017.8206269. [Online]. Available: http://ieeexplore.ieee.org/document/8206269/ (cit. on p. 27).

[141] K. Kaneko, K. Harada, F. Kanehiro, *et al.*, "Humanoid robot HRP-3", in *2008 IEEE/RSJ International Conference on Intelligent Robots and Systems*, Nice: IEEE, Sep. 2008, pp. 2471–2478. DOI: 10.1109/IROS.2008.4650604. [Online]. Available: http://ieeexplore.ieee.org/document/4650604/ (cit. on p. 57).

[142] K. Kaneko, F. Kanehiro, M. Morisawa, *et al.*, "Humanoid robot HRP-4 - humanoid robotics platform with lightweight and slim body", in *2011 IEEE/RSJ International Conference on Intelligent Robots and Systems*, San Francisco, CA: IEEE, Sep. 2011, pp. 4400–4407. DOI: 10.1109/IROS.2011.6094465. [Online]. Available: http://ieeexplore.ieee.org/document/6094465/ (cit. on p. 57).

[143] K. Kaneko, H. Kaminaga, T. Sakaguchi, *et al.*, "Humanoid robot HRP-5p: An electrically actuated humanoid robot with high-power and wide-range joints", *IEEE Robotics and Automation Letters*, vol. 4, no. 2, pp. 1431–1438, Apr. 2019. DOI: 10.1109/LRA.2019.2896465. [Online]. Available: https://ieeexplore.ieee.org/document/8630006/ (cit. on p. 57).

[144] R. Kang, F. Meng, X. Chen, *et al.*, "Structural design and crawling pattern generator of a planar quadruped robot for high-payload locomotion", *Sensors*, vol. 20, no. 22, p. 6543, Nov. 16, 2020. DOI: 10.3390/s20226543. [Online]. Available: https://www.mdpi.com/1424-8220/20/22/6543 (cit. on p. 19).

[145] B. Katz, J. D. Carlo, and S. Kim, "Mini cheetah: A platform for pushing the limits of dynamic quadruped control", in *IEEE Int. Conf. on Robotics and Automation*, 2019, pp. 6295–6301. DOI: 10.1109/ICRA.2019.8793865 (cit. on p. 19).

[146] N. Kau, *Stanford pupper: A low-cost agile quadruped robot for benchmarking and education*, Feb. 3, 2022. arXiv: 2110.00736[cs]. [Online]. Available: http://arxiv.org/abs/2110.00736 (cit. on p. 20).

[147] G. Kenneally, A. De, and D. E. Koditschek, "Design principles for a family of direct-drive legged robots", *IEEE Robotics and Automation Letters*, vol. 1, no. 2, pp. 900–907, Jul. 2016. DOI: 10.1109/LRA.2016.2528294. [Online]. Available: http://ieeexplore.ieee.org/document/7403902/ (cit. on p. 59).

[148] H. Kikukawa, N. Okada, and H. Kimura, "Simulation of quadruped robot running with visual adaptation", *The Proceedings of JSME annual Conference on Robotics and Mechatronics (Robomec)*, vol. 2020, no. 0, 2P1–J04, 2020. DOI: 10.1299/jsmermd.2020.2P1-J04. [Online]. Available: https://www.jstage.jst.go.jp/article/jsmermd/2020/0/2020_2P1-J04/_article/-char/ja/ (cit. on p. 19).

[149] S. Kim and P. M. Wensing, "Design of dynamic legged robots", *Foundations and Trends in Robotics*, vol. 5, no. 2, pp. 117–190, 2017. DOI: 10.1561/2300000044. [Online]. Available: http://www.nowpublishers.com/article/Details/ROB-044 (cit. on pp. 15, 58, 91).

[150] S. Kitano, S. Hirose, A. Horigome, *et al.*, "TITAN-XIII: Sprawling-type quadruped robot with ability of fast and energy-efficient walking", *ROBOMECH Journal*, vol. 3, no. 1, p. 8, Dec. 2016. DOI: 10.1186/s40648-016-0047-1. [Online]. Available: http://www.robomechjournal.com/content/3/1/8 (cit. on pp. 19, 91).

[151] C. Knabe, J. Seminatore, J. Webb, *et al.*, "Design of a series elastic humanoid for the DARPA robotics challenge", in *2015 IEEE-RAS 15th International Conference on Humanoid Robots (Humanoids)*, Seoul, South Korea: IEEE, Nov. 2015, pp. 738–743. DOI: 10.1109/HUMANOIDS.2015.7363452. [Online]. Available: http://ieeexplore.ieee.org/document/7363452/ (cit. on p. 58).

[152] K. H. Koch, K. Mombaur, and P. Souères, "Optimization-based walking generation for humanoid robot", *IFAC Proceedings Volumes*, vol. 45, no. 22, 2012, 10th IFAC Symposium on Robot Control (cit. on p. 129).

[153] K. Kojima, T. Karasawa, T. Kozuki, *et al.*, "Development of life-sized high-power humanoid robot JAXON for real-world use", in *2015 IEEE-RAS 15th International Conference on Humanoid Robots (Humanoids)*, Seoul, South Korea: IEEE, Nov. 2015, pp. 838–843. DOI: 10.1109/HUMANOIDS.2015.7363459. [Online]. Available: http://ieeexplore.ieee.org/document/7363459/ (cit. on p. 57).

[154] D. Krasny and D. Orin, "Evolution of dynamic maneuvers in a 3d galloping quadruped robot", in *Proceedings 2006 IEEE International Conference on Robotics and Automation, 2006. ICRA 2006.*, Orlando, FL, USA: IEEE, 2006, pp. 1084–1089. DOI: 10.1109/ROBOT.2006.1641854. [Online]. Available: http://ieeexplore.ieee.org/document/1641854/ (cit. on p. 75).

[155] P. Kry, L. Reveret, F. Faure, *et al.*, "Modal locomotion: Animating virtual characters with natural vibrations", *Computer Graphics Forum*, vol. 28, no. 2, pp. 289–298, Apr. 2009. DOI: 10.1111/j.1467-8659.2009.01368.x. [Online]. Available: https://onlinelibrary.wiley.com/doi/10.1111/j.1467-8659.2009.01368.x (cit. on p. 75).

[156] V. R. Kumar and K. J. Waldron, "Adaptive gait control for a walking robot", *Journal of Robotic Systems*, vol. 6, no. 1, pp. 49–76, Feb. 1989. DOI: 10.1002/rob.4620060105. [Online]. Available: https://onlinelibrary.wiley.com/doi/10.1002/rob.4620060105 (cit. on p. 17).

[157] Q. Le Lidec, I. Kalevatykh, I. Laptev, *et al.*, "Differentiable simulation for physical system identification", *IEEE Robotics and Automation Letters*, vol. 6, no. 2, pp. 3413–3420, Apr. 2021. DOI: 10.1109/LRA.2021.3062323. [Online]. Available: https://ieeexplore.ieee.org/document/9363565/ (cit. on p. 34).

[158] P.-A. Léziart, "Locomotion control of a lightweight quadruped robot", Theses, UPS Toulouse, Oct. 2022. [Online]. Available: https://hal.laas.fr/tel-03936109 (cit. on p. 15).

[159] Q. Li, W. Zhang, and L. Chen, "Design for control - a concurrent engineering approach for mechatronic systems design", *Mechatronics, IEEE/ASME Transactions on*, vol. 6, pp. 161–169, Jul. 2001. DOI: 10.1109/3516.928731 (cit. on pp. 73, 85).

[160] R. Liston and R. Mosher, "A versatile walking truck", in *Transportation Engineering Conference*, 1968 (cit. on p. 15).

[161] K. S. Luck, H. B. Amor, and R. Calandra, "Data-efficient co-adaptation of morphology and behaviour with deep reinforcement learning", in *Proceedings of the Conference on Robot Learning*, L. P. Kaelbling, D. Kragic, and K. Sugiura, Eds., ser. Proceedings of Machine Learning Research, vol. 100, PMLR, Oct. 2020, pp. 854–869. [Online]. Available: https://proceedings.mlr.press/v100/luck20a.html (cit. on p. 77).

[162] B. MacIntyre, M. Gandy, S. Dow, *et al.*, "Dart: A toolkit for rapid design exploration of augmented reality experiences", in *Proceedings of the 17th Annual ACM Symposium on User Interface Software and Technology*, ser. UIST '04, Santa Fe, NM, USA: Association for Computing Machinery, 2004, pp. 197–206. DOI: 10.1145/1029632.1029669. [Online]. Available: https://doi.org/10.1145/1029632.1029669 (cit. on p. 34).

[163] V. Makoviychuk, L. Wawrzyniak, Y. Guo, *et al.*, *Isaac gym: High performance GPU-based physics simulation for robot learning*, Aug. 25, 2021. arXiv: 2108.10470[cs]. [Online]. Available: http://arxiv.org/abs/2108.10470 (cit. on p. 34).

[164] D. Marchal, T. Morzadec, and C. Duriez, "Toward shape optimization of soft robots", Apr. 2019. DOI: 10.1109/ROBOSOFT.2019.8722822 (cit. on p. 98).

[165] C. Mastalli, R. Budhiraja, W. Merkt, *et al.*, "Crocoddyl: An Efficient and Versatile Framework for Multi-Contact Optimal Control", in *IEEE Int. Conf. on Robotics & Automation*, 2020 (cit. on pp. 97, 108).

[166] D. Mayne, "A second-order gradient method for determining optimal trajectories of non-linear discrete-time systems", *International Journal of Control*, vol. 3, no. 1, Jan. 1966 (cit. on pp. 127, 131).

[167] L. J. Maywald, F. Wiebe, S. Kumar, *et al.*, "Co-optimization of acrobot design and controller for increased certifiable stability", in *IEEE Int. Conf. on Intelligent Robots and Systems*, 2022 (cit. on p. 106).

[168] T. McGeer, "Passive dynamic walking", *The International Journal of Robotics Research*, vol. 9, pp. 62–82, 1990 (cit. on p. 74).

[169] R. B. McGhee, "Vehicular legged locomotion", *Advanced in Automation and Robotics*, 1983 (cit. on p. 15).

[170] V. Megaro, J. Zehnder, M. Bächer, *et al.*, "A computational design tool for compliant mechanisms", *ACM Transactions on Graphics*, vol. 36, no. 4, pp. 1–12, Aug. 31, 2017. DOI: 10.1145/3072959.3073636. [Online]. Available: https://dl.acm.org/doi/10.1145/3072959.3073636 (cit. on p. 74).

[171] G. Metta, L. Natale, F. Nori, *et al.*, "The iCub humanoid robot: An open-systems platform for research in cognitive development", *Neural Networks*, vol. 23, no. 8, pp. 1125–1134, Oct. 2010. DOI: 10.1016/j.neunet.2010.08.010. [Online]. Available: https://linkinghub.elsevier.com/retrieve/pii/S0893608010001619 (cit. on p. 58).

[172] K. Mombaur, H. Bock, and R. Longman, "Stable, unstable and chaotic motions of bipedal walking robots without feedback", in *2nd Int. Conf. Control of Oscillations and Chaos*, vol. 2, 2000 (cit. on p. 129).

[173] K. Mombaur, "Using optimization to create self-stable human-like running", *Robotica*, vol. 27, no. 3, pp. 321–330, May 2009 (cit. on p. 105).

[174] K. D. Mombaur, R. W. Longman, H. G. Bock, *et al.*, "Open-loop stable running", *Robotica*, vol. 23, no. 1, 2005 (cit. on pp. 75, 79, 129).

[175] E. Moore, D. Campbell, F. Grimminger, *et al.*, "Reliable stair climbing in the simple hexapod 'RHex'", in *Proceedings 2002 IEEE International Conference on Robotics and Automation (Cat. No.02CH37292)*, vol. 3, Washington, DC, USA: IEEE, 2002, pp. 2222–2227. DOI: 10.1109/ROBOT.2002.1013562. [Online]. Available: http://ieeexplore.ieee.org/document/1013562/ (cit. on p. 91).

[176] I. Mordatch, K. Lowrey, and E. Todorov, "Ensemble-CIO: Full-body dynamic motion planning that transfers to physical humanoids", in *IEEE/RSJ Int. Conf. on Intelligent Robots and Systems*, 2015 (cit. on p. 106).

[177] M. Neunert, M. Stäuble, M. Giftthaler, *et al.*, "Whole-body nonlinear model predictive control through contacts for quadrupeds", *IEEE RAL*, vol. 3, no. 3, pp. 1458–1465, (cit. on p. 108).

[178] E. Nieto, S. Rezazadeh, and R. Gregg, "Minimizing energy consumption and peak power of series elastic actuators: A convex optimization framework for elastic element design", *IEEE/ASME Transactions on Mechatronics*, vol. 24, pp. 1334–1345, Jun. 2019. DOI: 10.1109/TMECH.2019.2906887 (cit. on p. 93).

[179] K. Ogata *et al.*, *Modern control engineering*. Prentice hall Upper Saddle River, NJ, 2010, vol. 5 (cit. on p. 40).

[180] D. E. Orin, A. Goswami, and S.-H. Lee, "Centroidal dynamics of a humanoid robot", *Autonomous Robots*, vol. 35, no. 2, Oct. 2013 (cit. on p. 129).

[181] P. Ouyang, Q. Li, W. Zhang, *et al.*, "Design, modeling and control of a hybrid machine system", *Mechatronics*, vol. 14, pp. 1197–1217, Dec. 2004. DOI: 10.1016/j.mechatronics.2004.06.004 (cit. on p. 73).

[182] PAL robotics, *Kangaroo*, https://pal-robotics.com/robots/kangaroo/ (cit. on p. 27).

[183] X. Pan, A. Garg, A. Anandkumar, *et al.*, "Emergent hand morphology and control from optimizing robust grasps of diverse objects", in *2021 IEEE International Conference on Robotics and Automation (ICRA)*, Xi'an, China: IEEE, May 30, 2021, pp. 7540–7547. DOI: 10.1109/ICRA48506.2021.9562092. [Online]. Available: https://ieeexplore.ieee.org/document/9562092/ (cit. on p. 77).

[184] H.-W. Park, P. M. Wensing, and S. Kim, "High-speed bounding with the MIT cheetah 2: Control design and experiments", *The International Journal of Robotics Research*, vol. 36, no. 2, 2017 (cit. on pp. 19, 59).

[185] I.-W. Park, J.-Y. Kim, J. Lee, *et al.*, "Mechanical design of the humanoid robot platform, HUBO", *Advanced Robotics*, vol. 21, no. 11, pp. 1305–1322, Jan. 2007. DOI: 10.1163/156855307781503781. [Online]. Available: https://www.tandfonline.com/doi/full/10.1163/156855307781503781 (cit. on p. 57).

[186] J.-H. Park and H. Asada, "Concurrent design optimization of mechanical structure and control for high speed robots", *Journal of Dynamic Systems, Measurement, and Control*, vol. 116, no. 3, Sep. 1, 1994 (cit. on p. 73).

[187] D. L. Peters, P. Y. Papalambros, and A. G. Ulsoy, "Sequential co-design of an artifact and its controller via control proxy functions", *Mechatronics*, vol. 23, no. 4, pp. 409–418, (cit. on pp. 74, 106).

[188] J. Pieper, *Mjbots quad*, https://github.com/mjbots/quad (cit. on p. 126).

[189] M. Pirron and D. Zufferey, "MPERL: Hardware and software co-design for robotic manipulators ©", in *2019 IEEE/RSJ International Conference on Intelligent Robots and Systems (IROS)*, Macau, China: IEEE, Nov. 2019, pp. 7784–7790. DOI: 10.1109/IROS40897.2019.8968188. [Online]. Available: https://ieeexplore.ieee.org/document/8968188/ (cit. on p. 76).

[190] M. Posa, S. Kuindersma, and R. Tedrake, "Optimization and stabilization of trajectories for constrained dynamical systems", in *IEEE Int. Conf. on Robotics & Automation*, 2016 (cit. on pp. 128, 129).

[191] I. Poulakakis, J. A. Smith, and M. Buehler, "Modeling and experiments of untethered quadrupedal running with a bounding gait: The scout ii robot", *The International Journal of Robotics Research*, vol. 24, no. 4, pp. 239–256, 2005 (cit. on p. 17).

[192] G. Pratt and M. Williamson, "Series elastic actuators", in *Proceedings 1995 IEEE/RSJ International Conference on Intelligent Robots and Systems. Human Robot Interaction and Cooperative Robots*, vol. 1, Pittsburgh, PA, USA: IEEE Comput. Soc. Press, 1995, pp. 399–406. DOI: 10.1109/IROS.1995.525827. [Online]. Available: http://ieeexplore.ieee.org/document/525827/ (cit. on p. 57).

[193] M. Quigley, "ROS: An open-source robot operating system", in *IEEE ICRA*, Kobe, Japan, 2009 (cit. on p. 108).

[194] S. G. Radhakrishna Prabhu, R. C. Seals, P. J. Kyberd, *et al.*, "A survey on evolutionary-aided design in robotics", *Robotica*, vol. 36, no. 12, pp. 1804–1821, Dec. 2018. DOI: 10.1017/S0263574718000747. [Online]. Available: https://www.cambridge.org/core/product/identifier/S0263574718000747/type/journal_article (cit. on p. 73).

[195] M. Raff, N. Rosa, and C. D. Remy, "Generating families of optimally actuated gaits from a legged system's energetically conservative dynamics", in *2022 IEEE/RSJ International Conference on Intelligent Robots and Systems (IROS)*, Kyoto, Japan: IEEE, Oct. 23, 2022, pp. 8866–8872. DOI: 10.1109/IROS47612.2022.9981693. [Online]. Available: https://ieeexplore.ieee.org/document/9981693/ (cit. on p. 90).

[196] M. Raibert, K. Blankespoor, G. Nelson, *et al.*, "BigDog, the rough-terrain quadruped robot", *IFAC Proceedings Volumes*, vol. 41, no. 2, pp. 10 822–10 825, 2008. DOI: 10.3182/20080706-5-KR-1001.01833. [Online]. Available: https://linkinghub.elsevier.com/retrieve/pii/S1474667016407020 (cit. on pp. 17, 39).

[197] M. H. Raibert, H. B. Brown Jr, M. Chepponis, *et al.*, "Dynamically stable legged locomotion", Massachusetts Inst of Tech Cambridge Artificial Intelligence Lab, Tech. Rep., 1989 (cit. on p. 17).

[198] M. H. Raibert, H. B. Brown, and M. Chepponis, "Experiments in balance with a 3d one-legged hopping machine", *The International Journal of Robotics Research*, vol. 3, no. 2, pp. 75–92, Jun. 1984. DOI: 10.1177/027836498400300207 (cit. on p. 17).

[199] M. H. Raibert and J. K. Hodgins, "Animation of dynamic legged locomotion", in *Proceedings of the 18th annual conference on Computer graphics and interactive techniques - SIGGRAPH '91*, Not Known: ACM Press, 1991, pp. 349–358. DOI: 10.1145/122718.122755. [Online]. Available: http://portal.acm.org/citation.cfm?doid=122718.122755 (cit. on p. 75).

[200] R. Rajendra and D. K. Pratihar, "Particle swarm optimization algorithm vs genetic algorithm to develop integrated scheme for obtaining optimal mechanical structure and adaptive controller of a robot", in *Int. Conf. on Information Systems Design and Intelligent Applications*, Visakhapatnam, India, 2012 (cit. on p. 106).

[201] N. Rathod, A. Bratta, M. Focchi, *et al.*, "Mobility-enhanced MPC for legged locomotion on rough terrain", *arXiv: 2105.05998*, (cit. on p. 108).

[202] C. D. Remy, K. Buffinton, and R. Siegwart, "A MATLAB framework for efficient gait creation", in *2011 IEEE/RSJ International Conference on Intelligent Robots and Systems*, San Francisco, CA: IEEE, Sep. 2011, pp. 190–196. DOI: 10.1109/IROS.2011.6094452 (cit. on p. 90).

[203] C. D. Remy, K. Buffinton, and R. Siegwart, "Stability analysis of passive dynamic walking of quadrupeds", *The International Journal of Robotics Research*, vol. 29, no. 9, pp. 1173–1185, Aug. 2010. DOI: 10.1177/0278364909344635 (cit. on p. 106).

[204] J. A. Reyer and P. Y. Papalambros, "Combined Optimal Design and Control With Application to an Electric DC Motor ", *Journal of Mechanical Design*, vol. 124, 2002 (cit. on p. 73).

[205] S. Rezazadeh, A. Abate, R. L. Hatton, *et al.*, "Robot leg design: A constructive framework", *IEEE Access*, vol. 6, 2018 (cit. on p. 72).

[206] S. Rezazadeh and J. W. Hurst, "On the optimal selection of motors and transmissions for electromechanical and robotic systems", in *IEEE/RSJ Int. Conf. on Intelligent Robots and Systems*, 2014 (cit. on p. 72).

[207] W. Roozing, J. Malzahn, N. Kashiri, *et al.*, "On the stiffness selection for torque-controlled series-elastic actuators", *IEEE Robotics and Automation Letters*, vol. 2, no. 4, pp. 2255–2262, Oct. 2017. DOI: 10.1109/LRA.2017.2726141. [Online]. Available: http://ieeexplore.ieee.org/document/7976385/ (cit. on p. 58).

[208] ROS. [Online]. Available: https://wiki.ros.org/urdf/XML (cit. on p. 108).

[209] ——, [Online]. Available: http://wiki.ros.org/xacro (cit. on p. 108).

[210] N. Rudin, D. Hoeller, P. Reist, *et al.*, "Learning to walk in minutes using massively parallel deep reinforcement learning", in *Conference on Robot Learning*, PMLR, 2022, pp. 91–100 (cit. on p. 22).

[211] F. Ruppert and A. Badri-Spröwitz, "Learning plastic matching of robot dynamics in closed-loop central pattern generators", *Nature Machine Intelligence*, vol. 4, no. 7, pp. 652–660, Jul. 18, 2022. DOI: 10.1038/s42256-022-00505-4. [Online]. Available: https://www.nature.com/articles/s42256-022-00505-4 (cit. on pp. 20, 58).

[212] Y. Sakagami, R. Watanabe, C. Aoyama, *et al.*, "The intelligent ASIMO: System overview and integration", in *IEEE/RSJ International Conference on Intelligent Robots and System*, vol. 3, Lausanne, Switzerland: IEEE, 2002, pp. 2478–2483. DOI: 10.1109/IRDS.2002.1041641. [Online]. Available: http://ieeexplore.ieee.org/document/1041641/ (cit. on p. 57).

[213] J. Salisbury and M. Srinivasan, "Phantom-based haptic interaction with virtual objects", *IEEE Computer Graphics and Applications*, vol. 17, no. 5, pp. 6–10, Sep. 1997. DOI: 10.1109/MCG.1997.1626171. [Online]. Available: http://ieeexplore.ieee.org/document/1626171/ (cit. on p. 19).

[214] A. Sari, C. Espanet, and D. Hissel, "Particle swarm optimization applied to the co-design of a fuel cell air circuit", *Journal of Power Sources*, vol. 179, no. 1, (cit. on pp. 74, 106).

[215] C. Sartore, L. Rapetti, and D. Pucci, "Optimization of humanoid robot designs for human-robot ergonomic payload lifting", in *2022 IEEE-RAS 21st International Conference on Humanoid Robots (Humanoids)*, Ginowan, Japan: IEEE, Nov. 28, 2022, pp. 722–729. DOI: 10.1109/Humanoids53995.2022.10000222. [Online]. Available: https://ieeexplore.ieee.org/document/10000222/ (cit. on p. 76).

[216] A. Sathuluri, A. V. Sureshbabu, and M. Zimmermann, "Robust co-design of robots via cascaded optimisation", in *2023 IEEE International Conference on Robotics and Automation (ICRA)*, London, United Kingdom: IEEE, May 29, 2023, pp. 11 280–11 286. DOI: 10.1109/ICRA48891.2023.10161134. [Online]. Available: https://ieeexplore.ieee.org/document/10161134/ (cit. on p. 76).

[217] G. Saurel, J. Carpentier, N. Mansard, *et al.*, "A simulation framework for simultaneous design and control of passivity based walkers", Dec. 2016. DOI: 10.1109/SIMPAR.2016.7862383 (cit. on p. 74).

[218] ——, "A simulation framework for simultaneous design and control of passivity based walkers", in *IEEE Int. Conf. on Simulation, Modeling, and Programming for Autonomous Robots*, 2016 (cit. on p. 75).

[219] C. Schaff, A. Sedal, and M. R. Walter, *Soft robots learn to crawl: Jointly optimizing design and control with sim-to-real transfer*, Feb. 9, 2022. arXiv: 2202.04575[cs]. [Online]. Available: http://arxiv.org/abs/2202.04575 (cit. on p. 77).

[220] C. Schaff and M. R. Walter, *N-LIMB: Neural limb optimization for efficient morphological design*, Sep. 19, 2022. arXiv: 2207.11773[cs]. [Online]. Available: http://arxiv.org/abs/2207.11773 (cit. on p. 77).

[221] C. Schaff, D. Yunis, A. Chakrabarti, *et al.*, "Jointly learning to construct and control agents using deep reinforcement learning", *arXiv:1801.01432 [cs]*, Sep. 14, 2018, version: 3. arXiv: 1801.01432. [Online]. Available: http://arxiv.org/abs/1801.01432 (cit. on p. 76).

[222] SchedMD LLC, *SLURM: Workload manager*, 2023. [Online]. Available: https://slurm.schedmd.com/overview.html (cit. on p. 127).

[223] K. Schmidt-Nielsen, "Locomotion: Energy cost of swimming, flying, and running", *Science*, vol. 177, no. 4045, pp. 222–228, 1972, Publisher: American Association for the Advancement of Science. [Online]. Available: http://www.jstor.org/stable/1734532 (cit. on p. 91).

[224] S. Schoenholz and E. D. Cubuk, "JAX MD: A framework for differentiable physics", in *Advances in Neural Information Processing Systems*, H. Larochelle, M. Ranzato, R. Hadsell, *et al.*, Eds., vol. 33, Curran Associates, Inc., 2020, pp. 11 428–11 441 (cit. on p. 34).

[225] K. Schreiner, "Landmine detection research pushes forward, despite challenges", *IEEE Intelligent Systems*, vol. 17, no. 2, pp. 4–7, Mar. 2002. DOI: 10.1109/MIS.2002.999212. [Online]. Available: http://ieeexplore.ieee.org/document/999212/ (cit. on p. 21).

[226] J. Schulman, S. Levine, P. Abbeel, *et al.*, "Trust region policy optimization", in *International conference on machine learning*, PMLR, 2015, pp. 1889–1897 (cit. on p. 77).

[227] J. Schulman, F. Wolski, P. Dhariwal, *et al.*, *Proximal policy optimization algorithms*, Aug. 28, 2017. arXiv: 1707.06347[cs]. [Online]. Available: http://arxiv.org/abs/1707.06347 (cit. on p. 77).

[228] A. Schulz, C. Sung, A. Spielberg, *et al.*, "Interactive robogami: An end-to-end system for design of robots with ground locomotion", *The International Journal of Robotics Research*, vol. 36, no. 10, pp. 1131–1147, Sep. 2017. DOI: 10.1177/0278364917723465. [Online]. Available: http://journals.sagepub.com/doi/10.1177/0278364917723465 (cit. on p. 76).

[229] L. Sciavicco and B. Siciliano, *Modelling and control of robot manipulators*. Springer Science & Business Media, 2001 (cit. on p. 40).

[230] C. Semasinghe, D. Taylor, and S. Rezazadeh, "A unified optimization framework and new set of performance metrics for robot leg design", in *IEEE Int. Conf. on Robotics and Automation*, 2021 (cit. on p. 72).

[231] C. Semini, V. Barasuol, J. Goldsmith, *et al.*, "Design of the hydraulically actuated, torque-controlled quadruped robot HyQ2max", *IEEE/ASME Transactions on Mechatronics*, vol. 22, no. 2, pp. 635–646, Apr. 2017. DOI: 10.1109/TMECH.2016.2616284. [Online]. Available: http://ieeexplore.ieee.org/document/7587429/ (cit. on pp. 22, 40).

[232] C. Semini, J. Buchli, M. Frigerio, *et al.*, "HyQ - a dynamic locomotion research platform", Jan. 2011 (cit. on pp. 17, 40).

[233] S. Seok, A. Wang, M. Y. Chuah, *et al.*, "Design principles for highly efficient quadrupeds and implementation on the MIT cheetah robot", in *2013 IEEE International Conference on Robotics and Automation*, 2013, pp. 3307–3312. DOI: 10.1109/ICRA.2013.6631038 (cit. on p. 59).

[234] ——, "Design principles for highly efficient quadrupeds and implementation on the mit cheetah robot", in *2013 IEEE International Conference on Robotics and Automation*, 2013, pp. 3307–3312. DOI: 10.1109/ICRA.2013.6631038 (cit. on p. 90).

[235] S. Seok, A. Wang, D. Otten, *et al.*, "Actuator design for high force proprioceptive control in fast legged locomotion", in *2012 IEEE/RSJ International Conference on Intelligent Robots and Systems*, Vilamoura-Algarve, Portugal: IEEE, Oct. 2012, pp. 1970–1975. DOI: 10.1109/IROS.2012.6386252. [Online]. Available: http://ieeexplore.ieee.org/document/6386252/ (cit. on pp. 46, 47).

[236] M. A. Sherman, A. Seth, and S. L. Delp, "Simbody: Multibody dynamics for biomedical research", *Procedia Iutam*, vol. 2, pp. 241–261, 2011 (cit. on p. 34).

[237] P. Shiakolas, D. Koladiya, and J. Kebrle, "Optimum robot design based on task specifications using evolutionary techniques and kinematic, dynamic, and structural constraints", *Inverse Problems in Engineering*, vol. 10, no. 4, pp. 359–375, Jan. 2002. DOI: 10.1080/1068276021000004706. [Online]. Available: http://www.tandfonline.com/doi/abs/10.1080/1068276021000004706 (cit. on p. 73).

[238] M. F. Silva and J. T. Machado, "A literature review on the optimization of legged robots", *Journal of Vibration and Control*, vol. 18, no. 12, pp. 1753–1767, Oct. 2012. DOI: 10.1177/1077546311403180. [Online]. Available: http://journals.sagepub.com/doi/10.1177/1077546311403180 (cit. on p. 91).

[239] K. Sims, "Artificial evolution for computer graphics", in *Proceedings of the 18th annual conference on Computer graphics and interactive techniques - SIGGRAPH '91*, Not Known: ACM Press, 1991, pp. 319–328. DOI: 10.1145/122718.122752. [Online]. Available: http://portal.acm.org/citation.cfm?doid=122718.122752 (cit. on p. 73).

[240] ——, "Evolving 3d morphology and behavior by competition", *Artificial Life*, vol. 1, no. 4, pp. 353–372, Jul. 1994. DOI: 10.1162/artl.1994.1.4.353. [Online]. Available: https://direct.mit.edu/artl/article/1/4/353-372/2234 (cit. on p. 73).

[241] J. Skaf and S. Boyd, "Solving the LQR problem by block elimination", stanford.edu/class/ee363/notes/riccati-derivation.pdf (cit. on p. 109).

[242] M. Skouras, B. Thomaszewski, S. Coros, *et al.*, "Computational design of actuated deformable characters", *ACM Transactions on Graphics*, vol. 32, no. 4, pp. 1–10, Jul. 21, 2013. DOI: 10.1145/2461912.2461979. [Online]. Available: https://dl.acm.org/doi/10.1145/2461912.2461979 (cit. on p. 74).

[243] N. Smit-Anseeuw, R. Gleason, P. Zaytsev, *et al.*, "RAMone: A planar biped for studying the energetics of gait", in *2017 IEEE/RSJ International Conference on Intelligent Robots and Systems (IROS)*, Vancouver, BC: IEEE, Sep. 2017, pp. 4090–4095. DOI: 10.1109/IROS.2017.8206266. [Online]. Available: http://ieeexplore.ieee.org/document/8206266/ (cit. on p. 90).

[244] L. Smith, J. C. Kew, T. Li, *et al.*, "Learning and adapting agile locomotion skills by transferring experience", 2023, Publisher: arXiv Version Number: 1. DOI: 10.48550/ARXIV.2304.09834. [Online]. Available: https://arxiv.org/abs/2304.09834 (cit. on p. 22).

[245] L. Smith, I. Kostrikov, and S. Levine, "A walk in the park: Learning to walk in 20 minutes with model-free reinforcement learning", Aug. 16, 2022, [Online]. Available: http://arxiv.org/abs/2208.07860 (cit. on p. 22).

[246] R. Smith *et al.*, "Open dynamics engine", 2005 (cit. on p. 34).

[247] S.-M. Song and K. J. Waldron, *Machines that walk: the adaptive suspension vehicle*. MIT press, 1989 (cit. on p. 17).

[248] M. Sorokin, C. Fu, J. Tan, *et al.*, *On designing a learning robot: Improving morphology for enhanced task performance and learning*, Mar. 23, 2023. arXiv: 2303.13390[cs]. [Online]. Available: http://arxiv.org/abs/2303.13390 (visited on 11/27/2023) (cit. on p. 77).

[249] A. Spielberg, A. Amini, L. Chin, *et al.*, "Co-learning of task and sensor placement for soft robotics", *IEEE Robotics and Automation Letters*, vol. 6, no. 2, pp. 1208–1215, 2021. DOI: 10.1109/LRA.2021.3056369 (cit. on p. 78).

[250] A. Spielberg, B. Araki, C. Sung, *et al.*, "Functional co-optimization of articulated robots", *arXiv:1707.06617 [cs]*, (cit. on pp. 75, 79).

[251] A. Spröwitz, A. Tuleu, M. Vespignani, *et al.*, "Towards dynamic trot gait locomotion: Design, control, and experiments with cheetah-cub, a compliant quadruped robot", *The International Journal of Robotics Research*, vol. 32, no. 8, Jul. 2013 (cit. on pp. 19, 58, 72, 91).

[252] O. Stasse, T. Flayols, R. Budhiraja, *et al.*, "TALOS: A new humanoid research platform targeted for industrial applications", in *2017 IEEE-RAS 17th International Conference on Humanoid Robotics (Humanoids)*, Birmingham: IEEE, Nov. 2017, pp. 689–695. DOI: 10.1109/HUMANOIDS.2017.8246947. [Online]. Available: http://ieeexplore.ieee.org/document/8246947/ (cit. on p. 57).

[253] H. J. Suh, M. Simchowitz, K. Zhang, *et al.*, "Do differentiable simulators give better policy gradients?", in *Proceedings of the 39th International Conference on Machine Learning*, K. Chaudhuri, S. Jegelka, L. Song, *et al.*, Eds., ser. Proceedings of Machine Learning Research, vol. 162, PMLR, Jul. 2022, pp. 20 668–20 696. [Online]. Available: https://proceedings.mlr.press/v162/suh22b.html (cit. on p. 34).

[254] J. Tan, T. Zhang, E. Coumans, *et al.*, "Sim-to-real: Learning agile locomotion for quadruped robots", *arXiv: 1804.10332*, (cit. on pp. 19, 106).

[255] Y. Tassa, N. Mansard, and E. Todorov, "Control-limited differential dynamic programming", May 2014. DOI: 10.1109/ICRA.2014.6907001 (cit. on p. 98).

[256] R. Tedrake and the Drake Development Team, *Drake: Model-based design and verification for robotics*, 2019. [Online]. Available: https://drake.mit.edu (cit. on p. 33).

[257] B. Thomaszewski, S. Coros, D. Gauge, *et al.*, "Computational design of linkage-based characters", *ACM Transactions on Graphics*, vol. 33, no. 4, pp. 1–9, Jul. 27, 2014. DOI: 10.1145/2601097.2601143. [Online]. Available: https://dl.acm.org/doi/10.1145/2601097.2601143 (cit. on p. 74).

[258] E. Todorov, T. Erez, and Y. Tassa, "Mujoco: A physics engine for model-based control", in *2012 IEEE/RSJ International Conference on Intelligent Robots and Systems*, IEEE, 2012, pp. 5026–5033 (cit. on p. 34).

[259] N. G. Tsagarakis, D. G. Caldwell, F. Negrello, *et al.*, "WALK-MAN: A high-performance humanoid platform for realistic environments: A high-performance humanoid platform for realistic environments", *Journal of Field Robotics*, vol. 34, no. 7, pp. 1225–1259, Oct. 2017. DOI: 10.1002/rob.21702. [Online]. Available: https://onlinelibrary.wiley.com/doi/10.1002/rob.21702 (cit. on p. 58).

[260] I. Tsitsimpelis, C. J. Taylor, B. Lennox, *et al.*, "A review of ground-based robotic systems for the characterization of nuclear environments", *Progress in Nuclear Energy*, vol. 111, pp. 109–124, Mar. 2019. DOI: 10.1016/j.pnucene.2018.10.023. [Online]. Available: https://linkinghub.elsevier.com/retrieve/pii/S0149197018302750 (cit. on p. 21).

[261] V. A. Tucker, "The energetic cost of moving about: Walking and running are extremely inefficient forms of locomotion. much greater efficiency is achieved by birds, fish—and bicyclists", *American Scientist*, vol. 63, no. 4, pp. 413–419, 1975, Publisher: Sigma Xi, The Scientific Research Society. [Online]. Available: http://www.jstor.org/stable/27845576 (cit. on p. 91).

[262] Unitree, *Unitree A1*, https://unitreerobotics.net/robotdog/unitree-a1 (cit. on p. 20).

[263] M. Van De Panne, "Parameterized gait synthesis", *IEEE Computer Graphics and Applications*, vol. 16, no. 2, pp. 40–49, Mar. 1996. DOI: 10.1109/38.486679. [Online]. Available: http://ieeexplore.ieee.org/document/486679/ (cit. on p. 75).

[264] B. Vanderborght, A. Albu-Schaeffer, A. Bicchi, *et al.*, "Variable impedance actuators: A review", *Robotics and Autonomous Systems*, vol. 61, no. 12, pp. 1601–1614, Dec. 2013. DOI: 10.1016/j.robot.2013.06.009. [Online]. Available: https://linkinghub.elsevier.com/retrieve/pii/S0921889013001188 (cit. on p. 58).

[265] M. G. Villarreal-Cervantes, C. A. Cruz-Villar, J. Alvarez-Gallegos, *et al.*, "Robust structure-control design approach for mechatronic systems", *IEEE/ASME Transactions on Mechatronics*, vol. 18, no. 5, pp. 1592–1601, Oct. 2013. DOI: 10.1109/TMECH.2012.2208196 (cit. on p. 106).

[266] M. Vulliez and S. Zeghloul, "Multi-objective design optimization of the delthaptic, a new 6-dof haptic device", in *2016 IEEE 14th International Conference on Industrial Informatics (INDIN)*, Jul. 2016, pp. 248–253. DOI: 10.1109/INDIN.2016.7819167 (cit. on p. 102).

[267] A. Wächter and L. T. Biegler, "On the implementation of an interior-point filter line-search algorithm for large-scale nonlinear programming", *Mathematical Programming*, vol. 106, no. 1, Mar. 1, 2006 (cit. on p. 127).

[268] K. Wampler and Z. Popović, "Optimal gait and form for animal locomotion", in *ACM SIGGRAPH 2009 Papers*, ser. SIGGRAPH '09, New Orleans, Louisiana: Association for Computing Machinery, 2009. DOI: 10.1145/1576246.1531366 (cit. on pp. 75, 86).

[269] F. Wang, Z. Zhang, X. Mei, *et al.*, "Advanced control strategies of induction machine: Field oriented control, direct torque control and model predictive control", *Energies*, vol. 11, no. 1, p. 120, Jan. 3, 2018. DOI: 10.3390/en11010120. [Online]. Available: http://www.mdpi.com/1996-1073/11/1/120 (cit. on p. 63).

[270] Y. Wang and S. Boyd, "Fast model predictive control using online optimization", *IFAC Proceedings Volumes*, vol. 41, no. 2, 2008, 17th IFAC World Congress (cit. on p. 127).

[271] P. Wensing, "The rapid rise of quadruped robots [young professionals]", *IEEE Robotics & Automation Magazine*, vol. 28, no. 3, 2021 (cit. on p. 20).

[272] P. M. Wensing, A. Wang, S. Seok, *et al.*, "Proprioceptive actuator design in the MIT cheetah: Impact mitigation and high-bandwidth physical interaction for dynamic legged robots", *IEEE Transactions on Robotics*, vol. 33, no. 3, Jun. 2017 (cit. on pp. 19, 58, 72, 120).

[273] D. Wolz, "`fcmaes` - a Python3 derivative-free optimization library", [Online]. Available: `pypi.org/project/fcmaes` (cit. on p. 107).

[274] W. Xi and C. D. Remy, "Optimal gaits and motions for legged robots", in *2014 IEEE/RSJ International Conference on Intelligent Robots and Systems*, Chicago, IL, USA: IEEE, Sep. 2014, pp. 3259–3265. DOI: 10.1109/IROS.2014.6943015. [Online]. Available: http://ieeexplore.ieee.org/document/6943015/ (cit. on p. 90).

[275] W. Xi, Y. Yesilevskiy, and C. D. Remy, "Selecting gaits for economical locomotion of legged robots", *The International Journal of Robotics Research*, vol. 35, no. 9, pp. 1140–1154, Aug. 2016. DOI: 10.1177/0278364915612572 (cit. on p. 90).

[276] Z. Xie, G. Berseth, P. Clary, *et al.*, "Feedback control for cassie with deep reinforcement learning", in *2018 IEEE/RSJ International Conference on Intelligent Robots and Systems (IROS)*, Madrid: IEEE, Oct. 2018, pp. 1241–1246. DOI: 10.1109/IROS.2018.8593722. [Online]. Available: https://ieeexplore.ieee.org/document/8593722/ (cit. on p. 26).

[277] J. Xu, T. Chen, L. Zlokapa, *et al.*, "An end-to-end differentiable framework for contact-aware robot design", in *Robotics: Science and Systems XVII*, Jul. 12, 2021. DOI: 10.15607/RSS.2021.XVII.008. arXiv: 2107.07501[cs]. [Online]. Available: http://arxiv.org/abs/2107.07501 (cit. on p. 76).

[278] Y. Yesilevskiy, Z. Gan, and C. David Remy, "Energy-optimal hopping in parallel and series elastic one-dimensional monopeds", *Journal of Mechanisms and Robotics*, vol. 10, no. 3, 2018 (cit. on pp. 74, 75, 93, 127).

[279] Y. Yesilevskiy, Z. Gan, and C. Remy, "Optimal configuration of series and parallel elasticity in a 2D monoped", *IEEE Int. Conf. on Robotics & Automation*, 2016 (cit. on pp. 49, 74, 75, 93, 94, 127).

[280] Y. Yesilevskiy, W. Yang, and C. D. Remy, "Spine morphology and energetics: How principles from nature apply to robotics", *Bioinspiration & Biomimetics*, vol. 13, no. 3, p. 036 002, Mar. 14, 2018. DOI: 10.1088/1748-3190/aaaa9e. [Online]. Available: https://iopscience.iop.org/article/10.1088/1748-3190/aaaa9e (cit. on p. 90).

[281] E. A. Yildirim and S. J. Wright, "Warm-start strategies in interior-point methods for linear programming", *SIAM Jrnl. on Optimization*, vol. 12, no. 3, 2002 (cit. on p. 127).

[282] G. Zardini, A. Censi, and E. Frazzoli, "Co-design of autonomous systems: From hardware selection to control synthesis", in *2021 European Control Conference (ECC)*, Delft, Netherlands: IEEE, Jun. 29, 2021, pp. 682–689. DOI: 10.23919/ECC54610.2021.9654960. [Online]. Available: https://ieeexplore.ieee.org/document/9654960/ (cit. on p. 73).

[283] W. Zhang, Q. Li, and L. Guo, "Integrated design of mechanical structure and control algorithm for a programmable four-bar linkage", *IEEE/ASME transactions on mechatronics*, vol. 4, no. 4, pp. 354–362, 1999 (cit. on p. 85).

COLOPHON

This Ph.D. thesis uses the `classicthesis` typeset by André Miede, *vielen Dank*.

Final version